SVENSKA GEOFYSISKA FÖRENINGEN

VOLUME 9, NUMBER 1 **Tellus** FEBRUARY 1957

A QUARTERLY JOURNAL OF GEOPHYSICS

The Natural Distribution of Radiocarbon and the Exchange Time of Carbon Dioxide Between Atmosphere and Sea

By HARMON CRAIG, Scripps Institution of Oceanography, University of California, La Jolla, California

(Manuscript received Oct. 4, 1956)

Abstract

Steady-state equations governing the transfer and distribution of a radioactive isotope between its various exchange reservoirs are applied to the natural distribution of carbon 14. The radiocarbon enrichment or depletion in each reservoir, relative to the hypothetical state in which mixing is infinitely faster than the decay rate, is evaluated as a quantitative function of the exchange rates between the reservoirs. From the observed distribution of C^{12}, C^{13}, and C^{14} in the atmosphere, biosphere, and sea, and from the estimated production rate of C^{14} by cosmic rays, the residence time of a carbon dioxide molecule in the atmosphere, before entering the sea, is found to be between four and ten years.

The atmospheric residence time may also be evaluated, independently of the estimated C^{14} production rate, by considering the functional dependence of the C^{14} concentration in the oceanic mixed layer on the residence times in the atmosphere and the deep sea. This second method of evaluation also leads to an atmospheric residence time of about seven years. The average annual exchange flux of carbon dioxide into the sea is thus about 2×10^{-3} moles per square centimeter of sea surface. The average residence time of carbon dioxide in the deep sea is estimated as probably not more than about 500 years.

Introduction

Some years ago, the writer made a study of the expected and observed relationships between C^{13} and C^{14} variations in natural materials (CRAIG, 1954). The ratio C^{13}/C^{12} varies by some 5 % in natural sources of carbon (NIER and GULBRANSEN, 1939; CRAIG, 1953), and it was shown that for isotopic fractionation processes, the C^{14} fractionation factors should be the square of the equivalent C^{13} fractionation factors. Since the fractionation factors are close to 1, then barring effects due only to the radioactivity of C^{14}, the percentage enrichment of C^{14} in any compound should be approximately twice the C^{13} enrichment relative to the same source material. Thus, since the carbonate shells of marine mollusks are enriched some 2.5 % in C^{13} relative to terrestrial wood, such shells should show a C^{14} enrichment, relative to wood, of about 5 %. The analytical data then available indicated, however, that wood and shell have about the same radiocarbon concentration, and it was concluded therefore, that the exchange rate of CO_2 between atmosphere and sea was slow enough to produce an apparent radiocarbon age of 400 years for the surface ocean bicarbonate, corresponding to 5 % of the radiocarbon mean life of 8,033 years. It was further pointed out that only slow

Contribution from the Scripps Institution of Oceanography, New Series, No. 895. This paper represents in part results of research carried out by the University of California under contract with the Office of Naval Research.

transfer of carbon across the ocean-atmosphere interface could account for this isotopic discrepancy between the concentrations of the stable and radioactive isotopes.

Recently, more detailed studies of the natural distribution of radiocarbon have established unequivocally the reality of this effect, and it appears that the apparent age of the surface ocean bicarbonate may be taken as 400 ± 100 years for the sake of general calculations (SUESS, 1954, 1955; RAFTER, 1955). It is therefore possible to present a more detailed discussion of the factors affecting the concentration of radiocarbon in its natural reservoirs, and to derive some quantitative values for the exchange rate of carbon dioxide between the atmosphere and the sea.

Recent estimates of the residence time of a molecule of carbon dioxide in the atmosphere, before entering the sea, range from 16 hours (DINGLE, 1954) to the order of 1,000 years (PLASS, 1956). It is, therefore, of considerable interest to determine how precisely this figure may be evaluated from the known distribution and properties of the carbon isotopes. In the following study, we evaluate the characteristics of the radiocarbon distribution in a model of the atmosphere—sea system which is constructed in accord with the known layered structure of the sea, and deduce the atmospheric exchange time by two different methods which are quasi-independent. Both of these methods are based on considerations of the steady state transfer phenomena; a third method of evaluating the CO_2 exchange time, based on the dilution of the atmospheric radiocarbon concentration by the combustion of coal, has been given by SUESS (1953), and recently in a more detailed treatment by REVELLE and SUESS (1957). As we shall see, all these methods lead to the same atmospheric exchange rate but yield essentially no new information on the rate of internal mixing in the sea. However, we shall derive an estimated upper limit for the internal mixing time of the sea, by consideration of the possible dilution of radiocarbon activity in the mixed layer of the sea by production of dead CO_2. (The steady-state radiocarbon balance and the Suess effect have both been treated in a recent study by Arnold and Anderson, in which the internal mixing time of the sea is taken as fixed from recent measurements of M. Rubin; their calculations differ considerably from those given here and are commented on under Acknowledgements.)

Distribution of the carbon isotopes within the exchangeable system

We shall denote the total carbon in the active reservoirs of the atmosphere, biosphere, and sea, as the *exchangeable system*, containing about 7.9 grams of carbon per square centimeter of earth surface (cm_e^2). Table 1 shows the amounts of carbon assumed for the various components of the exchangeable system, the characteristic carbon 13 concentration in each of the components (given as per mil enrichments relative to the Chicago isotopic standard), and the carbon 14 fractionation factor relative to modern wood, computed as the square of the equivalent factor for carbon 13. The values of α_{14} are the C^{14} concentration factors relative to modern wood which would be observed if carbon 14 were stable, i.e. if the relative concentrations were unaffected by radioactive decay.

Figure 1 shows the model used for calculation; the exchangeable system is divided into five reservoirs containing amounts of carbon relative to N_a, the amount in the atmosphere, as shown in the various boxes. For convenience the term *biosphere* is restricted to denote the living terrestrial plants. The transfer between units is assumed to be determined by first order rate constants, denoted as shown, except in the case of biosphere assimilation, where the uptake is probably proportional to $N_a^{\varepsilon}N_b$, ε b ing a number between 0 and 1.

The amounts of carbon in the atmosphere, biosphere, humus, and in the entire ocean, are taken directly from Table 1. However, in accord with observation, the ocean has been taken as consisting of two reservoirs, a mixed layer and the deep sea, separated by the thermocline. The average depth of the thermocline is a question of considerable geochemical significance with respect to problems where rates of uptake or mixing are concerned. We are here interested in the average depth as defining the volumes of material in the two more or less permanent layers of the sea, relative to the total volume of material in the sea. Dr. Warren Wooster of the Scripps Institution has kindly made a study of this important relationship, using most of the

Table 1. Amounts of carbon, characteristic C^{13} concentration, and C^{14} fractionation factor relative to terrestrial wood, of the various components of the exchangeable system of natural carbon

	δC^{13} (‰) (1)	α_{14} (2)	Carbon content grams/cm^2
Atmospheric CO_2.	— 7	1.037	0.126 (3)
Terrestrial biosphere (living)..	—25	1	0.06 (4)
Terrestrial humus	—25	1	0.215 (5)
Marine biosphere.	—13.5	1.024	0.002 (6)
Dissolved organic carbon in sea..	—13.5	1.024	0.533 (7)
Total inorganic carbon in sea..	— 1.5	1.049	6.94 (7)
Total exchangeable system ...			7.88

(1) Data from H. Craig (1953, 1954). $\delta = [(R$ sample$/R$ standard$) - 1] \times 1{,}000$, where $R = C^{13}/C^{12}$ and the standard is the Chicago isotopic standard. Data on the various isotopic reference standards in use are given by Craig (1957).

(2) Fractionation factor for C^{14} relative to terrestrial wood; i.e. the expected C^{14}/C^{12} ratio in the component material, divided by the C^{14}/C^{12} ratio of modern wood. From column 1, the C^{13} fractionation factors relative to modern wood (— 25 ‰) were computed for each component; these values squared give the values in column 2 (see text). α is the chemical fractionation factor which would give the observed C^{14} concentration relative to wood if the mixing between components were infinitely fast.

(3) Data from Hutchinson (1954).

(4) Data from Schroeder and Noddack, as given by Goldschmidt (1954, p. 355). Hutchinson (1954) roughly estimates this figure as one order of magnitude lower; however he uses the estimates of Schroeder and Noddack for the rate of photosynthesis by terrestrial plants. Their calculated *rate* is based on their estimate of the size of the biosphere, and thus calculations of the atmosphere-biosphere flux cannot be consistent unless both (or neither) of their estimates are adopted.

(5) Mean of estimated values 0.29 by Goldschmidt (1954), and 0.14 by Rubey (1951).

(6) Estimated upper limit from data of Riley, Stommel, and Bumpus (1949). Using their data for the Sargasso sea only, one obtains an order of magnitude less, and according to them the Sargasso crop is about the same as the mean temperate ocean water crop, exclusive of the spring flowering period. In our units, their highest recorded value is 0.007 in Long Island Sound; the bulk of their data indicate the average ocean crop is an order of magnitude less.

(7) Data from Revelle and Suess (1957).

available records of observation of the variations in temperature and density in the various seas. He concludes that the mean thermocline depth, averaged over an entire year and over all oceans, is certainly between 50 and 100 meters. We have thus adopted the figure 75 ± 25 meters for the mean thermocline depth, for all calculations. The average depth of the ocean and all seas is taken as 3,800 meters (Sverdrup *et al.*, 1942), and thus the mixed layer and the deep sea are taken as containing respectively 2 % and 98 % of the total carbon in the sea. (The marine biosphere was assumed to be entirely in the mixed layer.) The amounts of carbon relative to the amount in the atmosphere are then $N_m = 1.2\ N_a$ and $N_d = 58.3\ N_a$.

Figure 1 also shows the values used for the observed radiocarbon concentrations in the various reservoirs, relative to R_w, the ratio C^{14}/C^{12} in terrestrial wood. Rafter (1955) has shown that the atmospheric ratio is about that expected on the basis of the C^{13} data, namely $1.037\ R_w$. The average radiocarbon activity in humus is not known, but must lie within limits of 0—1 R_w; the effect of this uncertainty on the following calculations is negligible. As discussed above, the activity in the mixed layer may be taken as equal to R_w; however the average activity in the deep sea is not known and we take this as a variable parameter. The absolute value of R_w is taken as 1.24×10^{-12} from the measurements of Suess (1955) on 19th century wood normalized for time and isotopic fractionation.

Notation and symbols:

N_i = amount of $(C^{12} + C^{13})$ in reservoir i.

N_i^* = amount of C^{14} in reservoir i.

k_{i-j} = rate constant for transfer of carbon from reservoir i to reservoir j, (first order process assumed, i.e. flux from i to $j = k_{i-j} N_i$, except for transfer from atmosphere to biosphere), years^{-1}.

k_{i-j}^* = rate constant for transfer of C^{14}, used when $k^* \neq k$.

τ_{i-j} = $1/k_{i-j}$ = residence time (years) of a stable carbon atom in reservoir i before transfer to reservoir j.

τ_{i-j}^* = $1/k_{i-j}^*$ = residence time of a C^{14} atom in reservoir i before transfer to reservoir j.

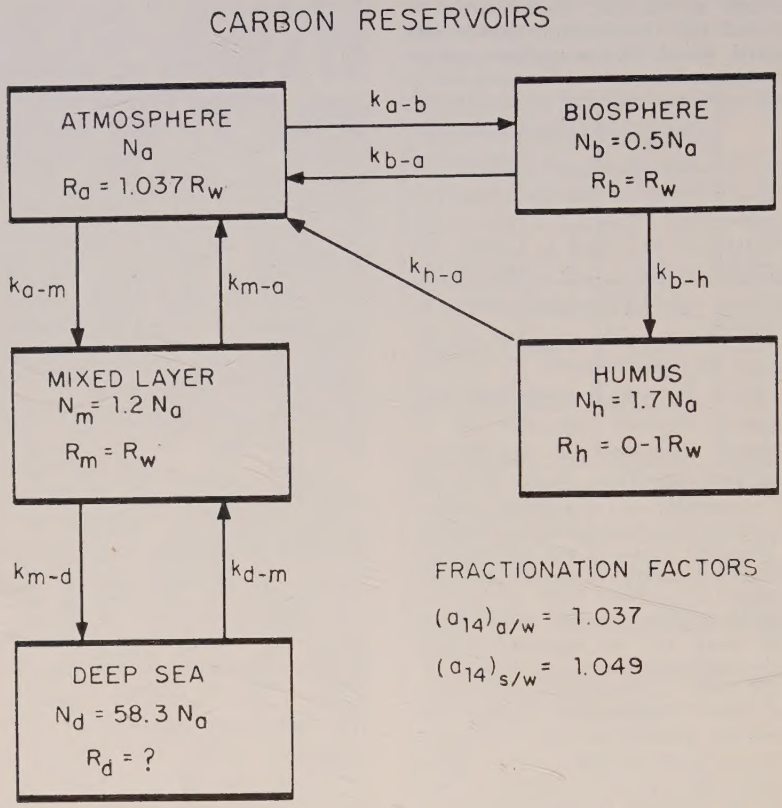

Figure 1. Carbon reservoirs in the exchangeable system. N_a = atmospheric carbon = 0.126 grams C/cm^2_e. $R_w = C^{14}/C^{12}$ ratio in standard wood = 1.14×10^{-12}.

τ_r = $1/\lambda$ ($\lambda = C^{14}$ decay constant) = radioactive mean life of $C^{14} = 8{,}033$ years.

R_i = $N_i^*/N_i = C^{14}/C^{12}$ ratio in carbon in reservoir i.

$\overline{Q}$ = mean production rate of C^{14} from cosmic ray flux, atoms/cm^2 sec.

The meaning of τ:

We shall define τ rigorously and identify its particular meanings with specific subscripts, in order to avoid possible confusion with respect to the many usages of this symbol. Assume a reservoir with a steady-state fixed content of N molecules of a substance, and a continuous flux into and out of the reservoir of ϕ molecules/year. At a particular time, $t = 0$, we have N_0 particular molecules in the reservoir, and at some later time t, we have N' of these original N_0 molecules still present. Then we define the average life of a molecule in the reservoir in the usual way, as

$$\tau = \frac{\Sigma_i\, t_i n_i}{\Sigma_i\, n_i} \approx -\frac{1}{N_0} \int_{\substack{t=0 \\ N'=N_0}}^{\substack{t=\infty \\ N'=0}} t\, dN'$$

where n_i is the number of molecules of the original N_0 which remain in the reservoir for each time t_i, and dN' is the number of molecules removed in the interval t and $t + dt$, i.e. the number of molecules with a reservoir lifetime equal to t.

The number of molecules of the original particular set of N_0 which are removed in any

interval dt is simply given by the concentration of such molecules in the reservoir, multiplied by the total flux from the reservoir, i.e.:

$$dN' = -\frac{N'}{N}\phi dt$$

which yields on integration $N' = N_0 \exp(-\phi t/N)$.

Substituting for dN' and then for N' in the integral expression for τ, and integrating between $t = 0$ and infinity, we obtain:

$$\tau = \frac{N}{\phi}$$

and from the expression for N' one sees that τ, the average life, is also the time required for the original number of N_0 particular molecules to be reduced to $1/e$ times the initial number. τ is thus formally equivalent to a radioactive mean life.

In many cases, the rate of removal is dependent only on the total amount of substance, N, in the reservoir, and we can write the outgoing flux as the product of N and a first order rate constant, i.e. $\phi = kN$. In such cases we see that $\tau = 1/k$, just as the radioactive mean life is equal to $1/\lambda$.

We shall call τ, as rigorously defined above, the residence time or average reservoir life. In particular, we denote by subscripts i and j, as shown above under *Notation*, a particular residence time in reservoir i before removal to a specific reservoir j. When a reservoir exchanges with n different reservoirs, then we denote the *total* residence time in reservoir i, relative to removal by all routes, as τ_{i-T} where:

$$\frac{1}{\tau_{i-T}} = \sum_{j=1}^{j=n} \frac{1}{\tau_{i-j}}$$

For a radioactive isotope, the average reservoir life will not be the same as for the corresponding stable isotope, because of the following effects. (1) There may be isotopic fractionation in the removal process. This effect is of course independent of the radioactivity and dependent only on the isotopic mass difference; when it occurs it will cause the residence times of the isotopic species, relative to that specific removal process, to be slightly different. (2) Because of the radioactivity, the total removal rate of a radioactive species will be the sum of the physical removal rates plus λN_i, the decay rate. (3) In the steady state, after normalizing for effects (1) and (2), the residence times of the isotopic species will always be the same. However, it should be noted that in a *transient* state, the concept of residence time, as given above, may break down, and a somewhat different rigorous definition may be required. In particular, it is well known that, for transfer from a reservoir i to a reservoir j, the transfer process for an isotope in low concentration will always be a first order process (the exponential exchange law, based on the low probability of interaction) as long as the rate of mixing in reservoir j is fast relative to the transfer process, so that the isotope does not pile up at the boundary. (Humus, and the deep-sea carbon, represent reservoirs where such a pile-up might occur in the transient state.) On the other hand, the transfer process for the abundant isotopic species may or may not be first order, depending on the specific chemical and physical processes involved. Conversely, the more abundant isotope may pile up at the surface of reservoir j and mix backwards more rapidly than forward, if this is the isotope involved in the transient process. (An example of this might be the $C^{12}O_2$ produced by the combustion of fossil fuel, which might pile up in the surface layers of the deep sea or the humus.)

We shall not be concerned with the transient state in this study and thus the effects given under (3) above may be disregarded in this paper. Moreover, we shall consider only those processes in the carbon cycle which happen to be so fast, relative to the decay rate of C^{14}, that the effect of its radioactivity on the residence times is negligible. However, considering isotopic fractionation, as discussed under (1) above, we shall denote the residence times and rate constants for C^{14} as τ^*_{i-j} and k^*_{i-j} for processes in which isotopic separation may be involved (specifically for absorption and release of CO_2 by the sea).

Calculation of the CO_2 exchange time from the radiocarbon production rate

We consider the radiocarbon material balance, relative to cosmic-ray production, physical removal, and decay, in the atmosphere. Equating the flux of C^{14} entering the atmosphere, from production and from the sea and biosphere, to that leaving by physical means

and decay, we write for the assumed steady state:

$$k^*_{a-m}N^*_a - k^*_{m-a}N^*_m = \bar{Q} - \lambda(N^*_a + N^*_b + N^*_h) \quad (1)$$

in terms of the isotopic rate constants for C^{14}. The steady state difference in the C^{14} flux between the atmosphere, and biosphere + humus, is simply $\lambda N^*_b + \lambda N^*_h$.

For $C^{12}O_2$ the steady state interaction of atmosphere and sea is:

$$k_{a-m}N_a = k_{m-a}N_m \quad (2)$$

and we then write the relation between the two sets of isotopic rate constants as:

$$\frac{k^*_{a-m}}{k^*_{m-a}} = \alpha_{s/a}\frac{k_{a-m}}{k_{m-a}} = \alpha_{s/a}\frac{N_m}{N_a} \quad (3)$$

where $\alpha_{s/a}$ is the ratio of the fractionation factor for C^{14} in the ocean bicarbonate, relative to wood, to the C^{14} factor in atmospheric CO_2 relative to wood; i.e. from table 1, $\alpha_{s/a} = 1.049/1.037 = 1.012$. (In these and the following derivations, we take all the factors relative to wood, which is the general radiocarbon standard.)

Substituting in (1) to eliminate k^*_{m-a}, and substituting $N^*_i = R_i N_i$, we obtain the expression for k^*_{a-m} in terms of the various R and N parameters, which may be written explicitly for the residence time of a $C^{14}O_2$ molecule in the atmosphere, before entering the sea, as:

$$\tau^*_{a-m} = \frac{\dfrac{\tau_r}{\alpha_{s/a}}\left[\alpha_{s/a} - \dfrac{R_m}{R_a}\right]}{\dfrac{\bar{Q}}{\lambda N^*_a} - \dfrac{R_b}{R_a}\dfrac{N_b}{N_a} - \dfrac{R_h}{R_a}\dfrac{N_h}{N_a} - 1} \quad (4)$$

wherein we note that the numerator of the expression is the fractional isotopic effect times the radiocarbon mean life. The denominator is the ratio of the total amount of radiocarbon in the sea to the amount in the atmosphere, $\bar{Q}/\lambda$ being equal to the total amount of radiocarbon in the world.

Using $\bar{Q}$ as 2 atoms/cm^2_e sec and $R_h/R_a = 0.5/1.037$ (see below for discussion of these values), setting $N^*_a = R_a N_a$, and using the various R and N values shown in Figure 1 and the other numerical values needed as given in the text, we find τ^*_{a-m} to be 6.2 years. The rate constant for absorption of $C^{12}O_2$ into the sea will be slightly greater than the rate constant for $C^{14}O_2$ because of an isotopic effect. For the case of absorption of $C^{12}O_2$ and $C^{13}O_2$ by barium hydroxide, the difference in rate is 1.5 % (Craig, 1953), and no significant error can be made by assuming a 3 % effect for the $C^{12} - C^{14}$ absorption by the sea. We thus find $\tau_{a-m} = .97\ \tau^*_{a-m} = 6$ years.

The range of possible error in the numerical values may be defined as follows. At present the most uncertain value is probably the cosmic ray production of C^{14}. Recent calculations of $\bar{Q}$ have yielded values of 2.6 (Anderson, 1953; Libby, 1955), and 2.4 (Ladenburg, 1952; Kouts and Yuan, 1952). Anderson suggests these values may be systematically too high because of uncertainty in the calculation of the capture rate of cosmic ray neutrons in the energy range just above the sharp increase in the cadmium cross section at 0.4 ev. More recently, Soberman (1956) has made a general study of the neutron intensity variations at high altitudes. With essentially the same experimental data, he calculates $\bar{Q}$ to be 1.1, neglecting the resonance capture, by nitrogen, of neutrons with energies greater than 0.5 Mev. Kouts and Yuan (1952) found that the local production rate at Princeton was increased from $Q = 3.50$ to 4.13 by inclusion of the resonance capture rate. They also pointed out that the counters used in the slow neutron measurements are calibrated to no greater accuracy than 20 %, reflecting the uncertainty in the flux values of the Argonne standard reactor. All things considered, it appears that $\bar{Q}$ should be assigned an uncertainty of 25 %, and we shall assume the value $2 \pm .5$, though as noted below, it seems unlikely that the correct value can be greater than 2.

The apparent age of carbon in the mixed layer of the sea may be taken as 400 ± 100 years[1] (Suess, 1954, 1955; Rafter, 1955). The

[1] Suess' measurements on Atlantic shells and organic carbon average 430 years relative to his standard. Rafter's measurements on Pacific shells, organic carbon, and surface sea water, average 290 years relative to a modern wood standard (Rafter, 1955). Correction of his wood standard for the Suess effect adds 110 years to all the Pacific measurements (Fergusson and Rafter, New Zealand C^{14} Age Measurements III, in press); thus the average age for Pacific samples, relative to age corrected 19th century wood, becomes 400 years, in exact agreement with the data of Suess. This age is obtained from the 5 % isotopic fractionation factor between wood and

data by Suess represent the apparent age relative to a composite 19th century wood standard, corrected for isotopic fractionation and age, and thus the Suess effect, i.e. the slight dilution of the activity of modern wood and the atmosphere by combustion of coal during the past decades, does not affect this figure. However, there may be a slight dilution of the activity of the oceanic mixed layer samples. The average Suess effect over the world is probably of the order of 1 %, since the highest values found are near areas subject to local industrial contamination and are thus not representative. As pointed out below, the residence time of carbon in the mixed layer, before entering the deep sea, is probably about the same as the atmospheric residence time, and thus the dilution effect on the mixed layer is probably not more than 1 %.

This effect is well within the over-all uncertainty, and we shall use the 400 year figure, taking the activity ratio R_m/R_a as $(1 \pm .01)/1.037$, introducing an error of ± 20 % in equation (4).

The counting error in the absolute value of R_w is 2 % (Suess, 1955) and the value itself is based on a mass spectrometrically calibrated C^{14} standard for which the calibration data showed a range of 3 %. The error in the C^{14} decay constant can scarcely exceed 2 % (Libby, 1955, p. 42). Finally, one sees that the term $\bar{Q}/\lambda N_a^*$ in the denominator of equation (4) is about 60, while the remaining terms are of the order of 1. In particular, with the amount of humus assumed as $N_h = 1.7\ N_a$, a possible range in R_h of 0 to R_w produces a range of only 3 % in τ^*_{a-m}. Thus we take $R_h = 0.5\ R_w$ for calculation, introducing an error of only ± 1.3 %. Even assuming that the humus value of $1.7\ N_a$ is underestimated by a factor of 10, and that all humus has modern activity, would cause an error of only 1.6 years in τ_{a-m}.

A reasonable estimate of the maximum error possible is a range of $\pm$ 50 %. The value obtained from (4) is then: $\tau_{a-m} = 6^{+4}_{-2}$ years; the maximum value representing assumed values of 1.5 for $\bar{Q}$ and 500 years for surface ocean carbon, and the minimum value representing assumed values of 2.5 and 300 years. (The actual errors are not symmetrical because one enters in the numerator and one in the denominator.)

Distribution of carbon 14 in the atmosphere and sea

We now proceed to derive equations expressing the functional dependence of the amounts and specific activities of radiocarbon in the atmosphere, mixed layer, and deep sea, on the various rate constants or residence times involved. We assume that the residence time of C^{14} in the deep sea, relative to physical removal, is the same as that for C^{12}, i.e. that no isotopic fractionation is involved in the internal mixing in the sea. We shall then show how τ^*_{a-m} can also be calculated as an explicit function of the rate of mixing within the sea.

Writing out the expressions for steady state material balance of the radiocarbon flux in the mixed layer and in the deep sea, we have:

$$k^*_{a-m}N^*_a + k_{d-m}N^*_d = N^*_m\,(k^*_{m-a} + k_{m-d} + \lambda) \quad (5)$$

$$k_{m-d}N^*_m = N^*_d\,(k_{d-m} + \lambda) \quad (6)$$

where we have assumed, as stated above, that the isotopic rate constants for mixing within the sea are identical. The steady state C^{12} balance between the mixed layer and deep sea is given by:

$$k_{m-d}N_m = k_{d-m}N_d \quad (7)$$

For simplification, we shall now omit from the model the terrestrial biosphere and humus, i.e. we take the total radiocarbon balance as:

$$\bar{Q} = \lambda\,(N^*_a + N^*_m + N^*_d) \quad (8)$$

The effect of the biosphere could be included by substituting for $\bar{Q}$ in all equations in this section, the expression: $[\bar{Q} - \lambda(N^*_b + N^*_h)]$. This would change the calculated percentage changes in activity of the various reservoirs for a given change in mixing rates (δ values) by only 1 % of their numerical values, and thus the error introduced by this simplification is negligible. (The percentage error is actually variable and roughly equal to δ_a in percent divided by 30.)

From the above expressions and equation (3), one may derive the explicit relationships for the amounts of C^{14} in the three reservoirs as functions of the C^{14} decay constant, the rate

shell; the observed radiocarbon activities of wood and shell are about the same, but apparent ages are usually tabulated instead of relative activities.

constants k^*_{a-m} and k_{d-m} $(=1/\tau_{d-m})$, the production rate, and the known distribution of C^{12}, which are as follows:

$$N^*_a = \frac{\bar{Q}}{\lambda}\left[1+\frac{1}{\frac{\lambda}{k^*_{a-m}}+\frac{1}{\alpha_{s/a}F}}\right]^{-1} \tag{9}$$

$$N^*_m = \frac{\bar{Q}}{\lambda}\frac{N_m}{N_a}\left[\frac{1}{F\left(1+\frac{\lambda}{k^*_{a-m}}+\frac{1}{\alpha_{s/a}F}\right)}\right] \tag{10}$$

$$N^*_d = N^*_m\left[\frac{N_a}{N_m}F-1\right] \tag{11}$$

$$F = \frac{N_m}{N_a}+\frac{N_d}{N_a}\left[\frac{1}{1+\frac{\lambda}{k_{d-m}}}\right] \tag{12}$$

From these expressions one sees that N^*_a varies inversely with both rate constants, i.e. slow exchange between atmosphere and sea and slow internal mixing in the sea will both increase the radiocarbon concentration in the atmosphere. The reason of course is that the rate of decay is constant and proportional to the concentration, so that if the rate of physical removal is decreased more C^{14} is removed by decay with a consequent increase in the concentration. In the same way, N^*_m is seen to vary directly with k^*_{a-m} but inversely with k_{d-m}, while N^*_d varies directly with both rate constants. Setting k_{d-m}/λ equal to infinity in the above expressions gives the equations governing the simple model of an atmosphere and a uniform ocean, and if k^*_{a-m}/λ is then also set equal to infinity, one obtains the simple statistical partitioning of C^{14} corrected by the isotopic fractionation factor.

The function F is seen to be the "effective volume" or "effective carbon reservoir" of the sea, relative to the amount of carbon in the atmosphere. As k_{d-m}/λ varies from infinity to 0, F varies from $(N_m+N_d)/N_a$, i.e. the total amount of carbon in the sea relative to the atmosphere, to N_m/N_a, i.e. the carbon in the mixed layer only. In the derivation of the above equations, F falls out quite naturally as an algebraic entity; the physical significance of this function is discussed in the next section. Values of F as a function of the residence time of carbon in the deep sea are tabulated in the next section, and we shall use these values here to demonstrate the magnitude of the concentration changes in the various reservoirs as functions of the mixing rates.

Noting that for each reservoir, $R_i = N^*_i/N_i$, we denote by δ_i the percentage difference in radiocarbon activity (C^{14}/C^{12}), for any pair of rate constants k^*_{a-m} and k_{d-m}, from the state in which these rate constants are both infinitely greater than the decay constant, i.e. when the radioactivity of C^{14} has no effect on its natural distribution. Thus we define:

$$\delta_i\,(\%) = \left[\frac{R_i}{R_i\,(\tau_{i-j}=0)}-1\right]\times 100 \tag{13}$$

where the notation $(\tau_{i-j}=0)$ signifies the hypothetical state in which the residence time in each reservoir before physical removal is essentially 0 relative to the residence time before radioactive decay (i.e. $k_{i-j}/\lambda =$ infinity). The following equations give δ for the atmosphere, mixed layer, and deep sea, as explicit functions of the residence time in the atmosphere before entering the sea, the residence time in the deep sea before entering the mixed layer, the radioactive mean life τ_r, and the fixed amounts of carbon 12 in the various reservoirs.

$$\delta_a = \frac{\alpha_{s/a}\frac{N_s}{N_a}\frac{\tau^*_{a-m}}{\tau_r}+\frac{N_s}{N_a}\frac{1}{F}-1}{\frac{\tau^*_{a-m}}{\tau_r}+\frac{1}{\alpha_{s/a}F}+1} \tag{14}$$

$$\delta_m = -\frac{\frac{\tau^*_{a-m}}{\tau_r}-\frac{N_s}{N_a}\frac{1}{F}+1}{\frac{\tau^*_{a-m}}{\tau_r}+\frac{1}{\alpha_{s/a}F}+1} \tag{15}$$

$$\delta_d = \frac{\tau_r\delta_m-\tau_{d-m}}{\tau_r+\tau_{d-m}} \tag{16}$$

In these expressions we have used N_s, the total stable carbon in the sea, $= N_m + N_d$. For the simpler model in which the ocean is taken as a single reservoir, uniformly mixed at a rate infinitely greater than the C^{14} decay rate, the function F is equal to N_s/N_a. The numerators of equations (14) and (15) are then reduced to containing the first term only, and one sees that, for a given atmospheric residence time, the percentage decrease in C^{14} activity in the

mixed layer is approximately N_a/N_s or $^1/_{60}$ of the increase in the atmospheric activity, as of course it must be. In this case, of course, δ_d and δ_m are identical, as shown by (16).

In table 2 we tabulate the calculated δ_i values for atmospheric residence times, relative

Table 2. Effect of the residence times of CO_2 in the atmosphere and deep sea, both relative to exchange into the mixed layer, on the specific activity of radiocarbon in the atmosphere, mixed layer, and deep sea. δ = per cent difference in activity (C^{14}/C^{12} ratio) from the condition of infinitely fast mixing relative to the radioactive decay rate

		τ^*_{a-m} = 5 y.	τ^*_{a-m} = 10 y.	τ^*_{a-m} = 20 y.
τ_{d-m} = 0	δ_a	+ 3.7	+ 7.4	+ 14.7
	δ_m, δ_d	— 0.06	— 0.12	— 0.24
τ_{d-m} = 500 y.	δ_a	+ 9.7	+ 13.4	+ 20.7
	δ_m	+ 5.93	+ 5.86	+ 5.73
	δ_d	— 0.28	— 0.34	— 0.46
τ_{d-m} = 1,000 y.	δ_a	+ 15.6	+ 19.3	+ 26.6
	δ_m	+ 11.88	+ 11.81	+ 11.67
	δ_d	— 0.51	— 0.57	— 0.69

to the mixed layer, of 5, 10, and 20 years, and deep sea residence times, relative to the mixed layer, of 0 (rapidly mixed sea), 500, and 1,000 years. For the case of rapid mixing of the sea, the C^{14} activity in the atmosphere is increased by about 0.74 % for each year of atmospheric residence time, relative to the condition of rapid atmospheric exchange with the sea, while the activity in the sea is reduced by $^1/_{60}$ of the atmospheric increase. If the internal mixing within the sea is slow, corresponding to a deep-sea residence time of 500 years relative to the mixed layer, the effect is to increase the activity in both the atmosphere and the mixed layer by 6 %, while reducing the deep-sea activity by 0.28 %; thus the *difference* in the observed activities in the atmosphere and mixed layer remains about the same. As the table shows, the atmospheric and mixed-layer activities are each increased by about 1.2 %, relative to the condition of a rapidly mixed sea, for each 100 years of residence time in the deep sea, or "age" of the deep sea water.

It is clear that the "apparent age" of the surface ocean bicarbonate does not reflect a simple decrease of activity due to slow transfer of radiocarbon into the sea, as is sometimes stated. The actual effect is a piling up of the radiocarbon in the atmosphere by the mixing barrier, amounting to several percent of the activity which would be observed in the case of very rapid exchange with the sea. The actual decrease in specific activity of the sea is seen to be an insignificant contribution to the observed difference of activity between the atmosphere and the sea. The "piling up" effect in the atmosphere and mixed layer, by slow internal mixing in the sea, is about the same for each of these reservoirs, because they contain about the same amounts of carbon (fixed by the chemical equilibrium between atmosphere and sea and the average depth of the thermocline); thus observations of the activity difference between the atmosphere and the mixed layer cannot yield much information about the rate of internal mixing in the sea.

Calculation of the CO_2 exchange time from the distribution of carbon 14

Table 2 shows that over the range of deep-sea residence time considered, the difference in activity between the atmosphere and mixed layer is practically unaffected by the internal mixing rate within the sea, and is essentially a function of the atmospheric residence time of CO_2 only. Thus we can estimate the atmospheric residence time rather closely by considering the atmosphere-mixed layer activity difference, if we have some idea of the order of magnitude of the mixing rate within the sea.

From equations (3), (5), (6), and (7), we derive the expression for the ratio of the radiocarbon activity in the atmosphere to the activity in the mixed layer, in terms of the mixing rate constants, as:

$$\frac{R_a}{R_m} = \frac{1}{\alpha_{s/a}} + \frac{\lambda F}{k^*_{a-m}} \qquad (17)$$

where the function F was given by (12). For an infinite deep-sea residence time, i.e. no mixing between the layers of the sea, F reduces to N_m/N_a and the activity ratio is seen to become dependent on the size of the mixed layer reservoir only. It should be noted that (17) is derived from considerations of the steady state balance in the mixed layer and in the deep

sea, and is *independent* of any assumptions about the terrestrial biosphere and humus.

Equation (17) may be rewritten as:

$$\tau^*_{a-m} = \frac{\tau_r}{F}\left[\frac{R_a}{R_m} - \frac{1}{\alpha_{s/a}}\right] \qquad (18)$$

and using R_a and R_m as given in figure 1, we now tabulate τ^*_{a-m} vs. τ_{d-m}, together with the function F and the ratio F/F_0 in percent, where $F_0 = N_s/N_a$ = the value of F for infinitely rapid mixing in the sea on the radiocarbon time scale.

τ_{d-m}(y)	F	F/F_0 (%)	τ^*_{a-m} (y)
0	59.5	100	6.54
100	58.8	98.8	6.62
300	57.4	96.5	6.78
500	56.1	94.3	6.93
1,000	53.0	89.1	7.34
5,000	37.1	62.4	10.5
10,000	27.2	45.7	14.3
20,000	18.9	31.8	20.6
50,000	9.3	15.6	41.8

By equating (18) with (4) we see that:

$$\frac{N^*_s}{N^*_a} = \frac{R_m}{R_a} F \qquad (19)$$

since, as noted in the discussion of (4), the denominator of (4) is equal to N^*_s/N^*_a. It is then easy to show rigorously the physical meaning which may be attached to F. For any given internal mixing rate in the sea, we may suppose the sea to be divided into two portions, the uppermost of which contains all the radiocarbon of the sea at a uniform concentration equal to that presently observed in the surface of the sea; i.e. the internal mixing in this portion is infinitely rapid on the radiocarbon time scale and the C^{14}/C^{12} ratio in this portion is $R_m (= R_w)$. The lowermost portion contains no radiocarbon. Then if X is the amount of C^{12} in the uppermost portion containing the radiocarbon, $X = FN_a$, and F is simply the ratio of the amount of stable carbon in the upper portion to the amount in the atmosphere. Moreover, $F/F_0 = X/N_s$, so that the ratio F/F_0 is simply the fraction of the total sea contained in the rapidly mixed upper portion.[1] Thus from the numerical values tabulated above, one sees that a deep-sea residence time of 5,000 years in the actual two-layer model assumed in this study, is equivalent to having 62 % of the sea, at C^{14} concentration R_m, rapidly mixed and functioning as an effective component of the exchangeable system, and 38 % of the sea completely isolated and containing no radiocarbon. This would correspond to complete mixing in the upper 2,400 meters of the sea and no communication with the bottom 1,400 meters.

The dependence of τ^*_{a-m} on τ_{d-m} is seen to be of such low order that a 5,000 year mixing time in the sea adds only 4 years to the atmospheric residence time calculated for a homogeneous sea with infinitely rapid internal mixing. This is simply the consequence of the long C^{14} half-life, coupled with the fact that one is dealing with a steady-state mixed system, rather than a case of simple exponential decay from an initial concentration.

Only one set of precise radiocarbon measurements on deep-sea water appears to exist at present. M. Rubin of the U.S. Geological Survey has found that in the area east of the Lesser Antilles, the water at 1,750 meters is only 200 years "older" than the surface water (personal communication). However, it appears to be well established that, in general, the internal mixing time of the sea is less than 1,000 years. Wooster and Ketchum (1956) have calculated the mean displacement time of the deep water of the North Atlantic as 250 years, from oceanographic data. Worthington (1954) has studied the secular decrease of dissolved oxygen in these waters and estimates the age, relative to the surface water, as 140 years. His data indicate that the North Atlantic deep water may be formed sporadically, rather than replenished by a continuous mixing process. The deep Pacific water is probably older than the deep waters of the Atlantic. However, Revelle and Maxwell (1952) found that the heat flux through the floor of the Pacific is such that the deep Pacific water must be replenished in less than a thousand years.

From the figures tabulated above, one sees that a range in the deep sea residence time of

[1] Alternatively one could assume a model in which the uppermost portion of the sea, containing all the radiocarbon, grades from a C^{14}/C^{12} ratio of R_m at the surface to 0 at the lower boundary. In this case $X = (R_m/R_x)FN_a$ and $X/N_s = (R_m/R_x)(F/F_0)$, where $R_x = N^*_s/X$ = the average C^{14}/C^{12} ratio in the upper layer. The correspondence with our actual model would then depend on the type of activity gradient assumed.

0—1,000 years corresponds to a range in τ^*_{a-m} of only 0.8 years, an insignificant error. Thus we take τ^*_{a-m} as 6.8 years, corresponding to $\tau_{a-m} = 6.6$ years, with an estimated uncertainty of about 40 %, reflecting uncertainties of 5 % due to the internal mixing rate in the sea, 20 % in the measured percentage activity difference between the atmosphere and mixed layer, perhaps 10 % in the absolute amount of carbon in the sea, and 2 % in the decay constant. The error in F due to the uncertainty in the average depth of the thermocline is only 1 %, as the absolute amount of carbon in the mixed layer alone does not enter into the calculation. (Thus the possible error in estimating the size of the marine biosphere is seen to be entirely negligible.)

The value 6.6 years is in excellent agreement with the previous figure of 6 years, calculated by (4) from the radiocarbon production rate with a very minor dependence on the size of the biosphere and humus. Both calculations, however, require the measured "apparent age" of the mixed layer carbon, and thus they are not completely independent. The errors in each of these results are probably such as to make the values slightly higher, and $\bar{Q}$ is more probably less than, rather than greater than, 2.0. Weighting the errors, and using (2) we adopt the values:

$$\tau_{a-m} = 7 \pm 3 \text{ years} \qquad \tau_{m-a} = 8.4 \text{ years}$$

$$k_{a-m} = 0.14 \qquad k_{m-a} = 0.12$$

and the mixing rate constants are thus a thousand times larger than the radioactive decay constant.

Taking the amount of CO_2 in the atmosphere as 2.35×10^{18} grams, (HUTCHINSON, 1954) and k_{a-m} as 0.14, we find the exchange rate of CO_2 between atmosphere and sea to be 2×10^{-3} moles of CO_2 per square centimeter of sea surface, per year, or about 45 cc (STP) of CO_2.

$\bar{Q}$ and the radiocarbon content of the deep sea

Using Suess' value for $R^=_w$ and the data given in table 1 and figure 1, we can calculate the maximum amount of radiocarbon on the earth by assuming the average "age" of the ocean water to be 600 years and all the humus to have modern activity. In this way we can account for 57 metric tons of C^{14} on the earth, corresponding to 260 megacuries of activity. Using the $\bar{Q}$ value of 2.4 (LADENBURG, 1952), the predicted amount of C^{14}, corresponding to secular equilibrium with the production rate, is 72 metric tons. The discrepancy is thus about equivalent to the 20 % uncertainty assigned to the production rate by KOUTS and YUAN (1952).

We may write the relationship between τ_{d-m} and $\bar{Q}$ as:

$$\frac{\tau_{d-m}}{\tau_r} = \frac{N_d R_m}{\frac{\bar{Q}}{\lambda} - N^*_{a+b+h+m}} - 1 \qquad (20)$$

and we calculate the following values of τ_{d-m} for the previously assumed mean and limits for $\bar{Q}$:

$\bar{Q}$	τ_{d-m} (y)
1.5	+2,580
2.0	− 265
2.5	−1,910

Thus from the uncertainty in $\bar{Q}$, the steady state conditions are consistent with any oceanic mixing time up to 2,500 years; however, the radiocarbon distribution data suggest that $\bar{Q}$ is actually about 1.8 and not greater than 2. In this calculation we have assumed all the humus to have modern activity; it seems unlikely that limestone can have acquired enough C^{14} by exchange to make up the balance required by the high value of $\bar{Q}$.

The relation between τ_{d-m} as defined for steady state mixing conditions, and t_c, the "age" of deep-sea water, relative to surface water, as calculated by the simple exponential decay relationship, is given by:

$$\frac{\tau_{d-m}}{t_c} = \frac{e^{\lambda t_c} - 1}{\lambda t_c} = 1 + \frac{1}{2}\frac{t_c}{\tau_r} + \frac{1}{6}\left[\frac{t_c}{\tau_r}\right]^2 \qquad (21)$$

and thus τ_{d-m} will be greater than t_c, the "measured age", by about 0.6 % for each 100 years of t_c.

Summation and discussion

Using the empirical data on the relative distribution of C^{12}, C^{13}, and C^{14} in the exchangeable system of carbon, and a model for the sea consisting of a rapidly-mixed surface

layer, coupled with the deep sea, a quantitative evaluation of the effects of the carbon transfer rates on the radiocarbon concentration in the various reservoirs has been made. Relative to the hypothetical state in which the various mixing rates are infinitely faster than the radiocarbon decay rate, we find that the specific activity of C^{14} in the atmosphere is increased about 5 %, while the activity in the mixed layer is decreased by about 0.08 %, by an atmospheric residence time, relative to the sea, of 7 years. However, slow mixing between the mixed layer and the deep sea increases the activity in both the atmosphere and the mixed layer, relative to the rapidly mixed state, by 1.2 % for each 100 years of deep-sea residence time of carbon. Thus, if the residence time in the deep sea is assumed to be about 250 years, as several lines of evidence indicate, the total effects of the mixing rates on the reservoir concentrations are: an 8 % increase in the atmospheric activity, a 2.9 % increase in the mixed-layer activity, and a 0.2 % decrease in the activity in the deep sea, all relative to the activities which would be observed if the transfer of carbon were so rapid that there were no effects from the radioactivity.

The exchange time of CO_2 between atmosphere and sea was found by two methods which are quasi-independent. The first method depends on the cosmic-ray production rate of radiocarbon, as calculated by various workers, on the C^{14} concentration in the mixed layer of the sea, and on the steady-state material balance in the atmosphere. The second method considers the steady-state material balance in the mixed layer, and the mixed-layer C^{14} concentration as a function of the exchange time between the mixed layer and the deep sea. Both these methods yield an atmospheric residence time of CO_2, relative to entrance into the sea, of 7 ± 3 years, corresponding to a rate constant $k_{a-m} = 0.14$.

According to HUTCHINSON (1954) the flux of atmospheric CO_2 into the biosphere corresponds to about 3 % of the amount in the atmosphere per year. In our notation, with $\tau_{a-m} = 7$ years, and $\tau_{a-b} = 33$ years, the total residence time of a CO_2 molecule in the atmosphere is $\tau_{a-T} = 6$ years, after which it goes either into the sea (9 chances out of 11) or into the terrestrial biosphere (2 chances out of 11). Thus the carbon dioxide flux into the sea is about 4.5 times larger than the flux into the biosphere, and about 82 % of the CO_2 leaving the atmosphere goes into the sea, while only 18 % goes into the terrestrial plants. This ratio represents a considerable departure from previous estimates, and indicates that the spatial distribution of plants and soils is probably not the dominant factor in determining the steady-state CO_2 concentration in the atmosphere, contrary to what has been supposed (HUTCHINSON, 1954, p. 391). In fact it appears more likely that the spatial pattern of absorption and release of CO_2 by the sea, and the seasonal variations in this pattern, are the dominant factors.

If the residence time of CO_2 in the Northern hemisphere atmosphere is even a few years, then the rapid rate of transfer into the sea should produce an appreciable difference in the observed Suess effects in the Northern and Southern hemispheres, because of the much greater industrial concentration in the Northern hemisphere. Thus, if the Northern hemisphere residence time, relative to cross-hemisphere mixing, is from 2 to 5 years, the Southern hemisphere Suess effect should be from 75 to 50 %, respectively, of the effect observed in the Northern hemisphere. There is some indication that the Southern effect may in fact be only about half the Northern effect (SUESS, 1955), but a great many precise measurements will be needed to establish the exact nature of the effect. Nevertheless, it is clear that the rapid exchange of CO_2 with the sea will allow one to make rather close estimates of the cross-hemispheric exchanges; the precision with which this can be done is of course a direct function of the exchange rate with the sea.

Turning to the mixed layer in the sea, we see that τ_{m-a}, the residence time of CO_2 relative to entrance into the atmosphere, is equal to N_m/N_a times τ_{a-m}, and is thus 8.4 years, corresponding to $k_{m-a} = 0.12$. If the residence time in the deep sea, τ_{d-m}, is about 200 years, the residence time in the mixed layer, before transfer into the deep sea, is τ_{m-d} = about 4 years, corresponding to k_{m-d} about 0.25. The total residence time is then $\tau_{m-T} = 2.7$ years, after which a CO_2 molecule can go into the deep sea (2 chances out of 3), or into the atmosphere (1 chance out of 3). Thus with τ_{d-m} about 200 years, about $^2/_3$ of

the carbon cycled into and out of the mixed layer would exchange with the deep sea, and about $^1/_3$ with the atmosphere. The precise ratio depends of course on the actual residence time in the deep sea, but it is clear that for any reasonable mixing time of the deep sea, the exchange of the mixed layer is about equally proportioned between the atmosphere and the deep sea.

It should be emphasized that the indicated uncertainty in the atmospheric exchange time refers only to the rigorous model calculation; there is, of course, an additional uncertainty concerning the relationship of the model to the real physical situation. Our model does not exclude the existence of large horizontal gradients across the surfaces of the reservoirs, since we are dealing with steady-state average fluxes. However, the basic construction of the model assumes that the two reservoirs in the sea are each internally mixed over times comparable with their residence times, so that the material removed from each of these reservoirs has the average radiocarbon concentration of the reservoir as a whole.

Fortunately, the two methods of calculating τ_{a-m} depend on different assumptions. The calculation based on $\overline{Q}$ considers the material balance in the atmosphere only, and requires only that the CO_2 entering the atmosphere from the sea have the radiocarbon concentration corresponding to the measured activity of the mixed layer carbon; i.e. only a negligible amount of the CO_2 should be contributed directly from the deep sea to the atmosphere, without passing through the mixed layer first. Since the exchange of water between near-surface and deep waters takes place predominantly in high latitudes where the thermocline ceases to exist, there may well be some direct exchange of CO_2 between deep water and the atmosphere. On the other hand, inspection of equation (4) shows that decreasing R_m/R_a to correspond with *all* the CO_2 furnished to the atmosphere from a carbon source with an apparent age of 650 years relative to the atmosphere (i.e. $\tau_{d-m}=250$ years), increases the calculated value of τ_{a-m} to only 10 years. Since it is hardly likely that all the CO_2 released from the sea comes directly from the deep sea to the atmosphere, we conclude that the calculation of τ_{a-m} from $\overline{Q}$ cannot be significantly in error from the model assumption.

Our second calculation of τ_{a-m}, by equation (18) is more dependent on the actual model of oceanic mixing constructed; it assumes that the mixed layer is well mixed over times of the order of a few years, so that the bulk of the mixed layer has the same C^{14} concentration as the portions exchanging with the atmosphere and the deep sea, and that the deep sea is internally mixed over times of the order of the average reservoir life in the deep sea. The first assumption is fulfilled, for the mixed layer is known to mix by convection and wind action over times of the order of days. If the second assumption were not valid, the function F would be slightly changed because the C^{14} concentration in the carbon exchanged with the mixed layer would not represent the average reservoir concentration (as assumed in equation (6)). However, the very minor dependence of the value of τ_{a-m} on F was shown, and moreover, it seems not unlikely that in the mixing process by which exchange with the mixed layer is effected, the deep sea is itself mixed at least partially in a time equivalent to the residence time.

The close agreement of the two values of τ_{a-m}, based on the assumption that the deep-sea residence time is not more than several thousand years, indicates that the model approximates well enough the actual mixing conditions in the sea. The additional assumption of the steady state has of course also been made; from the close agreement between the historical ages and the radiocarbon dates on samples of known age, this assumption is clearly valid enough for our purposes. (For the most recent data on comparison of measured and historical ages, see LIBBY, 1955, p. 10.)

SUESS (1953) has attacked the problem of the atmosphere-sea exchange rate from an entirely different viewpoint, namely the dilution of the atmospheric radiocarbon activity by the dead CO_2 from the combustion of fossil fuels, as recorded in the tree rings of the last 100 years. His measurements indicated a "Suess effect", as we shall indicate it for convenience, of about 3 %, from which he deduced an atmospheric CO_2 residence time, relative to the sea, of 20—50 years. The integrated amount of "dead" CO_2 which has been produced by

human activity is equivalent to a constant production rate of 0.25 % of N_a for the past 40 years (REVELLE and SUESS, 1957), which is long enough for the atmosphere to have reached secular equilibrium (to a close enough approximation) with the production rate. Thus from our present figure of $\tau_{a-m} = 7$ years, the predicted Suess effect is 7×0.25 or 1.75 % dilution of the atmospheric radiocarbon activity.

More recent and extensive measurements by SUESS (1955) have shown that the observed effect is actually less than 3 %, and that effects of about 3 %, as previously observed, represent local effects in areas near industrial concentrations. As Revelle and Suess point out, the average figure obtained from the recent data of Suess turns out, by coincidence, to be 1.73 %. They reverse the present procedure, evaluating the atmospheric residence time from the Suess effect with a more detailed treatment than made previously by Suess, and conclude that, all things considered, the atmospheric CO_2 residence time is of the order of magnitude of 10 years relative to the sea. The close agreement of their value, obtained from considerations of the transient state and the measured changes in atmospheric radiocarbon activity over past decades, and the value found in this study of the steady-state distribution of C^{14}, is gratifying, and indicates that the factors governing the natural distribution of radiocarbon are now fairly well understood.

Some comment should be made on the differences between the treatment by REVELLE and SUESS (1957) and by the present writer. Their conclusions are based on a generalized evaluation of the interaction of all the following parameters: τ_{a-m}, the "apparent age" of surface ocean carbonate, and an "effective" sea reservoir, essentially as related by equation (18), an "effective" atmospheric reservoir (as a function of interaction with the biosphere and humus), and the Suess effect. The reason for the much larger uncertainty assigned to their estimate of τ_{a-m}, compared to the estimate of ± 3 years for the figure deduced in this paper, is twofold. First, their treatment involves the Suess effect, which, being very small, is not amenable to precise measurement, and moreover, is directly related to the interaction between atmosphere and biosphere. Thus given the exact magnitude of the Suess effect and the "apparent age" of surface sea carbon as fixed values, then e.g., if the CO_2 in the atmosphere is in rapid exchange with an equivalent amount of carbon in the biosphere, the value of τ_{a-m} deduced for no interaction is doubled. The amounts of carbon tied up in the biosphere and humus, and the rate and extent of their interaction with the atmosphere, are subject to order of magnitude uncertainty.

Secondly, they take the ocean as a single reservoir and deliberately refrain from attempting to construct a model of the sea to which physical significance must be attached. On the other hand, the model constructed for the present study is based on breaking the sea into two reservoirs, which correspond, more or less, to those actually observed in the sea. As was shown in the second calculation of the atmospheric residence time, the interaction of the deep sea with the atmosphere in the present model is so weak that a precise estimate of the atmospheric exchange time can be made, even though the internal mixing rate of the sea is not known to within several thousand years. In fact, the mixed layer of the sea functions as a buffer, both in nature and in the present model, serving to damp out almost completely the interaction between the atmosphere and the deep sea.

We turn, finally, to the question of the internal mixing rate in the sea, and to what one can say about this rate from the present knowledge of the distribution of radiocarbon. As pointed out in the previous section of this paper, the uncertainty in the production rate of C^{14} is consistent with deep-sea residence times up to about 2,500 years. Unfortunately, the Revelle-Suess analysis provides no closer estimate.

Revelle and Suess define an "effective sea reservoir", smaller than the actual amount of carbon in the sea because of incomplete mixing, but as noted above, do not attach a physical meaning to their definition. The reason for our discussion of the physical significance of the function F, in a previous section, is now apparent; this function is their "effective sea reservoir", and their ratio S^*/S, where S in our notation is N_s, the total amount of stable carbon in the sea, is simply the ratio F/F_0. Values of F and F/F_0 were tabulated as functions of the deep-sea residence time, τ_{d-m}, at the point where equations (18) and (19) were

introduced. Revelle and Suess find that the interaction of their various parameters is such that ratios of S^*/S as low as 70 % are acceptable, and from the tabulated values of F/F_0 given with (18), we see that τ_{d-m} could then be as long as about 3,000 years and still be consistent with their requirements. Even if the effective sea reservoir can be restricted to 90 % of N_s, the deep-sea residence time can still be 1,000 years.

There is, however, one way in which the mixing rate of the sea can be defined more closely, from the radiocarbon data, than the 0—3,000 range obtained by the two methods discussed above. As mentioned above, the atmosphere can be considered to be essentially in secular equilibrium with a flux of dead CO_2 amounting to a constant input of 0.25 % of N_a over the past 40 years. From the discussion of τ_{a-T} given above, it appears that about 80 % of the CO_2 leaving the atmosphere goes into the sea, and thus we can assume a flux of about 0.2 % of N_a into the sea of dead CO_2. We may then ask what the maximum dilution of the radiocarbon activity in the mixed layer can have been.

The difference between the expected and observed radiocarbon activity of the mixed layer, relative to 19th century wood corrected for age, appears to be about 5 % and probably cannot be more than 6 % (Suess, 1955). From the calculation based on $\bar{Q}$, equation (4), we found that τ_{a-m} is probably not less than 4 years; it is almost certainly not less than 3 years. These minimum figures for τ_{a-m} would account for 3 % and 2 %, respectively, of the observed 5 %, or maximum 6 %, mixed-layer effect, by virtue of the effect of the mixing rates on the atmospheric concentration, which was discussed in a previous section. Thus it appears that the maximum dilution of C^{14} activity the mixed layer can have suffered is most probably 2 %, and almost certainly not more than 4 %.

The forward mixing residence time in the mixed layer, τ_{m-d}, is found by dividing the percentage dilution by the percentage flux, assuming secular equilibrium (which is shown by the result to be valid enough). If τ_{a-m} is as low as 4 years, then actually 90 % of the atmospheric CO_2 goes into the sea, and the mixed layer carbon, N_m, is 1.2 times N_a, thus the dead CO_2 from industrial combustion has a flux rate through the mixed layer of approximately 0.2 % of N_m. Dividing the percentages given above, we find that τ_{m-d} is most probably not more than 10 years, and almost certainly not more than 20 years.

The residence time of a CO_2 molecule in the deep sea, τ_{d-m}, as given by (7) is about 50 times the residence time in the mixed layer before transfer to the deep sea. We thus find that τ_{d-m} is most probably not more than 500 years, and almost certainly not greater than 1,000 years.

The above statement on the mixing rate in the sea is the most precise limitation which can be put on the average mixing time in the sea by the present radiocarbon data. Direct measurements on deep waters should, of course, delineate the situation much more precisely. Nevertheless, it should be pointed out that measurements on 50 or 100 year old shells and seaweed to determine the Suess effect in the sea will give an independent check on the average mixing rates in the sea.

The detailed analysis of the steady-state distribution of a radioactive isotope is seen to be a powerful tool for the evaluation of rates of mixing in natural reservoirs. An analysis, similar to the present study of radiocarbon, has been made of the distribution of natural tritium in the atmosphere and the sea. The results indicate that the production rate of tritium from cosmic rays is probably five to seven times higher than the rates currently estimated by consideration of the cosmic-ray flux. Because of the short mean life of tritium (18 years), as contrasted with radiocarbon, a closer estimate of the internal mixing rate in the sea can be made from the steady-state distribution observed in the atmosp ere and the mixed layer. The tritium distribution was found to indicate a deep-sea residence time of about 200—300 years, as a world average. Details of the tritium study will be published shortly.

Acknowledgements

This paper represents in part the results of a general study of the use of natural isotopic effects in the analysis of mixing rates in the atmosphere and the sea, begun while the writer was a member of a National Academy of Sciences Study Group on applications of

nuclear phenomena to oceanography; some of the material presented here is included in the final report of that group. It will be obvious from the text that I am greatly indebted to Drs. Hans Suess and Roger Revelle for discussion of many aspects of the subject, and that this paper has benefited in many ways from their own contribution (1957) and from the extensive radiocarbon studies of Suess. The present work was not aimed at duplication of their study, which is mainly concerned with the problem of the possible increase in the atmospheric carbon dioxide, and the limits which can be placed on this effect by knowledge of the CO_2 exchange rate between atmosphere and sea. Rather, the purposes of the writer's investigation were, first, to evaluate, on as quantitative a level as possible, the general factors affecting the distribution of natural radiocarbon in its various reservoirs, and second, to determine precisely what could be said, from the radiocarbon distribution, about the mixing of this isotope into the deep sea, because of the importance of this aspect relative to the study of the distribution of natural tritium.

Drs. James Arnold and Ernest Anderson had made calculations similar to some of the ones presented here, and I thank them for a preprint of their paper received during the early stages of this study. The present considerations were carried out independently of their work and we have not discussed our differences. Their estimate of the atmospheric residence time, as here defined, of about 14 years is obtained by a material balance calculation, independent of $\bar{Q}$, but they do not give their method of calculation and it is difficult to determine how their calculation differs from the method given by equation (18) above. They assume the flux of CO_2 into the sea to be proportional to the sum of $N_a + N_b + N_h$ as used in this paper, treating these three units as one large reservoir, and they assume the radiocarbon concentration in the deep se[illegible] be given by Rubin's measurement, th[illegible] ing a figure of 250 years for τ_{a-m}. [illegible] they use a figure for the amount of the marine biosphere 80 times hig[illegible] maximum possible value estimated as an upper limit in the present study (see table 1); this essentially doubles the amount of carbon assumed to be in the mixed layer. (In the present study, the material balance for the mixed layer was derived in such a way that, as shown by (18), the calculated value of τ_{a-m} is decreased by only 2 % if the amount of carbon in the mixed layer is doubled.) It seems likely that our different results for τ_{a-m} are due to the interaction of these factors, and it is, in fact, gratifying, that with such serious differences in initial assumptions, the figures differ by no more than a factor of two.

Finally, I wish to thank Dr. Warren Wooster for extensive discussion of mixing phenomena in the sea, and for his efforts in examining the question of the average thermocline depth; and Dr. Meyer Rubin for the information on his radiocarbon measurements on deep-sea samples.

REFERENCES

Anderson, E. C., 1953: The production and distribution of natural radiocarbon. *Ann. Rev. Nuclear Science* **2**, pp. 63—78.

Craig, H., 1953: The geochemistry of the stable carbon isotopes. *Geochim. et Cosmochim. Acta* **3**, pp. 53—92.

Craig, H., 1954: Carbon 13 in plants and the relationships between carbon 13 and carbon 14 variations in nature. *Journ. Geol.* **62**, pp. 115—149.

Craig, H., 1957: Isotopic standards for carbon and oxygen and correction factors for mass spectrometric analysis of carbon dioxide. *Geochim. et Cosmochim. Acta* (in press).

Dingle, A. N., 1954: The carbon dioxide exchange between the North Atlantic Ocean and the atmosphere. *Tellus* **6**, pp. 342—350.

Goldschmidt, V. M., 1954: *Geochemistry* (A. Muir, ed.). Oxford: Clarendon Press, 730 pp.

Hutchinson, G. E., 1954: In *The Earth as a Planet* (G. Kuiper, ed.). Chicago: University of Chicago Press, Chapter 8.

Kouts, H. and Yuan, L., 1952: The production rate of cosmic-ray neutrons and C^{14}. *Phys. Rev.* **86**, pp. 128—129.

Ladenburg, R., 1952: The absorption rate of cosmic-ray neutrons producing C^{14} in the atmosphere. *Phys. Rev.* **86**, p. 128.

Libby, W. F., 1955: *Radiocarbon Dating*. 2nd edition, Chicago, University of Chicago Press, 175 pp.

Nier, A. O. and Gulbransen, E. A., 1939: Variations in the relative abundance of the carbon isotopes. *Journ. Am. Chem. Soc.* **61**, pp. 697—698.

Plass, G. N., 1956: Carbon dioxide theory of climatic change. *Tellus* **8**, pp. 140—154.

Rafter, T. A., 1955: C^{14} variations in nature and the

effect on radiocarbon dating. *N. Zealand Journ. Sci. Tech. B* **37**, pp. 20—38.

REVELLE, R. and MAXWELL, A. E., 1952: Heat flow through the floor of the eastern North Pacific Ocean. *Nature* **170**, p. 199.

REVELLE, R. and SUESS, H. E., 1957: Carbon dioxide exchange between atmosphere and ocean and the question of an increase of atmospheric CO_2 during the past decades. *Tellus* **9**, p. 18.

RILEY, G. A., STOMMEL, H., and BUMPUS, D. F., 1949: Quantitative ecology of the plankton of the western North Atlantic. *Bull. Bingham Ocean. Coll.* **12**, Art. [illegible].

[illegible] W., 1951: Geologic history of sea water. *Bull. Geol. Soc. Amer.* **62**, pp. 1111—1147.

[illegible] K., 1956: High-altitude cosmic-ray neutron intensity variations. *Phys. Rev.* **102**, pp. 1399—1409.

SUESS, H. E., 1953: Natural radiocarbon and the rate of exchange of carbon dioxide between the atmosphere and the sea. *Nuclear Processes in Geologic Settings*, National Academy of Sciences — National Research Council Publication, pp. 52—56,

SUESS, H. E., 1954: Natural radiocarbon measurements by acetylene counting. *Science* **120**, pp. 5—7.

SUESS, H. E., 1955: Radiocarbon concentration in modern wood. *Science* **122**, pp. 415—417.

SVERDRUP, H. U., JOHNSON, M. W., and FLEMING, R. H., 1942: *The Oceans*. New York: Prentice-Hall, Inc. 1087 pp.

WOOSTER, W. S. and KETCHUM, B. H., 1956: Transport and dispersal of radioactive elements in the sea. Final report, *National Academy of Sciences Committee on Effects of Atomic Radiation on Oceanography and Fisheries* (in press).

WORTHINGTON, L. V., 1954: A preliminary note on the time scale n North Atlantic circulation. *Deep-Sea Research* **1**, pp. 244—251.

Carbon Dioxide Exchange Between Atmosphere and Ocean and the Question of an Increase of Atmospheric CO_2 during the Past Decades

By ROGER REVELLE and HANS E. SUESS, Scripps Institution of Oceanography, University of California, La Jolla, California

(Manuscript received September 4, 1956)

Abstract

From a comparison of C^{14}/C^{12} and C^{13}/C^{12} ratios in wood and in marine material and from a slight decrease of the C^{14} concentration in terrestrial plants over the past 50 years it can be concluded that the average lifetime of a CO_2 molecule in the atmosphere before it is dissolved into the sea is of the order of 10 years. This means that most of the CO_2 released by artificial fuel combustion since the beginning of the industrial revolution must have been absorbed by the oceans. The increase of atmospheric CO_2 from this cause is at present small but may become significant during future decades if industrial fuel combustion continues to rise exponentially.

Present data on the total amount of CO_2 in the atmosphere, on the rates and mechanisms of exchange, and on possible fluctuations in terrestrial and marine organic carbon, are inadequate for accurate measurement of future changes in atmospheric CO_2. An opportunity exists during the International Geophysical Year to obtain much of the necessary information.

Introduction

In the middle of the 19th century appreciable amounts of carbon dioxide began to be added to the atmosphere through the combustion of fossil fuels. The rate of combustion has continually increased so that at the present time the annual increment from this source is nearly 0.4 % of the total atmospheric carbon dioxide. By 1960 the amount added during the past century will be more than 15 %.

Callendar (1938, 1940, 1949) believed that nearly all the carbon dioxide produced by fossil fuel combustion has remained in the atmosphere, and he suggested that the increase in atmospheric carbon dioxide may account for the observed slight rise of average temperature in northern latitudes during recent decades. He thus revived the hypothesis of T. C. Chamberlin (1899) and S. Arrhenius (1903) that climatic changes may be related to fluctuations in the carbon dioxide content of the air. These authors supposed that an increase of carbon dioxide in the upper atmosphere would lower the mean level of back radiation in the infrared and thereby increase the average temperature near the earth's surface.

Subsequently, other authors have questioned Callendar's conclusions on two grounds. First, comparison of measurements made in the 19th century and in recent years do not demonstrate that there has been a significant increase in

Contribution from the Scripps Institution of Oceanography, New Series, No. 900. This paper represents in part results of research carried out by the University of California under contract with the Office of Naval Research.

Table 1. CO_2 added to atmosphere by consumption of fossil fuels

Decade	Average amount added per decade Measured		Cumulative total added			
	10^{18} gms	% Atm CO_2	10^{18} gms	% Atm CO_2	10^{18} gms	% Atm CO_2
1860—69	0.0054	0.23	0.0054	0.23		
1870—79	0.0085	0.36	0.0139	0.59		
1880—89	0.0128	0.54	0.0267	1.13		
1890—99	0.0185	0.79	0.0452	1.92		
1900—09	0.0299	1.27	0.0751	3.19		
1910—19	0.0405	1.72	0.1156	4.91		
1920—29	0.0470	2.00	0.1626	6.91		
1930—39	0.0497	2.11	0.2123	9.02		
1940—49	0.0636	2.71	0.2759	11.73		
	Forecast					
	Assuming fossil fuels are used to meet future requirements of fuel and power as estimated by UN (1955)				Assuming fossil fuel consumption remains constant at estimated 1955 rate	
1950—59	0.091	3.9	0.367	15.6	0.367	15.6
1960—69	0.128	5.4	0.495	21.0	0.458	19.5
1970—79	0.176	7.5	0.671	28.5	0.549	23.4
1980—89	0.247	10.5	0.918	39.0	0.640	27.2
1990—99	0.340	14.5	1.258	53.5	0.731	31.1
2000—09	0.472	20.0	1.730	73.5	0.822	35.0

atmospheric CO_2 (SLOCUM, 1955; FONSELIUS *et al.* 1956). Most of the excess CO_2 from fuel combustion may have been transferred to the ocean, a possibility suggested by S. ARRHENIUS (1903). Second, a few percent increase in the CO_2 content of the air, even if it has occurred, might not produce an observable increase in average air temperature near the ground in the face of fluctuations due to other causes. So little is known about the thermodynamics of the atmosphere that it is not certain whether or how a change in infrared back radiation from the upper air would affect the temperature near the surface. Calculations by PLASS (1956) indicate that a 10 % increase in atmospheric carbon dioxide would increase the average temperature by 0.36° C. But, amplifying or feed-back processes may exist such that a slight change in the character of the back radiation might have a more pronounced effect. Possible examples are a decrease in albedo of the earth due to melting of ice caps or a rise in water vapor content of the atmosphere (with accompanying increased infrared absorption near the surface) due to increased evaporation with rising temperature.

During the next few decades the rate of combustion of fossil fuels will continue to increase, if the fuel and power requirements of our world-wide industrial civilization continue to rise exponentially, and if these needs are met only to a limited degree by development of atomic power. Estimates by the UN (1955) indicate that during the first decade of the 21st century fossil fuel combustion could produce an amount of carbon dioxide equal to 20 % of that now in the atmosphere (Table 1).[1] This is probably two orders of magnitude greater than the usual rate of carbon dioxide production from volcanoes, which on the average must be equal to the rate at which silicates are weathered to carbonates (Table 2). Thus human beings are now carrying out a large scale geophysical experiment of a kind that could not have happened in the past nor be reproduced in the future. Within a few centuries we are returning to the atmosphere and oceans the concentrated organic carbon stored in sedimentary rocks over hundreds of millions of years. This experiment, if adequately

[1] World production of CO_2 from the use of limestone for cement, fluxing stone and in other ways was about 1 % of the total from fossil fuel combustion in 1950.

documented, may yield a far-reaching insight into the processes determining weather and climate. It therefore becomes of prime importance to attempt to determine the way in which carbon dioxide is partitioned between the atmosphere, the oceans, the biosphere and the lithosphere.

The carbon dioxide content of the atmosphere and ocean is presumably regulated over geologic times by the tendency toward thermodynamic equilibrium between silicates and carbonates and their respective free acids, silica and carbon dioxide (UREY, 1952). The atmosphere contains and probably has contained during geologic times considerably more CO_2 than the equilibrium concentration (HUTCHINSON, 1954), although uncertainties in the thermodynamic data are too great for an accurate quantitative comparison. Equilibrium is approached through rock weathering and marine sedimentation. Estimated rates of these processes give a very long time constant of the order of magnitude of 100,000 years. Rapid changes in the amount of carbon dioxide produced by volcanoes, in the state of the biosphere, or as in our case, in the rate of combustion of fossil fuels, may therefore cause considerable departures from average conditions.

Table 2. Estimated present annual rates of some processes involving atmospheric and oceanic carbon dioxide, in part after HUTCHINSON (1954)

	10^{18} gms	In units of atm $CO_2(A_0)$
Consumption of fossil fuels—CO_2 produced.	0.0091	0.0039
Bicarbonate and carbonate added to ocean by rivers (as CO_2)[1] . .	0.00103	0.0004
Photosynthesis on land —CO_2 consumed	0.073 ± 0.018	0.031
Photosynthesis in ocean —CO_2 consumed	0.46 ± 0.3	0.20

[1] According to CONWAY (1942) and HUTCHINSON (1954) 87 % of the river borne bicarbonate and carbonate comes from weathering of carbonate rocks, the remainder from weathering of silicates.

The answer to the question whether or not the combustion of coal, petroleum and natural gas has increased the carbon dioxide concentration in the atmosphere depends in part upon the rate at which an excess amount of CO_2 in the atmosphere is absorbed by the oceans. The exchange rate of isotopically labeled CO_2 between atmosphere and ocean, which, in principle, could be deduced from C^{14} measurements, is not identical with the rate of absorption, but is related to it.

Notations and geochemical constants

In our discussion of exchange and absorption rates we shall use the following notations:

S_0: Total carbon of the marine carbon reservoir at equilibrium condition, at time zero.

A_0: Atmospheric CO_2 carbon at time zero.

i: Annual amount of industrial CO_2 added to the atmosphere.

t: Time in years.

$s = S_t - S_0$: Amount of CO_2 derived from industrial fuel combustion in the sea at time t.

$r = it - s$: Amount of CO_2 derived from industrial fuel combustion in the atmosphere at time t.

r^*: Observed decrease in C^{14} activity.

τ(atm): Average lifetime of a CO_2 molecule in the atmosphere, before it becomes dissolved in the sea.

τ(sea): Average lifetime of carbon in the sea, before it becomes atmospheric CO_2.

$k_1 = 1/\tau$(atm): Rate of CO_2 transfer per year from the atmosphere to the sea.

$k_2 = 1/\tau$(sea): Rate of CO_2 transfer per year from the sea to the atmosphere.

P_{CO_2}: Partial CO_2 pressure in the atmosphere.

Table 3 gives the amount of carbon, expressed in CO_2 equivalents, in the various geochemical reservoirs on the surface of the Earth.

The symbols S^* and A^* shall be used for denoting respective "effective" reservoirs.

Rate of CO_2 exchange between sea and atmosphere

Two types of C^{14} measurements independently allow calculation of the exchange rate

Table 3. Amount of carbon, computed as CO_2, in sedimentary rocks, hydrosphere, atmosphere and biosphere from data given by RUBEY (1951), HUTCHINSON (1954), and SVERDRUP et al. (1942)

	Total on Earth: 10^{18} gms	In units of A_0
Carbonate in sediments...	67,000	28,500
Organic carbon in sediments	25,000	10,600
CO_2 in the atmosphere (A_0)	2.35	1
Living matter on land[1]....	0.3	0.12
Dead organic matter on land.....	2.6	1.1
$CO_2+H_2CO_3$ in ocean[2]....	0.8	0.3
CO_2 as HCO_3^- in ocean[2]..	114.7	48.7
CO_2 as $CO_3^=$ in ocean[2]....	14.2	6.0
Total inorganic carbon in ocean.....	129.7	55.0
Dead organic matter in ocean.....	10	4.4
Living organic matter in ocean.....	0.03	0.01
Total carbon in ocean (S_0)	140	59.4

[1] Living organic matter on land estimated from assays of standing timber in the world's forests. 30 % of land surface is relatively thick forest, averaging about 5,000 board feet/acre of commercial size timber or 0.26 gm CO_2/cm^2 of forest. Assuming that total living matter in forests is twice the amount of timber, and that other components of the biosphere are $^1/_3$ of total gives 0.34×10^{18} gm CO_2 in land biosphere.

[2] Carbon dioxide components in sea water are assumed to be in equilibrium with a CO_2 partial pressure of 3×10^{-4} atmospheres; chlorinity: 20 ‰; temperature: 10° C; alkalinity: 2.46×10^{-3} meq/L. Under these conditions pH = 8.18. Volume of the Ocean = 1.37×10^{24} cm^3. This is probably an underestimate, because the water below the thermocline contains CO_2 produced by oxidation of organic matter, and the average temperature of the ocean is somewhat less than 10° C.

through the sea-air interface, if assumptions are made with respect to mixing rates of the water masses in the oceans: (*a*) the apparent C^{14} age of marine materials and (*b*) the effects of industrial coal combustion on the C^{14} concentration in the atmosphere (SUESS 1953). Experimental data on these two subjects are inadequate for rigorous quantitative interpretation but are sufficiently accurate to allow estimates of the order of magnitude of the rate constant for the exchange.

Considering the combined marine and atmospheric carbon reservoir as a closed system in equilibrium, the following relation holds by definition:

$$\frac{\tau\,(\text{sea})}{\tau\,(\text{atm})}=\frac{k_1}{k_2}=\frac{S_0}{A_0}\,. \qquad (1)$$

τ (sea), the average lifetime of a carbon atom as a member of the marine reservoir, is equal to the average apparent C^{14} age of marine material.

An apparent C^{14} age of marine material is obtained by comparison of the C^{14} activity with that of a wood standard corrected for isotopic fractionation effects in nature or in the laboratory by mass spectrometric measurement of the C^{13}/C^{12} ratios. In marine carbonate the C^{13}/C^{12} ratio is about 2.5 % higher than in land plants (NIER and GULBRANSEN, 1939 and CRAIG 1953, 1954). Because of the double mass difference the effect for C^{14} should be twice as large as that for C^{13}, if the isotopic distribution is established sufficiently rapidly so that radioactive decay of C^{14} can be neglected. If, after normalizing to equal C^{13}/C^{12} ratios, a lower C^{14} concentration is found than that of the wood standard, then this difference is attributed here to the effect of radioactivity, and is expressed as apparent age. A detailed study of the expected relationship between the isotopic fractionation factors for C^{13} and C^{14} in the bio-geochemical cycle of carbon has been made by CRAIG (1954).

Assuming from the then available C^{14} measurements that shell and wood have the same specific C^{14} activity, CRAIG (1954) attributed this unexpected result to slow transfer of CO_2 across the ocean-atmosphere interface resulting in a radiocarbon age of 400 years for surface ocean bicarbonate. Since then, more precise C^{14} measurements, supplemented by mass spectroscopic C^{13} determinations, have been published by SUESS (1954, 1955) and by RAFTER (1955) (see also HAYES ET AL., 1955). The standard error of about 0.5 % corresponds to an uncertainty in the age values of about 40 years. The apparent ages calculated from the published measurements are as follows:

Atlantic: (SUESS, 1954).

Mercenaria mercenaria Nantucket sound (from under 45 ft of water)	Shells	440 yrs.
	Flesh	540 yrs.
Sargassum weed from sea surface, 36°24′ N, 69°37′ W		320 yrs.

New Zealand area: (RAFTER, 1955).

Pauna Shells	350 yrs.
Limpet shells	360 yrs.
Cockle shells	280 yrs.
Pauna flesh	290 yrs.
Limpet flesh	140 yrs.
Seaweed	250 yrs.
Seawater (East Cape area)	370 yrs.

The average of the ages given here is 430 yrs. for the Atlantic samples and 290 yrs. for the New Zealand samples. The difference of 140 yrs. is due to the fact that the ages of the first group were calculated using wood grown in the 19th century as standard, whereas contemporaneous wood was used as standard for the New Zealand samples.[1]

Assuming that these apparent ages for marine surface materials are representative for the average age of marine carbon, or in other words, that mixing times of the oceans are short compared to the ages measured, an apparent age of about 400 years for marine carbon corresponds, according to Eq. (1), to an exchange time τ (atm) of about 7 years.

This *lower* limit for the exchange time of CO_2 between the atmosphere and the sea can now be compared with computations of this quantity from the observed effect of industrial fuel combustion on the specific C^{14} activity of wood. This second way, however, will lead to an *upper* limit for the exchange time if rapid mixing in the oceans is assumed.

At present 9.1×10^{15} grams of C^{14} free CO_2, or a fraction of 3.9×10^{-3} of the atmospheric CO_2, is added per year to the atmosphere by artificial burning of fossil fuels. The total amount added during the 100 years prior to 1950 corresponds to about 12 % of the atmospheric carbon reservoir.

Neglecting any effect of the industrial CO_2 on the rate constants k_1 and k_2 one obtains:

$$\frac{ds}{dt} = k_1 (it - s) - k_2 s \qquad (2)$$

and integrated:

$$s = it \frac{k_1}{k_1 + k_2} - i \frac{k_1}{(k_1 + k_2)^2} \left(1 - e^{-(k_1 + k_2)t}\right) \qquad (3)$$

[1] See FERGUSSON and RAFTER. These authors have now found that 110 years should be added to all of their previous age determinations to correct for the difference of the standards.

for the amount of industrial CO_2 in the sea at the time t. As $k_1 \approx 60\ k_2$, we may neglect k_2 as small compared to k_1. We then obtain:

$$s = it - \frac{i}{k_1} \left(1 - e^{-k_1 t}\right) \qquad (4)$$

or

$$r = it - s = \frac{i}{k_1} \left(1 - e^{-k_1 t}\right) \qquad (5)$$

Expressing i, s, and r in units of the atmospheric CO_2, we obtain with $i = 0.25$ % (corresponding to the value during the 1940's) and $t = 40$ years, the following values of r for exchange times τ (atm) $= \frac{1}{k_1}$ as listed:

Table 4

$1/k_1 = \tau$(atm) years	r %
5	1.2
10	2.5
20	4.4
30	5.5
40	6.3
100	8.3
∞	10.0

Empirical values for the decrease in the specific C^{14} activity r^* were obtained by comparing C^{14} activities of wood samples grown in the 19th century with those grown more recently, taking into account isotope fractionation effects by C^{13} measurements and correcting for the C^{14} decay by normalizing to equal age (SUESS 1955).

With the assumption that the total atmospheric carbon reservoir is only negligibly greater than the amount of CO_2 in the atmosphere, r^* will be equal to r.

Table 5

Tree	Years of growth from annual rings	r^* %
Spruce, Alaska.....	1945—1950	1.77
White Pine, Massachusetts	1936—1946	3.40
	1946—1953	2.90
Incense Cedar, California	1940—1944	1.85
	1950—1953	1.05
Cedrela, Peru	1943—1946	0.05
	1948—1953	1.05

It might be tempting to assume that the effects found in the samples investigated and their individual variations are due to local contamination of air masses by industrial CO_2 and that the world-wide decrease in the C^{14} activity of wood is practically zero. This, however, implies a too fast exchange rate and is inconsistent with the lower limit of τ (atm) given above. By coincidence, it so happens that taking the average of the r^* values listed, 1.73 %, an exchange time τ (atm) of 7 years is obtained as an upper limit, identical with the lower limit obtained previously from the C^{14} age of marine surface material. An exchange time of 7 years, however, makes it necessary to assume unexpectedly short mixing times for the ocean.[1]

By reconsidering the relative size of the marine and atmospheric carbon reservoirs, and the assumptions necessary for treating the combined reservoirs as a closed system, we may approximate more closely to the conditions prevailing in nature. First, it seems possible that some of the organic matter and carbonate present in soils may have to be added to the carbon that constitutes the atmospheric carbon reservoir. Practically nothing is known about the C^{14} age of soils and it may be that some of the soil carbon, partly through bacterial action, is in more rapid isotopic exchange with atmospheric CO_2 than the data on plant assimilation and biological oxidation indicate. The total amount of carbon in soils may be equal to, or larger by as much as a factor of two than that in the CO_2 of the atmosphere. Rapid exchange with such carbon would decrease the change in C^{14} activity resulting from industrial fuel combustion by a factor equal to the ratio of the total "effective" atmospheric carbon reservoir to the atmospheric CO_2. However, the overturn time of the atmospheric CO_2 through the terrestrial biological cycle and the soil is probably at least several decades and it therefore seems improbable that a mechanism exists that might account for an atmospheric reservoir of more than 1.5 times the CO_2 in the atmosphere.

Nevertheless, it is interesting, in order to demonstrate how the uncertainty in the size of the atmospheric carbon reservoir affects our results, to introduce "effective" reservoirs A^* and S^*, so that $A^* > A$, because of exchange with soil carbon, and $S^* < S$, because of incomplete mixing in the oceans. A^* and S^* are defined in such a way that Eq. (1) becomes

$$\frac{k_1}{k_2} = \frac{S^*}{A^*} \qquad (1\,a)$$

For Eq. (5):

$$r^* = \frac{A}{A^*}\,\frac{i}{k_1}\,(1 - e^{-k_1 t}) \qquad (5\,a)$$

is to be substituted.

Then the relationships of the three unknown quantities k_1, S^* and A^* according to the two equations (1 a) and (5 a) are shown graphically in figure 1.

With an average age of surface sea carbon of 400 years, i.e., $k_2 = 1/400$, one finds, even with an improbably large A^* equal to 3 A, that S^* is only 10 to 30 % smaller than S, so that the resulting mixing times of the oceans cannot be larger than a few 100 years.

The overturn time for the marine carbon through rock weathering and precipitation can be estimated to be of the order of 100,000 years (table 3). During an average lifetime of sea carbon of 400 years an amount corresponding to 0.3 % of the marine reservoir will be added to the oceans through rock weathering in the form of C^{14} free carbon and be precipitated after isotopic equilibration. On the average, this will cause the C^{14} age of sea carbon to appear about 35 years older. Locally, and especially along shores, the effect may well be considerably greater, so that the ages measured so far may, on the average, be too great by as much as 100 years. In figure 1, solutions are shown for $1/k_2 = 300$ years, indicating a value of S^*/S of about $^2/_3$ for acceptable values of A^*.[1]

A possibility that the addition of C^{14} free CO_2 to the atmosphere from volcanic eruptions in the 19th century may obscure the

[1] In a separate paper in this issue, H. Craig evaluates the exchange time by considering present data on the C-14 production rate by cosmic rays, and obtains a value of 7 ± 3 years. He further finds that a more detailed model of ocean mixing gives the same value. An earlier estimate of 20 to 50 years (Suess 1953) was based on C-14 measurements of woods grown in an area of industrial contamination.

[1] For a discussion of the physical significance of S^*/S in terms of mixing times in the ocean see H. Craig's paper in this issue.

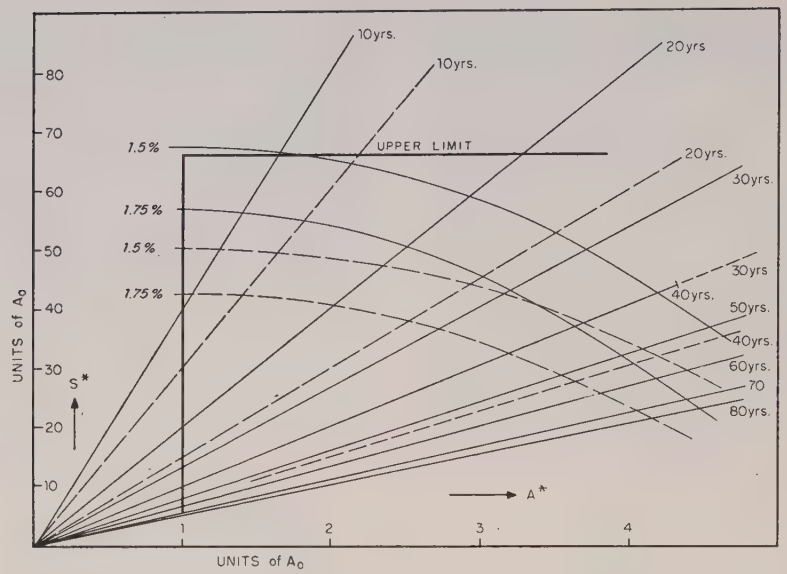

Fig. 1. Graphic solutions of Eq. (1 a) for values $1/k_1$ ranging from 10 to 80 years (straight lines), and of Eq. (5 a) for $r^* = 1.5$ % and 1.75 % (curved lines), for average apparent C^{14} age of sea water $1/k_2 = 400$ years (solid lines) and 300 years (broken lines). Points of intersection of straight lines and curves are possible solutions of the two equations for effective reservoirs A^* and S^*.

effect from industrial fuel combustion needs further experimental investigation.

We conclude that the exchange time τ (atm) = $= 1/k_1$, defined as the time it takes on the average for a CO_2 molecule as a member of the atmospheric carbon reservoir to be absorbed by the sea, is of the order of magnitude of 10 years. This corresponds to a net exchange rate of the order of 10^{-7} mol CO_2 per second and square meter of the ocean surface, larger by a factor of 100 than that postulated by PLASS (1956) and smaller by a factor of 10,000 than that deduced by DINGLE (1954) as a lower limit from numerical values of the various rate controlling constants. These are, as HUTCHINSON (1954) has forcefully pointed out, too uncertain to allow any definite conclusions. On the other hand, our exchange data give a value for the "invasion coefficient" of carbon dioxide close to that determined experimentally by BOHR (1899) for a stirred liquid surface.

Secular variation of CO_2 in the atmosphere

In the preceding section of this paper, two simplifying assumptions were made when estimating the exchange rate of CO_2 between the atmosphere and the oceans: (1) that the rate constants k_1 and k_2 were not affected by a small increase of the exchangeable carbon reservoir such as that from industrial fuel combustion, and (2) that, except for that increase, no other changes in the sizes of the oceanic and atmospheric carbon reservoirs have taken place. If these assumptions were rigorously correct, the increase in atmospheric CO_2 due to an addition of C^{14} free CO_2 would be nearly equal to r, as given by Eq. (5) and in table 4, and equal to the decrease in the specific C^{14} activity r^*, multiplied by a factor A^*/A.

Because of the peculiar buffer mechanism of sea water, however, the increase in the partial CO_2 pressure is about 10 times higher than the increase in the total CO_2 concentration of sea water when CO_2 is added and the alkalinity remains constant (BUCH, 1933, see also HARVEY, 1955), so that under equilibrium conditions at a given alkalinity

$$\frac{r}{A_0} = \frac{\gamma s}{S_0} \text{ or } \frac{A_0}{S_0} = \frac{k_1}{k_2} = \frac{r}{\gamma s},$$

γ being a numerical factor of the order of 10

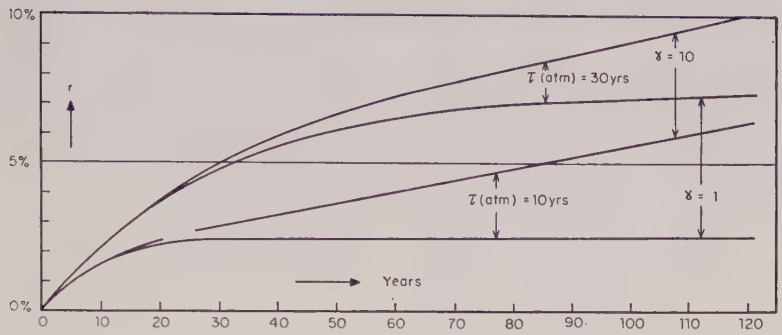

Fig. 2. Expected secular increase in the CO_2 concentration of air (r) according to Eq. (7), for average lifetimes of CO_2 in the atmosphere τ(atm) = 10 years and 30 years, with and without correction for the increase in the partial CO_2 pressure with total CO_2 concentration of sea water (curves for $\gamma = 10$ and $\gamma = 1$ respectively), for a constant rate of addition of industrial CO_2 of $i = 2.5 \cdot 10^{-3} \times A_0$.

for r and s small compared to A_0 and S_0 respectively.

As a reasonable approximation we may write instead of Eq. (3):

$$s = it\frac{k_1}{k_1+\gamma k_2} - i\frac{k_1}{(k_1+\gamma k_2)^2}\left(1 - e^{-(k_1+\gamma k_2)t}\right) \quad (6)$$

or

$$r = it\frac{\gamma k_2}{k_1+\gamma k_2} + i\frac{k_1}{(k_1+\gamma k_2)^2}\left(1 - e^{-(k_1+\gamma k_2)t}\right) \quad (7)$$

Figure 2 shows r as a function of time calculated from Eq. (7) for two values of k_1 corresponding to an exchange time of 10 and 30 years respectively, assuming constant addition of industrial CO_2 equal to 0.25 % of the CO_2 in the atmosphere per year. At present the integrated amount of industrial CO_2 corresponds to about 40 to 50 years of addition at this constant rate. The increase in CO_2 in the atmosphere plus biosphere and soil due to industrial fuel combustion should therefore at present amount to 3 to 6 %, depending on the assumptions made with respect to the size of the "effective" atmospheric carbon reservoir that exchanges with the ocean.

Eq. (7) and figure 2 show that addition of industrial CO_2 at a constant rate should eventually lead to a situation in which the secular increase in CO_2 in the atmosphere plus biosphere and soil equals $\frac{i\gamma k_2/k_1}{1+\gamma k_2/k_1}$ per year. With $S_0/A_0 = k_1/k_2 \approx 60$ and $i = 0.25$ an increase of 3.6 % per century is obtained. We have neglected the present rate of increase in alkalinity, which is small compared to the rate of CO_2 production from fossil fuels. However, over a sufficiently long period of time the alkalinity of the ocean must be expected to rise more rapidly as a consequence of the higher total CO_2 concentration in the atmosphere and ocean which will tend to increase the rate of rock weathering and to decrease the rate of deposition of $CaCO_3$. The secular increase in r should therefore be less than that calculated from Eq. (7) with $\gamma = 10$ and somewhere between the curves shown in figure 2 for $\gamma = 10$ and $\gamma = 1$.

It seems therefore quite improbable that an increase in the atmospheric CO_2 concentration of as much as 10 % could have been caused by industrial fuel combustion during the past century, as Callendar's statistical analyses indicate. It is possible, however, that such an increase could have taken place as the result of a combination with various other causes. The most obvious ones are the following:

1) Increase of the average ocean temperature of 1° C increases P_{CO_2} by about 7 %. However, such increase would also raise the sea level by about 60 cm, due to thermal expansion of the ocean water. Actually, according to MUNK and REVELLE (1952), although the sea level has risen about 10 cm during the last century, this rise can be accounted for almost quantitatively by addition of melt water from retreating glaciers and ice caps. The increase in the average ocean temperature is probably not more than 0.05° C, which corresponds to an increase in P_{CO_2} of 0.35 %. In the case of slow oceanic mixing, the increase could be somewhat larger, if only

the top layers of the sea were affected by a rise in temperature.

2) Decrease in the carbon content of soils: HUTCHINSON (1954) considers this the most probable additional cause of the Callendar effect. The increase in arable lands of about 4×10^{16} cm^2 since the middle of the 19th century has resulted in a corresponding decrease of forest land of about 10 %. Assuming that 70 % of all the soil carbon is in forests (probably a considerable over-estimate), and that cultivation reduced this by 50 %, the total decrease in soil carbon would correspond to 9×10^{16} gms of CO_2 which is 4 % of that in the atmosphere. At least four-fifths of this amount should have been transferred to the ocean.

3) Change in the amount of organic matter in the oceans. About 7 % of the marine carbon reservoir consists of organic material. The amount of organic matter must depend on the balance between the rates of reduction of CO_2 by photosynthesis and of production of CO_2 by oxidation. As pointed out previously, a change in the CO_2 content of sea water by a certain factor without a corresponding change in alkalinity changes P_{CO_2} by about 10 times this factor. Therefore a 1 % change in the concentration of organic material in the sea will change the partial CO_2 pressure and hence the atmospheric CO_2 by roughly 1 %. During the past 50 years, the increase in marine carbon from absorption of industrial CO_2 of about 0.2 % might have increased the rate of photosynthesis without a corresponding change in the rate of oxidation per unit mass of organic matter, and thus decreased P_{CO_2}. An increase in the temperature of surface water might have increased the rate of oxidation per unit mass of organic matter, and hence increased P_{CO_2}. We suspect that fluctuations in the amount of organic marine carbon might be an important cause for changes in the atmospheric CO_2 concentration.

ERIKSON and WELANDER (1956) have discussed a mathematical model of the carbon cycle between the atmosphere, the land biosphere and dead organic matter, and the ocean, in which it is assumed that the rate of input of carbon to the biosphere is directly proportional, not only to the total size of the biosphere but also to the amount of CO_2 in the atmosphere. Their estimate of the land biosphere is 7 times larger than that given in Table 3. They conclude that most of that part of the CO_2 added by fossil fuel consumption, which has not been absorbed by the ocean, has probably gone into the biosphere. Erikson and Welander's basic assumption that the amount of atmospheric carbon dioxide limits the growth of the terrestrial biosphere seems highly unlikely, in view of the fact that the principal photosynthetic production on land is in forests, where a deficiency of plant nutrients might be expected. In any case as HUTCHINSON (1954) has shown, the amount of carbon in the biosphere and soil humus has probably decreased, rather than increased, during the past century, because of the clearing of forests.

In contemplating the probably large increase in CO_2 production by fossil fuel combustion in coming decades we conclude that a total increase of 20 to 40 % in atmospheric CO_2 can be anticipated. This should certainly be adequate to allow a determination of the effects, if any, of changes in atmospheric carbon dioxide on weather and climate throughout the earth.

Present data on the total amount of CO_2 in the atmosphere, on the rates and mechanisms of CO_2 exchange between the sea and the air and between the air and the soils, and on possible fluctuations in marine organic carbon, are insufficient to give an accurate base line for measurement of future changes in atmospheric CO_2. An opportunity exists during the International Geophysical Year to obtain much of the necessary information.

Acknowledgements

A paper on the same subject by James R. Arnold and Ernest C. Anderson appears in this issue of this journal; we are grateful to Drs. Arnold and Anderson for the opportunity of discussing the problem before publication. We are happy to note that these authors have simultaneously and independently derived essentially the same conclusions as presented in this paper. We hope that the somewhat different approach will make both contributions equally valuable to the reader. We also wish to thank Dr. Carl Eckart for valuable discussions and Dr. Harmon Craig for much constructive criticism. Dr. Craig's own careful analysis of the subject appears in a separate paper in this issue.

REFERENCES

Arrhenius, Svante, 1903: *Lehrbuch der kosmischen Physik* **2**. Leipzig: Hirzel.

Bohr, C., 1899: Die Löslichkeit von Gasen in Flüssigkeiten. *Ann. d. Phys.* **68**, p. 500.

Buch, K., 1933: Der Borsäuregehalt des Meerwassers und seine Bedeutung bei der Berechnung des Kohlensäuresystems. *Rapp. Cons. Explor. Mer.* **85**, p. 71.

Callendar, G. S., 1938: The artificial production of carbon dioxide and its influence on temperature. *Quarterly Journ. Royal Meteorol. Soc.* **64**, p. 223.

Callendar, G. S., 1940: Variations in the amount of carbon dioxide in different air currents. *Quarterly Journ. Royal Meteorol. Soc.* **66**, p. 395.

Callendar, G. S., 1949: Can carbon dioxide influence climate? *Weather* **4**, p. 310.

Chamberlin, T. C., 1899: An attempt to frame a working hypothesis of the cause of glacial periods on an atmospheric basis. *J. of Geology* **7**, pp. 575, 667, 751.

Conway, E. J., 1942: Mean geochemical data in relation to oceanic evolution. *Proc. Roy. Irish Acad., B.* **48**, p. 119.

Craig, H., 1953: The geochemistry of the stable carbon isotopes. *Geochim. et Cosmochim. Acta* **3**, p. 53.

Craig, H., 1954: Carbon 13 in plants and the relationship between carbon 13 and carbon 14 variations in nature. *Journ. Geol.* **62**, p. 115.

Dingle, H. N., 1954: The carbon dioxide exchange between the North Atlantic Ocean and the atmosphere. *Tellus* **6**, p. 342.

Erikson, E., and Welander, P., 1956: On a mathematical model of the carbon cycle in nature. *Tellus* **8**, p. 155.

Fergusson, G. J., and Rafter, T. A.: *New Zealand C-14 Age Measurements III.* In press.

Fonselius, S., Koroleff, F., and Wärme, K., 1956: Carbon dioxide variations in the atmosphere. *Tellus* **8**, p. 176.

Harvey, H. W., 1955: *The Chemistry and Fertility of Sea Water.* Cambridge: University Press.

Hayes, F. N., Anderson, E. C., and Arnold, J. R., 1955: Liquid scintillation counting of natural radiocarbon. *Proc. of the International Conference on Peaceful Uses of Atomic Energy, Geneva,* **14**, p. 188.

Hutchinson, G. E., 1954: In *The Earth as a Planet,* G. Kuiper, ed. Chicago: University Press. Chapter 8.

Munk, W., and Revelle, R., 1952: Sea level and the rotation of the earth. *Am. Journ. Sci.* **250**, p. 829.

Nier, A. O., and Gulbransen, E. A., 1939: Variations in the relative abundance of the carbon isotopes. *Journ. Am. Chem. Soc.* **61**, p. 697.

Plass, G. N., 1956: Carbon dioxide theory of climatic change. *Tellus* **8**, p. 140.

Rafter, T. A., 1955: C^{14} variations in nature and the effect on radiocarbon dating. *New Zealand Journ. Sci. Tech. B.* **37**, p. 20.

Rubey, W. W., 1951: Geologic history of sea water. *Bull. Geol. Soc. Amer.* **62**, p. 1111.

Slocum, Giles, 1955: Has the amount of carbon dioxide in the atmosphere changed significantly since the beginning of the twentieth century? *Monthly Weather Rev.* Oct., p. 225.

Suess, H. E., 1953: Natural Radiocarbon and the rate of exchange of carbon dioxide between the atmosphere and the sea. *Nuclear Processes in Geologic Settings,* National Academy of Sciences — National Research Council Publication, pp. 52—56.

Suess, H. E., 1954: Natural radiocarbon measurements by acetylene counting. *Science* **120**, p. 5.

Suess, H. E., 1955: Radiocarbon concentration in modern wood. *Science* **122**, p. 415.

Sverdrup, H. U., Johnson, M. W., and Fleming, R. H., 1942: *The Oceans.* New York: Prentice-Hall, Inc.

United Nations, 1955: World requirements of energy, 1975—2000. *International Conference on Peaceful Uses of Atomic Energy, Geneva,* **1**, p. 3.

Urey, H. C., 1952: *The Planets.* New Haven: Yale Univ. Press.

The Distribution of Carbon-14 in Nature

By JAMES R. ARNOLD, Department of Chemistry, Princeton University, Princeton, N.J., and ERNEST C. ANDERSON, Los Alamos Scientific Laboratory, University of California, Los Alamos, New Mexico

(Manuscript received September 4, 1956)

Abstract

The carbon-14 activity of oceanic materials indicates that the mixing half-time for carbon between the atmosphere and ocean surface waters is one or two decades, while the turnover time for the ocean as a whole is several hundred years. This conclusion is consistent with estimates based on the measured decrease in carbon-14 specific activity of wood grown in recent years compared with 19th century wood.

1. Introduction

Early studies on the distribution of carbon-14 in diverse samples of living matter (ANDERSON and LIBBY, 1951) indicated the essential constancy of the activity (or concentration) of carbon-14 in the carbon of these materials. It was postulated that the specific activity is constant except for the effect of isotopic fractionation throughout what is now called the "exchange reservoir", consisting of the atmosphere, living matter (biosphere), and the seas. (The C-13/C-12 ratio permits accurate correction for the fractionation effect which can amount to as much as 6 % between materials such as wood and carbonate ion.)

Two small deviations from this state of affairs are now known to occur:

1) Age of the oceans. Measurements seem to show that the specific activity of surface ocean water is lower by perhaps 4 to 8 % than its equilibrium value if mixing with the atmosphere were rapid. The deeper water seems to be even older.

2) The Suess effect (SUESS, 1955). Twentieth century wood shows a lower specific activity than expected from earlier samples. This is ascribed to the rapidly increasing rate of combustion of fossil fuels. The resulting inert carbon dioxide dilutes the radioactivity of the carbon with which it mixes.

We propose to use these two effects, which are to be regarded as minor nuisances in radiocarbon dating work, as indicators of the rates of mixing of various parts of the exchange reservoir. In addition, we will employ our knowledge of the rate of production Q and of the absolute specific activity of carbon-14 to set certain important limits.

We shall be forced to simplify the complex situation in order to make practical calculations. As a result of this and the uncertainties in the data the computed mixing times must be regarded as rough approximations.

The data we shall employ are given in Table I. The quantities of carbon in various parts of the reservoir shown in column two are taken from LIBBY (1955), with the addition of 0.2 g/cm^2 for humus, and a partially compensating lowering of the "biosphere" component. In column three are given the values increased by a factor of 1.05 for the atmosphere and 1.06 for ocean "carbonate", an artificial device which takes into account isotopic fractionation for purposes of our model calculations. The

Table I. Assumed size and specific activity of the components of the exchange reservoir

	Carbon content g/cm^{-2}	Carbon content (corr. for fractionation)	Relative specific activity (corr. for fractionation)
Atmosphere.....	0.12	0.13	1.00
Biosphere.....	0.21	0.21	
Land.....	0.05	0.05	1.00
Ocean.....	0.16	0.16	0.960
Ocean, dissolved organic.....	0.6	0.6	0.928
In top 100 metres	0.02	0.02	0.960
Humus.....	0.2	0.2	1.00
Ocean carbonate.	7.25	7.7	0.928
In top 100 meters	0.2	0.2	0.960

relative specific activities for average oceanic materials are estimates from the data of RUBIN (1956). Other measurements are available. It is assumed that humus and dissolved organic matter are in fairly rapid equilibrium with the local life.

It should be stressed that these numbers are all more or less inaccurate, and may not even represent the best values available currently. The conclusions we shall draw from our model calculations will not depend at all strongly on the numbers used.

2. Models

The simplest useful model which we can make of the mixing process divides the exchange reservoir into two parts whose boundary is the ocean surface. The upper reservoir A is taken to include the atmosphere, land-life and humus, or a total of 0.38 g/cm^2. Reservoir C contains ocean "carbonate", the remainder of the living matter and dissolved organic carbon, a total of 8.5 g/cm^2.

Consider the transfer of ordinary carbon and of carbon-14 from one reservoir to the other. We have for the equilibrium $A \underset{k_{-1}}{\overset{k_1}{\rightleftharpoons}} C$, a pair of first order rate constants related to the half-times for mixing by the definition $t_{1/2} = 0.693/k$. Exchange of normal carbon between the two reservoirs, in steady state, leads to two equations:

$$\left.\begin{aligned} \frac{dn_A}{dt} = 0 = -k_1 n_A + k_{-1} n_c \\ \frac{dn_c}{dt} = 0 = k_1 n_A - k_{-1} n_c \end{aligned}\right\} \quad (1)$$

The second equation is redundant. For the C-14 distribution there is again a pair of equations, one of which is redundant. For reservoir A:

$$\frac{df_A}{dt} = 0 = \lambda(f_A + f_c) - \lambda f_A - k_1 f_A + k_{-1} f_c \quad (2)$$

In these equations n_A is the quantity of normal carbon in gm per cm^2 in reservoir A, and f_A the quantity of C-14, the latter in arbitrary units. λ is the decay constant of C-14, 1.25 × × 10^{-4}yr^{-1}. Equation 1 serves to define the ratio k_{-1}/k_1; equation 2 gives us the individual values if the quantities n, f, λ are given. Calculations for more complex models follow the same form.

In the ocean there is a rather striking difference between a surface layer which is well mixed both vertically and horizontally by thermal convection and wind action, and middle and deep waters of nearly uniform temperature and slow circulation. To approximate the effect of such a division a second model has been constructed in which a surface sea layer B appears. In this model, $A \underset{k_{-1}}{\overset{k_1}{\rightleftharpoons}} B \underset{k_{-2}}{\overset{k_2}{\rightleftharpoons}} C$. Reservoir A remains as before and reservoir B is taken to represent the ocean to a depth of 100 meters, approximately the level of the thermocline. It is assumed that reservoir B contains all the ocean life and that dissolved organic matter is uniformly mixed through the sea.

The results, shown in Table II, indicate that the mixing times depend on reservoir size, on the model used, and on the choice of C^{14} data. At the same time the orders of magnitude are fixed within rather narrow limits. In the second model, the reverse mixing times of 12 and 250 years may seem too short to account for the 600-yr age of C corresponding to a specific activity of 0.926. It must be remembered that the 10-yr half-time for B to A is the time to cycle half of the 0.38 g/cm^{-2} reservoir B through A. Since C is 20 times as large as B, the half-time of cycling the mass of C from B to A is 20 × 10 or 200 yr. This combined

Table II. Mixing times for several reservoir models

System	Reservoir	Carbon Content[1] g cm^{-2}	Specific Activity[2]	Total C^{14} Content	Mixing half-time, years	
					Forward	Reverse
AC	A	0.38	1	0.38	20	440
	C	8.46	0.928	7.85		
ABC	A	0.38	1	0.38	10	10
	B	0.38	0.965	0.367	12	250
	C	8.08	0.926	7.48		
ACD	A	0.38	1	0.38	13	290
	C	8.46	0.928	7.85		
	D	large	small	3.0	15,000	...

[1] corrected for isotopic fractionation.
[2] relative to reservoir A.

with the 250-yr $t_{1/2}$ for $C-B$ is sufficient to give the required 600-yr average life ($=416$ yr $t_{1/2}$).

Several other models, breaking up reservoirs A and C into sub-reservoirs in different ways, have been used to calculate mixing times. The results are essentially similar to those given above.

The "age" of the sea might be explained by another hypothesis, namely, that carbon of low or zero activity in the underlying sediments might be redissolving at an appreciable rate and diluting this reservoir. The preservation of the isotopic gradients in ocean bottom cores excludes the possibility of large-scale chemical exchange between sediments and sea, but gross solution and redeposition in different regions are still possible. To demonstrate the consequences of such an effect, we have set up a model in which $A \underset{k_{-1}}{\overset{k_1}{\rightleftharpoons}} C \underset{k_{-2}}{\overset{k_2}{\rightleftharpoons}} D$(sediments). Here reservoirs A and C are as in the first model. The size of reservoir D is indeterminate, since we cannot estimate the quantity of sediments available for solution. If this is large compared with the size of reservoir C, however, so that the specific activity of sediment carbon remains low, only the total amount of C^{14} in reservoir D is important.

An upper limit to this quantity can be given based on our knowledge of the C^{14} production rate Q, as compared with the known specific activity of carbon in reservoir A. In steady state the production rate of C^{14} is equal to its disintegration rate, and the existence of a steady state is implied by the success of the C^{14} dating method. The decay rate is about 15 min^{-1} g^{-1} in reservoir A (Suess, 1955). The disintegration rate Q is then 2.0 sec^{-1} cm^{-2} if all the C^{14} is in A and C. A rough upper limit for Q from the cosmic ray neutron flux is 2.6 sec^{-1} cm^{-2}. If recent measurements of Soberman (1955) are correct, the value is much lower. Thus, at most 0.6 sec^{-1} cm^{-2} or about 30 % of the C^{14} inventory might be in D. Using this number we compute the ACD mixing times shown in Table II. It is clear that the mixing times between A and C are not much affected by the existence of reservoir D. In fact, in order to decrease these mixing times by an order of magnitude, an order of magnitude increase in Q would be necessary. This is, of course, entirely excluded by the cosmic ray data.

3. Fossil fuel

The effect of fossil fuel consumption on the CO_2 content of the atmosphere has been considered by a number of writers (Callendar, 1940; Buch, 1942, 1948; Stepanova, 1952; Suess, 1953). Production of CO_2 by this process has reached truly geochemical proportions and the rate of introduction of "new" (i.e., "old") carbon into the exchange reservoir by fuel consumption seems to exceed the natural production rate of juvenile carbon by two orders of magnitude. As long ago as 1919 Krogh (1919) was able to show that local increases in the CO_2 of the air of Copenhagen were due to combustion processes by measuring the concomitant decrease of O_2 and the respiratory quotient. The quantitative effect of this fossil CO_2 on the C^{14} assay depends strongly on the rates of mixing of the several components of the exchange reservoir. The total amount of dead C added to the atmosphere since 1900 amounts to 0.016 g cm^{-2}. The rate of production of fossil CO_2 has been exponential with a half-time of 17 yr up to 1910 and about 40 yr since then. If all this were to remain in the atmosphere, it would lead to a world-wide depression of the C^{14} assay of atmospheric CO_2 of about 12 %. If it mixed with the atmosphere, land-life and humus,

the depression would be 4 %. If diluted with the entire exchange reservoir, the effect would be only 0.2 %.

Because the CO_2 of the atmosphere appears to have increased by some 10 % since 1900, it has been postulated by CALLENDAR (1940) that the fossil fuel CO_2 has indeed remained in the atmosphere so that the atmosphere-sea and atmosphere-biosphere mixing times must be long compared with 50 yr. The observed level of the SUESS effect is very difficult to reconcile with CALLENDAR's hypothesis. While local depressions of the assay of up to 4 % are observed, the world-wide depression must be of the order of 1 %. In order for 0.016 g/cm^{-2} of inert carbon to produce this small reduction in the assay, it must be exchanged with at least reservoirs *A* and *B*. On the basis of the detailed analysis of the sea-water-air equilibrium by BUCH *et al.* (1932), one can compute that a given per cent increase in the CO_2 partial pressure in the air results in a 10-fold smaller per cent increase in total CO_2 concentration of the sea (this was called to our attention by R. REVELLE). The entire reservoir *B* is, therefore, available for specific activity reduction by exchange while in terms of actual removal of CO_2 from the air, it is only $^1/_{10}$ as effective. Putting in these numbers one finds that a specific activity reduction of 0.016/0.76 = = 2.1 % is predicted, which is not much too high, along with an increase in partial pressure of 0.016/0.42 = 3.8 %. This is a factor of three too small to account for the observed increase in atmospheric CO_2.

One can make the numbers fit by assuming the land biosphere to be very small or to mix very slowly. In this case the predicted SUESS effect for *A* and *B* is 0.016/0.50 = 3.2 % and the atmosphere concentration increase is 9 % in good agreement with some of the local results in the northern hemisphere. However, the southern hemisphere numbers seem to show no SUESS effect as large as 1 % and since inter-hemisphere atmospheric mixing is probably rapid, this indicates the large SUESS effects to be purely local phenomena. One is, therefore, compelled to return to something like the first formulation, in which case CALLENDAR's explanation of atmospheric CO_2 increase cannot be maintained.

The reason for the increase in atmospheric CO_2 remains obscure. HUTCHINSON (1954) has suggested an agricultural origin for the excess. Another possibility is the effect of the increase in temperature of the oceans during the past 50 yr which may have displaced the complex dynamic equilibrium between CO_2 in the sea and the air.

The data used in the calculation of the SUESS effect are those previously reported by SUESS (1955) and ARNOLD (HAYES, ANDERSON, and ARNOLD, 1955). Samples were tree-ring sections from selected localities. The C^{14} activity and the C^{13} content were determined and the C^{14} values corrected for age and for isotopic fractionation. The results are summarized in Figure 1. The Wisconsin and Massachusetts trees are assumed to represent local conditions near industrial centers; the Yosemite and Alaska trees perhaps represent a non-industrial northern hemisphere average; and the Peruvian tree (analyzed by both investigators) the southern hemisphere.

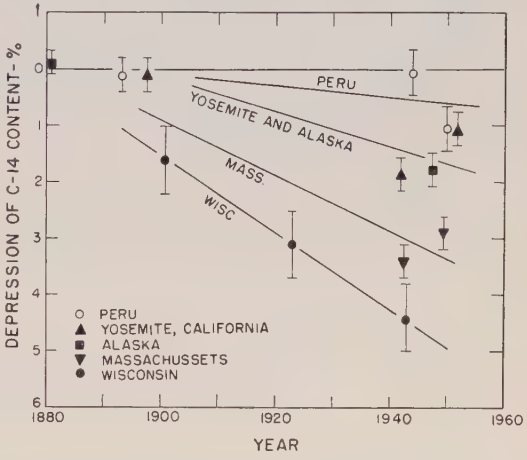

Fig. 1. Decrease in C^{14} assay of wood in the twentieth century. Activity corrected for radioactive decay. Data from SUESS (1955) and HAYES, ANDERSON and ARNOLD (1955).

Because the effect is so small and the number of samples so limited, no quantitative estimate of mixing times can be derived from these results, but comparison of orders of magnitude with the model is possible. The 4 % depression near industrial centers is reasonable in terms of known total fossil fuel consumption. If Yosemite and Alaska are indeed representative of the general northern hemisphere effect, then dilution with a reservoir 2 to 3 times the size of *A* is indicated, requiring mixing with a total

of 1.0—1.5 g/cm² C on a time-scale of the order of 20 yr. It is gratifying to note that these quantities are close to those obtained in the *ABC* model based on the ocean "age". *A* and *B* together contain about 0.8 g/cm⁻² with a mixing time of 10 yr and the short turnover of *B* through *C* (12 yr) in effect enlarges the "dilution capacity" of *B*.

The interpretation of the southern hemisphere Suess effect is less clear. If the time for ocean mixing is indeed years and if inter-hemisphere atmospheric mixing time is short compared to inter-reservoir mixing times, then the average Suess effect in the southern hemisphere should be comparable to that in the northern hemisphere. The limited data so far available seem to indicate that this is not so. The southern Suess effect appears to be less than 0.5 % if indeed it is not zero. More data are needed to clarify this situation.

4. Conclusions

The discussion based on the carbon-14 activity of marine samples has indicated that the mixing half-time for carbon between the atmosphere and ocean surface water is perhaps one or two decades, while the turnover time for the ocean as a whole is several hundred years. This conclusion is consistent with the data on the Suess effect, which would tend if anything to favor the lower values. As more reliable data are accumulated, and as the analysis are made more detailed, these figures will doubtless change. However, their order of magnitude seems reasonably well defined at the present time.

Acknowledgements

We wish to thank Dr. Hans E. Suess and Dr. Roger Revelle for the opportunity to discuss these matters with them before publication. We are indebted also to Dr. Meyer Rubin for his data on the activity of some ocean samples. One of us (J.R.A.) acknowledges generous support by the Office of Ordnance Research. U. S. Army. Part of this work was done under the auspices of the Atomic Energy Commission.

REFERENCES

Anderson, E. C., and Libby, W. F., 1951: World-wide distribution of natural radiocarbon. *Phys. Rev.* **81**, p. 64.

Buch, K., 1942: Kohlensäure in Atmosphäre und Meer. *Ann. d. Hydr.* **70**, p. 193.

Buch, K., 1948: Der Kohlendioxydgehalt der Luft als Indikator der meteorologischen Luftqualität. *Geophysica* **3**, p. 63.

Buch, K., Harvey, H. W., Wattenberg, H., and Gripenberg, S., 1932: Über das Kohlensäuresystem in Meerwasser. *Conseil. Perm. Explor. Mer. Rapp. Proc.-Verb.* **79**, p. 1.

Callendar, G. S., 1940: Variations of the amount of carbon dioxide in different air currents. *Quart. J. Royal Meteorological Soc.* **66**, p. 395.

Hayes, F. N., Anderson, E. C., and Arnold, J. R., 1955: Liquid scintillation counting of natural radiocarbon. *Proc. of the International Conf. in Geneva, August 1955, Vol.* **14**, p. 188.

Hutchinson, G. E., 1954: *The Earth as a Planet*, Gerard P. Kuiper, ed., University of Chicago, 1954, Chapter 8.

Krogh, A., 1919: The compositions of the atmosphere. *Dan. Mat. Fys. Medd.* **1**, No. 12.

Libby, W. F., 1955: Radiocarbon dating (Second Edition). *University of Chicago Press.*

Rubin, M., 1956: Personal communication.

Soberman, R. K., Beiser, A., and Korff, S. A., 1955: Variation of position of cosmic-ray neutron intensity maximum with geometric latitude. *Physical Review* **99**, p. 608.

Stepanova, N. A., 1952: A selective annotated bibliography on carbon dioxide in the atmosphere. *Meteorological Abstracts* **3**, p. 137.

Suess, H. E., 1953: Natural radiocarbon and the rate of exchange of carbon dioxide between the atmosphere and the sea. *Nuclear Processes in Geologic Settings*, National Research Council, Wastington, p. 52.

Suess, H. E., 1955: Radiocarbon concentration in modern wood. *Science* **122**, p. 415.

Trade Cumulus Cloud Groups: Some Observations Suggesting a Mechanism of Their Origin[1]

By JOANNE STARR MALKUS. Woods Hole Oceanographic Institution

(Manuscript received June 18, 1956)

Abstract

On a recent field trip to the western Caribbean, temperature gradients in the surface layers of the trade-wind oceans were found and related to the presence of cumulus cloud groups. The cloud groups generally formed over and slightly downwind of warm spots which were several kilometers in extent along the wind and 0.1—0.3° C in amplitude. Clouds were not found in the absence of warm spots although warm spots were occasionally encountered without clouds.

Air circulations, similar to but weaker than those produced by heated land masses, are hypothesized to exist over oceanic warm spots and their magnitude is estimated from previous work on heated islands. Observed differences in low-level moisture structure between clear and cloudy areas may be interpreted in terms of such circulations and their evolution with time. Some suggestions are made concerning the life cycles of trade cumuli.

I. Introduction

Oceanic trade cumulus commonly appear in irregular groups about 10—50 km across separated by somewhat wider clear spaces. Cloud grouping and structure do not seem to vary from day to night. Early observations showed that individual trade cumuli do not have "roots" in thermals extending up from the sea surface, nor are they observed in regular patterns suggesting polygonal convection cells. In fact, these two possibilities of their origin are excluded because the air layer below cloud is actually slightly stable at all elevations above the first few meters.

Time-lapse motion pictures suggest that trade-wind clouds almost always form in groups, and that the groups themselves go through a life cycle, beginning their existence as a large number of small cloudlets, a considerable fraction of which may later attain the precipitation stage together. Isolated swelling cumulus or shower clouds are exceptional. In view of the probable importance of large precipitating cloud areas in the initiation of tropical storms and of the interaction of cloud elements with one another to form larger clouds, we have become concerned with the original formation of these groups. We wish to ask what processes are at work below cloud to permit large numbers of moist air parcels simultaneously to reach the condensation level in particular localities.

The base of trade-wind clouds averages about 650 meters, with extreme variations ranging between 300 and 1,000 m. The lowest four-fifths of this subcloud layer is well mixed, with a temperature lapse rate about 0.9 adiabatic and a very slow vertical decay of mixing ratio (about 10^{-8} cm^{-1} or less). The upper 100—200 m is usually more stable, with a mean potential temperature increase of 1° C and an order of magnitude increase in moisture

[1] Contribution No. 843 from theWoods Hole Oceanographic Institution.

lapse rate. The stable layer is more pronounced in the clear regions than in those topped by clouds, where it is often absent altogether. On the average in clear areas the top of the mixed layer is at about 85 % of the height of the lifting condensation level of the air composing it, while in cloudy areas the mixed region reaches to 95—100 % of the L.C.L. or 75 m higher. These figures suggest that the origin of trade cumulus groups is to be sought in factors producing weak convergences on the 10—50 km horizontal scale in the subcloud layer. Small variations in one or more sea surface properties such as roughness, radiative character, temperature, or evaporation might suffice to set up such circulations; in particular it seemed desirable to determine whether or not slight differences in sea surface temperature (below the sensitivity of standard oceanographic instruments) might not be common and perhaps associated with cloud groups.

The latter suggestion arose from theoretical and observational studies of air flow over small heated islands, both in the tropics and in middle latitudes. In the sunny hours, islands in the trades are vigorous sources of cumulus, and in fact the cloud towers have often been used by pilots and mariners to locate an island when too far away to discern the land mass itself. The theory of flow over a heat source (Stern and Malkus, 1953) shows why these islands are such excellent producers of cumulus. Corresponding to each heated island may be derived an "equivalent mountain", its height depending directly upon the land temperature excess and inversely upon the stability of the undisturbed air, with a shape corresponding closely to that of the island temperature profile. This "mountain" builds up and decays diurnally. For islands in the trade stream, every degree (Centigrade) temperature excess adds about 500 m to the mountain's magnitude. The mountain itself, rather than being a solid obstacle, consists of a deeper turbulent mixed layer which has been thickened due to the added heat flux and the convergent circulation, so that the low-level streamlines crossing it are deformed upward corresponding to its amplitude and shape.

Thus over the oceans themselves, very slight surface temperature patchiness might be responsible for the initial formation of cloud groups. Since the top of the mixed layer falls short of the condensation level by 50—100 meters or less, island-sized warm spots exceeding the temperature of their surroundings by just a few tenths of a degree could give rise to "equivalent hills" high enough to permit the air in the subcloud layer to reach the height of its average condensation level, so that the moister eddies near its top attain saturation and appear as small cloudlets. The surrounding areas would be clear spaces in which compensatory subsidence occurs, similar to the clear subsidence rings observed around the islands (Malkus, 1955). Randomly distributed low hills of 10—50 km scale, giving rise to clouds clustered over and slightly downwind of them, would present a picture of cloud patterns similar to those photographed and mapped by the Wyman-Woodcock expedition to the trades (Fig. 1). It remained to determine whether adequate temperature gradients are present in the surface layers of the tropical oceans.

Recently an airborne instrument has been developed at the Woods Hole Oceanographic Institution which detects slight sea surface temperature differences. In April 1956, a short field trip to the western Caribbean was made, flying this instrument in the Institution's PBY airplane. The observations were made in such a manner that it was possible to relate sea surface thermal structure to cloud formations. In the few flights made to date, a remarkably clear relation between these patterns was observed. The first part of this paper describes the methods and results of the field work. Then some deductions are made concerning the convective air motions associated with surface thermal gradients of the sizes and magnitudes observed. These are used to interpret previously obtained data on the structure of clear and cloudy areas and to discuss the life cycles of trade cumulus clouds and cloud groups.

II. Observations of surface temperature anomalies and their relation to cloud groups

The airborne radiation thermometer is a device which measures the long wave-length radiation from the surface over which it is being flown. The detector looks through an optical system alternately at the surface and at a reference black body and compares the temperature of the two. The black body is main-

Fig. 1. Map made from cloud photographs showing a typical distribution of oceanic trade cumuli. Calculated from high altitude photographs Nos. 13—26 made by the Wyman-Woodcock Caribbean expedition. The radius of the dashed circle is 53 km; location of its center at 20°00′ N, 64°25′ W. The wind was east-southeast decreasing slightly with elevation. Note the rather irregular spacing of clear and cloudy areas. Only the medium and large clouds within the 53-km circle have been accurately located. The shaded areas are distant cloud banks.

tained at a temperature about five degrees higher than ambient in the aircraft. The instrument is calibrated so that the recorded signal is linearly proportional to the difference between the temperature of the surface and the constant temperature of the black body; at maximum sensitivity it resolves gradients of hundredths of a degree occurring over horizontal distances down to 50—100 m (when carried at the speed of the PBY). On the recent field trip, it was flown at 1,000 ft across the coastline of Jamaica (18° N, 77°30′ W) and neighboring small islands, and up- and downwind over the surrounding oceans. A small source of error arises from water vapor variations in the air column between the instrument and sea level; however, the column would have to possess sudden humidity gradients greater than five times the observed maxima to make this error larger than a few hundredths of a degree. It may be shown further that this error slightly minimizes the oceanic gradients detected. The best corroboration of the records presented here, however, lies in similar measurements obtained in the same area on the same days by the Research Vessel ATLANTIS, which was equipped with sensitive recording thermometers mounted near the surface and at several depths down to 80 ft.

On the aircraft flights, the locations of cloud formations were marked on the surface temperature records by hand punching a key from

the blister as each cloud passed overhead and by a motion picture camera aimed vertically upward. Examination of the results shows that sea surface temperature differences from about 0.1—0.3° C were common on days with active cumulus convection. On days of light winds the gradients were often extremely sharp, a "step" up or down occupying less than 50 m in the horizontal, while with strong winds the edges appeared more diffuse, the same temperature change taking about 1 km. Both "warm spots" and "cold spots" were found, the sizes of which could often be determined from the records. Over the open sea these ranged from 4—20 km in extent along the direction of the wind. Larger scales probably also occurred, since frequently the aircraft crossed a gradient up or down without crossing any noticeable one in the opposite sense before the run had to be ended. Insufficient cross-wind flying was done to determine scales in that direction.

The association of thermal and cloud patterns was surprisingly good and may be summarized as follows: For four flights near Jamaica (10—60 miles offshore)

1) Clouds when present were always associated with warm spots (not cold spots) although they frequently were best developed at the downwind boundary of a warm spot where the temperature gradient was steepest.

2) Cloud groups were generally displaced slightly downwind relative to warm spots, as would be the case over a hill or island.

3) Groups of clouds were generally associated with warm spots, individual clouds being of a much smaller scale. Some individual clouds could be detected on the temperature records since their shadows occasionally produced cloud-sized cool spots as much as a few hundredths of a degree in amplitude.

4) Warm spots were sometimes found without any clouds. In the majority of those cases over the open sea, however, the temperature anomalies did not exceed about one-half the amplitude of those with which clouds were associated on a given day. Warm spots without clouds were also occasionally encountered within the subsidence zone surrounding Jamaica.

5) Oceanic cloud groups were not found in the absence of temperature anomalies.

The temperature records were quite reproducible: on return flights across the "step" zone the same gradients in the opposite sense were invariably found although on one occasion successive crossings made it appear that both the step and associated cloud group were

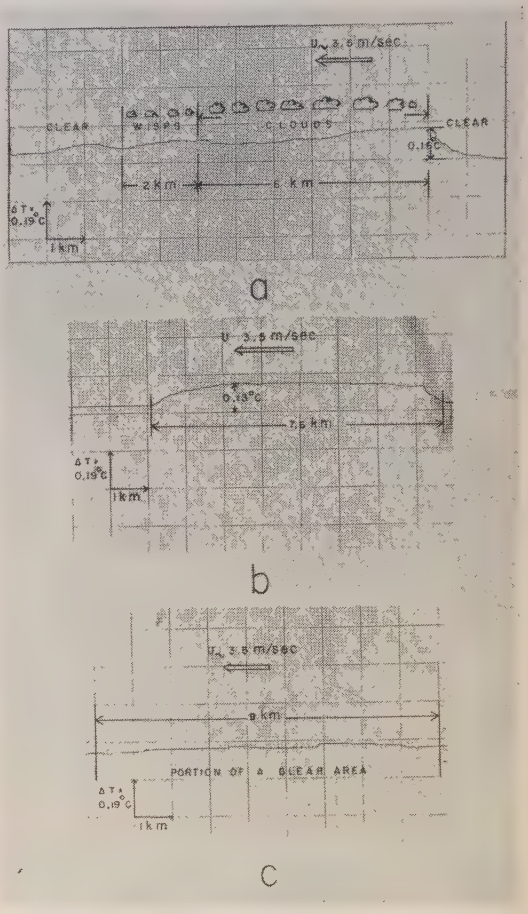

Fig. 2. Sea surface temperature records from radiation thermometer on day of light wind ($U \sim 3.5$ m/sec) and fair trade cumulus. All flights made into wind. Temperature increases upward.

a. Warm spot with cumulus. Clouds drawn somewhat larger than actual widths. Only beginning and end of group marked accurately.

b. Warm spot without cumulus. Found within subsidence ring off island of Jamaica (about 15 miles north). This warm spot has typical temperature profile for light wind day, steeper on upwind edge and more gradual on lee edge.

c. Typical record from clear zone on same day. On this occasion the clear zones were much wider than the cloudy ones and the warm spots were few and far between. No temperature anomalies greater than about 0.04° C were found in clear zones except near the island (see b.).

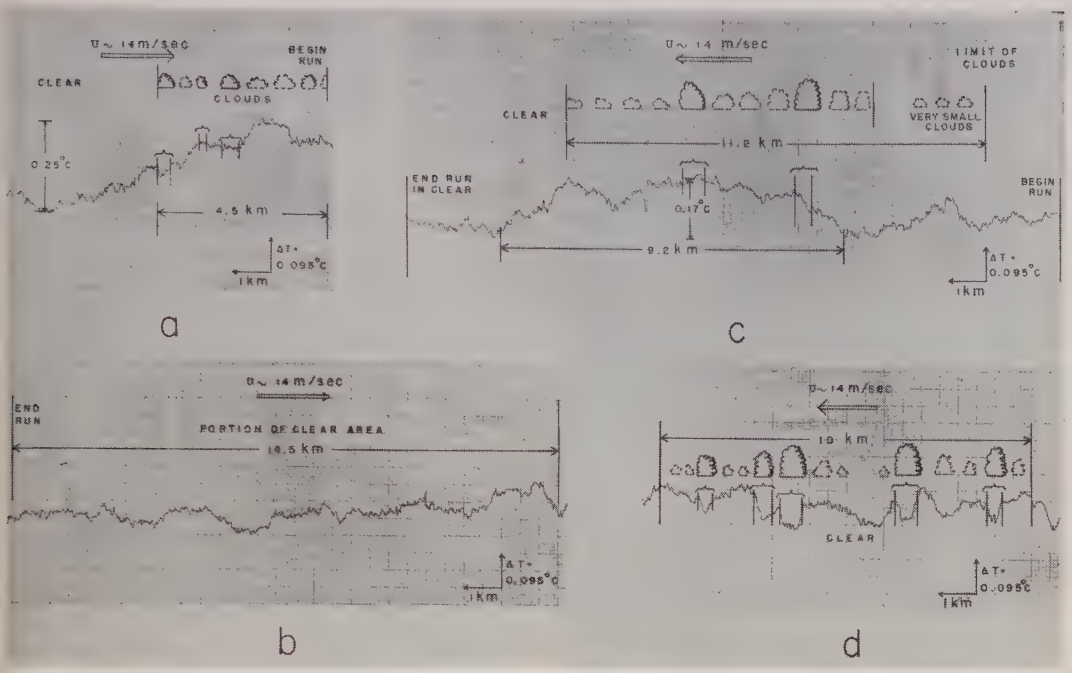

Fig. 3. Sea surface temperature records from radiation thermometer on day of strong wind ($U \sim 14$ m/sec) Some of the increased small-scale fluctuations on these records are real (some small dips are cloud shadows; a few are marked) and some are undoubtedly instrumental. The instrument was operated on this occasion in a manner bound to give more noise than on the occasions of Fig. 1 and 4. Temperatures increase upward.

a. Warm spot 0.25° C in amplitude associated with clouds. Run was made upwind and begins at right edge of figure (within cloudy area) and continued past its downwind edge far into clear area to left. Some of the cloud shadows were marked on the record and are denoted by small brackets with solid-line clouds above. The remaining (dotted) clouds are located approximately.

b. Typical clear area record for the same day. Direct continuation of upwind run begun in Fig. 3 a. Some of the small-scale noise may be instrumental in origin.

c. Upwind run completely traversing 9-km warm spot 0.17° C in amplitude. This warm spot was located on repeated traverses up- and downwind across it and showed little change in amplitude in the time studied. The solid-line clouds were coded accurately on the record as was the beginning and end of the cloud group. The remaining (dotted) clouds are located approximately.

d. Portion of a downwind run made within a warm spot at least 20 km across. Reproduced to show cloud shadows which had the most pronounced effect on the temperature record of any observed over water, due probably to clouds of greater vertical thickness and blacker appearance from below. The bracketed shadows with solid-line clouds drawn above were coded accurately on the record. The remaining (dotted) clouds are sketched approximately.

gradually dying out. No good idea of the duration of the warm spots could be obtained from the flights, although time-lapse photographs from the Jamaica beach (which were directed to following the life histories of cloud groups as a whole) suggest that often they persisted in nearly the same locality for at least 3—4 hours.

The ATLANTIS records confirmed the aircraft temperature data, and on certain rather calm days showed even sharper steps than the gradients reported above; on occasions a 0.1—0.2° C temperature rise or fall occupied only about 10—20 ft in the horizontal. Steps of the same amplitude were recorded on all the lower-level thermometers, with only very slight changes in shape with increasing depth. It appears that this temperature patchiness of the sea surface layers is not a peculiarity of the waters around Jamaica, for the Atlantis obtained similar anomalies on the homeward voyage to Charleston, South Carolina.

Several typical records from the airborne instrument are reproduced in Figures 2—4.

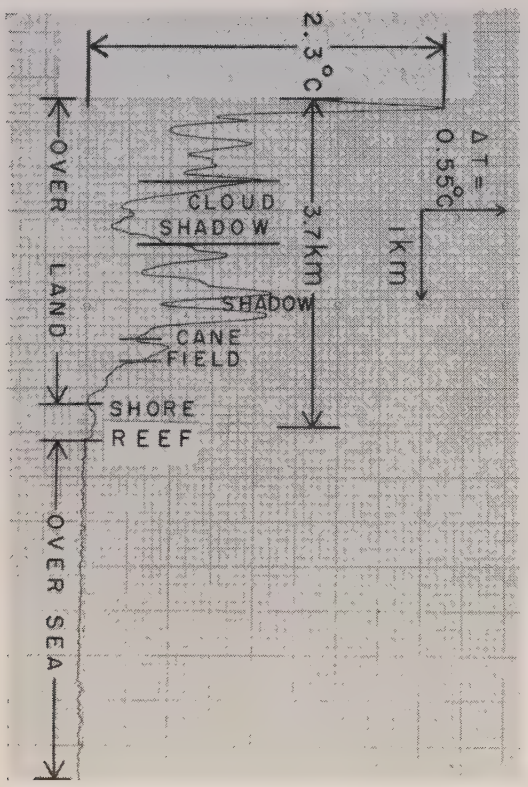

Fig. 4. Island run made at 10.00 a.m. local time on the same strong wind day as the records of Fig. 3. Run made from land to sea across Jamaica north coastline, which lies east-west or nearly parallel to the wind. All fluctuations shown over land are real. Some could be associated with terrain features and several marked dips occurred under cloud shadows; two of these were coded on the record. Instrument is operated on much lower sensitivity than preceding records so that maximum land temperature excess was 2.3° C.

One trace obtained from flying across the Jamaica coastline on a sunny day is shown for comparison. Even though the island record was not made at the maximum of diurnal heating (when the island thermal excess might be expected to be about 25 % greater), the land warming may at first appear small. To understand this it should be pointed out that the radiation instrument operates in the infra-red wave length range 8—13 microns, in order to minimize absorption by the water vapor intervening between the surface and the detector.

While a water surface is a nearly perfect black body in this part of the spectrum, a beach and soil surface undoubtedly has significant albedo. Thus what was measured here might be called the "equivalent black body temperature" of the island. The actual ground temperature, if measured, probably would have been much higher. However, the island temperature rise of Figure 4 is quite in keeping with the land thermal profiles deduced elsewhere as consistent with observed convective and sea-breeze circulations (see MALKUS and STERN, 1953; MALKUS, 1955). This agreement between "equivalent black body temperature" of the land surface and the temperature excess necessary to drive convective motions is probably more than coincidence—if the emission of infra-red radiation is one of the major processes controlling the heat flux from the boundary to the lowest air. Thus we may hypothesize that the radiation thermometer gives approximately the "effective" (for convective motions) boundary temperature of a land as well as a water surface. The contrast between the observed sea and land thermal profiles of Figures 2—4 is striking, the land showing enormously larger fluctuations, due both to differences in soil character and to cloud shadows.

III. Air circulations produced by differential heating

A mechanism for the initiation of cumulus groups over sea surface warm spots was suggested by the "equivalent mountain" analogy which, in fact, provided the incentive for the observations reported above. The "equivalent mountain" effect is associated with a horizontally convergent circulation across the warmed region and concomitant weak updrafts above it, superimposed upon the mean wind flow. If we may continue applying the island model of differential heating to the trade-wind oceans, the approximate magnitude and structure of similar convergent circulations over the warm spots is readily deduced. This permits derivation of a quantitative relation between the observed temperature excess and the expected differences in air structure across a warm spot. While this picture undoubtedly oversimplifies the complex interactions between ocean and atmosphere, circulations of the deduced strength and scale account for several features of the subcloud air which were inexplicable in terms of turbulent fluxes alone,

and in so doing provide a plausible connection between the evolution of cloud groups and processes occurring below cloud.

The maximum height of the "equivalent mountain" corresponding to a heated island has been shown to be

$$M = \frac{\tau}{\Gamma - \gamma} \tag{1}$$

where M is in cm; τ is the effective island temperature excess in °C; Γ is the adiabatic lapse rate, and γ is the lapse rate of the undisturbed air upwind. This maximum is reached at a distance sufficiently inshore from the upwind beach to allow for the establishment by turbulence of a well-mixed ground layer. Thus the equivalent mountain slope may be more gradual than that of the temperature profile and in mid-latitudes on days of poor mixing the maximum height may not be attained in passage across the island. In the trades, the lower air is nearly adiabatic to begin with and the amplitude prescribed by the temperature profile is normally reached within 3—5 km downwind of the island boundary. The greatest "mountain" elevation and streamline deformation are thus commonly encountered at the lee shore where τ is largest. Since the average lapse rate of the trade-region moist layer (surface to inversion height at 2—3 km) varies little from about 0.8 adiabatic, the height of the equivalent mountain in kilometers is usually close to one-half the temperature excess in degrees.

The main features of the heat-produced circulation may now be deduced if we know the height at which the "sea breeze" reverses direction, because this is also the height of maximum vertical velocity: that is to say, it is the height at which the streamline deformation reaches the full amplitude prescribed by equation (1). This height has been derived as

$$h = \frac{\pi}{2} \frac{U}{\sqrt{gs}} \tag{2}$$

where h is in cm; U is the undisturbed wind in cm/sec; s is the upwind static stability, $\Gamma - \gamma / \overline{T}$, where $\overline{T}$ is the mean absolute temperature of the air layer and g is the acceleration of gravity. Since in the trades gs varies little from about 7×10^{-5} sec^{-2}, this relation may be written approximately

$$h \text{ (km)} \cong 0.2\, U \text{ m/sec} \tag{3}$$

Thus for a normal wind speed of 5 m/sec the height of the sea-breeze reversal is about 1 km, being proportionally higher or lower for a stronger or weaker trade.

It is now possible to estimate the average vertical motion at level h, since the air must ascend the height of the equivalent mountain in the time it requires to cross the island, namely U/d where d is the island width. Thus

$$\overline{w} = \frac{\tau}{\Gamma - \gamma} \frac{U}{d} \tag{4}$$

Clearly this is only the average upward motion, for the vertical ascent rate depends on the slope of the equivalent mountain and thus on the features of the temperature profile; it no doubt varies across the island. Larger islands will show weaker mean ascent rates than smaller ones since τ does not rise linearly with island width. The prediction of equation (4) was borne out in comparing the vertical motions over Anegada (2 by 10 km) with those over Puerto Rico (50 by 160 km).

Thus up to maximum $\overline{w}$, its average rate of increase with height is $\overline{w}/h$ and if the island is larger in its cross-stream than down-stream extent, the average horizontal wind difference across it is approximately

$$\frac{\overline{\Delta u}}{\tau} \cong \frac{U}{(\Gamma - \gamma)\, h} \tag{5}$$

and when h is substituted from (2)

$$\frac{\overline{\Delta u}}{\tau} \cong \frac{2}{\pi \overline{T}} \sqrt{\frac{g}{s}} \tag{6}$$

or

$$\frac{\overline{\Delta u}\ \text{(m/sec)}}{\tau} \cong 2.5 \tag{7}$$

for normal trade-region stabilities. Equation (7) gives the wind difference across an island averaged from the surface up to the height where it vanishes. Observations indicate that the tropical sea breeze is about constant up to 300 m or so, from which it decreases roughly linearly to zero at h. Thus we deduce that the low-level wind difference across a heated region should be approximately 3.6 m/sec per °C

mean effective surface temperature excess or that the sea-breeze component at each boundary should be about 1.8 m/sec per degree. Therefore for islands and oceanic warm spots in the trades, the "sea-breeze" strength and equivalent mountain height should depend primarily on the effective temperature excess. The height of sea-breeze reversal (maximum updraft) should vary directly as the wind speed.

These relations have been tested satisfactorily for three islands in the Atlantic trade-wind region, two large (about 50 by 150 km) and one small (about 2 by 10 km). The methods, observations used, and results are reported elsewhere (Malkus, 1955; 1956). If they may now be applied to the oceanic warm spots, the expected circulations are inferred as follows: For a typical warm region 0.2° C in amplitude and 10 km horizontal extent in the direction of the wind, the equivalent mountain is 100 m high; $\triangle u$ at the surface is 0.7 m/sec, and if the trade is blowing at 6.7 m/sec (15 miles per hour) the height of "sea-breeze" reversal is 1,350 m. The air would take about 25 minutes to cross the warm spot and the upward motions at 650 m (average level of cloud base) will be 4.3 cm/sec so that the streamline starting at that height at the upwind edge will have risen 65 m by the downwind boundary. The wind profiles expected at the two edges of the warm region are shown in Figure 5. These have been obtained by adding the heat-produced motions to an average oceanic trade-wind profile.

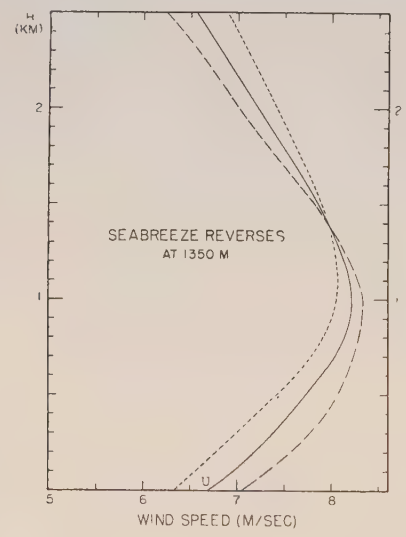

Fig. 5. Calculated wind anomalies associated with typical warm spot. An average oceanic trade-wind distribution with height is given by the solid curve *U*. The long dashed curve shows the modified profile expected at the upwind edge of a 0.2° C warm spot 10 km across, and the short dashed curve is the expected profile at the downwind edge. The surface value of the "sea breeze", its elevation of reversal, and its height distribution are obtained as outlined in text and equations. These profiles are believed to prevail after the warm spot has been in existence long enough for a quasi-steady circulation to develop.

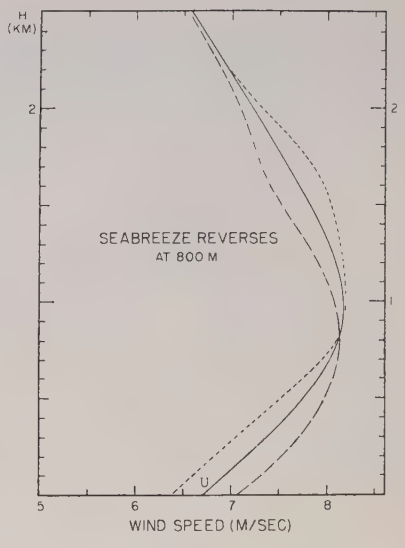

Fig. 6. Calculated wind anomalies associated with an oceanic warm spot in an intermediate stage of development. The solid curve *U* is the same as the solid curve of Fig. 5. In this case the expected profiles at the upwind (long dashed curve) and downwind short dashed curve) edges of the warm spot have been obtained assuming that the sea breeze changes sign at 800 m, instead of 1,350 m as in Fig. 5. The surface wind anomalies are the same in the two figures.

This situation is envisaged after the warm spot has been in existence long enough for the establishment of a quasi-steady flow pattern. The time dependence of the motion field should not be ignored. Island observations suggest that although the offshore subsidence ring is formed and the sea breeze sets in at the coast within an hour after the land becomes warmer than the water, the growth in size of the cell is slower, the maximum depth and inshore penetration requiring several hours. Thus it is probable that the main feature of the

aging of the circulation is its deepening with time up to the maximum-depth configuration of Figure 5. A likely intermediate flow condition might be the one of Figure 6 in which the surface $\triangle u$ is the same but the "sea breeze" reverses at 800 m. The corresponding $\overline{w}$ at cloud-base level is 3.3 cm/sec. The effects of such circulations and their changes with time upon the air flowing through them is considered in the next section.

IV. Effects upon the air structure

During the Wyman-Woodcock expedition to the trades in 1946, numerous vertical soundings of air temperature and humidity were made over the open ocean. On many of the observing days, soundings were taken both in clear and cloudy areas. These have been segregated and the features of the lower air compared. Marked differences in moisture structure below cloud-base level were apparent. The top of the mixed layer averaged 550 m, or less than 100 m below cloud base. In this layer, the air in cloudy regions contained 2 % more moisture than that in the clear, with a 0.3—0.4 gm/kgm higher mixing ratio at the top. This means that the moisture lapse rate in the cloudy-zone mixed layer was on the average 22 % less than in the clear-zone mixed layer. In the 100-m "stable" layer just below cloud base, the differences were even more striking. The moisture lapse rate in cloudy zones fell short of that in clear zones by 33 %, and at cloud-base level (but generally away from clouds) the mixing ratio in cloudy zones exceeded that in clear zones by an average of about 1 gm/kgm. On three occasions in cloudy areas, the upward moisture lapse rate was actually zero or negative in this last 100 m below cloud base and the mixing ratio at cloud-base level exceeded that in nearby clear zones by 1.5—2.0 gm/kgm. The mean surface wind varied little throughout the observation period.

Turbulent fluxes do not account for these distributions. Furthermore, the effects upon turbulent transports of the small surface temperature excesses are unlikely to alter the air structure appreciably above the lowest 100 m or so in the time the air spends crossing the warm spot. Evaporation from the sea surface is increased by 4 % at most. On the other hand, weak circulations caused by the heating can account for the differences. The effectiveness of these scales of motion in transporting water vapor is illustrated when we calculate that the moisture flux produced by a 4 cm/sec vertical velocity exceeds locally the observed evaporation rate and turbulent flux by an order of magnitude. This does not imply that the net integrated upward flux due to these motions exceeds the turbulent transports, as will be seen later, but it does suggest local variations depending upon position relative to the flow pattern.

A typical trade-wind air stream flowing across a warm spot and through its circulation is now considered. The air starts at the upwind edge with the moisture structure typical of a clear area and the laws of mass and water vapor conservation are applied assuming that the air passes through the region in a time small compared to that needed for the motion field to change. Fluxes into and out of the mixed and stable layers are balanced successively using the circulations shown in Figures 5 and 6. The tacit assumption has been made that the evaporation and the upward turbulent flux through cloud-base level are about equal to each other and vary little with position. The results may be discussed using Figure 7. If we consider the mixed layer and apply first the circulation of Figure 6 and then the more mature flow of Figure 5, we get the results in Figures 7 a and 7 b respectively. Although the motion field differs slightly between a and b the resulting differences in moisture structure are negligible. If the air crosses the upwind boundary of the warm spot with the water vapor distribution typical of a clear area, then it may cross the downwind boundary with a distribution typical of a cloudy area. The depicted average mixing ratio increase of about 2 % is required by the superposition of the motion field upon an air stream which dries out with height in the manner of the trades: To satisfy continuity in a steady, horizontally convergent flow, the air column with the smaller wind must be more moist than the column with the stronger wind, in direct proportion that the mixing ratio at the top boundary is less than the average value at the inflow end. It is not a unique solution from these diagrams, which deal with the mixed layer as a single box, that the greatest

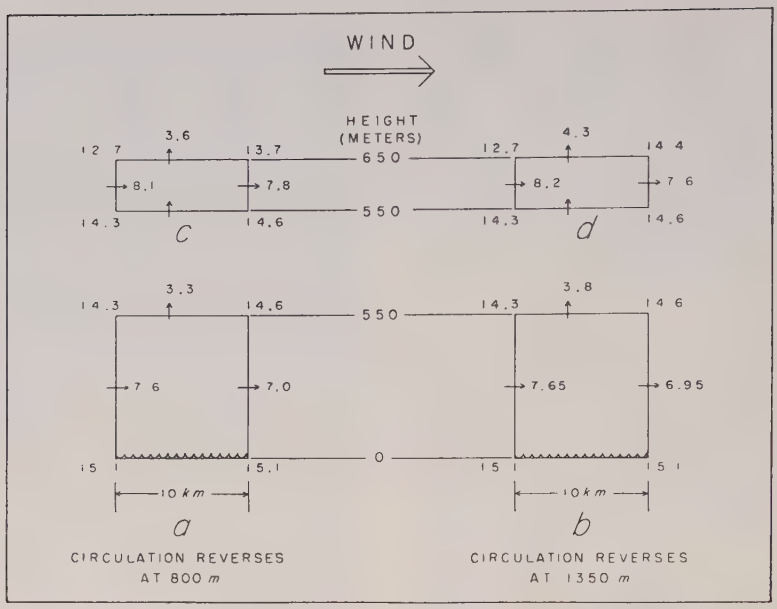

Fig. 7. Diagrams showing mixing ratio and velocity structures obeying mass and moisture conservation laws when typical trade-wind air flows across a 10-km warm spot. The horizontal arrows are wind speeds in m/sec; vertical arrows are mean vertical motions in cm/sec; and the numbers at the corner of each box are mixing ratios in gm/kgm. All figures are rounded off. Boxes a and c use the velocities of the shallower circulation of Fig. 6; boxes b and d use those of the deeper circulation of Fig. 5. In a and b the 550-m deep mixed layer is dealt with as a section 10 km across and unit width into the page. The air and water vapor entering per sec at the upwind (left-hand) side must equal the outflow per sec through the top and downwind (right-hand) side. In c and d the next higher stable layer is treated as a similar section 100 m deep. In each case the inflow air has the moisture distribution of a clear area. The moisture distribution at the outflow end is adjusted to satisfy continuity.

vapor accumulation occurs at the top. This must be so, however, if the moisture lapse rate increases upward as it does in the trade. The greatest moisture addition has thus been made at 550 m, which gives a diminution of mixing ratio lapse rate of 38 % between the extreme ends of the warm spot. This is consistent with the average difference of 22 % between clear and cloudy areas and gives a downwind-end sounding identical to many actually made in cloudy zones.

The required downstream accumulation of moisture becomes greater in the next higher layer through which the vertical decay of mixing ratio is much stronger. Applying the circulation of Figure 6 ("sea breeze" changing sign at 800 m) to the 100-m thick stable layer, we get the results of Figure 7 c. The upwind (left-hand) air column has the moisture structure of a clear area. Continuity is satisfied when the air leaving (right-hand column) has the structure of a cloudy area, with a 1 gm/kgm greater mixing ratio at cloud-base height and a moisture lapse rate smaller by 50 %. The deeper circulation of Figure 5 has a more striking effect, which is shown in Figure 7 d. The mixing ratio at cloud base must now be 1.7 gm/kgm greater at the downwind edge of the warm spot and the moisture lapse rate there practically disappears. This corresponds closely to the observed cases of vanishing or negative mixing ratio gradient just below cloud base. These distributions cannot be produced by turbulent fluxes alone, which on the contrary would shortly destroy such accumulations were not other scales of motion operating to maintain them. The observations and calculations presented here suggest a plausible origin

of circulations of approximately the required amplitude and size.

Although the upward flux of water vapor is large above these warm regions due to the gradual ascent of air, mass continuity requires that it be large in the opposite sense in the surrounding regions of subsidence. Whether or not flows of the sort hypothesized lead to any net upward transport of moisture through cloud-base level depends upon the correlation between vertical motions and mixing ratio, which is unknown. If the correlation were perfect and if the clear areas were twice as wide as the cloudy ones, these circulations could produce a net upward flux through cloud-base level of about 1.3×10^{-6} gm cm^{-2} sec^{-1}. This is 33 % of the evaporation rate or about 43 % of the total moisture flux at that height. While this maximum figure is undoubtedly too large, there is evidence that motions of this scale contribute to the net upward pumping of moisture in the lower trade. If small-scale turbulence alone were to be responsible, it has been found that overly large eddy exchange coefficients are required (see BUNKER, HAURWITZ, MALKUS, STOMMEL, 1949, p. 70).

V. The life cycles of trade-wind clouds and cloud groups

If the velocity profiles of Figures 6 and 5 represent successive time stages in the development of the flow over an oceanic warm spot, it appears likely that the air below cloud will accumulate moisture as the circulation ages, particularly at the downwind edge. For a typical trade-wind sounding, an increase of mixing ratio of 1 gm/kgm would lower the condensation level by about 260 m or 850 ft. Between Figures 7 c and 7 d, the mean mixing ratio of the 100-m layer just below cloud base has risen by 0.35 gm/kgm. Therefore, as a typical circulation reached maximum growth, we might expect cloud base to descend by about 90 m or 300 ft. Some corroborative observational evidence has been gathered by Woodcock[1] near Hawaii. On successive flights below cloud in a fixed locality, he frequently found the cumulus bases lowering from 100—500 ft in one or two hours.

Some of the factors controlling the lifetimes of individual clouds within a group may also be understood in terms of these temperature anomalies and associated circulations. For the observed horizontal dimensions of the warm spots, the time required for normal trade-wind air to pass across them ranges from about five minutes to two hours. This coincides with the range of lifetimes of individual tropical cumuli. While the warm spot circulation remains relatively steady, it can be envisaged that individual clouds will form at some interval after the air crosses the temperature up-step and will dissipate shortly after passing the down-step, many kilometers further downwind. During passage across the warm spot, each cumulus may put up several towers, depending upon the time available. This picture has received support from a series of time-lapse films of some small oceanic clouds north of Jamaica. The group as a whole remained in nearly the same location for more than four hours, despite a 5—6 m/sec wind. The lifetime of a single cumulus measured about 30 minutes, or just the time required to cross the group. Each cloud first appeared at the upwind edge of the population, travelled across the region at approximately the wind speed, and perished as it became the last cloud on the downwind edge. This behavior of the group could not be accounted for in terms of the wind shear, which was strongly negative. Each cloud leaned upwind, put up new towers ahead (downwind) of itself, and evaporated on its rear (upwind) edge, consistent with the predicted asymmetry of a single cumulus in a windfield decreasing upward. None of these small clouds produced showers, which upon occurrence could give rise to different mechanisms of cloud propagation and production.

VI. Concluding remarks

Further observations with the airborne radiation thermometer are planned in other parts of the Atlantic trade and at other seasons. It is hoped to learn whether or not sea surface temperature patchiness of the sort described here is a common phenomenon and how generally it is related to cloud formations. More detailed measurements of the lowest air temperature, moisture, wind and turbulent structure directly over the warm regions are desired to shed light on the mechanisms of interaction between sea and air and to check the predictions concerning the circulations presented here.

[1] Reported in conversation with the writer.

It is hoped that such meteorological observations may be combined with measurements from a surface vessel in an attempt to elucidate the oceanographic factors controlling the origin, scale, and duration of these thermal anomalies, about which little or nothing is known at the present time.

Acknowledgments

An essential contribution to this work was made by Dr. William S. Richardson, who designed and developed the radiation thermometer, and who generously took part in the field program described here, and by Mr. Charles Wilkins who operated the instrument on many of the flights. Much gratitude is also due to Mr. Claude Ronne who participated in every phase of the effort.

This study has been supported by the United States Office of Naval Research.

REFERENCES

Bunker, A. F., Haurwitz, B., Malkus, J. S., and Stommel, H., 1949: Vertical distribution of temperature and humidity over the Caribbean Sea. *Pap. Phys. Oceanogr. Meteorol., Mass. Inst. of Tech. and Woods Hole Oceanogr. Inst.*, **11**, 82 pp.

Malkus, J. S., 1955: The effects of a large island upon the trade-wind air stream. *Quart. J. Roy. Meteor. Soc.*, **81**, pp. 538—550.

Malkus, J. S., 1956: Differential heating in the trades and its relation to cloud formations. Unpublished manuscript on file at the Woods Hole Oceanogr. Inst.

Stern, M. E., and Malkus, J. S., 1953: The flow of a stable atmosphere over a heated island, Part II. *J. Meteor.*, **10**, pp. 105—120.

Wind Action on a Shallow Sea: Some Generalizations of Ekman's Theory

By PIERRE WELANDER

Institute of Theoretical Physics, University of Stockholm,
and International Meteorological Institute in Stockholm

(Manuscript received October 15, revised November 26, 1956)

Abstract

In 1923 EKMAN developed a theory for the sea-level changes produced in a deep sea by the action of a steady wind. In the present paper the theory has been extended to a shallow sea, for which the Ekman "depth of frictional influence" d is comparable to the actual depth h. It is pointed out that the wind-stress divergence may be of the same importance as the wind-stress curl in this case.

The theory is furthermore extended to the transient case. It is demonstrated how the velocity profile and the flow can be expressed in terms of the local time-histories of the wind-stress and the surface slope, and a single integro-differential equation is derived for the sea-level elevation. This equation could possibly be used for prediction of meteorologic tides and storm surges.

I. Introduction

In considering the wind action on the sea Ekman used a model described by the following two equations of motion:

$$\left.\begin{aligned} \frac{\partial u}{\partial t} - fv &= -g\frac{\partial \zeta}{\partial x} + \nu\frac{\partial^2 u}{\partial z^2} \\ \frac{\partial v}{\partial t} + fu &= -g\frac{\partial \zeta}{\partial y} + \nu\frac{\partial^2 v}{\partial z^2} \end{aligned}\right\} \qquad (1)$$

The boundary conditions are

$$\left.\begin{aligned} \nu\left(\frac{\partial u}{\partial z}\right)_{z=0} &= \tau_x^w\,, \qquad \nu\left(\frac{\partial v}{\partial z}\right)_{z=0} = \tau_y^w \\ u_{z=-h} &= 0\,, \qquad v_{z=-h} = 0 \end{aligned}\right\} (2)$$

Here x, y are horizontal locally Cartesian coordinates, and u, v are the corresponding velocities. z is the vertical coordinate counted positive upwards. The free surface is at $z = \zeta(x, y)$ and the bottom at $z = -h(x, y)$ (Fig. 1). f is the Coriolis parameter, g the acceleration of gravity and ν the coefficient of vertical friction. These are considered as constants. τ_x^w, τ_y^w, finally, are the components of the wind-stress acting on the sea surface ($\varrho = 1$). In the derivation of the equations it has been assumed that the water is homogeneous, that the pressure is hydrostatic, and that lateral friction and non-linear acceleration terms can be neglected.

The steady state velocity profile obtained from this model for given values of the wind-stress τ_x^w, τ_y^w and surface slope $\frac{\partial \zeta}{\partial x}$, $\frac{\partial \zeta}{\partial y}$ has been discussed in detail by EKMAN in his paper of 1905. Computing the components of the total flow

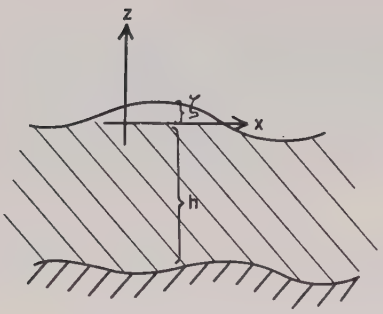

Fig. 1. Coordinate system.

$$\left.\begin{aligned} U &= \int_{-h}^{0} u\,dz \\ V &= \int_{-h}^{0} v\,dz \end{aligned}\right\} \qquad (3)$$

and inserting these in the continuity equation

$$\frac{\partial U}{\partial x} + \frac{\partial V}{\partial y} = 0 \qquad (4)$$

Ekman derived furthermore, in his paper of 1923, a single steady state equation for the sea-level elevation ζ, and discussed this equation in certain simple cases. Ekman was, of course, most interested in the possible application of his theory to the wind-driven ocean circulation, and accordingly he assumed the "depth of frictional influence" $d = \pi\sqrt{\frac{2\nu}{f}}$ to be small compared with the actual depth h. As it has turned out later, however, Ekman's model is not realistic for the deep oceans, because of the neglection of such important factors as the variation of the Coriolis parameter with latitude, the decrease of the horizontal pressure gradient with depth due to the density stratification, and the large-scale lateral mixing. On the other hand, Ekman's model may depict the conditions in a small, shallow sea, with linear dimensions comparable to, say, the North Sea. In a small sea the variation of the Coriolis parameter is insignificant, and for small depths the lateral friction will probably become negligible in comparison with the vertical friction. Also, stratification should have a relatively small influence on the pressure gradient in a shallow sea. It must be pointed out, however, that the stratification may have a strong indirect effect through the coefficient of friction. For instance, in a layer where the density gradient is very large ("discontinuity layer"), the coefficient of vertical friction will fall to practically zero, and the frictional transport of momentum down to the bottom is accordingly reduced. This is of course of greatest significance in a very shallow sea, where most momentum is transported by the frictional stresses. Also in other cases, the assumption of a constant coefficient of vertical friction is not very realistic. Both experiments and theory suggest that the coefficients of turbulent friction should in turn depend on the type of flow set up, and several refined frictional laws have been presented. By introducing such refined laws in this problem one would, however, complicate the mathematical treatment considerably and no simple discussion of frictional influence on the flow would be possible. By using a constant coefficient of friction to represent the "effective friction" the mathematics becomes fairly simple and straight-forward, and the solution can be discussed in terms of a single non-dimensional number, giving the combined effect of friction, Coriolis force and the finite depth.

In the time-dependent case, Fredholm computed the velocity profile developing under the action of a suddenly introduced constant wind-stress, when the depth is infinite (Ekman 1905). This investigation has later on been extended to the case of a sea of finite depth by Fjeldstad (1930) and Hidaka (1933).

Knowing the above mentioned responses, one may find the velocity profile and flow at any place and time expressed in terms of the local time-histories of the wind-stress and surface slope. The continuity equation

$$\frac{\partial \zeta}{\partial t} + \frac{\partial U}{\partial x} + \frac{\partial V}{\partial y} = 0 \qquad (5)$$

will then provide a relation between the rate of change of the sea-level and the local time-histories of the wind-stress, the surface slope, and the surface curvature. This equation can be integrated step by step to give the changes in sea-level of a given sea from the knowledge of the wind-stress values. The

boundary condition is that the normal flow vanishes at the coast. In special, the equation could be used for numerical prediction of storm-surges. Such predictions have been attempted recently for the North Sea by HANSEN (1956) with good success. Hansen's model is based on the vertically integrated equations, where except U, V and ζ also the bottom stress components τ_x^b, τ_y^b appear as unknown variables. The bottom stress has then to be expressed in terms of these other variables through an extra equation, and Hansen uses here a relation based on certain formulae from steady channel flow. According to the present investigation one can, however, give an exact relation between the bottom stress and the integrated variables, and one might hope that the prediction equation (34, 35), which utilizes this exact relation, would improve Hansen's result. Practical experiments with the equation have accordingly been planned.

The author wants to thank Dr. Fischer, now at the International Meteorological Institute in Stockholm, for valuable discussions on the subject.

II. Sea-level in steady state

In the steady state the equations of motion reduce to

$$\left.\begin{aligned} \nu \frac{\partial^2 u}{\partial z^2} + fv &= g \frac{\partial \zeta}{\partial x} \\ \nu \frac{\partial^2 v}{\partial z^2} - fu &= g \frac{\partial \zeta}{\partial y} \end{aligned}\right\} \qquad (6)$$

with unchanged boundary conditions (2).

It is found convenient to introduce a complex notation as follows:

$$\left.\begin{aligned} w &= u + iv \\ \frac{\partial \zeta}{\partial n} &= \frac{\partial \zeta}{\partial x} + i \frac{\partial \zeta}{\partial y} \\ \tau^w &= \tau_x^w + i\tau_y^w \end{aligned}\right\} \qquad (7)$$

Equation (6) can then be written

$$\nu \frac{\partial^2 w}{\partial z^2} - ifw = g \frac{\partial \zeta}{\partial n} \qquad (8)$$

with boundary conditions

$$\left.\begin{aligned} \nu \left(\frac{\partial w}{\partial z}\right)_{z=0} &= \tau^w \\ w_{z=-h} &= 0 \end{aligned}\right\} \qquad (9)$$

Consider for the moment both the wind-stress τ^w and the surface slope $\frac{\partial \zeta}{\partial n}$ as prescribed, they are functions of x and y only. The general solution to equation (8) is

$$w = C_1 e^{\sqrt{\frac{if}{\nu}} \cdot z} + C_2 e^{-\sqrt{\frac{if}{\nu}} \cdot z} + \frac{ig}{f} \frac{\partial \zeta}{\partial n}$$

The boundary conditions (9) determine C_1 and C_2 uniquely and one gets

$$w = \frac{1}{\sqrt{if\nu}} \frac{\sinh \sqrt{\frac{if}{\nu}}\,(h+z)}{\cosh \sqrt{\frac{if}{\nu}}\, h} \tau^w - \frac{ig}{f} \left(\frac{\cosh \sqrt{\frac{if}{\nu}}\, z}{\cosh \sqrt{\frac{if}{\nu}}\, h} - 1 \right) \frac{\partial \zeta}{\partial n} \qquad (10)$$

This solution represents the sum of the Ekman "drift-current" and "gradient current" for finite depth (EKMAN 1905). Integrating the velocity profile (10) gives for the total complex flow,

$$W = U + iV = \int_{-h}^{0} w dz = \frac{A}{f} \tau^w + \frac{ghB}{f} \frac{\partial \zeta}{\partial n}$$

where A and B are functions only of $\frac{h}{d}$,

$$\text{where } d = \pi \sqrt{\frac{2\nu}{f}}.$$

Writing $A = C + iD$, $B = E + iF$, the flow components become

$$\left.\begin{aligned} U &= \frac{1}{f}(C\tau_x^w - D\tau_y^w) + \frac{gh}{f}\left(E\frac{\partial \zeta}{\partial x} - F\frac{\partial \zeta}{\partial y}\right) \\ V &= \frac{1}{f}(D\tau_x^w + C\tau_y^w) + \frac{gh}{f}\left(F\frac{\partial \zeta}{\partial x} + E\frac{\partial \zeta}{\partial y}\right) \end{aligned}\right\} \qquad (11)$$

and the complete expressions for C, D, E and F are

$$\left.\begin{aligned} C &= \frac{2\sin\pi\frac{h}{d}\sinh\pi\frac{h}{d}}{\cos 2\pi\frac{h}{d}+\cosh 2\pi\frac{h}{d}} \\ D &= \frac{2\cos\pi\frac{h}{d}\cosh\pi\frac{h}{d}}{\cos 2\pi\frac{h}{d}+\cosh 2\pi\frac{h}{d}} - 1 \\ E &= \frac{1}{2\pi\frac{h}{d}}\,\frac{\sin 2\pi\frac{h}{d}-\sinh 2\pi\frac{h}{d}}{\cos 2\pi\frac{h}{d}+\cosh 2\pi\frac{h}{d}} \\ F &= -\frac{1}{2\pi\frac{h}{d}}\,\frac{\sin 2\pi\frac{h}{d}+\sinh 2\pi\frac{h}{d}}{\cos 2\pi\frac{h}{d}+\cosh 2\pi\frac{h}{d}} + 1 \end{aligned}\right\} \quad (12)$$

These are shown graphically as functions of $\frac{h}{d}$ in Fig. 2 a—d.

Inserting the values for U and V in the continuity equation (4) one obtains the wanted equation for the sea-level elevation. It becomes

$$ghE\nabla^2\zeta + \gamma_1\frac{\partial\zeta}{\partial x} + \gamma_2\frac{\partial\zeta}{\partial y} =$$
$$= -C\ \mathrm{div}\,\tau^w + D\ \mathrm{curl}\,\tau^w + \delta_1\tau_x^w + \delta_2\tau_y^w \quad (13)$$

where

$$\left.\begin{aligned} \gamma_1 &= \frac{\partial}{\partial x}(ghE) + \frac{\partial}{\partial y}(ghF) \\ \gamma_2 &= -\frac{\partial}{\partial x}(ghF) + \frac{\partial}{\partial y}(ghE) \\ \delta_1 &= -\left(\frac{\partial C}{\partial x}+\frac{\partial D}{\partial y}\right) \\ \delta_2 &= \frac{\partial D}{\partial x}-\frac{\partial C}{\partial y} \end{aligned}\right\} \quad (14)$$

and

$$\left.\begin{aligned} \mathrm{div}\ \tau^w &= \frac{\partial\tau_x^w}{\partial x}+\frac{\partial\tau_y^w}{\partial y} \\ \mathrm{curl}\,\tau^w &= \frac{\partial\tau_y^w}{\partial x}-\frac{\partial\tau_x^w}{\partial y} \\ \nabla^2\zeta &= \frac{\partial^2\zeta}{\partial x^2}+\frac{\partial^2\zeta}{\partial y^2} \end{aligned}\right\} \quad (15)$$

The equation is of the elliptic type and can be solved numerically for any closed basin, using the boundary condition that the normal flow vanishes at the coasts. In terms of ζ this condition becomes

$$gh\left(E\frac{\partial\zeta}{\partial r} - F\frac{\partial\zeta}{\partial s}\right) = -C\tau_r^w + D\tau_s^w \quad (16)$$

where r is the normal and s the tangential coordinate counted positive inwards and *cum sole*, respectively. In the special case of constant depth (13) reduces to

$$ghE\nabla^2\zeta = -C\ \mathrm{div}\,\tau^w + D\ \mathrm{curl}\,\tau^w \quad (17)$$

and in the case of infinite depth it simplifies further to

$$\frac{gd}{2\pi}\nabla^2\zeta = -\mathrm{curl}\,\tau^w \quad (18)$$

In Ekman's derivation of the steady-state equation for ζ it was assumed that $\frac{h}{d} \gg 1$, and consequently the terms C div τ^w, $\delta_1\tau_x^w$, and $\delta_2\tau_y^w$ were missing.

The appearance of the wind-stress divergence in the more general equation (13) is of special interest. The wind-stress divergence will have its maximum effect in a sea of depth $h \sim \frac{d}{2}$, in which case the effect is about half of that from a wind-stress curl of the same magnitude.

One may think that the wind-stress divergence should be a small quantity compared to the wind-stress curl, but this seems not to be the case. Assuming that the wind-stress is proportional to the square of the surface wind speed, one can put

$$\tau^w = kW\mathbf{W} \quad (19)$$

where $\mathbf{W}$ is the wind-vector and $W = |\mathbf{W}|$, and the wind-stress divergence becomes

$$\mathrm{div}\,\tau^w = kW\ \mathrm{div}\,\mathbf{W} + kW\frac{\partial W}{\partial s} \quad (20)$$

where s is a coordinate in the wind-direction. The first one of the two terms appearing in the above expression is generally negligible since the divergence of the wind is quite small, but the second one may well be comparable with the wind-stress curl in regions

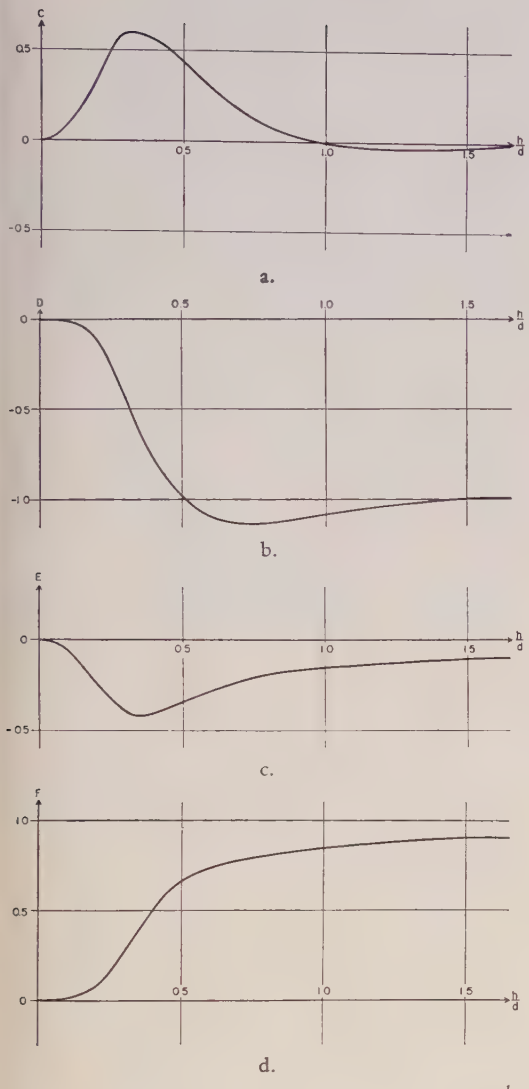

Fig. 2 a—d. Coefficients *C, D, E, F* as dependent on $\frac{h}{d}$.

where the streamlines converge or diverge. In fact, a computation of the ratio of the wind-stress divergence and curl over a number of hemispheric weather maps gave as high an average value as 0.45.

A case that can be treated very simply is the one of a uniform wind-stress acting over a sea of uniform depth. This case has been discussed by EKMAN (1923) and SCHALKWIJK (1947). Introducing the angle φ for the deviation of the "stau-direction" $\left(\text{direction of } \frac{\partial \zeta}{\partial n}\right)$ to the right of the wind-direction and the angle $\gamma = \left|\frac{\partial \zeta}{\partial n}\right|$ for the magnitude of the slope, one has

$$\operatorname{tg} \varphi = \frac{FC - ED}{FD + EC} \tag{21}$$

$$\frac{gh}{\tau^w} \cdot \gamma = \frac{\sqrt{(FC - ED)^2 + (FD + EC)^2}}{E^2 + F^2} \tag{22}$$

In this case the surface slope will be independent of the horizontal extensions of the sea, it depends only on the wind-stress value and the ratio $\frac{h}{d}$. The angle φ is small and positive, with a maximum value $\sim 12°$ occurring when $\frac{h}{d} \sim 1$, and it tends to zero both for very small and very large depths. $\frac{gh}{\tau^w} \cdot \gamma$ approaches $\frac{3}{2}$ for small values of $\frac{h}{d}$ and 1 for large values of $\frac{h}{d}$, and the sea-surface slope is thus in both cases inversely proportional to the depth. The actual variations of φ and γ with $\frac{h}{d}$ according to (21) and (22) are seen in Figs. 3—4.

The qualitative effects of an added wind-stress curl and wind-stress divergence can be seen from an inspection of equation (13) and Figs. 2a—c. It is found that a positive wind-stress curl contributes with a positive $\nabla^2 \zeta$, i.e. a sea-surface concavity, while a negative wind-stress contributes with a negative $\nabla^2 \zeta$, i.e. a sea-surface convexity. This corresponds to a sea-level rising and sea-level sinking, respectively, at the coast, if the sea-level is assumed to be unchanged out in the open sea. The effect will increase numerically with the depth of the sea up to the limiting value given by (18).

In the same way it is found that a positive wind-stress divergence contributes with a sea-surface convexity, a negative wind-stress divergence with a sea-surface concavity, in the range $0 < \frac{h}{d} < 1$. For larger values of $\frac{h}{d}$ the sign may change (in fact it changes each

time $\frac{h}{d}$ passes an integer), but the effect is then very small.

If the depth is variable a uniform wind will also give rise to sea-surface concavities and convexities, because of the terms $\delta_1 \tau_x^w$, $\delta_2 \tau_y^w$, $\gamma_1 \frac{\partial \zeta}{\partial x}$, and $\gamma_2 \frac{\partial \zeta}{\partial y}$. From an inspection of these terms it is found that a decrease of the depth in the direction of the wind or to the right of the wind gives rise to a sea-surface concavity, an increase of the depth in these directions to a sea-surface convexity, provided that the sea is sufficiently shallow $\left(\frac{h}{d} < 0.5\right)$. For larger depths the effects will be reversed but then also their magnitudes become small. Finally, a decrease of the depth in the "stau-direction" or to the right of the stau-direction gives rise to a sea-surface convexity, an increase of the depth in these directions to a sea-surface concavity. When the depth h becomes very large the effect of a variation of the depth in the stau-direction disappears, while the effect of a variation perpendicular to the "stau-direction" remains finite.

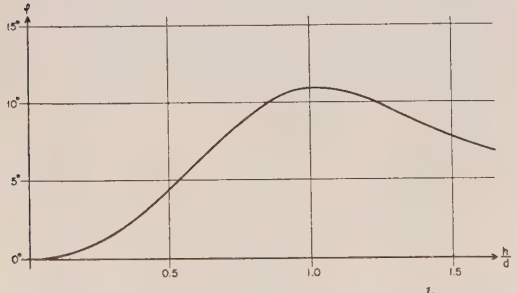

Fig. 3. The angle φ as dependent on $\frac{h}{d}$.

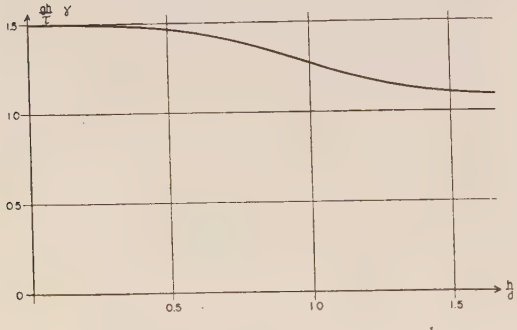

Fig. 4. The angle γ as dependent on $\frac{h}{d}$.

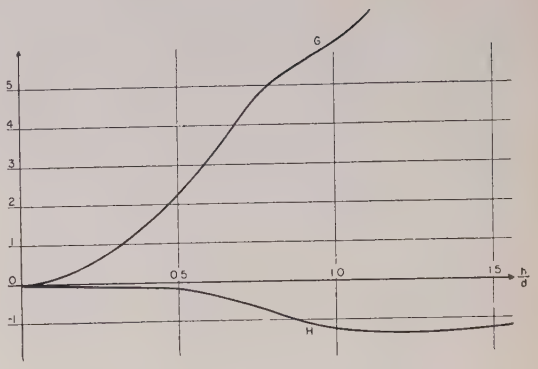

Fig. 5. Appearance of $G\left(\frac{h}{d}\right)$ and $H\left(\frac{h}{d}\right)$.

This last result is of course not very realistic. It is due to the fact that the horizontal divergence disappears outside the frictional layers in this model, forcing all vertical velocities that are induced at the bottom to penetrate up to the surface layer. In a real sea there exist compensating divergencies outside these layers due to stratification, variation of the Coriolis parameter and non-linear terms.

It may be of interest to derive the expression for the vorticity of the flow $\eta = \frac{\partial V}{\partial x} - \frac{\partial U}{\partial y}$ in terms of the wind-stress field. This is made here only for the case of a uniform depth. From (11) is obtained

$$\eta = \frac{1}{f}(C \operatorname{curl} \tau^w + D \operatorname{div} \tau^w) + \frac{gh}{f} F \nabla^2 \zeta \quad (23)$$

and eliminating $\nabla^2 \zeta$ with the aid of equation (17) one gets

$$\eta = \frac{1}{f}(G \operatorname{curl} \tau^w + H \operatorname{div} \tau^w) \quad (24)$$

where

$$\left.\begin{aligned} G &= C + \frac{F}{E} \cdot D \\ H &= D - \frac{F}{E} \cdot C \end{aligned}\right\} \quad (25)$$

G and H are given as function of $\frac{h}{d}$ in Fig. 5. G and H are of comparable magnitude for shallow water, and the wind-stress divergence will then contribute to the horizontal circulation. For deep water the divergence term is small compared to the curl-term. Introducing a stream-function Ψ through

$U = -\frac{\partial \Psi}{\partial y}$, $V = \frac{\partial \Psi}{\partial x}$ (24) can be written

$$\nabla^2 \Psi = \frac{1}{f}(G \operatorname{curl} \tau^w + H \operatorname{div} \tau^w) \quad (26)$$

and this can be integrated, numerically at least, over any closed basin to give the streamlines. The boundary condition is $\Psi = 0$. This equation should be compared with the one obtained by introducing a frictional resistance proportional to the flow,

$$\tau^b = rW \quad (27)$$

which law is often used in discussions of wind-driven circulations. In this latter case one gets

$$\nabla^2 \Psi = \frac{1}{r} \operatorname{curl} \tau^w \quad (28)$$

and the effect of wind-stress divergence is completely lost. For the curl-term the expressions agree if $r = \frac{1}{G} f$.

III. Sea-level in transient state

In the steady state it was possible to find the velocity profile at each point as expressed in terms of the local wind-stress τ^w, the surface slope $\frac{\partial \zeta}{\partial n}$, and the number $\frac{h}{d}$. Substitution of the expressions for the flow components in the continuity equation (4) then gave a differential equation for ζ only.

In the time-dependent case the velocity profile cannot of course be determined by the local, instantaneous values of the wind-stress and the surface slope. It is true, however, that *the velocity profile is uniquely determined by the local time-histories of the wind-stress and the surface slope at each point and instant.* The bottom-stress and the flow are thus also determined by the time-histories.

From a physical point of view it may seem peculiar that only the *local* wind-stress and surface slope should enter in the determination, since this would allow us to create any wanted local velocity field without considering the development at other neighbouring points. One must remember, however, that the surface slope is not a "forcing function" at our disposal (forcing the surface by any outer action to take on a certain wanted form must give rise to extra pressure gradients and equations (1) will then be violated), but it is in turn related to the spatial variations of the flow through the continuity equation. Hereby one gets a coupling between different regions of the fluid. Nevertheless, in the mathematical discussion of the local velocity profile, one may formally look at the surface slope as a forcing function prescribed from the outside.

To find the explicit expression for the velocity profile, one should start from two special profiles $w_a(z,t)$ and $w_b(z,t)$ satisfying the following equations and boundary conditions, respectively:

$$\frac{\partial w}{\partial t} + ifw = \nu \frac{\partial^2 w}{\partial z^2},$$

$$\nu \left(\frac{\partial w}{\partial z}\right)_{z=0} = 1, \quad w_{z=-h} = 0, \quad w_{t=0} = 0 \quad (29\,a)$$

$$\frac{\partial w}{\partial t} + ifw = -g + \nu \frac{\partial^2 w}{\partial z^2},$$

$$\nu \left(\frac{\partial w}{\partial z}\right)_{z=0} = 0, \quad w_{z=-h} = 0, \quad w_{t=0} = 0 \quad (29\,b)$$

w_a gives the response to a suddenly introduced wind-stress of unit magnitude, w_b the response to a suddenly introduced surface slope of unit magnitude. For the special case of infinite depth the solution to the problem (29 a) was given by Fredholm (Ekman 1905). The general solutions have been derived by Fjeldstad (1930) and Hidaka (1933). These can be written on the form

$$w_a = -\frac{1}{\pi^2} \frac{h}{\nu} \left(\frac{d}{h}\right)^2 \sum_{n=0}^{\infty} \frac{1}{\mu_n^2 + i} \cos \frac{2n+1}{2} \pi \frac{z}{h} e^{-(\mu_n^2 + i)tf} + \overline{w}_a \quad (30\,a)$$

$$w_b = -\frac{\sqrt{2}}{\pi} \frac{g}{f} \frac{d}{h} \sum_{n=0}^{\infty} \frac{(-1)^n}{\mu_n^2 + i} \cos \frac{2n+1}{2} \pi \frac{z}{h} e^{-(\mu_n^2 + i)tf} + \overline{w}_b \quad (30\,b)$$

where

$$\mu_n = \frac{1}{2\sqrt{2}}(2n+1)\frac{h}{d} \qquad (31)$$

and $\overline{w}_a$, $\overline{w}_b$ stand for the corresponding steady state solutions.

The response to a suddenly introduced differential wind-stress $\triangle\tau^w$ and sea-surface slope $\triangle \frac{\partial\zeta}{\partial n}$ is

$$w = \triangle\tau^w w_a(z,t) + \triangle \frac{\partial\zeta}{\partial n} w_b(z,t)$$

Putting

$$\triangle\tau^w = \frac{\partial\tau^w}{\partial t}\triangle t$$

$$\triangle \frac{\partial\zeta}{\partial n} = \frac{\partial^2\zeta}{\partial t\,\partial n}\triangle t$$

and summing up the contributions from such differential steps in the wind-stress and surface slope for past times ($\alpha < t$) gives

$$w = \int_0^\infty \left[\frac{\partial\tau^w}{\partial t}(t-\alpha)\,w_a(z,\alpha) + \right.$$
$$\left. + \frac{\partial^2\zeta}{\partial t\,\partial n}(t-\alpha)\,w_b(z,\alpha)\right] d\alpha \qquad (32)$$

It is then assumed that τ^w and $\frac{\partial\zeta}{\partial n}$ start from zero values.

After a partial integration the following more convenient form of (32) is obtained.

$$w = \int_0^\infty \left[\tau^w(t-\alpha)\frac{\partial w_a}{\partial t}(z,\alpha) + \right.$$
$$\left. + \frac{\partial\zeta}{\partial n}(t-\alpha)\frac{\partial w_b}{\partial t}(z,\alpha)\right] d\alpha \qquad (33)$$

Integrating vertically and inserting the expressions for w_a and w_b one obtains for the total flow

$$W = \frac{4}{\pi}\int_0^\infty \tau^w(t-\alpha)\sum_{n=0}^\infty \frac{(-1)^n}{2n+1} e^{-(\mu_n^2+i)\alpha f}\,d\alpha$$
$$- \frac{8}{\pi^2} gh \int_0^\infty \frac{\partial\zeta}{\partial n}(t-\alpha)\sum_{n=0}^\infty \frac{1}{(2n+1)^2} e^{-(\mu_n^2+i)\alpha f}\,d\alpha \qquad (34)$$

By using this expression in the continuity equation, written in the form

$$\frac{\partial\zeta}{\partial t} = -\operatorname{div} W \qquad (35)$$

one arrives at a single prediction equation for ζ. On the right side of the equation the time-histories of the wind-stress, the surface slope and surface curvature enter. It is thus an integro-differential equation for ζ. It may be solved numerically for a given basin and stress-field by using a step-by-step technique. The boundary condition $W_r = 0$ at the coast, can be formulated as a condition for $\frac{\partial\zeta}{\partial n}$ at each step.

It should be possible to use (34, 35) for actual predictions of meteorological tides and storm surges. The method would probably improve the results obtained by other methods in the case of fairly shallow water, where bottom friction is of importance. So far no computations have been performed, but some experiments for the North Sea basin are planned.

REFERENCES:

Ekman, V. W., 1905: On the influence of the earth's rotation on ocean-currents. *Arkiv Mat. Astr. Fysik* **2**, No. 4.

Ekman, V. W., 1923: Ueber Horizontalcirkulation bei winderzeugten Meeresströmungen. *Arkiv Mat. Astr. Fysik* **17**, No. 26.

Hansen, W., 1956: Theorie zur Errechnung des Wasserstandes und der Strömung in Randmeeren nebst Anwendungen. *Tellus* **8**, pp. 287—300.

Hidaka, K., 1933: Non-stationary ocean currents. Part I. *Mem. Imp. Mar. Obs. Kobe* **5**, No. 3.

Fjeldstad, J. R.: *Zeits. für Angew. Math. Mech.* **10**.

Schalkwijk, W. F., 1947: A contribution to the study of storm surges on the Dutch coast. *Koninklijk Nederlandsch Meteorologisch Instituut*, No. 125, *Medeelingen en Verhandelingen*, Serie B, Deel I, No. 7.

Some Remarks About Nonlinear Oscillations In Tidal Channels

By H. KREISS, International Institute of Meteorology in Stockholm

(Manuscript received July 15, revised October 25, 1956)

Abstract

In tidal rivers one observes an unsymmetry between flood and ebbcurrent. This phenomenon is examined for channels with constant mean depth and mean cross-section area. The hydrodynamic equations are integrated over the vertical and it is shown that one is not allowed to introduce the usual simplifications (linearisation, neglection of friction) if one wants to describe this phenemenon. With the aid of a perturbation method the equations are integrated and it is shown that for sufficiently small ratio maximum of the flow/mean depth one can approximate the solution of by two harmonics. This approximation is examined in detail.

1. Introduction

In tidal estuaries one often observes that the floodcurrent u_F is of shorter duration than the ebb-current u_E and that the maximum value of u_F is greater than the maximum value of u_E. These facts are of importance for the transport of sediments and do explain why a river sometimes gets filled with sand. (Figure 1.)

Of late effective numerical methods have been developed for the computation of such tidal currents (HANSEN, 1956). These methods are the only ones that permit us to compute tides in rivers with varying cross-section and varying mean depth. On the other hand they do not readily give an insight into the physical structure of the motions since each computation gives just one special numerical solution and does not tell anything about what would happen if the controlling parameters were changed. For this reason it may be useful to develop analytical theories for simple examples and to study their physical structure in detail. In this paper we shall discuss such a theory for the simple case of tidal motions in channels with constant mean depth and constant cross-section.

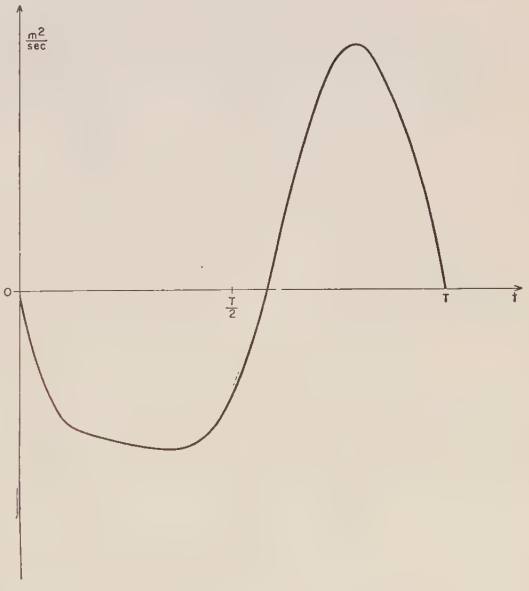

Fig. 1. Flow-values in a fixed point as a function of time. The positive values represent the flood current u_F the negative the ebb current u_E.

2. Basic equations

In the theoretical study of tidal motions in channels, one usually assumes that the channel is connected with the open sea at one end and closed at the other. Using the symbols u, ζ, h for velocity, the surface elevation and the mean depth respectively, one starts with the vertically integrated hydrodynamical equations in the form:

$$\left.\begin{aligned} &\bar{u}_t + \frac{\lambda}{h}\bar{u}\bar{u}_x + R(\bar{u}) + g(h+\zeta)\zeta_x = 0 \\ &\bar{u}_x + \zeta_t = 0 \\ &\bar{u} = \int_{-h}^{\zeta} u\,dz \end{aligned}\right\} \quad 2.1$$

f_t, f_x, f_{xt} etc. being defined by

$$f_t = \frac{\partial f}{\partial t};\quad f_x = \frac{\partial f}{\partial x};\quad f_{xt} = \frac{\partial^2 f}{\partial x\,\partial t}$$

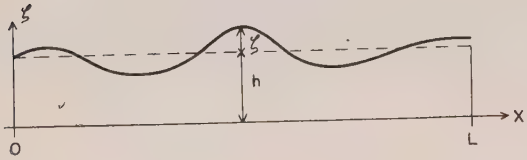

Fig. 2.

The boundary conditions are:

$$\text{for } x = 0 \quad \zeta(0,t) = f(t) = A\cos\frac{2\pi}{T}t$$

$$\text{and for } x = L, \quad \bar{u} = 0 \quad \text{(Figure 2)}$$

In 2.1 $R(\bar{u})$ is the friction-term and one generally assumes:

$$R(\bar{u}) = -R(-\bar{u})$$

This assumption is only true when the friction is independent of the history of the motion; it is well known that in some tidal rivers one has to choose different friction-laws for ebb- and flood-currents.

The factor λ derives from the fact that the velocity is a function of depth. This factor most likely varies from section to section and from time to time. One can write $\lambda = 1 + \varepsilon(x,t)$. In many cases, however, ε is small compared with 1. Later it will be shown that the entire term $\frac{\lambda}{h}\bar{u}\bar{u}_x$ normally does not influence the solution of 2.1 strongly. Under those circumstances the assumption $\lambda = 1$ is a reasonable one.

In the study of tides one is not interested in the transient solution of 2.1 and we shall therefore restrict this investigation to the T-periodical solution.

In all earlier analytical investigations the equations 2.1 have been simplified in one or both of the following two ways:

a) One neglects the nonlinear terms $\frac{\lambda}{h}\bar{u}\bar{u}_x$ and $\zeta\zeta_x$ and investigates:

$$\left.\begin{aligned} &\bar{u}_t + R(\bar{u}) + gh\zeta_x = 0 \\ &\bar{u}_x + \zeta_t = 0 \end{aligned}\right\}$$
$$\left.\begin{aligned} &\zeta(0,t) = A\cos\frac{2\pi}{T}t \\ &\bar{u}(L,t) = 0 \end{aligned}\right\} \quad 2.1\,a$$

There is no possibility to describe the previously mentioned lack of symmetry between ebb and flood currents by this system, since the transformation:

$$x = x^*;\quad t = t^* + \frac{T}{2};\quad \zeta = -\zeta^*;\quad u = -u^*$$

does not change the system 2.1 a. In fact:

$$\left.\begin{aligned} &\bar{u}\left(t + \frac{T}{2}\right) = -\bar{u}(t) \\ &\zeta\left(t + \frac{T}{2}\right) = -\zeta(t) \end{aligned}\right\}$$

b) One neglects the friction term and investigates:

$$\left.\begin{aligned} &\bar{u}_t + g(h+\zeta)\zeta_x + \frac{\lambda}{h}\bar{u}\bar{u}_x = 0 \\ &\bar{u}_x + \zeta_t = 0 \end{aligned}\right\}$$
$$\left.\begin{aligned} &\zeta(0,t) = A\cos\frac{2\pi}{T}t \\ &\bar{u}(L,t) = 0 \end{aligned}\right\} \quad 2.1\,b$$

(H. Lamb 1932; J. Stoker 1948.)

But also these equations do not lead further

since they remain unchanged by the transformation:

$$x = x^*;\quad t = -t^*;\quad \bar{u} = -\bar{u}^*;\quad \zeta = \zeta^*$$

Therefore

$$\bar{u}(-t) = -\bar{u}(t)$$
$$\zeta(-t) = \zeta(t)$$

and we get again symmetry between ebb and flood current.

It follows that we must take into account both friction and the nonlinear terms. The simplest way to do this is to choose

$$R(\bar{u}) = \text{const} \cdot \bar{u} = \sigma\bar{u}$$

In accordance with earlier investigations we put

$$\sigma = \frac{\varrho}{h};\quad \varrho = 2 \cdot 10^{-3}\ \left[\frac{\text{meter}}{\text{sec.}}\right]$$

Thus we shall investigate the system

$$\left.\begin{cases} \bar{u}_t + \frac{\lambda}{h}\bar{u}\bar{u}_x + \varrho\,\frac{\bar{u}}{h} + g(h+\zeta)\zeta_x = 0 \\ \bar{u}_x + \zeta_t = 0 \end{cases}\right\} \quad 2.2$$
$$\left.\begin{cases} \zeta(0, t) = A\cos\frac{2\pi}{T}t \\ \bar{u}(L, t) \equiv 0 \end{cases}\right\}$$

It is convenient to write 2.2 in nondimensional form:

Putting

$$\left.\begin{aligned} \bar{u} &= \frac{2\pi hL}{T}\,\bar{u}'; & \xi &= h\zeta' \\ t &= \frac{T}{2\pi}\,t'; & x &= Lx' \end{aligned}\right\} \quad 2.3$$

we get

$$\alpha^2(\bar{u}'_{t'} + \beta\bar{u}' + \lambda\bar{u}'\bar{u}'_{x'}) + (1+\zeta')\zeta'_{x'} = 0 \quad 2.4\,a$$
$$\bar{u}'_{x'} + \zeta'_{t'} = 0 \quad 2.4\,b$$

with

$$\alpha = \frac{2\pi L}{\sqrt{gh}\,T};\quad \beta = \frac{\varrho T}{2\pi h}$$

From the continuity equation 2.4 b it follows, that a function φ exists with the properties:

$$\bar{u}' = -\varphi_{t'} \qquad \zeta' = \varphi_{x'} \quad 2.5$$

Dropping the ′ we get from 2.4 a and 2.5

$$\left.\begin{cases} -\alpha^2(\varphi_{tt} + \beta\varphi_t) + \varphi_{xx} + \alpha^2\lambda\varphi_t\varphi_{xt} + \\ +\varphi_{xx}\varphi_x = 0 \\ \varphi(1, t) = 0 \\ \varphi_x(0, t) = \frac{A}{h}\cos t \end{cases}\right\} \quad 2.6$$

As far as I know, is it not possible to represent the solution of 2.6 by a finit number of elementary functions.

But if the ratio amplitude A/mean depth h is small compared with unity we shall see that the solution of 2.6 is "situated in the neighbourhood" of the solution of the linearised equation 2.1 a. With the aid of the perturbation method we can then approximate the solution of 2.6 by means of a number of solutions of linear equations.

We can write 2.6 in the form:

$$\left.\begin{cases} -\alpha^2(\varphi_{tt} + \beta\varphi_t) + \varphi_{xx} + \\ +\varepsilon(\alpha^2\lambda\varphi_t\varphi_{tx} + \varphi_{xx}\varphi_x) = 0;\ \varepsilon = 1 \\ \varphi(1, t) = 0 \\ \varphi_x(0, t) = \frac{A}{h}\cos t \end{cases}\right\} \quad 2.7$$

Writing formally $\varphi = \Sigma\varphi_\nu\varepsilon^\nu$, introducing this expression into 2.7 and arranging after powers of ε we get:

$$-\alpha^2(\varphi_{\nu tt} + \beta\varphi_{\nu t}) + \varphi_{\nu xx} +$$
$$+(\varphi_{0xx}\varphi_{\nu-1,\,x} \cdot \ldots \cdot \varphi_{\nu-1,\,xx}\varphi_{0x}) +$$
$$+\alpha^2\lambda(\varphi_{0t}\varphi_{\nu-1,\,tx} \cdot \ldots \cdot \varphi_{\nu-1,\,t}\varphi_{0tx}) = 0 \quad 2.8$$

The boundary conditions are fulfilled by the demand

$$\left.\begin{aligned} \varphi_0(1, t) &= 0 \quad \varphi_{0x}(0, t) = \frac{A}{h}\cos t \\ \varphi_\nu(1, t) &= 0 \quad \varphi_{\nu x}(0, t) = 0 \quad \nu > 0 \end{aligned}\right\} \quad 2.9$$

Then

$$\varphi = \Sigma\varphi_\nu \quad 2.10$$

is a formal solution of 2.6 and by the aid of 2.5 we get formal expressions for $\bar{u}'$ and ζ'.

This whole development is of any use only if already $\varphi_0 + \varphi_1$ gives a sufficiently good approximation to the solution φ of 2.6. If one has to take additional φ_ν into account the

mathematical apparatus increases immensely and becomes unwieldy.

Therefore we shall restrict us to the case that $\varphi_0+\varphi_1$ and its first derivatives gives a sufficiently good approximation to φ and its first derivatives. To investigate under which conditions this is true we shall derive a differential-equation for $\psi=\varphi-(\varphi_0+\varphi_1)$. From equation 2.8 we get the equations for φ_0 and φ_1.

$$\left.\begin{aligned} &-\alpha^2(\varphi_{0tt}+\beta\varphi_{0t})+\varphi_{0xx}=0\\ &\varphi_0(1,t)=0\\ &\varphi_{0x}(0,t)=\frac{A}{h}\cos t \end{aligned}\right\} \quad 2.11$$

$$\left.\begin{aligned} &-\alpha^2(\varphi_{1tt}+\beta\varphi_{1t})+\varphi_{1xx}=\\ &-\frac{1}{2}\frac{\partial}{\partial x}(\varphi_{0x}^2+\lambda\alpha^2\varphi_{0t})\\ &\varphi_1(1,t)=0;\quad \varphi_{1x}(0,t)=0 \end{aligned}\right\} \quad 2.12$$

Subtracting these two equations from equation 2.7 we get for ψ

$$\left.\begin{aligned} &-\alpha^2(\psi_{tt}+\beta\psi_t)+\psi_{xx}+\\ &+\frac{1}{2}\frac{\partial}{\partial x}\left\{\alpha^2\lambda[\psi_t^2+2(\varphi_{0t}+\varphi_{1t})\psi_t]+\right.\\ &\left.+2(\varphi_{0x}+\varphi_{1x})\psi_x+\psi_x^2\right\}=\\ &=-\frac{1}{2}\frac{\partial}{\partial x}\{\alpha^2\lambda(2\varphi_{0t}\cdot\varphi_{1t}+\varphi_{1t}^2)+\\ &+2\varphi_{0x}\varphi_{1x}+\varphi_{1x}^2\}\\ &\psi_0(1,t)=\psi_{1x}(0,t)=0 \end{aligned}\right\} \quad 2.13$$

Now we assume that the ratio of the amplitude A to the mean depth h is small compared with unity. It then follows, as we shall see in the next section, that also $|\varphi_{0t}|, |\varphi_{0x}| \ll 1$ and $|\varphi_{1t}| \ll |\varphi_{0t}|$; $|\varphi_{1x}| \ll |\varphi_{0x}|$ and we can approximate ψ by $\bar{\psi}$. $\bar{\psi}$ is defined by the equation (all "small terms" in equation 2.13 are neglected)

$$\left.\begin{aligned} &-\alpha^2(\bar{\psi}_{tt}+\beta\bar{\psi}_t)+\bar{\psi}_{xx}=\\ &=-\frac{\partial}{\partial x}(\alpha^2\lambda\varphi_{0t}\varphi_{1t}+\varphi_{0x}\varphi_{1x})\\ &\bar{\psi}_0(1,t)=\bar{\psi}_{1,x}(0,t) \end{aligned}\right\} \quad 2.14$$

This simplification of 2.13 is permissible, because we are only interested in the order of magnitude of ψ and its first derivatives. One can also justify it by numerical examples. I have solved both equations 2.13 and 2.14 for some examples in which $\frac{A}{h}=0.2$ and found that maximum $|\psi| < 1.5$ maximum $|\bar{\psi}|$ and that this inequality also is valid for the first derivatives.

We shall discuss equation 2.14 at the end of section 3 and give some estimates of $\bar{\psi}$, when we have determined φ_0 and φ_1. But we can point out already here the analogy between the equation 2.12 for φ_1 and 2.14 for $\bar{\psi}$. We have mentioned, that if $|\varphi_0|$ is small compared with unity, $|\varphi_1|$ is small compared with $|\varphi_0|$. From 2.12 and 2.14 it is then at least plausible that $|\bar{\psi}|$ is small compared with $|\varphi_1|$.

We shall now introduce some notations which will be useful in the following.

Putting $-\varphi_{it}=\bar{u}_i'$ $\varphi_{ix}=\zeta_i'$ $(i=0,1)$ we can write

$$\left.\begin{aligned} &\bar{u}'=\bar{u}_0'+\bar{u}_1'\\ &\zeta=\zeta_0'+\zeta_1' \end{aligned}\right\} \quad 2.15$$

$\bar{u}_0'$, ζ_0' is the solution of the linearized equation 2.1 a in nondimensional form.

$\bar{u}_1'$, ζ_1' gives us the deviation of the solution of the nonlinear equation 2.2 from $(\bar{u}_0', \zeta_0')$.

Therefore we shall often use the phrases

the linear part for $(\bar{u}_0', \zeta_0')$
the nonlinear part for $(\bar{u}_1', \zeta_1')$

3. Determination of φ_0

a) φ_0

We know from 2.11 that for φ_0

$$\left.\begin{aligned} &-\alpha^2(\varphi_{0tt}+\beta\varphi_{0t})+\varphi_{0xx}=0\\ &\varphi_{0x}(0,t)=\frac{A}{h}\cos t\quad \varphi_0(1,t)=0 \end{aligned}\right\} \quad 3.1$$

holds.

Writing the boundary conditions of 3.1 in complex form, we get that $\varphi_0=$realpart ω_0 and that for ω_0

$$\left.\begin{aligned} &-\alpha^2(\omega_{0tt}+\beta\omega_{0t})+\omega_{0xx}=0\\ &\omega_{0x}(0,t)=\frac{A}{h}e^{it}\quad \omega_0(1,t)=0 \end{aligned}\right\} \quad 3.2$$

holds. As usual, we get the 2π-periodic solution ω_0 of 3.2 by assuming

$$\omega_0 = f(x)\, e_{it}$$

Putting this expression into 3.2 we get for $f(x)$

$$\left.\begin{aligned} &\alpha^2(1-i\beta)\cdot(\times)+f''(x)=0 \\ &f'(0)=\frac{A}{h}, \quad f(1)=0 \end{aligned}\right\} \qquad 3.3$$

Therefore

$$f(x)=\frac{A}{hK_1\left(e^{K_1}+e^{-K_1}\right)}\left(e^{K_1(x-1)}-e^{-K_1(x-1)}\right)$$

with $K_1^2=-\alpha^2(1-i\beta)$ thus $K_1=K_{1r}+iK_{1i}=$

$$=\frac{\alpha}{\sqrt{2}}\left(\sqrt{\sqrt{1+\beta^2}-1}+\frac{i\beta}{\sqrt{\sqrt{1+\beta^2}-1}}\right) \qquad 3.4$$

and we get

$$\omega_0=\frac{Ae^{it}}{hK_1\left(e^{K_1}+e^{-K_1}\right)}\left(e^{K_1(x-1)}-e^{-K_1(x-1)}\right)=$$

$$\frac{Ae^{it}}{hK_1\left(1+e^{-2K_1}\right)}\left(e^{K_1(x-2)}-e^{-K_1x}\right) \qquad 3.5$$

$$\text{with}\quad \varphi_0=\text{realpart}\ \omega_0=\frac{1}{2}\left(\omega_0+\bar{\bar{\omega}}_0\right)$$

$\bar{\bar{\omega}}_0$ being defined as the conjugate complex value of ω_0.

b) φ_1

From the equations 2.12 and 3.6 it follows that for φ_1

$$-\alpha^2\left(\varphi_{1tt}+\beta\varphi_{1t}\right)+\varphi_{1xx}=-\frac{1}{2}\frac{\partial}{\partial x}\left(\varphi_{0x}^2+\lambda\alpha^2\varphi_{0t}^2\right)=$$

$$=-\frac{1}{8}\frac{\partial}{\partial x}\left(\omega_{0x}^2+\bar{\omega}_{0x}^2+2\,\omega_{0x}\bar{\omega}_{0x}+\right.$$

$$\left.+\lambda\alpha^2\left(\omega_{0t}^2+\bar{\bar{\omega}}_{0t}^2+2\,\omega_{0t}\bar{\bar{\omega}}_{0t}\right)\right) \qquad 3.7$$

holds. 3.7 is a linear equation and therefore we can split it up into

$$-\alpha^2\left(\varphi_{1tt}^{(1)}+\beta\varphi_{1t}^{(1)}\right)+\varphi_{1xx}^{(1)}=$$

$$=-\frac{1}{4}\frac{\partial}{\partial x}\left(\omega_{0x}\bar{\bar{\omega}}_{0x}+\lambda\alpha^2\omega_{0t}\bar{\bar{\omega}}_{0t}\right) \qquad 3.8\,a$$

$$-\alpha^2\left(\varphi_{1tt}^{(2)}+\beta\varphi_{1t}^{(2)}\right)+\varphi_{1xx}^{(2)}=$$

$$=-\frac{1}{8}\frac{\partial}{\partial x}\left(\omega_{0x}^2+\bar{\bar{\omega}}_{0x}^2+\lambda\alpha^2\left(\omega_{0t}^2+\bar{\bar{\omega}}_{0t}^2\right)\right) \qquad 3.8\,b$$

$$\varphi_{1x}^{(i)}(0,t)=\varphi_1^{(i)}(1,t);\quad (i=1.2)$$

Thus $\varphi_1=\varphi_1^{(1)}+\varphi_1^{(2)}$

The right side of 3.8 a is independent of t, therefore also $\varphi_1^{(1)}$ is independent of t and we get by simple integration

$$\varphi_{1x}^{(1)}=\frac{1}{4}\int_0^x\frac{\partial}{\partial x}\left(\omega_{0x}\bar{\omega}_{0x}+\lambda\alpha^2\omega_{0t}\bar{\bar{\omega}}_{0t}\right)dx \qquad 3.9$$

From 3.8 b we see that we can write $\varphi_1^{(2)}$ as the realpart of a function ω_1 for which

$$\left.\begin{aligned} &-\alpha^2\left(\omega_{1tt}+\beta\omega_{1t}\right)+\omega_{1xx}= \\ &=-\frac{1}{4}\frac{\partial}{\partial x}\left(\omega_{0x}^2+\lambda\alpha^2\omega_{0t}^2\right) \\ &\omega_{1x}(0,t)=\omega_1\ (1,t)=0 \end{aligned}\right\} \qquad 3.10$$

holds. From 3.5 we have

$$\frac{\partial}{\partial x}\omega_{0x}^2=\frac{2A^2K_1e^{it}}{h^2\left(1+e^{-2K_1}\right)^2}\left(e^{2K_1(x-2)}-e^{-2K_1x}\right)$$

$$\lambda\alpha^2\frac{\partial}{\partial x}\omega_{0t}^2=$$

$$=-\frac{2A^2\lambda\alpha^2e^{2it}}{Kh^2\left(1+e^{-2K_1}\right)^2}\left(e^{2K_1(x-2)}-e^{-2K_1x}\right)=$$

$$=-\frac{\lambda\alpha^2}{K_1^2}\frac{\partial}{\partial x}\omega_{0x}^2$$

Therefore we get

$$-\alpha^2\left(\omega_{1tt}+\beta\omega_{1t}\right)+\omega_{1xx}=-\frac{1}{2}\left(1-\frac{\lambda\alpha^2}{K_1^2}\right)\cdot$$

$$\cdot\frac{A^2K_1e^{2it}}{h^2\left(1+e^{-2K_1}\right)}\left(e^{2K_1(x-2)}-e^{-2K_1x}\right) \qquad 3.11$$

$$\omega_{1x}(0,t)=\omega_1(1,t)=0 \qquad 3.11\,a$$

A particular solution of 3.11 we get in the form

$$\omega_{1P}=\left(1-\frac{\lambda\alpha^2}{K_1^2}\right)\frac{iA^2}{h^2}\cdot$$

$$\cdot\frac{K_1e^{2it}}{4\alpha^2\beta\left(1+e^{-2K_1}\right)^2}\left\{e^{2K_1(x-2)}-e^{-2K_1x}\right\} \qquad 3.12$$

Now we must find a solution ω_{1H} of the homogenous equation 3.11 so that $\omega_1=\omega_{1P}+\omega_{1H}$ fulfills the boundary conditions 3.11 a.

Because ω_{1P} is of the form $f(x)e^{2it}$, ω_{1H} must be of the same form:

$$\omega_{1H}=g(x)\,e^{2it}$$

From the homogenous equation 3.11 we get for $g(x)$

$$4\alpha^2\left(1-\frac{i\beta}{2}\right)g(x)+g''(x)=0 \qquad 3.13$$

and therefore

$$\left.\begin{aligned} &g(x)=De^{K_2(x-2)}+Ee^{-K_2x}\\ &\text{with}\quad K_2^2=-4\alpha^2\left(1-\frac{i\beta}{2}\right)\end{aligned}\right\} \qquad 3.14$$

$$\left.\begin{aligned}&\text{thus}\quad K_2=K_{2r}+iK_{2i}=\frac{\alpha}{\sqrt{2}}\cdot\\ &\cdot\left(2\sqrt{\sqrt{1+\frac{\beta^2}{4}}-1}+\frac{i\beta}{\sqrt{\sqrt{1+\frac{\beta^2}{4}}-1}}\right)\end{aligned}\right\} \qquad 3.14$$

D and E we can determine in such a way, that ω_1 fulfills the boundary conditions 3.11 a and we find finally:

$$\omega_1=\omega_{1P}+\omega_{1H}=$$

$$=\frac{iA^2K_1e^{2it}}{h^2\,4\beta\alpha^2}\,\frac{\left(1-\frac{\lambda\alpha^2}{K_1^2}\right)}{(1+e^{-2K_1})^2}\left\{e^{2K_1(x-2)}-e^{-2K_1x}-\frac{2K_1}{K_2}\,\frac{(1+e^{-4K_1})}{(1+e^{-2K_2})}\left(e^{K_2(x-2)}-e^{-K_2x}\right)\right\}=$$

$$=\left(1-\frac{\lambda\alpha^2}{K_1^2}\right)\frac{iA^2K_1e^{2it}}{h^2\,4\beta\alpha^2\left(e^{-K_1}+e^{K_1}\right)}$$

$$\left\{e^{2K_1(x-1)}-e^{-2K_1(x-1)}-\frac{2K_1}{K_2}\,\frac{\left(e^{-2K_1}+e^{2K_1}\right)}{\left(e^{K_2}+e^{-K_2}\right)}\left(e^{K_2(x-1)}-e^{-K_2(x-1)}\right)\right\} \qquad 3.15$$

$$\text{with}\quad \alpha=\frac{2\pi L}{\sqrt{gh}\,T};\quad \beta=\frac{\varrho T}{2\pi h};\quad K_\nu=\frac{\alpha}{\sqrt{2}}\left(\nu\sqrt{\sqrt{1+\frac{\beta^2}{\nu^2}}-1}+\frac{i\beta}{\sqrt{\sqrt{1+\frac{\beta^2}{\nu^2}}-1}}\right)$$

and

$$\varphi_1^{(2)}=\frac{1}{2}\left(\omega_1+\bar{\bar{\omega}}_1\right) \qquad 3.16$$

4. Validity of approximating φ by $\varphi_0+\varphi_1$

It was shown in section 3 that we can approximate $\psi=\varphi-(\varphi_0+\varphi_1)$ by $\bar{\psi}$, where $\bar{\psi}$ is determined by

$$\left.\begin{aligned}&-\alpha^2\left(\bar{\psi}_{tt}+\beta\bar{\psi}_t\right)+\bar{\psi}_{xx}=\\ &=-\frac{\partial}{\partial x}\left(\varphi_{0x}\varphi_{1x}+\lambda\alpha^2\varphi_{0t}\varphi_{1t}\right)\\ &\psi_{0x}(0,t)=\bar{\psi}_0(1,t)=0\end{aligned}\right\} \qquad 4.1$$

There are no mathematical difficulties to solve this equation. We shall only integrate it for the case of a long channel for which we may neglect the reflected wave and merely state the result for the general case. From 3.5, 3.9 and 3.15 we get:

$$-\frac{\partial}{\partial x}\left(\varphi_{0x}\varphi_{1t}x+\lambda\alpha^2\varphi_{0t}\varphi_{1t}\right)=$$

$$=-\frac{1}{4}\frac{\partial}{\partial x}\left[\left(\omega_{0x}+\bar{\bar{\omega}}_{0x}\right)\left(\omega_{1x}+\bar{\bar{\omega}}_{1x}\right)+\right.$$

$$\left.+\lambda\alpha^2\left(\omega_{0t}+\bar{\bar{\omega}}_{0t}\right)\left(\omega_{1t}+\bar{\bar{\omega}}_{1t}\right)\right]-$$

$$-\frac{1}{2}\frac{\partial}{\partial x}\left[\left(\omega_{0x}+\bar{\bar{\omega}}_{0x}\right)\varphi_{1x}^{(2)}\right]$$

Therefore we can introduce functions $\bar{\psi}_\nu$ $(\nu=1,2,3)$ for which

$$\left.\begin{aligned}&-\alpha^2\left(\bar{\psi}_{\nu tt}+\beta\bar{\psi}_{\nu t}\right)+\bar{\psi}_{\nu xx}=\\ &=\begin{cases}-\frac{1}{2}\frac{\partial}{\partial x}\left(\omega_{0x}\omega_{1x}+\lambda\alpha^2\omega_{0t}\omega_{1t}\right) & \nu=1\\ -\frac{1}{2}\frac{\partial}{\partial x}\left(\bar{\bar{\omega}}_{0x}\omega_{1x}+\lambda\alpha^2\bar{\bar{\omega}}_{0t}\omega_{1t}\right) & \nu=2\\ -\frac{\partial}{\partial x}\varphi_{1x}^{(2)}\omega_{0x} & \nu=3\end{cases}\end{aligned}\right\} \qquad 4.2$$

holds, and we get then

$$\bar{\psi}=\text{realpart}\left(\bar{\psi}_1+\bar{\psi}_2+\bar{\psi}_3\right) \qquad 4.3$$

For long channels we may neglect e^{-K_ν} compared with one and we get from 3.5, 3.9 and 3.15:

$$\omega_0 = -\frac{A}{hK_1} e^{it} e^{-K_1 x}$$

$$\omega_1 = -\frac{iA^2 K_1}{h^2 4\beta\alpha^2}\left(1 - \frac{\lambda\alpha^2}{K_1^2}\right)\left(e^{-2K_1 x} - \frac{2K_1}{K_2} e^{-K_2 x}\right) e^{2it}$$

Without introducing appreciable errors we may put $\frac{2K_1}{K_2} = 1$ and get

$$f(x) = -\frac{1}{2}\frac{\partial}{\partial x}(\omega_{0x}\omega_{1x} + \lambda\alpha^2\omega_{0t}\omega_{1t}) =$$

$$= Ce^{3it}\frac{\partial}{\partial x}\left[2K_1^2 e^{-K_1 x}(e^{-2K_1 x} - e^{-K_2 x}) - 2\lambda\alpha^2 e^{-K_1 x}\left(e^{-2K_1 x} - \frac{2K_1}{K_2} e^{-K_2 x}\right)\right] =$$

$$= C^*[3K_1 e^{-3K_1 x} - (K_1 + K_2) e^{-(K_1+K_2)x}]$$

with

$$C^* = \left(1 - \frac{\lambda\alpha^2}{K_1^2}\right)^2 \frac{A^3 K_1^2}{h^3 4\beta\alpha^2}$$

Then we can write the equation for $\bar{\psi}$ in the form:

$$\left.\begin{aligned} -\alpha^2(\bar{\psi}_{1tt} + \beta\bar{\psi}_{1t}) + \bar{\psi}_{xx} &= f(x)\, e^{3it} \\ \bar{\psi}_{1x}(0, t) = \bar{\psi}_1(1, t) &= 0 \end{aligned}\right\} \quad 4.4$$

assuming $\bar{\psi}_1 = g(x)e^{3it}$ we get for $g(x)$

$$\left.\begin{aligned} 9\alpha^2\left(1 - \frac{i\beta}{3}\right)g(x) + g''(x) &= \\ = C^*\{3K_1 e^{-3K_1 x} - (K_1 + K_2) e^{-(K_1+K_2)x}\} & \\ g'(0) = g(1) &= 0 \end{aligned}\right\} \quad 4.5$$

Putting $K_3^2 = -9\alpha^2\left(1 - \frac{i\beta}{3}\right)$; realpart $K_3 \geq 0$ we have

$$\frac{g(x)}{C^*} = \frac{3K_1}{9\alpha^2\left(1 - \frac{i\beta}{3}\right) + 9K_1^2}(e^{-3K_1 x} - e^{-(K_1+K_2)x}) -$$

$$-\left[\frac{K_1 + K_2}{9\alpha^2\left(1 - \frac{i\beta}{3}\right) + (K_1 + K_2)^2} - \frac{3K_1}{9\alpha^2\left(1 - \frac{i\beta}{3}\right) + 9K_1^2}\right](e^{-(K_1+K_2)x} - e^{-K_3 x})$$

We only introduce small errors if assuming $K_\nu = K_{1r} + i\nu K_{1i}$. Thus

$$\left|\frac{3K_1}{9\alpha^2\left(1 - \frac{i\beta}{3}\right) + 9K_1^2}(e^{-3K_1 x} - e^{-(K_1+K_2)x})\right| \leq \frac{3|K_1|}{6\beta\alpha^2}\left|e^{-3K_1 x} - e^{-(K_1+K_2)x}\right| \leq \frac{2}{27}\cdot\frac{|K_1|}{\beta\alpha^2}$$

$$\left|\frac{K_1 + K_2}{9\alpha^2\left(1 - \frac{i\beta}{3}\right) + (K_1 + K_2)^2} - \frac{3K_1}{9\alpha^2\left(1 - \frac{i\beta}{3}\right) + 9K_1^2}(e^{-(K_1+K_2)x} - e^{-K_3 x})\right| \leq$$

$$< \frac{1}{4}\left|\frac{K_1 + K_2}{9\alpha^2\left(1 - \frac{i\beta}{3}\right) + (K_1 + K_2)^2} - \frac{3K_1}{9\alpha^2\left(1 - \frac{i\beta}{3}\right) + gK_1^2}\right|$$

and from the last expression one can show that it is smaller than

$\frac{|K_1|}{8\beta\alpha^2}$ for $0 \leq \beta \leq 2$. Therefore

$\bar{\psi}_1 = g(x)e^{3it}$ with $|g(x)| \leq C^*\frac{|K_1|}{\alpha^2\beta}\left(\frac{1}{8} + \frac{2}{27}\right)$

In the same way one can show that the same inequality holds for $\bar{\psi}_2$ and that $\bar{\psi}_3$ is small compared with $\bar{\psi}_1$ and $\bar{\psi}_2$. Now we can decide under which conditions our approximation is valid.

We accept the approximation if

$$\frac{\text{Maximum } |\bar{\psi}_t|}{\text{Maximum } |\varphi_{0t}|} = \frac{\text{maximum } |\text{flow } \varphi_t - \text{approximation } \varphi_{0t} + \varphi_{1t}|}{\text{maximum } |\text{“linear flow”} \ \varphi_{0t}|} \leq$$

Now

$$\frac{\text{maximum } |\bar{\psi}_t|}{\text{maximum } |\varphi_{0t}|} = \frac{h}{A} \frac{|K_1|^2}{\alpha^2 \beta} 4 \left(\frac{1}{8} + \frac{2}{27}\right) |C^*| \leq 0.8 \left|1 - \frac{\lambda \alpha^2}{K_1^2}\right| \frac{A^2}{4h^2} \cdot \frac{1+\beta^2}{\beta^2}$$

therefore the approximation is valid if

$$\frac{A}{h} \leq \sqrt{0.15 \frac{\beta^2}{1+\beta^2} \cdot \frac{1}{\left|1 - \frac{\lambda \alpha^2}{K_1^2}\right|^2}} \qquad 4.7 \qquad \left(\text{Example } \beta = 2; \frac{A}{h} \leq 0.275\right)$$

In the general case we get a similar result

$$\frac{\text{maximum } |\bar{\psi}_t|}{\text{maximum } |\varphi_{0t}|} \leq 0.6 \left|1 - \frac{\lambda \alpha^2}{K_1^2}\right| \left\{ \frac{1}{|1+e^{-2K_1}|} \left(\frac{1}{|1+e^{-2K_2}|} + \frac{1}{3} \frac{1}{|1+e^{-2K_3}|} \right) \frac{A^2}{4h^2} \frac{1+\beta^2}{\beta^2} \right\} \qquad 4.8$$

About the factor $\left|\frac{1}{1+e^{-2K_1}}\right|$ see the next section. $\left|\frac{1}{1+e^{-2K_3}}\right|$ takes its maximum if the channel is so long that the corresponding free oscillation has the period $\frac{T}{3}$. Then $\left|\frac{1}{1+e^{-2K_3}}\right|$ can become quite big if β is small and it may happen that the approximation for this length is not useful. But $\left|\frac{1}{1+e^{-2K_3}}\right|$ can only become as big as 2 or 1.5 for values of $\beta = 2$ and 3 repectively.

5. Estimates of the linear part $\bar{u}_0'$ and the nonlinear part $\bar{u}_1'$

In the first four sections it has been shown that the flow distribution of tidal motions can be approximated—under certain conditions—as the sum of two terms $\bar{u}_0'$ and $\bar{u}_1'$, the first of which represents the solution of the linearized equation 2.4. We can interprete this representation in the following way:

The tides in the open sea (boundary conditions $\zeta'(0,t) = \frac{A}{h} \cos \frac{2\pi}{T} t$) induces the T-periodical oscillation $\bar{u}_0'$. This oscillation itself induces the $1/2 \cdot T$-periodical oscillation $\bar{u}_1'$.

In this section we shall establish some rough measures for $\bar{u}_0'$ and the ratio between the linear part $\bar{u}_0'$ and the nonlinear part $\bar{u}_1'$ in order to get estimates for these quantities. Besides we shall also obtain some important information about the oscillations.

a) measure for $\bar{u}_0'$

From 2.14, 2.15, 3.5 and 3.6 we get

$$\bar{u}_0' = -\text{realpart} \left\{ \frac{A i e^{it}}{(1+e^{-2K_1})} \cdot \frac{1}{hK_1} \left(e^{K_1(x-2)} - e^{-K_1 x}\right) \right\} \qquad 5.1$$

Therefore we can use as a measure for $\bar{u}_0'$

$$m(\bar{u}_0') = \left| \frac{A}{hK_1} \cdot \frac{1}{(1+e^{-2K_1})} \right| = \frac{A}{\alpha h \sqrt[4]{1+\beta^2}} \cdot \frac{1}{|1+e^{-2K_1}|} \qquad 5.2$$

This measure is quite good for not too short channels. For short channels (that means short compared with the wavelength of $\bar{u}_0$)[1] it is bad because α is small compared with one and therefore also $e^{K_1(x-1)} - e^{-K_1(x-1)}$ is small.

Quite interesting is the factor

$$\frac{1}{|1+e^{-2K_1}|} = \frac{1}{\sqrt[2]{(1+e^{-2K_{1r}} \cos 2K_{1i})^2 + e^{-4K_{1r}} \sin^2 2K_{1i}}} \qquad 5.3$$

[1] $\bar{u}_0$ is the velocity in dimensional form; we get it from the nondimensional velocity $\bar{u}_0'$ by inverting the transformation 2.3

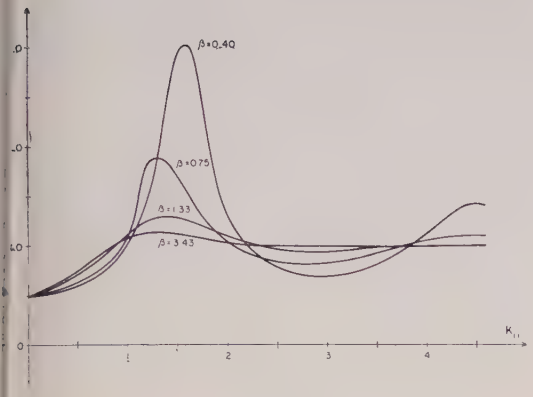

Fig. 3. $\frac{1}{|1+e^{-2K_1}|}$ for different values of β.

This factor reaches its maximum value when the channel is just of the length, for which the corresponding free oscillation has the period T. In Figure 3 we have plotted $|1+e^{-2K_1}|^{-1}$ as a function of the ratio $\frac{\text{channel length } L}{\text{wave length of } \bar{u}_0} = K_{1i} = \frac{\alpha\beta}{\sqrt{2}\cdot\sqrt{\sqrt{1+\beta^2}-1}}$ for different values of β that means for different values of frictional influence, and we see:

in general $|1+e^{-2K_1}|^{-1} \sim 1$ but in the "neighbourhood of resonance" $|1+e^{-2K_1}|^{-1}$ can be quite big if the frictional influence is small.

From 5.3 we see that $|1+e^{-2K_1}|^{-1}$ reaches its first maximum when

$$\cos 2K_{1i} \sim -1$$

or

$$K_{1i} = \frac{\alpha\beta}{\sqrt{2}\cdot\sqrt{\sqrt{1+\beta^2}-1}} = \frac{\pi}{2}$$

now

$$\alpha = \frac{2\pi L}{\sqrt{gh}\,T}$$

and thus resonance for the linear part occurs when

$$L_T = \frac{\sqrt{gh}}{4}\cdot T\cdot\frac{\sqrt{2}\sqrt{\sqrt{1+\beta^2}-1}}{\beta} \qquad 5.4$$

As a mean value for $m(\bar{u}_0')$ we get

$$\frac{1}{\alpha h}\cdot\frac{1}{\sqrt[4]{1+\beta^2}}$$

If we invert the transformation 2.3 we get a measure for the mean velocity

$$\frac{\bar{u}_0}{h} = \frac{1}{h}\int_{-h}^{\zeta} u_0\,dz \text{ and we obtain}$$

$$m\left(\frac{\bar{u}_0}{h}\right) = \sqrt{\frac{g}{h}}\cdot A\cdot\frac{1}{\sqrt[4]{1+\beta^2}} \qquad 5.5$$

b) measure for $r = \frac{\bar{u}_1'}{\bar{u}_0'}$

From equation 3.9, 3.14, 3.15 and 2.15 we get:

$$\bar{u}_1' = -\text{realpart}\left(1-\frac{\lambda\alpha^2}{K_1^2}\right)\frac{A^2K_1^2}{h^2\beta K_2\alpha^2}\cdot\frac{1+e^{-4K_1}}{(1+e^{-2K_1})^2(1+e^{-2K_2})}$$

$$\left\{e^{K_2(x-2)} - e^{-K_2x} - \frac{K_2}{2K_1}\frac{(1+e^{-2K_2})}{(1+e^{-4K_2})}\left(e^{2K_1(x-2)} - e^{-2K_1x}\right)\right\} \qquad 5.6$$

and therefore we can choose as a measure for $r = \frac{\bar{u}_1'}{\bar{u}_0'}$

$$m(r) = \frac{1}{m(\bar{u}_0')}\cdot\left|1-\frac{\lambda\alpha^2}{K_1^2}\right|\frac{A^2|K_1^2|}{h^2\beta|K_2|\alpha^2}\cdot\frac{|1+e^{-4K_1}|}{|1+e^{-2K_1}|^2|1+e^{-2K_2}|} =$$

$$= \left|1-\frac{\lambda\alpha^2}{K_1^2}\right|\cdot\frac{A}{2h}\cdot\frac{\sqrt{1+\beta^2}}{\beta}\cdot\sqrt[4]{\frac{1+\beta^2}{1+\frac{\beta^2}{4}}}\cdot\frac{1}{|1+e^{-2K_1}|}\cdot\frac{|1+e^{-4K_1}|}{|1+e^{-2K_2}|} \qquad 5.7$$

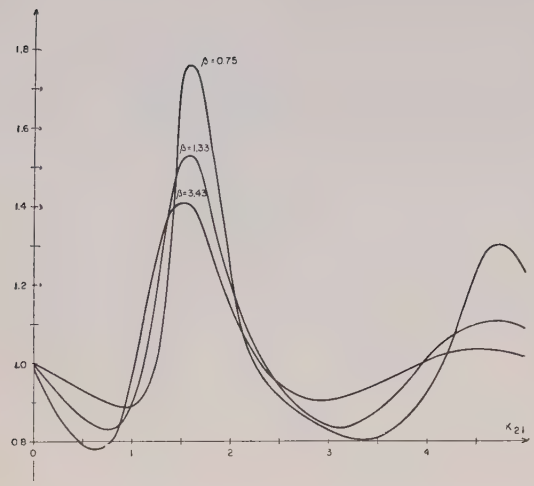

Fig. 4. $|D|^{-1} = \left|\frac{1+e^{-4K_1}}{1+e^{-2K_2}}\right|$ for different values of β.

Besides the already mentioned resonance another resonance can influence $m(r)$ strongly. The length of the channel is such that the corresponding free oscillation has the period $1/2\ T$. Then $|1+e^{-2K_2}|^{-1}$ takes its maximum.

However, the influence of $|1+e^{-2K_2}|^{-1}$ cannot become too strong, because $|1+e^{-4K_1}|$ then is small. In Figure 4 we have plotted $\left|\frac{1+e^{-4K_1}}{1+e^{-2K_2}}\right|$ as a function of

$$K_{2i} = \frac{\text{channel length } L}{\text{wavelength of the nonlinear part } u}$$

for different values of β. We see that $\left|\frac{1+e^{-4K_1}}{1+e^{-2K_2}}\right|$ may become as big as two.

In the same way we can compute when resonance for the nonlinear part $\bar{u}_1$ occurs. We must have

$$K_{2i} = \frac{\alpha\beta}{\sqrt{2}\cdot\sqrt{\sqrt{1+\frac{\beta^2}{4}}-1}} = \frac{\pi}{2}$$

and therefore

$$L_{T/2} = \frac{\sqrt{gh}}{8}\,T\cdot\frac{\sqrt{2}\cdot\sqrt{\sqrt{1+\frac{\beta^2}{4}}-1}}{\frac{\beta}{2}} \qquad 5.8$$

As a mean value for $m(r)$ we get:

$$m(r) = \frac{A}{2h}\,\frac{\sqrt{1+\beta^2}}{\beta}\cdot\sqrt[4]{\frac{1+\beta^2}{1+\frac{\beta^2}{4}}}\cdot\left|1-\frac{\lambda\alpha^2}{K_1^2}\right| = \frac{A}{2h}\,\frac{\sqrt{1+\beta^2}}{\beta}\cdot\sqrt[4]{\frac{1+\beta^2}{1+\frac{\beta^2}{4}}}\cdot\frac{\sqrt{(\lambda+1)^2+\beta^2}}{\sqrt{1+\beta^2}} \qquad 5.9$$

for small β-values we may approximate this expression by

$$m(r) = \frac{A}{h\beta} = \frac{2\pi A}{\varrho T} \quad \text{because } \beta = \frac{\varrho T}{2\pi h};\ \lambda = 1$$

$$\left(\text{example: } T = 12^h = 4.32\cdot 10^4 \text{ sec};\ \varrho = 2\cdot 10^{-3}\left[\frac{\text{m}}{\text{sec}}\right] \text{ and therefore } m(r) = 0.07\,\frac{A}{[\text{meter}]}\right)$$

The last equation shows that for small values of frictional influence $m(r)$ is independent of the depth and only dependent on the coefficient of friction, the period T and the amplitude A. Therefore the nonlinear part is also important, when the depth is large and its influence is particularly strong when resonance occurs, because the frictional influence is small.

But we can go one step further. In hydraulics one uses the following friction law:

$$R(\bar{u}) = \varrho^*\,\frac{|\bar{u}|\bar{u}}{h^2}$$

If therefore the velocities are small we may replace our friction law

$$R(\bar{u}) = \frac{\varrho\bar{u}}{h}$$

by

$$R^*(\bar{u}) = \frac{\varrho^*|\bar{u}_{\max}|\bar{u}}{h^2}$$

From 5.5 we get $|\bar{u}_{\max}| \sim \sqrt{gh}A$ and thus

$$R(\bar{u}^*) = \frac{\varrho^{**}\sqrt{gh}A}{h^2}\bar{u} = \varrho\frac{\bar{u}}{h} \text{ with } \varrho = \varrho^{**}\sqrt{\frac{g}{h}}A.$$

Using this expression for ϱ in equation 5.10 we get

$$m(r) = \frac{2\pi}{\varrho^{**} T}\sqrt{\frac{h}{g}}$$

Now $m(r)$ is also independent of the amplitude A and proportional to $\sqrt{h}$. Even if the depth is large and the amplitude is small the influence of the nonlinear part might be relatively strong. The reason why the influence of the nonlinear part does not tend to 0 more rapidly than the linear part when we let $h \to \infty$, $L \to \infty$ and $A \to 0$ is found from the equation 3.10.

The right side $\omega_{0x}\omega_{0xx}$ of this equation represents an oscillation which converges towards a free oscillation of 3.10 when β tends to 0. Therefore also $\omega_{0x}\omega_{0xx}$ must tend to 0 if ω_1 is to remain finite.

Now we are also in the position to say something about the influence of the term $\frac{\lambda}{h}\bar{u}\bar{u}_x$. We can regard $\bar{u}_1' = \bar{u}_1'(\lambda)$ as a function of λ. We want to compare the influence of this term and the term $gh\zeta\zeta_x$. Therefore we examine the ratio $\left|\frac{\bar{u}_1'(\lambda=1) - \bar{u}_1'(\lambda=0)}{\bar{u}_1'(\lambda=0)}\right|$. From 5.6 we get

$$\left|\frac{\bar{u}_1'(\lambda=1) - \bar{u}_1'(\lambda=0)}{\bar{u}_1'(\lambda=0)}\right| = \frac{1}{\sqrt{1+\beta^2}}, \quad 5.11$$

if β is small compared with one $\frac{1}{\sqrt{1+\beta^2}} \sim 1$. In this case the influence of the term $\frac{\lambda}{h}\bar{u}\bar{u}_x$ is as big as the influence of the term $gh\zeta\zeta_x$. But for $\beta = 3$ its influence is only 30 % of the influence of $gh\zeta\zeta_x$.

6. Discussion of the solution for different cases

In the previous sections we have seen that the flow $\bar{u}'$ is composed by two harmonics $\bar{u}_0'$, $\bar{u}_1'$ which have the periods T, $1/2\ T$ respectively, and that the "nonlinear influence" is particularly strong when resonance occurs. We have also seen that in general only the first resonance is pronounced, which is due to the frictional influence. Therefore we can divide all channels into different classes, with respect to their lengths.

1) The length is small compared with the "resonance length" $L_{T/2}$ (5.8), where resonance for the nonlinear part occurs.
2) The length is in the "neighbourhood" of $L_{T/2}$.
3) The length is in the "neighbourhood" of L_T, where resonance for the linear part occurs. (5.4)
4) The channel is so long that the reflected wave is negligible.

We are therefore going to discuss the following four important cases:

a) short channels
b) infinitely long channels (the reflected wave is negligible)
c) the length is equal to $L_{T/2}$
d) the length is equal to L_T

a) Short chaunels

For a short channel α is small compared with one and we may therefore approximate e^{2K_1} sufficiently well by $1 + 2K_1 + 2K_1^2$. From 5.1 and 5.6 we then get:

$$\bar{u}_0' = -\text{realpart}\ \frac{iA}{h}\frac{e^{it}}{\left(1 + \frac{K_1^2}{2}\right)}(x-1)$$

$$\bar{u}_1' = \text{realpart}\ \frac{4A^2K_1^2(x-1)\,e^{2it}}{h^2(2+K_1)^2(2+K_2^2)}$$

if $|K_1| \leq 0.3$[1] then $|K_2| \leq 0.6$ and we may neglect $\frac{K_1^2}{2}$ against 1.

Therefore:

$$\left.\begin{aligned} \bar{u}_0' &= -\frac{A}{h}|x-1|\sin\frac{2\pi}{T}t \\ \frac{|\bar{u}_1'|}{\max|\bar{u}_0'|} &\leq 0.06\,\frac{A}{h} \end{aligned}\right\} \quad 6.1$$

[1] $|K_1| = \alpha\sqrt[4]{1+\beta^2} = \frac{2\pi L}{\sqrt{gh}\,T}\cdot\sqrt[4]{1+\beta^2}$, if $|K_1| \leq$ ≤ 0.3 then $L \leq \frac{0.3\sqrt{gh}\,T}{2\pi\sqrt[4]{1+\beta^2}}$

Thus we see that we can neglect $\bar{u}_1'$ even when $\frac{A}{h}=0.3$. From the continuity-equation 2.4 b we get

$$\zeta' = \frac{A}{h}\cos\frac{2\pi}{T}t \quad \text{thus} \quad \frac{\partial\zeta'}{\partial x}=0 \qquad 6.2$$

Thus for short rivers with varying cross-section one can put $\frac{\partial\zeta}{\partial x}=0$ and determine $\bar{u}$ from the continuity equation.

Before discussing the other three cases we shall derive a formula for the flow $\bar{u}$ and discuss some general properties of this expression.

From 5.1 and 5.6 we get

$$\bar{u}' = \text{realpart}\left\{\frac{A}{(1+e^{-2K_1})hK_1}\left\{ie^{it}\left(e^{K_1(x-2)}-e^{-K_1x}\right)+\left(1-\frac{\lambda\alpha^2}{K_1^2}\right)\frac{A}{h\beta}\frac{K_1^3}{K_2\alpha^2}\cdot\right.\right.$$

$$\left.\left.\cdot\frac{(1+e^{-4K_1})}{(1+e^{-2K_1}(1+e^{-2K_2})}e^{2it}\left(e^{K_2(x-2)}-e^{-K_2x}-\frac{K_2}{2K_1}\frac{(1+e^{-2K_2})}{(1+e^{-4K_1})}\left[e^{2K_1(x-2)}-e^{-2K_1x}\right]\right)\right\}\right\} \qquad 6.3$$

writing

$$\left.\begin{aligned} K_1=|K_1|e^{i\vartheta_1} \quad K_2=|K_2|e^{i\vartheta_2} \quad \left(1-\frac{\lambda}{K_1^2}\right)=|E|e^{i\vartheta_3} \\ \frac{1}{1+e^{-2K_1}}=|B|e^{ib};\ \frac{(1+e^{-4K_1})}{(1+e^{-2K_1})(1+e^{-2K_2})}=|C|e^{ic};\ \frac{1+e^{-2K_2}}{1+e^{-4K_1}}=|D|\cdot e^{id} \end{aligned}\right\} \qquad 6.4$$

we get

$$\bar{u}'=\frac{A|B|}{h|K_1|}\,\text{realpart}\left\{l_1(-K_1x)+\frac{A|K_1|^3}{h\beta|K_2|\alpha^2}|E||C|\left[l_2(-K_2x)-\frac{|K_2|}{2|K_1|}|D|\,l_2(-2K_1x+d)\right]\right\}-$$

$$-\frac{A|B|}{h|K_1|}\,\text{realpart}\left\{l_1[K_1(x-2)]+\frac{A|K_1|^3}{h\beta|K_2|\alpha^2}|E||C|\left[l_2[K_2(x-2)-\frac{|K_2|}{2|K_1|}|D|\,l_2[2K_1(x-2)+d]\right]\right\}$$

$$\text{where } l_1(s)=e^{i\left(t+\frac{\pi}{2}-\vartheta_1+b+s\right)} \quad l_2(s)=e^{i(2t+2\vartheta_1-\vartheta_2+c+b+\vartheta_3+s)} \qquad 6.5$$

In general we may put $d=0$, $K_{1r}=K_{2r}$, $K_{2i}=2K_{1i}$, without introducing too large errors.

Using the abbreviation $t^*=t-\vartheta_1-K_{1i}x+b$ we get

$$\bar{u}_1'=-\frac{A}{h}\frac{B}{|K_1|}e^{-K_{1r}x}\cdot$$

$$\cdot\left\{\sin t^*+\frac{EA|K_1|^3}{h\beta|K_2|\alpha^2}|C|\cos\left[2t^*+(4\vartheta_1-\vartheta_2-180)+\vartheta_3\right]\left(1-\frac{|K_2|}{2|K_1|}\cdot|D|e^{-K_{1r}x}\right)\right\}+$$

$$+\frac{A}{h}\frac{|B|}{|K_1|}e^{K_{1r}(x-2)}\left\{\sin\left[t^*+2K_{1i}(x-1)\right]+\frac{EA|K_1|^3}{h\beta|K_2|\alpha^2}|C|\right.$$

$$\left.\cos\left[2t^*+(4\vartheta_1-\vartheta_2-180)+\vartheta_3+4K_1(x-1)\right]\cdot\left(1-\frac{|K_2|}{2|K_1|}|D|e^{K_{1r}(x-2)}\right)\right\} \qquad 6.8$$

From the last equation we see that $\bar{u}'$ is composed of two waves which are of the same structure and only differ in magnitude and phase. The first part represents the entering wave while the second part represents the reflected wave. Both waves consist of a linear part and a nonlinear part and there are two extreme cases for the superposition of the nonlinear parts.

i) if $2K_{1i}(x-1)=-\frac{\pi}{2}$ both parts are of the same form with respect to time and have the same sign.

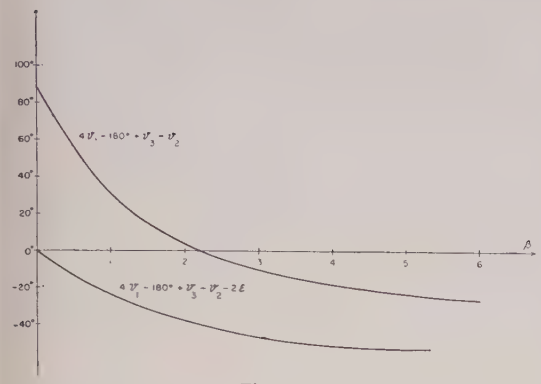

Fig. 5.

ii) if $2K_{1i}(x-1) = -\pi$ the parts are of the same form with respect to time but have different signs. We thus find that the nonlinear influence is strongest in the case i) while in case ii) it is much reduced. A closer examination follows.

i) $2K_{1i}(x-1) = -\frac{\pi}{2}$

From 3.4 we get

$$\frac{2K_{1r}(x-1)}{2K_{1i}(x-1)} = \frac{K_{1r}}{K_{1i}} = \frac{\sqrt{1+\beta^2}-1}{\beta}$$

$$\text{now } 2K_{1i}(x-1) = -\frac{\pi}{2}$$

$$\text{and therefore } 2K_{1r}(x-1) = -\frac{\pi}{2}\frac{\sqrt{1+\beta^2}-1}{\beta}$$

Introducing this value into 6.8 we get

$$\bar{u}' = -\frac{A|B|}{h|K_1|}e^{-K_{1r}x}\left\{\sin t^* + e^{-\frac{\pi}{2}\frac{\sqrt{1+\beta^2}-1}{\beta}}\cdot\cos t^* + H\cos\left[2t^* + (4\vartheta_1 - \vartheta_2 - 180) + \vartheta_3\right]\right\} \quad 6.9$$

with

$$H = \frac{EA|K_1|^3}{h\beta|K_2|\alpha^2}|D|\left\{1 - \frac{|K_2|}{2|K_1|}|D|e^{-K_{1r}x} + \left(1 - \frac{|K_2|}{2|K_1|}|D|e^{K_{1r}(x-2)}\right)e^{2K_{1r}(x-1)}\right\}$$

therefore we can write 6.9 in the form

$$\bar{u}' = -\frac{A|B|}{h|K_1|}e^{-K_{1r}x}$$

$$\{F\sin(t^*+\varepsilon) + H\cos[2t^* + (4\vartheta_1 - \vartheta_2 - 180) + \vartheta_3]\} \quad 6.10$$

From figure 5 we see that $|4\vartheta_1 - \vartheta_2 - 180° + \vartheta_3 - 2\varepsilon| < 90°$. Now two cases are possible: 1) $H > 0$ then we have for all β-values

$$\text{maximum } \bar{u}_F > \text{maxium } \bar{u}_E$$

One can see this from figure 6—7 where we have plotted the curves

$$\left.\begin{aligned} &-[\sin t + 0.2\cos(2t + 90°)]; \\ &-(\sin t + 0.2\cos 2t) \end{aligned}\right\} \quad 6.11$$

and we see that if $\bar{u}' = -[\sin t^* + a\cos(2t^* + \eta)]$ with $0 \leq |\eta| < 90°$, $a > 0$ the last inequality holds and that the unsymmetry is most pronounced for $\eta = 0°$ while it vanishes for $\eta = 90°$.

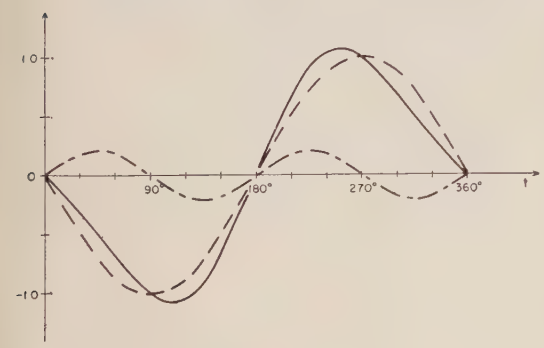

Fig. 6.

— — — — = − sint —·—·—· = − 0.2 cos (2t + 90)

——————— = − (sint + 0.2 cos (2t + 90))

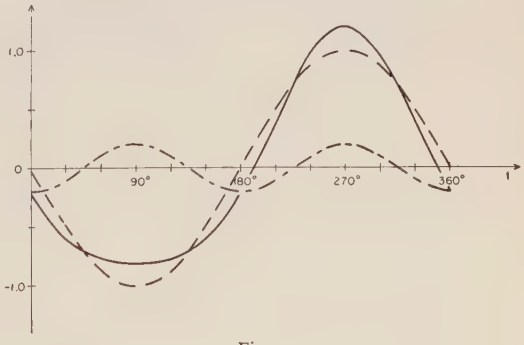

Fig 7.

— — — — = − sint —·—·—· = − 0.2 cos 2t

——————— = − (sint + 0.2 cos 2t)

2) $H \leq 0$

Then: maximum $\bar{u}_F \leq$ maximum $\bar{u}_E$. [This can only happen for extreme values of β. With aid of Fig. 3 one can compute that $H > 0$ for $\beta \geq 0.5$, and this condition for β is usually fulfilled.]

ii) $2K_{1i}(x-1) = -\pi$

Now

$$\bar{u}' = -\frac{A|B|}{h|K_1|} e^{-K_{1r}x} \{M \sin t^* + N \cos [2t^* + (3\vartheta_1 - 180) + \vartheta_3]\} \qquad 6.12$$

with

$$M = 1 + e^{2K_{1r}(x-1)} \quad N = \frac{|K_1|^3}{h\beta|K_2|\alpha^2} |C| \left\{ 1 - \frac{|K_2|}{2|K_1|} |D| e^{-K_{1r}x} - \left(1 - \frac{|K_2|}{2|K_1|} |D| e^{K_{1r}(x-2)} \right) e^{2K_{1r}(x-1)} \right\}$$

In the previous case we found that in general

maximum $\bar{u}_F >$ maximum $\bar{u}_E$

but now

maximum $\bar{u}_F <$ maximum $\bar{u}_E$ 6.13

at the mouth of the channel. Then $2K_{1i} \sim \pi$, $e^{-K_{1r}x} \sim 1$, $|D| > 1$, and with the aid of Fig. 3, one can compute that

$$1 - \frac{|K_2|}{2|K_1|} |D| - \left(1 - \frac{|K_2|}{2|K_1|} |D| e^{-2K_{1r}} \right) e^{-2K_{1r}} < 0$$

for not too big values of β (for ex. $\beta = 1.3$) and therefore $N < 0$. We get the inequality 6.13 since Figure 5 shows that $4\vartheta_1 - \vartheta_2 - 180 + \vartheta_3$ is varying between 90° and − 20° while β is changing from 0 till 5.

b) Long channels

We may neglect the reflected wave and put $|B| = |C| = |D| = 1$; $b = c = d = 0$.

Then

$$\bar{u}' = -\frac{A}{h|K_1|} e^{-K_{1r}x} \left\{ \sin t^* + E \frac{A|K_1|^3}{h\beta|K_2|\alpha^2} \cos [2t^* + (4\vartheta_1 - \vartheta_2 - 180) + \vartheta_3] \left(1 - \frac{|K_2|}{2|K_1|} e^{-K_{1r}x} \right) \right\} \qquad 6.14$$

From this equation and Fig. 5 we get for tidal currents in long channels

maximum $\bar{u}_F >$ maximum $\bar{u}_E$

when friction is taken into account, because $1 - \frac{|K_2|}{2|K_1|} e^{-K_{1r}x} > 0$. Furthermore we see that the relatively strongest influence of the non-linear component occurs at the end of the channel and that this component takes its absolute biggest value W when $e^{-K_{1r}x} = 1 - \frac{|K_1|}{|K_2|}$

$$W = \frac{EA^2|K_1|^2}{\beta h^2|K_2|\alpha^2} \left(1 - \frac{|K_1|}{|K_2|} \right) \left(\frac{3}{2} - \frac{|K_2|}{2|K_1|} \right) \cdot \frac{2\pi L}{T} \qquad 6.15$$

Examples:

$h = 5$ m $\quad \beta = 2 \quad A = 1.5$ m $\quad W = 0.11$ m/sec.

$h = 5$ m $\quad \beta = 3 \quad A = 1.5$ m $\quad W = 0.2$ m/sec.

c) Channels with length equal to $L_{T/2}$

Here $2K_{1i} = \frac{\pi}{2}$ (see 5.8) and for $x = 0$ we get the case that has been discussed earlier (see 6.10). The nonlinear components of the two waves (see 6.8) are of the same form with respect to time and have the same sign. Because of resonance these components are relatively large and therefore the nonlinear influence is particularly strong. With aid of equation 6.8 one can show that also for the points $0 < x < 1$

maximum $u_F >$ maximum u_E

d) Channels with length equal to L_T

We have $2K_{1i} = \pi$. For $x = 0$, $x = 1/2$ we get the cases discussed in connection with equation 6.10, 6.12 respectively. Therefore we get for the first part of the channel

maximum $u_F <$ maximum u_E

For $x = 1/2$, the inequality changes into

maximum $u_F >$ maximum u_E

and one can show that this last inequality holds for all points with $1 > x > 1/2$.

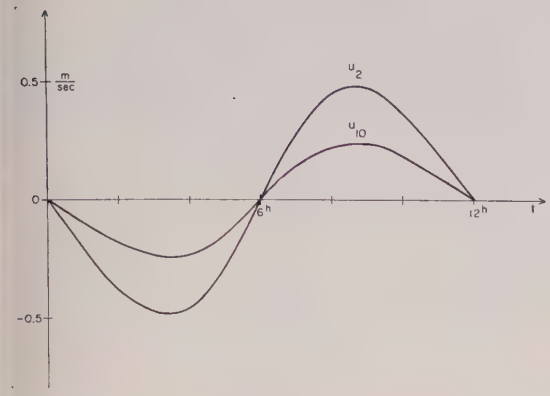

Fig. 8.

: 20 km long channel. Mean velocity $u_i = \dfrac{\overline{u}_i}{(h_i + \zeta_i)}$ in the points $x_i = i$ km. x_i = distance from the mouth. The positive values represent the flood current.

7. Some numerical computations

For comparison with our theory we shall discuss some numerical solutions of the equation 2.1 which have been obtained using the method of finite differences (cf. HANSEN, 1956.) The friction term is changed to

$$R(\bar{u}) = \frac{\varrho|\bar{u}|\bar{u}}{h^2}$$

and it is interesting to see that this does not change the structure of the solutions.

In Figure 8 we have plotted the tidal currents in a 20 km long and 10 meter deep channel.[1] Our theory is confirmed because at every point the deviation from the theoretically expected value is ≤ 0.02 m/sec (sec equations 6.1, 6.2).

In Figure 9 the tidal currents in a 50 km long and 10 meter deep channel have been plotted. According to our theory we have resonance for the nonlinear part and the numerical computation shows the same: very pronounced nonlinear influence.

In Figure 10 the tidal currents in a 98 km long and 10 meter deep channel is shown. Also here theory and computation give qualitatively the same result: resonance for the linear component occurs and we get a flow distribution as theoretically obtained for channels with length equal to L_T.

[1] In all cases is $\varrho = 1 \cdot 10^{-3}$.

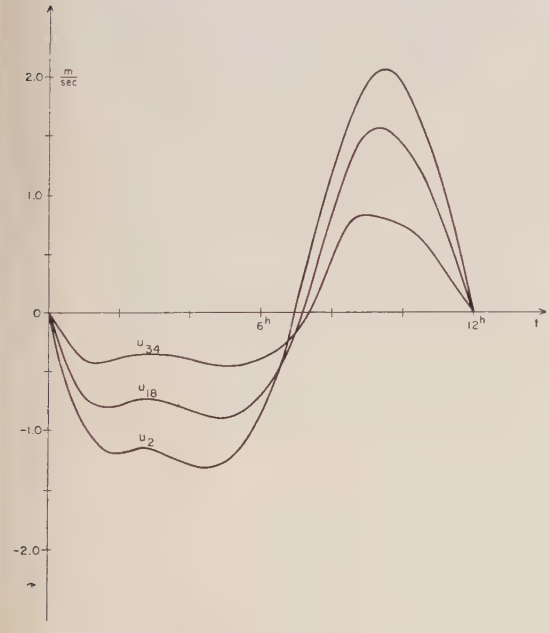

Fig. 9. : 50 km long channel. Mean velocity u_i in the points $x_i = i$ km.

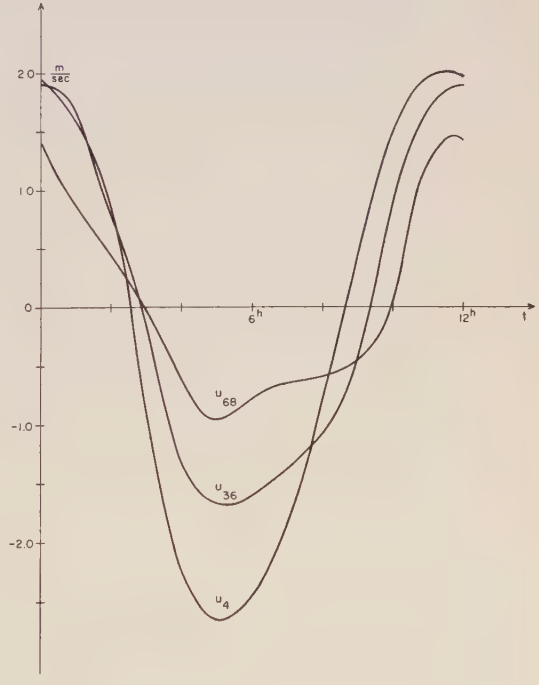

Fig. 10. 98 km long channel. Mean velocity u_i in the points $x_i = i$ km.

8. Acknowledgements

The author wishes to express his sincere thanks to Professor C.-G. Rossby and to Dr. P. Welander for many valuable discussions. Parts of this investigation has been made possible by grants from the "Deutsche Forschungsgemeinschaft". The numerical computations has been carried out on the electronic computer BESK in Stockholm.

REFERENCES

Hansen, W., 1956: Theorie zur Errechnung des Wasserstandes und der Strömungen in Randmeeren nebst Anwendungen, *Tellus*, **8**, pp. 287—300.

Lamb, H., 1932: *Hydrodynamics*, pp. 251—281.

Stoker, J., 1948: *Comm. Appl. Math.*, **11**, pp. 1—80.

A Heuristic Theory of Large-Scale Turbulence and Long-Period Velocity Variations in Barotropic Flow

By PHILIP DUNCAN THOMPSON, Lt. Colonel, U.S. Air Force. Joint Numerical Weather Prediction Unit, Washington, D.C.

(Manuscript received March 23, 1956)

Abstract

By combining an equation for the conservation of zonal momentum with the eddy vorticity equation for nondivergent barotropic flow through a channel, it has been found possible to express the time variations of the longitude-averaged zonal wind in terms of the mean zonal wind itself and certain statistics of the eddy velocity field. In large-scale turbulence—where the characteristic dimension of the eddies is comparable with the entire "width" of the flow—these eddy statistics take on the properties of autocorrelation functions; thus, they depend primarily on the overall scale of the eddies and intensity of turbulence, rather than on details of the flow pattern. Changes in the scale and intensity of large-scale turbulence are related to changes in the mean zonal flow through the principles of conservation of total kinetic energy and variance of vorticity. Under a general hypothesis regarding the "stability" of the eddy statistics, the equations for the zonally-averaged motion comprise a complete system of nonlinear equations, which can be integrated by finite-sum and -difference methods. Accordingly, these equations constitute a mathematical theory of large-scale "free" turbulence, and provide the basis for a numerical method of predicting the zonally-averaged motion.

With the assumption that the eddy scale is invariant, the equation governing the mean zonal wind takes a form related to that of the classical wave equation. Numerical integrations of this equation verify that extremes of mean zonal wind (e.g., pronounced jets) maintain their identity over long periods of time, and migrate either northward or southward (or in both directions at once) in a very regular way—a phenomenon that has been observed by RIEHL ET AL. (1950). The results also show that a strong jet in the mean westerlies tends to split into two weaker jets, which then move in opposite directions to produce the separated double jet structure typical of widespread blocking. The latter has been described as a characteristic denouement from strong zonal flow by CRESSMAN (1950). The theoretical speed of migration of extremes in the mean zonal wind is found to agree closely with the observed speed in a case where published data are available.

Since these features of long-period velocity variations—the most striking and regular discovered to date—have a characteristic time scale of a week or two, numerical prediction methods based on the present theory show some promise of aiding in the preparation of extended-range forecasts.

1. Introduction and General Remarks

During the past year or so, increasing attention has been focussed on the possibility of applying hydrodynamical theory to the problem of long range weather prediction. The modest and rather recent successes of dynamical methods in *short* range prediction have shown that even the simple theory underlying present methods is a fair description of the atmosphere's behavior on a large scale and over short periods of time. In a manner of speaking, the theory of adiabatic nonviscous flow appears

to describe the "internal" dynamics of the atmosphere—i.e., the manner in which the state of the atmosphere would evolve from a given initial state, without absorption of heat energy from external sources, and without the forces of viscosity whereby kinetic energy is dissipated into heat energy and (in the latter form) ultimately emitted to space. Accordingly, since the general physical laws that govern the atmosphere's internal dynamics are also those which control its reaction to energy input and output, one should expect that some more general formulation of hydrodynamical theory would provide a sound basis for methods of long range prediction.

Considering the problem in extreme, it is evident that a special theory of adiabatic nonviscous flow is not general enough to account for *very long* period changes—as, for instance, the change of seasons. In this case, it is clear that the change does not depend as much on the state of the atmosphere at some arbitrarily specified time in the remote past as it does on the cumulative effect of energy input and output. In short, whether the theory of adiabatic nonviscous flow is or is not capable of predicting changes over a period of given length is probably a question of degree, depending on the length of the period. The "transition" period, which is undoubtedly related in some way to the time required to dissipate a large fixed fraction of the relative kinetic energy in the absence of heat sources (or to build it up from the state of relative rest), has been variously estimated from several days to a week or so.

Viewed in this light, the problem of forecasting over periods of a few days might reasonably be approached from the standpoint of integrating the equations for adiabatic nonviscous flow in their usual "two"- or three-dimensional form. This is a particularly attractive approach, for it involves merely extending the period over which the present equations[1] for short range prediction are to be integrated. Preliminary efforts to explore this approach have already been made, in fact, by Bergthorsson and collaborators (1955), and more recently by the Joint Numerical Weather Prediction Unit (JNWPU). Both groups have found that the simplest of methods (based on the equations for barotropic flow) predicts most of the change in the very large scale flow patterns over periods up to three days, without regard to the actual input or output of energy or, for that matter, the transformation of potential to kinetic energy. In the few instances where the predictions were extended over longer periods, there was a marked decrease in accuracy—partially, no doubt, due to shortcomings of the *physical* model, but possibly due to the accumulation of errors that are purely *mathematical* in origin.

This same general approach to the problem of long range forecasting is also illustrated in the recent work of Phillips (1955), who has integrated equations for a model whose *internal* dynamics are expressed in the usual short range prediction equations, but in which the intensity of heat sources varies with latitude and in which kinetic energy is dissipated by simple diffusion of vorticity. Although Phillips' computations were carried out for random initial conditions and were not directly aimed at long range forecasting per se, they still point up the merits and disadvantages of an approach centered around the integration of the hydrodynamical equations in two- or three-dimensional form. In general, Phillips' model displays the main features of behavior of the atmosphere, taken over a long period of time and on a large scale. As in previous attempts at extended numerical integration, the quality of the predictions began to deteriorate rapidly within a few days after the disturbances had grown to appreciable amplitude. In this case, however, the predictions were incorrect only in the sense that they did not reflect some mathematical property of the *differential* equations for the model. Thus, the "errors" of Phillips' computations were due entirely to approximations of the numerical method by which the equations were solved.

Apart from incomplete or inaccurate initial data, the errors of predictions based on hydrodynamical theory may be lumped under the following two main headings:

(1) Errors arising from the introduction of approximations into the general hydrodynamical equations. Since such approximations may radically alter the range and types of phenomena describable by the equations, this kind of error is due essentially to defects of the *physical model.*

[1] Based on the so-called theory of quasi-geostrophic flow.

(2) Errors which are inherent in the numerical methods by which the differential equations are solved—e.g., errors due to finite-difference approximations and roundoff errors. Errors of this class are purely mathematical in character, in the sense that they would be present in numerical integrations of the *general* hydrodynamical equations.

With errors of the first type we shall not be concerned here, except to remark that the *physical* problem confronting us is not so much to discover the general mechanisms of long period changes, as it is to give simple and interpretable mathematical expression to the operation of more or less known mechanisms, in terms of meteorological observables.

With regard to purely mathematical errors, it should be noted that the difficulties of the approach outlined earlier are essentially those of integrating the usual "two"- or three-dimensional form of the equations for quasi-geostrophic flow—difficulties that are enhanced by the fact that the equations are now to be integrated over extended periods of time. Since the quasi-geostrophic equations are nonlinear, they are usually replaced by a corresponding set of finite-difference equations, which are solvable by a sequence of algebraic operations. Now, the condition for (computational) stability of solutions of the finite-difference equations is quite severe, requiring that the integrations be carried out over a long succession of short time intervals, each of the order of an hour. For a forecast period of *fixed* duration, the cumulative effect of roundoff error, truncation error, and nonlinear interactions with those errors does not decrease to zero with an increasing number of submultiple time increments. Thus, if the forecast period is long enough, this effect will obscure all features of meteorological interest.

The situation is further aggravated by the fact that first and higher order finite-differences of the unaveraged isobaric height do not vary smoothly from one point to the next, producing large truncation errors in the approximation of derivatives. Taken together, errors of the type described above generally manifest themselves in increasingly "ragged" contour and vorticity patterns, a symptom of computational distress that is recognizable in the extended predictions of PHILLIPS (1955), BERGTHORSSON ET AL. (1955), and the JNWPU. The *symptoms* may be alleviated rather arbitrarily by any of several methods of intermittent smoothing,[1] but none of these methods guarantees to preserve the correct interaction between components of different scale.

A second difficulty arises from the inaccuracy with which the phase speed of individual circulation centers can be predicted. Owing to the uncertainties of initial state, systematic truncation error and defects of the physical models, the probability that the predicted phase angle is *more* than 90 degrees away from the correct value approaches the probability that it is *less, when the period of the forecast is much in excess of the typical period of the transient fluctuations.* If this is indeed the case, as appears likely, one might as well abandon any attempt to predict zonal variations over long periods, and deal only with zonal averages. This argument alone strongly suggests that the fundamental equations for long range weather prediction should be made to apply to zonally-averaged variables, rather than to their point values.

Returning temporarily to questions of cumulative roundoff and truncation error, one would expect that equations for zonally-averaged motion would involve smaller phase velocities and correspondingly less stringent conditions for computational stability. Further, latitudinal and time variations of zonally averaged variables are quite smooth, so that truncation errors should not accumulate as rapidly in this case as they do in numerical integration of the full "two-" or three-dimensional form of the quasi-geostrophic equations. This surmise is borne out by the results of later sections.

In summary, it appears desirable from the standpoint of reducing purely mathematical errors, and sufficient (in view of ultimate limitations on the detail of accurate long range forecasts) to deal with a new set of derived hydrodynamical equations, which applies to the zonally averaged state of the atmosphere.

There is, in retrospect, another reason for developing a theory of mean motions. Aside from pragmatic questions of forecasting, it would be desirable to interpret the behavior of the atmosphere over long periods of time in terms of relatively simple geometrical and physical concepts. On the face of it, the three-dimensional form of the equations for even

[1] e.g., the methods proposed by PHILLIPS (1955) and SHUMAN (1955).

quasi-geostrophic flow does not lead to such simple concepts. The equations of mean motion, however, do admit of a rather clearcut geometrical interpretation.

Having discussed at length some of the difficulties in applying hydrodynamical theory to the problem of long and "extended" range forecasting, and having discussed several strong motives for dealing with equations for the zonally averaged motions of the atmosphere, we can now state briefly the principal objectives of the remainder of this paper. They are simply to derive a complete system of equations that applies to "zonally averaged" motions, with particular emphasis on an equation for predicting the mean zonal wind profile, and to present a numerical method by which these equations can be integrated. It should also be made clear that the main purpose of this work is not to develop a method of prediction that is immediately applicable to long range forecasting, but to outline and explore a methodology or approach that may lead to greater insight into less special problems of long range prediction.

For simplicity, and to clarify general features of method, we shall deal with the motions of a barotropic, nonviscous fluid, flowing through an infinitely long channel bounded by rigid parallel walls. Our problem, then, is to derive a complete system of equations that applies to the mean motions of this fluid, averaged along lines parallel to the walls and at variable distance from one of the boundaries. In particular, we shall seek to derive and solve an equation for the changes in the mean component of velocity parallel to the walls.

Since the flow under consideration is barotropic and essentially nondivergent, one can state at the outset that it cannot exhibit any feature of behavior which depends in a vital way on energy input or output—simply because potential energy, the intermediary form through which heat energy must pass to be converted into kinetic energy, cannot be transformed into kinetic energy in this model. Nevertheless, it is still conceivable that this model will display some important and typical aspects of long period velocity variations in the atmosphere, *when taken in the mean*. It is generally observed, in fact, that the mechanism of baroclinic instability (by which potential energy is transformed into kinetic energy of the large scale disturbances) operates only sporadically and in sudden bursts, and over only a small fraction of a hemisphere at any given time. Further, sudden increases in the total zonal momentum of the atmosphere over a whole hemisphere occur only once every week or two (vide RIEHL ET AL., 1950), and are percentagewise not very great. For these reasons, one might expect that the variations of *mean* zonal wind in the barotropic model (beginning with equivalent initial conditions) would parallel those of the atmosphere for periods approaching or perhaps slightly exceeding the "transition" period, particularly during the stage immediately following an almost impulsive increase of total kinetic energy. It has already been pointed out that forecasts based on the equation for barotropic flow are fairly accurate *in detail* for periods up to three days. Finally, having excluded the transformation of potential to kinetic energy, it is only consistent to exclude also the dissipation of kinetic energy by viscosity. These conjectures will be confirmed qualitatively and semiquantitatively by reference to data published by CRESSMAN (1950) and RIEHL, YEH and LASEUR (1950).

Turning to the ingredients of any theory of mean motion, one soon sees that a *complete* system of equations for the zonally-averaged motion cannot be derived from the equations of barotropic flow alone. Owing to the fact that the configuration of *unaveraged* flow is not uniquely determined by a given configuration of *averaged* flow, some information is irretrievably lost in the process of averaging. To make up for this loss, it is necessary to state some hypothesis regarding the statistical properties of the "eddies"[1]—i.e., deviations from zonal averages—and/or their interaction with the mean flow itself. The hypothesis to be introduced here capitalizes on the geometry of very large scale eddies, and strictly applies only when the characteristic horizontal dimension of the eddies is comparable with the distance between the "walls" that contain the flow. Interpreted in terms of the atmosphere's dimensions, the distance between "walls" corresponds roughly to the distance from equator to pole; thus, in view of the tre-

[1] It will frequently be convenient to adopt the language of turbulence, so that "eddy", "fluctuation", "disturbance", "deviation", and "perturbation" will be used more or less interchangeably.

mendous scale of atmospheric motions, the "hypothesis of large scale" is superficially a reasonable one. In this same connection, it is important to note that the most effective agencies of mean zonal momentum transport are the disturbances of largest scale.

The aims and viewpoints expressed above are, of course, far from new. In essence, they are the aims and viewponts of a theory of large-scale turbulence, in which the large-scale disturbances are regarded as eddies in a nonlaminar flow; a complete theory of mean motions would, in fact, be a bona fide theory of turbulence. The type of "turbulence" in question is quite different, to be sure, from the usual variety—in that the mean state probably does not approach a quasi-steady asymptotic state. The mean state of the atmosphere's boundary layer, on the other hand, can and does approach such a steady state, simply because small scale eddies are continuously generated by mechanical means and continuously dissipated by viscosity. For this reason, one might characterize large-scale atmospheric disturbances as "free turbulence". Other distinctions between these two types of turbulence —as, for instance, the nondiffusive nature of large-scale eddies—have been pointed out by STARR (1953) and others.

The development of the mathematical theory will center around an equation that expresses the way in which changes in the mean flow depend on the eddy velocity. By introducing the way in which changes in the eddy velocity are related in turn to the mean flow, it is then possible to state how changes in the mean zonal wind depend on the mean flow itself. The information required to arrive at a complete system of equations is the form of certain cross-correlations between turbulent fluctuations. The key point in the development is that, with the introduction of the "hypothesis of large-scale", those cross-correlations take on the properties of normalized auto-correlations—properties that vary only slightly from one day to the next.

The resulting prognostic equation for the mean zonal wind can be integrated by finite-difference methods, beginning with the initial profile of mean zonal wind and the initial transport of zonal momentum. By-products of the integration are indices of the intensity of meridional flow, the characteristic scale of the disturbances, and the latitude of maximum eddy circulation.

To make sure that the behavior of solutions of the mean zonal wind equation is not enforced by a fortuitous choice of initial conditions, the method of integration mentioned above will be applied in a case when the initial transport of zonal momentum vanishes everywhere. In this case, it is easy to see that the fundamental equation has the mathematical form of a wave equation, and that a pronounced "jet" in the mean zonal wind profile tend to move northward or southward at a definite speed, depending partly on the relative dimensions of the disturbances and the jet itself, and partly on the RMS value of the meridional wind. This effect is strongly reminiscent of the phenomenon described by RIEHL (1950). Finally, according to this theory, there is also a tendency for a sharp maximum of mean zonal wind (such as would correspond to strong zonal flow around a large sector of a hemisphere) to split into two distinct maxima, which move apart to produce the "double-jet" structure typical of widespread blocking. The latter phenomenon has been reported by CRESSMAN (1950) as being a fairly characteristic development from strong zonal flow.

2. Fundamental Equations and Boundary Conditions for Barotropic Flow between Parallel Walls

The equations of motion for a nonviscous barotropic fluid may be written in the form:

$$\frac{\partial u}{\partial t}+\frac{\partial}{\partial x}\left(\frac{u^2+v^2}{2}\right)-v(\zeta+f)+\frac{\partial P}{\partial x}=0 \qquad (1)$$

$$\frac{\partial v}{\partial t}+\frac{\partial}{\partial y}\left(\frac{u^2+v^2}{2}\right)+u(\zeta+f)+\frac{\partial P}{\partial y}=0 \qquad (2)$$

where t is time; x and y are coordinate distances parallel and normal to the walls, respectively; u and v are the corresponding components of the horizontal velocity vector; ζ is $(\partial v/\partial x - \partial u/\partial y)$, the vertical component of relative vorticity; and f (assumed to be a linear function of y only) is the Coriolis parameter or vertical component of the earth's vorticity. The function P is

$$\int_{p_0}^{p}\alpha(p')dp'$$

where p is pressure, p_0 is a fixed reference pressure, p' is a dummy variable corresponding to p and α is the specific volume, which in this model is a function of pressure only. Partial differentiations with respect to x, y, and t are carried out holding height fixed.

Since the percentage variations of pressure experienced by individual fluid elements next to the surface are very small over most of the globe, large-scale barotropic flow is essentially nondivergent. Thus, the equation of mass continuity reduces to:

$$\frac{\partial u}{\partial x}+\frac{\partial v}{\partial y}=0 \tag{3}$$

Taken together, Eqs. (1), (2), and (3) comprise a complete system of equations involving the three dependent variables u, v, and P.

One of the fundamental equations in a theory of mean motion may be derived simply by applying the zonal average to each term of Eq. (1). Thus, noting that the averaging operation may be commuted with differentiations with respect to y and t,

$$\frac{\partial \bar{u}}{\partial t}-\overline{v\zeta}-f\bar{v}=0 \tag{4}$$

where the "bar" above a variable denotes its zonal average, defined as

$$\bar{\phi}\equiv\lim_{M\to\infty}\frac{1}{2M}\int_{-M}^{M}\phi\,dx$$

The averages of the second and fourth terms in Eq. (1) vanish, since

$$\overline{\frac{\partial\phi}{\partial x}}\equiv\lim_{M\to\infty}\frac{1}{2M}\left[\phi(M,y,t)-\phi(-M,y,t)\right]$$

In general, therefore, *the zonal average of the x-derivative* of any continuous variable which is always and everywhere finite *must vanish.*[1] This property will be invoked frequently throughout the mathematical development. Eq. (4) may be simplified further by introducing the condition for nondivergent flow—that is, since no fluid passes through either of the walls, the net volume transport across any line parallel to the walls must vanish. Thus, $\bar{v}=0$ and Eq. (4) becomes

$$\frac{\partial \bar{u}}{\partial t}=\overline{v\zeta}=\overline{v'\zeta'} \tag{5}$$

in which the primes denote deviations from zonal means. The equation above simply states that the rate at which the mean zonal wind changes at any "latitude" (line of constant y) is equal to the mean "northward" transport of vorticity at that latitude. In particular, since v vanishes at the walls, it implies that $\bar{u}$ at the walls does not change with time. This boundary condition, as it turns out, is necessary to determine a unique solution of the equations of mean motion.

Eq. (5) may be put into a more familiar form by introducing the definition of ζ and integrating by parts.

$$\overline{v\zeta}=\overline{\frac{\partial}{\partial x}\left(\frac{v^2}{2}-\frac{u^2}{2}\right)}-\frac{\partial}{\partial y}\overline{uv}=-\frac{\partial}{\partial y}\overline{uv}$$

so that Eq. (5) becomes

$$\frac{\partial \bar{u}}{\partial t}=-\frac{\partial}{\partial y}\overline{uv} \tag{6}$$

or, since $\bar{v}=0$

$$\frac{\partial \bar{u}}{\partial t}=-\frac{\partial}{\partial y}\overline{u'v'} \tag{7}$$

Eq. (7) states the well-known fact that the rate at which the mean zonal momentum increases is equal to the convergence of the mean eddy flux of zonal momentum. Integrating both sides of Eq. (6) with respect to y from one wall (at $y=0$) to the other (at $y=W$), we find that

$$\frac{\partial}{\partial t}\int_0^W \bar{u}\,dy=-\left[uv\right]_0^W=0$$

Thus, the total zonal momentum does not vary with time, another fact that will be of considerable use later in the development.

Eq. (5) or Eq. (7) states how changes in the mean zonal wind depend on deviations from purely zonal flow. Our next concern is to express the manner in which changes of the eddy velocity depend on the mean zonal flow itself. The required relationship is found in the

[1] This property can be retained in averages over a finite interval if the flow is periodic—e.g., if the fluid covers the surface of a sphere. In this case, the appropriate modification of the zonal average is to fix the interval of integration at 2π radians of longitude.

vorticity equation, obtained by differentiating Eq. (1) with respect to y, differentiating Eq. (2) with respect to x, and subtracting the first from the second. Since the flow is nondivergent, the vorticity equation takes the form

$$\frac{\partial \zeta}{\partial t} + u\frac{\partial \zeta}{\partial x} + v\frac{\partial \zeta}{\partial y} + \beta v = 0 \qquad (8)$$

where $\beta = df/dy$. Writing each variable as the sum of its zonal mean and the deviation from the mean, applying the averaging operator to Eq. (8), and subtracting the *averaged* equation from Eq. (8), we then find that

$$\frac{\partial \zeta'}{\partial t} + \bar{u}\frac{\partial \zeta'}{\partial x} + v'\frac{\partial \bar{\zeta}}{\partial y} + \beta v' + (\mathbf{V}' \cdot \nabla \zeta')' = 0 \qquad (9)$$

in which $\mathbf{V}$ is the horizontal velocity vector, and ∇ is the horizontal vector gradient. It will be noted that the fifth term in Eq. (9) is the only one that contains products of deviations, a property that distinguishes its statistics from those of terms in which the deviations enter linearly.

As it stands, Eq. (9) does not alone comprise a complete system of equations, for it involves the two dependent variables u and v. The missing information is contained in Eq. (3)—which, since $\bar{v} = 0$, may be written as

$$\frac{\partial u'}{dx} + \frac{\partial v'}{\partial y} = 0$$

This equation implies that there exists an "eddy streamfunction" ψ, such that

$$u' = -\frac{\partial \psi}{\partial y} \qquad v' = \frac{\partial \psi}{\partial x} \qquad \zeta' = \nabla^2 \psi$$

where ∇^2 is the horizontal Laplacian operator. Substituting the expressions above into Eq. (9),

$$\frac{\partial}{\partial t}\nabla^2\psi + \bar{u}\frac{\partial}{\partial x}\nabla^2\psi - \frac{\partial \psi}{\partial x}\frac{\partial^2 \bar{u}}{\partial y^2} + \beta\frac{\partial \psi}{\partial x} + J'(\psi, \nabla^2\psi) = 0 \qquad (10)$$

Eq. (10) states how changes in the eddy streamfunction or eddy velocity depend on $\bar{u}$, the mean zonal flow.

Owing to the elliptic character of Eq. (10), regarded as a linear equation in which $\partial\psi/\partial t$ is the unknown, it is also necessary to specify the values of $\partial\psi/\partial t$ along the walls. To begin with, ψ must be constant along the walls at any given time, for v (or v') must vanish there. Now, the streamfunction contains an additive and arbitrary function of time—i.e., if the function Ψ is a solution of Eq. (10), then so also is the function $\psi = \Psi + f(t)$, simply because ψ does not enter undifferentiated with respect to x or y. Thus, we may choose the function $f(t)$ in such a way that ψ vanishes along $y = 0$ at all times. The value of ψ along $y = W$ may now be calculated from the relation between ψ and u'.

$$\psi(x, W, t) = -\int_0^W u' dy$$

But ψ along $y = W$ is constant at any given time, so that

$$\psi(x, W, t) = \bar{\psi}(W, t) = -\int_0^W \bar{u}' dy = 0$$

Finally, since ψ vanishes along both walls at all times, it follows that $\partial\psi/\partial t$ must also vanish along both walls at all times.

We may now regard Eqs. (5) and (10) as a complete system of equations involving the variables $\bar{u}$ and ψ. Beginning with initial values of ψ and $\bar{u}$ at every point in the flow, one can (in principle) compute $\partial\bar{u}/\partial t$ at all points in the flow from Eq. (5) and extrapolate $\bar{u}$ over a very short interval of time, *except along the walls*. It has already been shown, however, that $\bar{u}$ cannot vary along the walls, so that the distribution of $\bar{u}$ can be regenerated completely at a time slightly later than the initial instant. Similarly, it is possible to calculate $\partial\psi/\partial t$ from the initial distributions of ψ and $\bar{u}$ by solving Eq. (10), subject to the conditions that $\partial\psi/\partial t$ vanish on $y = 0$ and $y = W$. Thus ψ can also be extrapolated from its initial distribution. Finally, since the information available at the initial instant can be regenerated completely at a slightly later time, the process above may be repeated again and again, to compute the distributions of ψ and $\bar{u}$ over a period of any length desired.

This view of the problem of predicting the mean zonal wind speed is essentially the one that will be adopted in the remainder of the mathematical development.

3. The Equation for the Mean Zonal Flow

A method for predicting the mean zonal momentum, proposed several years ago by LORENZ (1952), will serve to point up one of the difficulties in synthesizing a general hypothesis. This method is based on an equation related to Eq. (7), and rests on an assumption whose validity depends on a rather loose empirical correlation between the net eddy transport of zonal momentum and the mean zonal momentum itself. From Eq. (5), however, we infer that the net eddy transport of zonal momentum is equivalent to the mean northward transport of vorticity or, in other words, the cross-correlation between the vorticity ζ and the "northward" component of velocity v. In general, since the fields of ζ and v tend to be almost exactly 90 degrees out of phase, the cross-correlation between them is usually quite small, and is extremely sensitive to small changes in the phase difference or to small changes in the general "shape" of the flow pattern. This suggests that the cross-correlation between v and ζ should not be specified by hypothesis, for the very reason that it is a cross-correlation between quantities which (at any fixed time) bear no direct geometrical relation to each other. Our next concern is to derive an equation for the mean zonal flow, in which the only statistics of the eddy velocity to appear are autocorrelations or cross-correlations between variables whose contemporaneous fields are geometrically related.

An equation of the desired form may be obtained by differentiating Eq. (5) with respect to time.

$$\frac{\partial^2 \bar{u}}{\partial t^2} = \overline{v' \frac{\partial \zeta'}{\partial t}} + \overline{\zeta' \frac{\partial v'}{dt}}$$

Thus, expressing v' and ζ' in terms of ψ, integrating by parts, and noting that $v' = v$,

$$\frac{\partial^2 \bar{u}}{\partial t^2} = \overline{v \nabla^2 \left(\frac{\partial \psi}{\partial t} \right) - \frac{\partial \psi}{\partial t} \nabla^2 v} \qquad (11)$$

This is one of the key equations in the present theory. An important variant of this same equation is derived by rewriting the right hand side of Eq. (11) as

$$\overline{\nabla \cdot \left(v \nabla \frac{\partial \psi}{\partial t} - \frac{\partial \psi}{dt} \nabla v \right)} = \frac{\partial}{\partial y} \overline{v \frac{\partial}{\partial y} \left(\frac{\partial \psi}{\partial t} \right)} - \overline{\frac{\partial \psi}{\partial t} \frac{\partial v}{\partial y}} \qquad (12)$$

The expression above verifies that the total zonal momentum is conserved, if its initial time derivative is zero.

The next step of the development is to eliminate the time derivatives from the right hand side of Eq. (11). This will be done by solving Eq. (10) for $\partial \psi / \partial t$. We first note that Eq. (10) can be put in the form

$$\nabla^2 \left(\frac{\partial \psi}{\partial t} \right) + \bar{u} \nabla^2 v - v \nabla^2 \bar{u} + \beta v + E = 0 \qquad (13)$$

where $E = J'(\psi, \nabla^2 \psi)$. To simplify matters still further, we shall rewrite Eq. (13) as

$$\nabla^2 \left(\frac{\partial \psi}{\partial t} + \bar{u} v \right) = 2 \nabla \cdot v \nabla \bar{u} - \beta v - E \qquad (14)$$

The equation above will now be multiplied by the function

$$G = -\frac{1}{4\pi} \ln \left[\frac{\sinh^2 \frac{\pi}{2W}(\xi - x) + \sin^2 \frac{\pi}{2W}(\eta - y)}{\sinh^2 \frac{\pi}{2W}(\xi - x) + \sin^2 \frac{\pi}{2W}(\eta + y)} \right]$$

in which ξ and η are dummy variables corresponding to x and y, respectively. This function is the so-called Green's function for an infinitely long strip of width W.[1] The relevant properties of G are that:

(1) $\nabla^2 G = \frac{\partial^2 G}{\partial \xi^2} + \frac{\partial G}{\partial \eta^2} = 0$ except at the point (x, y)

(2) G vanishes when $\eta = 0$, $\eta = W$, or when $\xi \to \pm \infty$

(3) $\frac{\partial G}{\partial \xi}$ vanishes when $\xi \to \pm \infty$

(4) G behaves like $-\frac{1}{2\pi} \ln r$, where $r^2 = (\xi - x)^2 + (\eta - y)^2$, for very small r.

[1] The Green's function may be visualized as the displacement at the point (ξ, η) of an elastic membrane rigidly fixed to two parallel rods a distance W apart, when a steady concentrated force is applied at the single point (x, y).

A consequence of this property is that

$$\lim_{\varrho \to 0} \int_0^{2\pi} \left(\frac{\partial G}{\partial r}\right)_C \varrho d\Theta = -1$$

in which ϱ is the radius of a very small circle C with center at (x, y), and Θ is the angle between the x-axis and a line from the fixed point (x, y) to the variable point (ξ, η) on the circle C. Making use of standard vector identities and property (1) of the function G, we may write Eq. (14) in the form

$$\nabla \cdot \left[G \nabla \left(\frac{\partial \psi}{\partial t} + \bar{u} v \right) - \left(\frac{\partial \psi}{\partial t} + \bar{u} v \right) \nabla G \right] =$$

$$= 2 \nabla \cdot G v \nabla \bar{u} - 2 v \nabla G \cdot \nabla \bar{u} - \beta G v - G E \quad (15)$$

Each term of the equation above is now integrated over the area A, bounded by the walls and a small circle C of radius ϱ with center at (x, y), as shown in Fig. 1. By the application

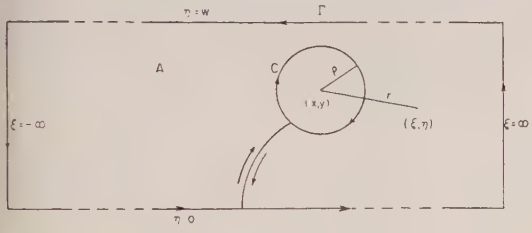

Fig. 1. Path of integration by Green's method.

of Gauss' theorem, the area integrals of the left hand side and first term on the right hand side of Eq. (15) can be transformed immediately into line integrals taken around the path Γ indicated by arrows on Fig. 1, with the result that

$$\oint_\Gamma \left[G \frac{\partial}{\partial n} \left(\frac{\partial \psi}{\partial t} + \bar{u} v \right) - \left(\frac{\partial \psi}{\partial t} + \bar{u} v \right) \frac{\partial G}{\partial n} \right] dl =$$

$$= 2 \oint_\Gamma G v \frac{\partial \bar{u}}{\partial n} dl - \int_A (2 v \nabla G \cdot \nabla \bar{u} + \beta G v + G E) dA \quad (16)$$

where a derivative with respect to n is the component of the vector gradient normal to the right of the path Γ, dl is an increment of length along Γ and dA is an area increment of A.

We now investigate the line integrals that enter into Eq. (16). To begin with, the contributions from integrating down one side and back along the other side of the "cut" adjoining the line $\eta = 0$ and the circle C exactly cancel. Moreover, owing to properties (2) and (3) of the function G, and because v and $\partial\psi/\partial t$ vanish on the walls, the line integrals around the outer boundary of A vanish. It remains to evaluate the limit of the line integrals around the circle C, as the radius ϱ approaches zero. Now, since $\bar{u}$, v, and $\partial\psi/\partial t$ are continuous at (x, y), the first term on the right hand side of Eq. (16) vanishes entirely in the limit, and the remainder of the equation reduces to:

$$\lim_{\varrho \to 0} \int_0^{2\pi} \left(\frac{\partial \psi}{\partial t} + \bar{u} v \right)_C \left(\frac{\partial G}{\partial r} \right)_C \varrho d\Theta$$

$$= - \int_A (2 v \nabla G \cdot \nabla \bar{u} + \beta G v + G E) dA$$

It is now understood that the region A covers the *entire* area between the walls. Making use of property (4) of the function G,

$$\frac{\partial \psi}{\partial t} + \bar{u} v = \int_0^W \int_{-\infty}^{\infty} (2 v \nabla G \cdot \nabla \bar{u} + \beta G v + G E) d\xi d\eta \quad (17)$$

where v, $\bar{u}$, and E are to be regarded as functions of ξ and η, wherever they appear under the integral signs. Finally, the expressions for $\nabla^2(\partial\psi/\partial t)$ and $\partial\psi/\partial t$, given by Eqs. (13) and (17), will now be substituted into Eq. (11).

$$\frac{\partial^2 \bar{u}}{\partial t^2} = \bar{v}^2 \frac{\partial^2 \bar{u}}{\partial y^2} - 2 \nabla^2 \overline{v \int_0^W \int_{-\infty}^{\infty} v \nabla G \cdot \nabla \bar{u} d\xi d\eta}$$

$$- \beta \left(\overline{v^2} + \nabla^2 \overline{v \int_0^W \int_{-\infty}^{\infty} G v d\xi d\eta} \right)$$

$$- \left(\overline{vE} + \nabla^2 \overline{v \int_0^W \int_{-\infty}^{\infty} G E d\xi d\eta} \right) \quad (18)$$

This equation forms the basis for most of the remaining discussion.

It was pointed out earlier that E is the only term of Eq. (13) that involves products of deviations. One may, therefore, think of E

as representing the interaction of the eddies with themselves, and regard $\overline{vE}$ as an effect of the auto-interaction of eddies on the mean zonal flow. By definition,

$$\overline{vE} = \overline{v\left(\mathbf{V}' \cdot \nabla \zeta' - \overline{\mathbf{V}' \cdot \nabla \zeta'}\right)}$$

or, since $\bar{v} = 0$,

$$\overline{vE} = \overline{v'\left(u' \frac{\partial \zeta'}{\partial x} + v' \frac{\partial \zeta'}{\partial y}\right)}$$

Integrating by parts, we find that the equation above can be rewritten in the form

$$\overline{vE} = \frac{\partial}{\partial y} \overline{\zeta'(v'^2)'} - \overline{u'(\zeta'^2)'} - \overline{\zeta' \frac{\partial}{\partial y}\left(\frac{u'^2 + v'^2}{2}\right)'}$$

Thus, $\overline{vE}$ depends essentially on correlations between the deviation of one quantity and the deviation of the *square of the deviation* of another quantity. Now, in very large scale eddies the deviation fields u', v', and ζ' are of about the same scale, whereas the scale of the deviations of the *squares* of u', v', and ζ' is almost exactly *half* that scale. Accordingly, the fields of u', v', and ζ' tend to be uncorrelated with the fields of $(u'^2)'$, $(v'^2)'$, and $(\zeta'^2)'$, *without regard to the relative phases of those fields.* For this and similar reasons, the terms in Eq. (18) that involve E will be omitted. This simplification implies that the changes in the *mean* zonal flow are brought about primarily through the interaction of the eddies with the mean flow itself, rather than by the auto-interaction of eddies.

Our next concern is to isolate the effect of the eddies on the mean zonal flow. To do so, we shall investigate the correlation between $\nabla^2 v$ and the integrals on the right hand side of Eq. (18), a typical example of which is the expression

$$\overline{I = L(x, y) \int_0^W \int_{-\infty}^{\infty} G(\xi - x, y, \eta) v(\xi, \eta) d\xi d\eta}$$

where the symbol $L(x, y)$ stands for $\nabla^2 v$ at the point (x, y). Noting that x and ξ enter into G only in the combination $(\xi - x)$, and introducing a new variable of integration τ, equal to $(\xi - x)$,

$$\overline{I = L(x, y) \int_0^W \int_{-\infty}^{\infty} G(\tau, y, \eta) v(x + \tau, \eta) d\tau d\eta}$$

or, rearranging the order of integration,

$$I = \int_0^W \int_{-\infty}^{\infty} G(\tau, y, \eta) \overline{L(x, y) v(x + \tau, \eta)} d\tau d\eta$$

Finally, since $\overline{L(x, y) v(x, y)}$ is not a function of τ or η,

$$I = \overline{v \nabla^2 v} \int_0^W \int_{-\infty}^{\infty} G(\tau, y, \eta) R(\tau, y, \eta) d\tau d\eta$$

in which $R(\tau, y, \eta)$

$$= \overline{L(x, y) v(x + \tau, \eta)} / \overline{L(x, y) v(x, y)}.$$

Analogous procedures may be applied to transform the second term on the right hand side of Eq. (18), with the result that

$$\frac{\partial^2 \bar{u}}{\partial t^2} = \overline{v^2}\left[\frac{\partial^2 \bar{u}}{\partial y^2} + \frac{2}{\lambda^2} \int_0^W \int_{-\infty}^{\infty} R \nabla G \cdot \nabla \bar{u} d\tau dn - \beta\left(1 - \frac{1}{\lambda^2} \int_0^W \int_{-\infty}^{\infty} R G d\tau d\eta\right)\right] \quad (19)$$

where $\lambda(y)$ is given by $\lambda^{-2} = -\overline{v \nabla^2 v} / \overline{v^2}$.

To simplify Eq. (19) still further, we note that the area integral in the second term in brackets may be transformed as follows:

$$J = \int_0^W \int_{-\infty}^{\infty} R \nabla G \cdot \nabla \bar{u} d\tau d\eta$$

$$= \int_0^W \int_{-\infty}^{\infty} (\nabla \cdot R \bar{u} \nabla G - \bar{u} \nabla R \cdot \nabla G - \bar{u} R \nabla^2 G) d\tau d\eta$$

$$= \bar{u}(y) R(0, y, y) - \int_0^W \int_{-\infty}^{\infty} \bar{u} \nabla R \cdot \nabla G d\tau d\eta$$

But, by definition, $R(0, y, y) = 1$. Moreover,

$$\int_0^W \int_{-\infty}^{\infty} \nabla R \cdot \nabla G d\tau d\eta = \int_0^W \int_{-\infty}^{\infty} (\nabla \cdot R \nabla G - R \nabla^2 G) d\tau d\eta = 1 \quad (20)$$

Thus, letting $\bar{u} = U + \frac{1}{W}\int_0^W \bar{u}dy$, we may rewrite the integral J as

$$J = \bar{u} - \frac{1}{W}\int_0^W \bar{u}dy - \int_0^W\int_{-\infty}^{\infty} U(\eta)\nabla R \cdot \nabla G d\tau d\eta$$

$$= U - \int_0^W U(\eta)F(y, \eta)d\eta$$

where $F(y, \eta) = \int_{-\infty}^{\infty} \nabla R \cdot \nabla G d\tau$. Finally, since it has already been shown that $\int_0^W \bar{u}\, dy$ does not vary with time, Eq. (19) can be put in the form

$$\frac{\partial^2 U}{\partial t^2} = \overline{v^2}\left[\frac{\partial^2 U}{\partial y^2} + \frac{2}{\lambda^2}\left(U - \int_0^W U(\eta)F(y, \eta)d\eta\right)\right.$$

$$\left. - \beta\left(1 - \frac{1}{\lambda^2}\int_0^W\int_{-\infty}^{\infty} RG d\tau d\eta\right)\right] \quad (21)$$

This is the general prognostic equation for deviations of the mean zonal wind from an unchanging grand average (taken over the entire flow), and is the fundamental physical basis for the present theory of mean motions.

Taken together, Eqs. (10) and (21) comprise a complete system of equations, which can be integrated by a modification of the procedure outlined at the end of Section 2. Beginning with initial values of U and ψ, it is possible to compute the eddy statistics $\overline{v^2}$, λ, F and R, and to calculate $\partial^2 U/\partial t^2$ from Eq. (21). Since the initial values of $\partial U/\partial t$ (i.e., $\partial\bar{u}/\partial t$) are given in terms of ψ by Eq. (5), one can then predict U and $\partial U/\partial t$ at a time slightly later than the initial moment. As before, ψ may be predicted by solving Eq. (10) and extrapolating, in order to regenerate the eddy statistics $\overline{v^2}$, λ, F and R at a time later than the initial moment, and so on.

In effect, however, the scheme outlined above is equivalent to integrating the equations for the *unaveraged* motion. The main objective, therefore, is to introduce a hypothesis by which the eddy statistics can be specified or predicted, without integrating the general equations in full detail.

4. The Statistics of Large-Scale Turbulence

According to Eq. (21), changes in the mean zonal wind profile depend partly on the shape of the mean zonal wind profile itself, and partly on certain statistics of the meridional wind component—namely $\overline{v^2}$, λ, R, and F. Our present purpose is to discuss the character and interpretation of these statistics, and the extent to which they depend on details of the flow.

The quantity R is defined as

$$\overline{v(x+\tau, \eta)\nabla^2 v(x, y)}\,/\,\overline{v(x, y)\nabla^2 v(x, y)}$$

Thus, R is essentially a normalized cross-correlation function for a variable "lag" or "shift", depending on τ, y, and η. Its value at $\tau = 0$ and $\eta = y$ is necessarily unity for all y, as shown in Fig. 2. Moreover, since v vanishes

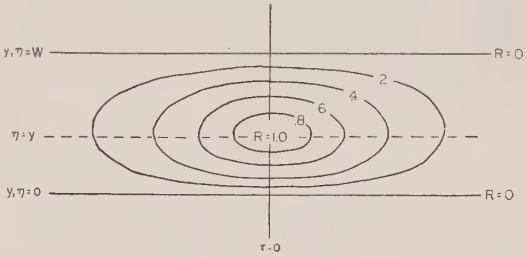

Fig. 2. Schematic pattern of $R(\tau, y, \eta)$ for $y = .4W$.

at the walls, R vanishes at $\eta = 0$ and $\eta = W$, for all y and τ. Now, the geometrical connection between v and $\nabla^2 v$ is given by the identity

$$\int_0^W\int_{-\infty}^{\infty} G\nabla^2 v d\xi d\eta = \int_0^W\int_{-\infty}^{\infty}[\nabla \cdot (G\nabla v - v\nabla G)$$

$$+ v\nabla^2 G]d\xi d\eta = -v(x, y)$$

Thus, since G has a singularity at (x, y) and decreases monotonically to zero as η goes to zero or W and as τ approaches $\pm\infty$, one may think of v as a weighted area average of $\nabla^2 v$, with greatest weight attached to the point (x, y) where the average applies. Accordingly, if the typical dimension of the eddies were much smaller than W, one would expect little

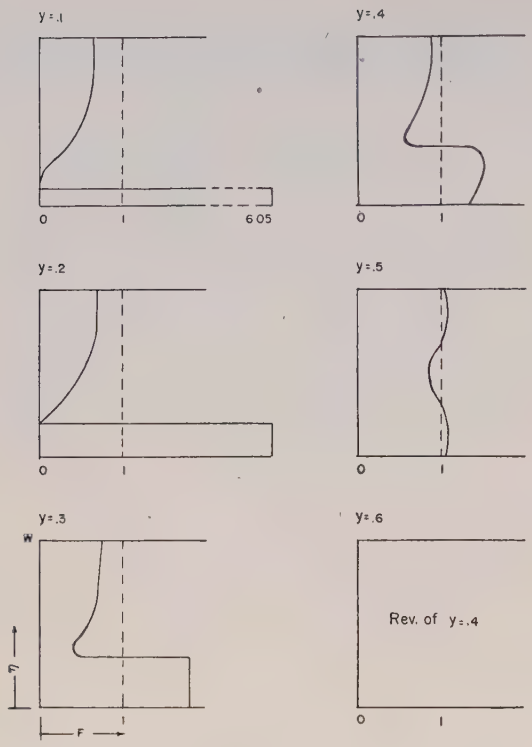

Fig. 3. The weighting-function $F(\gamma, \eta)$ for $v = V \sin \frac{\pi x}{L} \sin \frac{\pi y}{W}$.

or no correlation between v and $\nabla^2 v$. On the other hand, if the scale of the eddies were comparable with W, maxima and minima of v would very nearly coincide with minima and maxima (respectively) of $\nabla^2 v$, so that there would be a high negative correlation between v and $\nabla^2 v$. In this case, $R(\tau, \gamma, \eta)$ takes on the properties of an *auto*correlation function, attaining its maximum value near the point (x, y) and decreasing monotonically to zero as η goes to zero or W. Moreover, since the eddies are generally aperiodic, $R(\tau, \gamma, \eta)$ will tend to approach zero in a regular way as τ approaches $\pm\infty$, the rate at which R decreases being determined by the scale of the eddies.

The mere fact that the general character of $R(\tau, \gamma, \eta)$ can be described so completely in the case of large scale turbulence means that, it the typical scale of the eddies is comparable with the distance between walls, then $R(\tau, \gamma, \eta)$ depends very little on the details of the flow. In this case, R depends primarily (but not crucially) on the typical scale of the eddies, and its day-to-day variation is mainly a reflection of changes in scale.

The quantity $F(\gamma, \eta)$ is related to $R(\tau, \gamma, \eta)$ as follows:

$$F(\gamma, \eta) = \int_{-\infty}^{\infty} \nabla R \cdot \nabla G d\tau$$

In general, both R and G are positive, attain their maximum values at or near the point (x, y), and vanish as η goes to zero or W and as τ approaches $\pm\infty$. Thus, $F(\gamma, \eta)$ is generally positive, as shown in Fig. 3. Like $R(\tau, \gamma, \eta)$, $F(\gamma, \eta)$ depends very little on the details of the flow and, even less than R, depends on the scale of the eddies.

An important property of F is derivable from Eq. (20), which, together with the definition of F, implies that

$$\int_0^W F(\gamma, \eta) d\eta = 1$$

for all γ. We may, therefore, regard the expression

$$U^*(\gamma) = \int_0^W U(\eta) F(\gamma, \eta) d\eta$$

as a *normalized* weighted average of U, in which the weighting factor is $F(\gamma, \eta)$. As shown in Fig. 3, $F(\gamma, \eta)$ does not vary appreciably with η when γ lies near $W/2$. Thus, when γ is near $W/2$, the weighted average $U^*(\gamma)$ is very nearly the unweighted average

$$\frac{1}{W} \int_0^W U(\eta) d\eta$$

which, by the definition of U, vanishes. To see the consequences of this property, let us consider the behavior of U^* in the case of a very narrow, strong "jet" in the mean zonal flow, located near the middle of the channel and superimposed on a roughly *uniform* mean zonal flow. In this case, the mean zonal wind profile is characterized by large positive values of U in a narrow band around $\gamma = W/2$, and by small negative values over two rather broad regions adjacent to the walls. Now, as we have already seen, $U^*(\gamma)$ is very small when γ lies near $W/2$—certainly much smaller in magnitude than the *unaveraged* values of U.

near $y = W/2$. But $U^*(y)$ is also small elsewhere, simply because U is small in the broad regions of uniform mean zonal flow, and because least relative weight is attached to conditions in the middle of the channel when y is near zero or W. Thus, if the mean zonal wind profile is of the general type described above, U^* is negligible in comparison with U for purposes of solving Eq. (21). This conclusion will be verified by the results of a later section.

A further consequence: not only does $F(y, \eta)$ depend very little on the details of the flow (or even on the overall scale of the eddies), but the solution of Eq. (21) is still *less* affected by the small extent to which F *does* depend on scale.

The quantity $\lambda(y)$ is defined by the equation

$$\frac{1}{\lambda^2} = -\frac{\overline{v \nabla^2 v}}{\overline{v^2}}$$

Thus, λ has the units of a length, and is essentially a statistical measure of the scale or typical dimension of the eddies. Owing to the previously discussed relation between v and $\nabla^2 v$ in large-scale turbulence, λ has the properties of an autocorrelation function, and depends very little on the details of the v-field. For the same reason, moreover, one might expect that $\lambda(y)$ would vary only slowly across the width of the channel.[1]

Since the general behavior of solutions of Eq. (21) depends critically on λ, and because both R and F depend on the scale of the eddies to some extent, it is natural to ask if the *scale* of the turbulence can be specified or predicted with sufficient accuracy. Judging from the manner in which λ enters Eq. (21), the relevant question concerns the comparative magnitudes of the percentage time variations of scale and the maximum percentage variations of U. In order to estimate variations of scale, we shall consider another and equally legitimate statistical measure of the characteristic dimension of the eddies, denoted by S.[2]

$$S = \frac{V}{K}$$

where

$$V = \int_0^W \overline{(\nabla^2 \psi)^2} dy \qquad K = \int_0^W \overline{\nabla \psi \cdot \nabla \psi} dy$$

Thus, S is essentially the inverse of the square of the characteristic scale. Differentiating S with respect to t, we find that

$$\frac{\partial S}{\partial t} = \frac{1}{K}\left(\frac{\partial V}{\partial t} - S\frac{\partial K}{\partial t}\right) \tag{22}$$

The next concern is to express the changes of V and K—which are the total variance of eddy vorticity and total eddy kinetic energy, respectively—in terms of changes in U. Turning to the former, we first multiply Eq. (8) by ζ and apply the bar-operator. Simultaneously making use of Eq. (5) to eliminate $\overline{v\zeta}$,

$$\frac{1}{2}\frac{\partial}{\partial t}\overline{\zeta^2} + \frac{1}{2}\frac{\partial}{\partial y}\overline{v\zeta^2} + \beta\frac{\partial \overline{u}}{\partial t} = 0$$

Next, integrating the equation above with respect to y from $y = 0$ to $y = W$, noting that v vanishes at the walls, and recalling that the total zonal momentum is conserved,

$$\frac{\partial}{\partial t}\int_0^W \overline{\zeta^2}\, dy = 0$$

Finally, we decompose ζ into the eddy vorticity and mean vorticity, with the result that

$$\frac{\partial}{\partial t}\int_0^W \overline{(\nabla^2 \psi)^2}\, dy = -\frac{\partial}{\partial t}\int_0^W \left(\frac{\partial U}{\partial y}\right)^2 dy \tag{23}$$

The change in eddy kinetic energy may be calculated by multiplying Eq. (1) by u, multiplying Eq. (2) by v, and adding one equation to the other. At the same time applying the bar-operator,

$$\frac{1}{2}\frac{\partial}{\partial t}\overline{\mathbf{V}\cdot\mathbf{V}} + \frac{1}{2}\frac{\partial}{\partial y}\overline{v\mathbf{V}\cdot\mathbf{V}} + \frac{\partial}{\partial y}\overline{Pv} = 0$$

Thus, integrating this equation with respect to y from $y = 0$ to $y = W$ (where v vanishes),

$$\frac{\partial}{\partial t}\int_0^W \overline{\mathbf{V}\cdot\mathbf{V}}\, dy = 0$$

[1] In a fairly typical case, λ was found to vary by no more than 15 pct of its average value, taken across the entire width of the flow.

[2] For the present purpose, it is sufficient to deal with a "lump" measure of scale, since λ does not vary radically with y.

This equation, of course, expresses the well-known fact that the total kinetic energy of an enclosed barotropic fluid is invariant. Finally, splitting up the total kinetic energy into eddy kinetic energy and kinetic energy of the mean zonal flow,

$$\frac{\partial}{\partial t}\int_0^W \overline{\nabla\psi\cdot\nabla\psi}\,dy = -\frac{\partial}{\partial t}\int_0^W U^2\,dy \qquad (24)$$

Substituting from Eqs. (23) and (24) into Eq. (22), integrating by parts, and noting that $\partial U/\partial t$ vanishes at $y=0$ and $y=W$,

$$\frac{\partial S}{\partial t} = \frac{2}{K}\int_0^W \frac{\partial U}{\partial t}\left(\frac{\partial^2 U}{\partial y^2} + SU\right) dy \qquad (25)$$

The formula above is a general relationship between variations in the overall scale of the eddies and changes in the mean zonal flow.

The question as to the importance of variations of scale may now be dealt with by stating Eq. (25) as an inequality.

$$\left|\frac{\partial S}{\partial t}\right| < \frac{2}{K}\int_0^W \left|\left(\frac{\partial U}{\partial t}\right)\right| \left|\frac{\partial^2 U}{\partial y^2} + SU\right| dy$$

whence

$$\left|\frac{\partial S}{\partial t}\right| << \frac{2}{K}\left|\frac{\partial U}{\partial t}\right|_{\max}\int_0^W \left|\frac{\partial^2 U}{\partial y^2} + SU\right| dy$$

in which a repeated inequality sign indicates the number of intervening "links" in the chain of inequalities. Now, where U reaches a real extreme, its sign is necessarily opposite to that of $\partial^2 U/\partial y^2$. Thus, since $\partial^2 U/\partial y^2$ and SU are of the same order of magnitude,

$$\left|\frac{\partial S}{\partial t}\right| <<< \frac{2}{K}\left|\frac{\partial U}{\partial t}\right|_{\max} \cdot S\int_0^W |U|\,dy$$

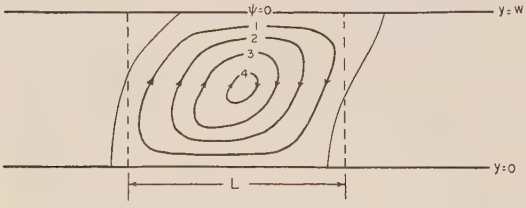

Fig. 4. Schematic pattern of the eddy streamfunction ψ in a large scale eddy. The eddy velocity is directed along the eddy streamlines, and is proportional to the gradient of the eddy streamfunction.

In well-developed turbulence, moreover, the average eddy speed is fully as great as the maximum value of $|U|$, so that

$$\frac{1}{K}\int_0^W |U|\,dy < \frac{1}{|U|_{\max}}$$

and finally,

$$\frac{1}{S}\left|\frac{\partial S}{\partial t}\right| <<<< \frac{1}{|U|_{\max}}\left|\frac{\partial U}{\partial t}\right|_{\max}$$

Despite its semi-quantitative character, the argument above shows that variations in the scale of the eddies are probably much smaller (taken percentagewise) than the maximum variations of U. This conclusion is amply supported, in fact, by the observed behavior of the atmosphere; changes in the overall scale of the transient disturbances are observed to be of the order of tens of percent over the course of a week, whereas the deviation of the mean zonal wind from its grand average may vary by 100 percent or even change sign. Thus, one might be justified in assuming that R and F (which depend primarily on the scale of the eddies) and λ are independent of time—a hypothesis that will be explored in later sections.

It remains to discuss $\overline{v^2}(y)$, a statistical measure of the intensity of turbulence. Since $\overline{v^2}$ is an autocorrelation function, one should expect that its general form would depend very little on details of the flow. Moreover, because $\overline{v^2}$ must vanish at the walls, geometrical constraints alone demand that $\overline{v^2}$ reach its maximum somewhere near the middle of the channel at all times. This, in fact, is borne out by the data published by RIEHL AND COLLABORATORS (1950).

The time variations of the intensity of turbulence may be investigated by considering the total kinetic energy of the meridional motion. Owing to the geometry of very large scale eddies (see Fig. 4), in which there is only one pronounced maximum or minimum of the eddy streamfunction in any section across the channel, the kinetic energy of zonal eddy motion is related to the kinetic energy of the meridional motion by a factor depending on the relative dimensions of the eddies in the x and y directions. That is, approximately,

$$\int_0^W \overline{u'^2} \cdot dy = \frac{L^2}{W^2} \int_0^W \overline{v'^2}\, dy$$

in which L is the typical dimension of the eddies in the x-direction. Thus, the total eddy kinetic energy is

$$\int_0^W \overline{\nabla\psi \cdot \nabla\psi}\, dy = \left(1 + \frac{L^2}{W^2}\right) \int_0^W \overline{v^2}\, dy$$

Now, the connection between the eddy kinetic energy and the kinetic energy of the mean zonal flow may be found by integrating Eq. (24) with respect to time.

$$\int_0^W U^2 dy + \int_0^W \overline{\nabla\psi \cdot \nabla\psi}\, dy = \int_0^W U_0^2 dy + \int_0^W \overline{\nabla\psi_0 \cdot \nabla\psi_0}\, dy$$

where the subscript "zero" denotes conditions at some fixed "initial" time. Finally, combining the two preceding equations,

$$\int_0^W \overline{v^2} dy = \int_0^W \overline{v_0^2} dy + \frac{W^2}{W^2 + L^2} \int_0^W (U_0^2 - U^2)\, dy \tag{27}$$

This formula expresses the total kinetic energy of the meridional motion at any time in terms of U at that same time, and automatically takes account of the decrease (or increase) in the intensity of turbulence as the kinetic energy of the mean zonal flow increases (or decreases).

Having related the time variations of both the *scale* and *intensity* of turbulence to changes in the mean zonal flow, we now possess the main ingredients of a theory of large-scale mean motions. At this point, however, one should note that the eddy statistics $\overline{v^2}$, λ, R and F are not actually independent, and not all hypotheses lead to physically consistent models —e.g., models in which the total zonal momentum is conserved. Let us now inquire whether or not Eq. (21) implies conservation of total zonal momentum at all times, if $\overline{v^2}$, λ, R, and F are specified independently and arbitrarily, but U is allowed to vary according to Eq. (21). The relevant fact is that Eq. (21) is derivable from Eq. (12) by *identities only*, with the consistent substitution of the solution of Eq. (13)[1] for $\partial\psi/\partial t$. Thus, no matter what distribution of U (or $\bar{u}$) prevails at any given time, Eq. (21) must be reducible to the *form* of Eq. (12), *provided the eddy statistics* $\overline{v^2}$, λ, R and F *are all computed from the same distribution of* v. But this, in turn, implies that the second derivative of the total zonal momentum vanishes at all times, whence the total zonal momentum is always conserved if it was unchanging initially.

With the assurance that the total zonal momentum will be conserved, we now state the following general hypotheses:

1) The most effective agencies of momentum transport are eddies of very large scale—i.e., the characteristic dimensions of the eddies are comparable with the entire "width" of the flow.

2) The statistical measures of the *scale* and *intensity* of turbulence *at any time* may be identified with the statistics of a v-field whose amplitude is a constant multiple of the amplitude of the *initial* v-field, and whose scale in the x-direction is a constant multiple of the scale of the *same* initial v-field.

In other words, for purposes of computing the eddy statistics $\overline{v^2}$, λ, R and F and for those purposes only, we suppose that

$$v(x, y, t) = k v_0(mx, y, 0)$$

in which $v_0\ (x, y, 0)$ is the *initial* distribution of v, and k and m are at most functions of time. With this assumption, the value of k at any time is determined by Eq. (27). That is,

$$k^2 = 1 + \frac{W^2}{W^2 + L^2} \cdot \frac{\int_0^W (U_0^2 - U^2) dy}{\int_0^W \overline{v_0^2} dy} \tag{27a}$$

The value of the "scaling factor" m at any time is chosen to be consistent with Eq. (25), which relates changes of eddy scale to time variations of the mean zonal flow. Thus, under the hypothesis stated above, Eqs. (21), (25), and (27) comprise a complete system of equations involving the mean zonal wind, the eddy

[1] With E omitted throughout.

scale, and the intensity of turbulence. Accordingly, they provide the basis for a general theory of large-scale mean motions.

It was pointed out earlier that, on both theoretical and observational grounds, it may be legitimate to assume that the scale of the eddies is independent of time, in which case $m=1$ at all times. The next and subsequent sections will deal entirely with this special hypothesis, which appears to embody the essential ingredients of the theory and which has the considerable virtue of simplicity.

5. A Numerical Method for Predicting the Mean Zonal Wind

With the introduction of the special hypothesis just discussed, Eq. (21) takes the form:

$$\frac{\partial^2 U}{\partial t^2} = k^2\overline{v_0^2}\left[\frac{\partial^2 U}{\partial y^2} + \frac{2}{\lambda_0^2}\left(U - \int_0^W U(\eta)F_0(y,\eta)d\eta\right) + \beta\left(1 - \frac{1}{\lambda_0^2}\int_0^W\int_{-\infty}^{\infty} R_0 G d\tau d\eta\right)\right] \quad (28)$$

where $\overline{v_0^2}$, λ_0, R_0, and F_0 are the values of $\overline{v^2}$, λ, R, and F computed from the initial distribution of v, and are regarded as independent of time after the initial moment. The quantity k^2 is related to U by Eq. (27a). Thus, Eq. (28) involves only one dependent variable U, the deviation of the mean zonal wind (at a variable latitude y) from an unchanging grand average taken over all latitudes. Accordingly, Eq. (28) provides the complete theoretical basis for a method of predicting the mean zonal wind profile.

The purpose of this section is to outline a numerical method for solving Eq. (28)—which, since k depends on U, is nonlinear and generally cannot be solved by exact analytic methods. To start with, we assume that the eddy statistics $\overline{v_0^2}$, λ_0, R_0 and F_0 have been computed from the distribution of v at the beginning of the forecast period. We suppose, further, that the initial values of U are known, and that the initial values of $\partial U/\partial t$ have been calculated from the initial flow pattern by means of Eq. (5) or (7). In addition to the initial conditions specified above, it is also necessary to state conditions on U at the walls. These are contained in Eq. (5), which implies that U remains unchanged at $y=0$ and $y=W$.

Beginning with the initial values of U and $\partial U/\partial t$, one can immediately predict U at a time $\triangle t$ later than the initial moment ($t=0$). It is then possible to compute the entire right hand side of Eq. (28) by finite-sums and finite-differences from the predicted values of U at $t=\triangle t$ in the interior of the channel, taken together with the specified values of U at the walls. Thus, Eq. (28) enables us to calculate $\partial^2 U/\partial t^2$ at $t=\triangle t$. But with the values of U known at $t=0$ and $t=\triangle t$, and with $\partial^2 U/\partial t^2$ known at $t=\triangle t$, one can compute the values of U at $t=2\triangle t$. Finally, since the information available at $t=2\triangle t$ and $t=\triangle t$ is as complete as it was at $t=\triangle t$ and $t=0$, it is possible to recompute $\partial^2 U/\partial t^2$ at $t=2\triangle t$, and so to predict U at $t=3\triangle t$, and so on. This scheme is essentially the one by which the computations to be described in the next section were carried out.

6. The Case of No Initial Momentum Transport

In order to study the general behavior of solutions of Eq. (28), the method of integration described in the preceding section was applied to two types of initial mean zonal wind profiles—both distinguished by the presence of a narrow intense jet, located in the middle of the channel in one case, and near one edge of the channel in the other. To make sure that the essential properties of the solutions would not be obscured by a fortuitous choice of initial values of $\partial U/\partial t$, the *initial* rate of change of U was constrained to vanish at all latitudes, by specifying an *initial* eddy velocity field in which the mean eddy transport of zonal momentum vanishes at all latitudes. This does not, of course, imply that there is no momentum transport at *later* times; it does, however, insure that the changes of mean zonal wind (or momentum) will reflect only the intrinsic dynamical properties of the system.

According to Eq. (5), the case of no mean transport of momentum is one in which v and $\nabla^2\psi$ are completely uncorrelated—i.e., in which the fields of v and $\nabla^2\psi$ are exactly 90 degrees out of phase. But this is also the case when v and $\nabla^2 v$ (or $\partial\nabla^2\psi/\partial x$) are almost exactly in phase, in which case v and $\nabla^2 v$ are

almost perfectly correlated. We therefore consider an initial eddy velocity field in which $\nabla^2 v_0 = -v_0/\mu^2$, an equation which has the simple solution

$$v_0 = V \sin\frac{\pi y}{W} \sin\frac{\pi x}{L} \qquad (29)$$

where V is the maximum meridional wind speed and

$$\frac{1}{\mu^2} = \left(\frac{\pi}{W}\right)^2 + \left(\frac{\pi}{L}\right)^2$$

It is readily verified that the mean zonal momentum transport implied by Eq. (29) vanishes everywhere. The eddy statistics are computed by substituting the expression for v_0 given by Eq. (29) into the definitions of $\overline{v_0^2}$, λ_0, R_0, and F_0. They are:

$$\overline{v_0^2} = \frac{V^2}{2} \sin^2\frac{\pi y}{W}$$

$$\lambda_0 = \mu$$

$$R_0 = -\frac{\sin\dfrac{\pi\eta}{W}\cos\dfrac{\pi\tau}{L}}{\sin\dfrac{\pi y}{W}}$$

$$F_0 \simeq \frac{\pi^2}{2L^2} \frac{\sin\dfrac{\pi\eta}{W}}{\sin\dfrac{\pi y}{W}} \cdot g(y,\eta) + \frac{\pi}{W} \frac{\cos\dfrac{\pi\eta}{W}}{\sin\dfrac{\pi y}{W}} \cdot \frac{\partial g}{\partial \eta}$$

$$\text{where } g(y,\eta) = \begin{cases} \eta\left(1 - \dfrac{y}{W}\right) & \text{if } \eta < y \\ y\left(1 - \dfrac{\eta}{W}\right) & \text{if } \eta > y \end{cases}$$

$F_0(y, \eta)$ is plotted as a function of η in Fig. 3, for nine values of y.[1] In the numerical integration of Eq. (28), L was taken equal to W, $\beta = 3/W$ day, and $V = .2\ W$/day. Lengths were expressed in units of W, time in units of days, and speeds in units of W/day.

The results of the numerical integration of Eq. (28) for the case of a narrow intense jet in the middle of the channel are summarized in Fig. 5(a), which shows the meridional profiles

[1] The values of F_0 given here are not exact. Certain approximations have been introduced to facilitate integration.

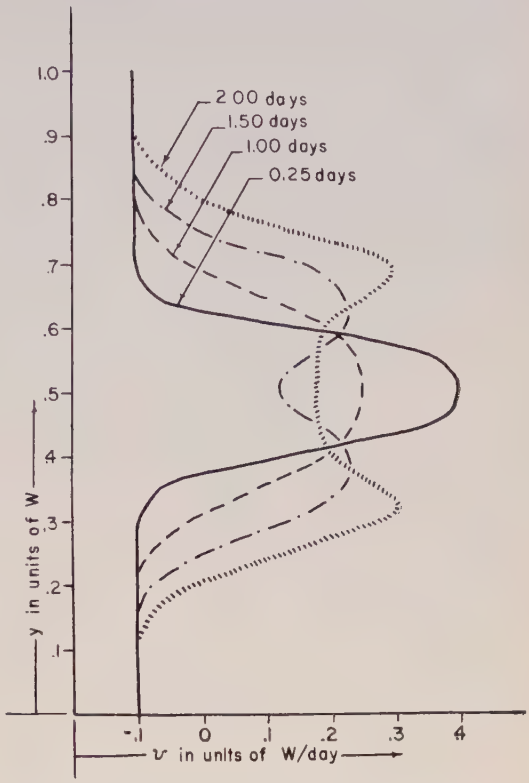

Fig. 5. Time sequences of mean zonal wind profiles for the case of zero initial momentum transport.
(a) based on numerical solution of Eq. (28).

of U at regular intervals of time after $t = 0$. The most striking features of this sequence of mean zonal wind profiles are (1) the weakening and broadening of the jet between $t = 0$ and $t = 1$, (2) the "splitting" of the jet at about $t = 5/4$ and (3) the regular progression of the two jets toward the north and south, each travelling at about .12 W/day. A similar phenomenon is reported by Cressman (1950), who observed that the formation of a double-jet structure is a characteristic and rather sudden denouement from situations of strong zonal flow. Cressman, in fact, states: "This study has suggested that a synoptic pattern consisting of a *single high-level west-wind maximum*, containing long waves of small amplitude, such as is found in the 22 February (1949) chart in Fig. 3, is in itself unstable, and must necessarily break down into a more complicated pattern *by means of a splitting of the maximum*."[1] Cressman's

[1] The italics are mine. Author.

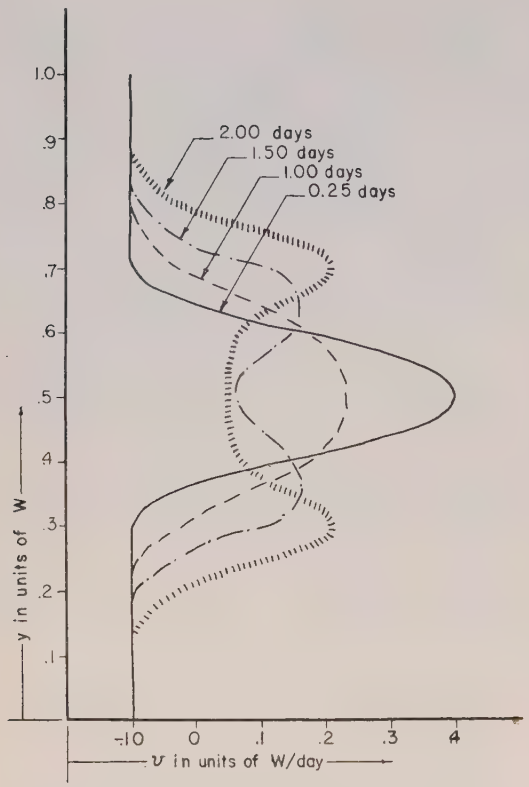

Fig. 5 (b). Same as (a) with $\beta = 0$.

conclusions, of course, were based entirely on a descriptive study of the observed behavior of the atmosphere. Since the double-jet structure is typical of well-developed "blocking" situations, it appears that the present theory of mean motions—whose sole physical content is expressed in the equations of barotropic flow—contains a mechanism for the initiation and development of "blocking".

During the course of the numerical integrations, it became apparent that the earth's rotation had very little effect on the changes of the mean zonal wind. To verify this suspicion, the computations summarized in Fig. 5(a) were repeated for conditions that were unchanged in all respects, except that β was set equal to zero. The results are shown in Fig. 5(b), which indicates that the earth's rotation had the main effect of increasing the total zonal momentum (a quantity which should be conserved), but did not significantly alter the general behavior of the mean zonal wind profile. For this reason and because the increase of total zonal momentum was directly traceable to approximations of integration, the effect of the earth's rotation was omitted from all subsequent calculations.

In section 4, during the discussion of the weighting function $F(\gamma, \eta)$, it was pointed out that the quantity

$$U^*(\gamma) = \int_0^W U(\eta) F(\gamma, \eta)\, d\eta$$

is generally negligible in comparison with U, for purposes of integrating Eq. (28). To support this conclusion, the computations summarized in Fig. 5(a) were repeated for conditions that were unchanged in all respects, except that both β and U^* were set equal to zero. The results are shown in Fig. 5(c). Comparing Figs. 5(b) and 5(c), we see that the omission of U^* has little effect on the evolution of the mean zonal wind profile, even to details, and certainly does not alter its general behavior.

The evidence presented in Figs. 5(a), 5(b),

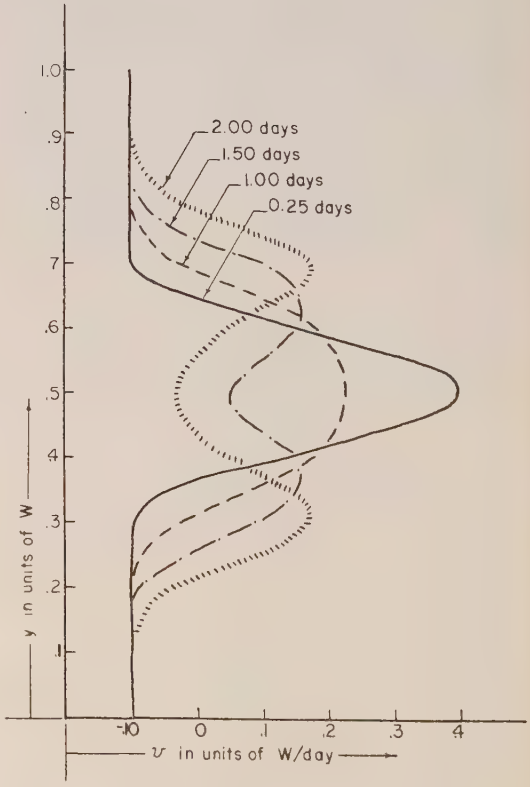

Fig. 5 (c). Same as (a) with $\beta = 0$ and $U^* = 0$.

and 5(c) strongly suggests that, with good approximation, the essential dynamical properties of the system are expressed in the following simplified form of Eq. (28):

$$\frac{\partial^2 U}{\partial t^2} = k^2 \overline{v_0^2} \left[\frac{\partial^2 U}{\partial y^2} + \frac{2U}{\lambda_0^2} \right] \qquad (30)$$

This equation is particularly convenient from the standpoint of computation, for it obviates the necessity of evaluating U^* by the method of finite-sums.

The results of the numerical integration of Eq. (28) for the case of a narrow intense jet near one edge of the channel are illustrated in Fig. 6(a), which, as before, shows the meridional profiles of U at regular intervals of time after $t=0$. The most striking single feature of this sequence of mean zonal wind profiles is the regular northward progression of the maximum mean zonal wind.[1] This feature stands out even more vividly in Fig. 6(b), a latitude-time diagram on which lines of constant U have been drawn. The effect described above is strongly reminiscent of the phenomenon reported by RIEHL ET AL. (1950), who observe that an extreme in the anomaly of mean zonal momentum typically migrates (either northward or southward) in a regular way, sometimes persisting over periods of several weeks. As did CRESSMAN (1949), they also find that distinct extremes of mean zonal momentum may travel in opposite directions. What is significant is that Eq. (28) contains a mechanism whereby extremes of mean zonal wind may be propagated toward the north, toward the south or in both directions at once, depending on the initial conditions.

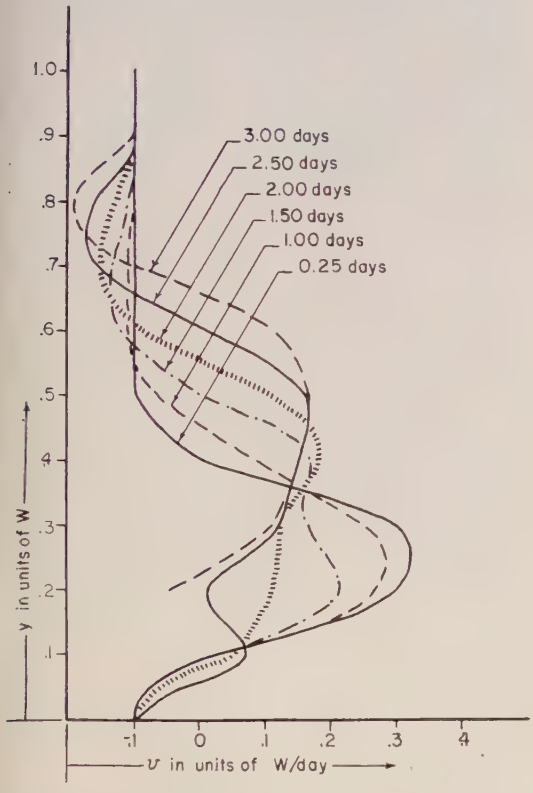

Fig. 6 (a). Time sequence of mean zonal wind profiles for the case of zero initial momentum transport.

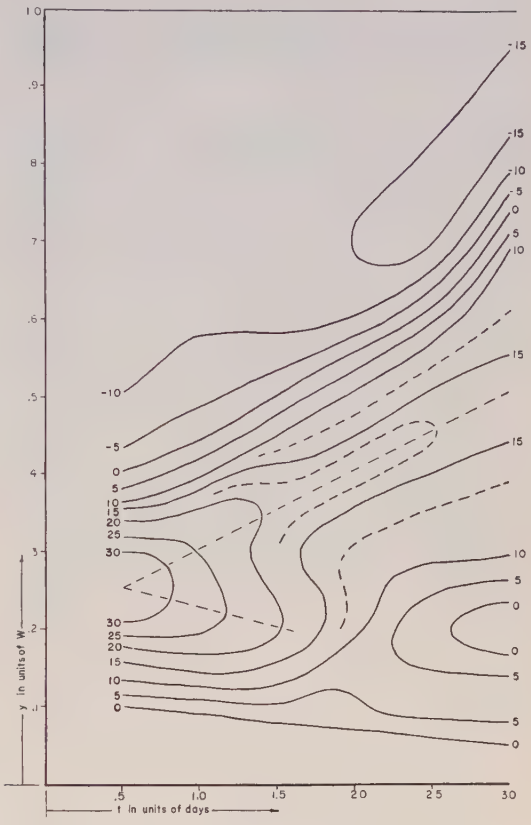

Fig. 6 (b). Lines of constant U (in units of .1 W/day) on a latitude-time diagram.

[1] The rather confused pattern of variations in the immediate vicinity of the southern wall is due to the "reflection" of a *southward* moving maximum, which reverses its sense upon being reflected at the boundary.

7. The General Nature of Long-Period Variations of Mean Zonal Wind in Barotropic Flow

The fundamental reason for the peculiar behavior of solutions of Eq. (28) is apparent when one realizes that Eq. (28) is essentially a "wave-equation"—i.e., a second order equation of hyperbolic type. Eq. (30) is, in fact, reducible to a generalized form of the so-called "telegraphic" equation by transformations of both the dependent and independent variables. It is characteristic of such second order equations that extremes which are present in the initial conditions are propagated in either or both directions in a regular way, and are preserved over long periods of time.

To make this point more concrete, the computations summarized in Fig. 5(a) were repeated for two special cases, in both of which the original conditions were unchanged, except that $\beta = 0$, $U^* = 0$, and $\lambda_0 = \infty$. In the first case, $\overline{v_0^2}$ varied from one latitude to another; in the second, $\overline{v_0^2}$ was regarded as a constant, equal to the average of the correct values over a narrow strip centered on $y = W/2$. The results of these computations are shown in Figs. 7(a) and 7(b).[1] Comparison of Figs. 7(a) and 7(b) with Figs. 5(a), 5(b), and 5(c) reveals that the most prominent features of the solutions of Eq. (28) also appear in the solutions of the simple equation

$$\frac{\partial^2 U}{\partial t^2} = c^2 \frac{\partial^2 U}{\partial y^2} \tag{31}$$

where c is a constant measure of the RMS meridional wind speed. It will be recognized that the form of Eq. (31) is that of the classical wave equation, which also governs the propagation of sound waves in air, or gravity waves on the surface of a shallow body of water.

In the cases of no initial momentum transport studied here, Eq. (31) leads to a very simple geometrical interpretation: The mean zonal wind profile at any time is the superposition of two virtual mean zonal wind profiles which:

1) both have the shape of the initial mean zonal wind profile, but one half its amplitude,
2) are initially in phase, and
3) travel in opposite directions at the speed c, without change in shape.

Qualitatively, at least, this description is in accord with the main features of Figs. 5(a), 5(b), and 5(c).

It remains to see if the speed at which extremes of mean zonal wind actually migrate is in agreement with the speed predicted from theory. Now, as indicated by Figs. 7(a) and 7(b), the speed of migration at a *particular* latitude is not much affected by taking $\overline{v^2}$ to be a constant, equal to the correct value of $\overline{v^2}$ at that latitude. With this simplification, Eq. (30) has wave solutions of the form

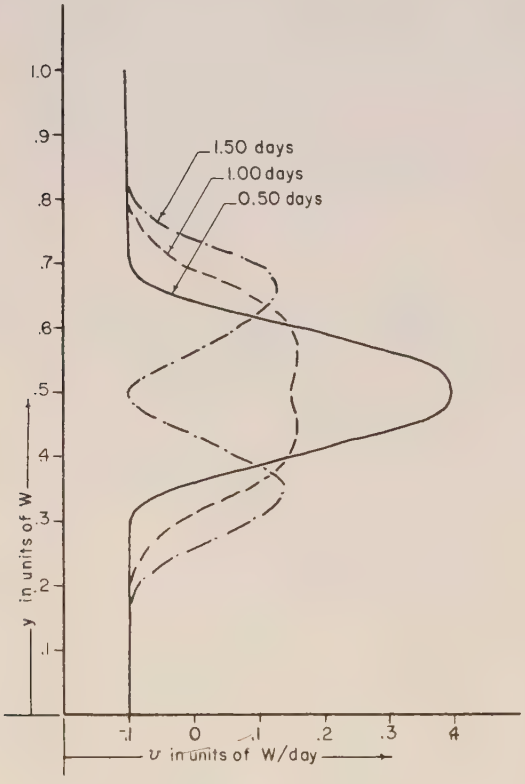

Fig. 7. Sequences of mean zonal wind profiles based on solutions of Eq. (28) with $\beta = 0$, $U^* = 0$, and $\lambda_0 = \infty$.
(a) $\overline{v^2}$ variable

[1] The solution shown by the solid curves on Fig. 7 (b) was computed by an exact analytic method. The circled points are values of U for $t = 1.5$, computed by *numerical* integration. Since those points fall on the exact curve for $t = 1.5$, the numerical solutions of Eq. (28) are evidently not subject to appreciable truncation and roundoff errors.

$$U = e^{\frac{i\pi}{w}(y-ct)}$$

in which c, the characteristic speed of migration, is given by

$$c = \pm \sqrt{\overline{v^2}\left[1 - 2\left(\frac{w^2}{L^2} + \frac{w^2}{W^2}\right)\right]} \qquad (32)$$

and w is a typical "half wavelength" of latitudinal variations in U.

One of the few cases for which published data are complete enough to make a rough estimate of c is that of 14 October 1945, which has been discussed by both CRESSMAN (1950) and RIEHL ET AL. (1950). Judging from Riehl's Figure 18, the "half wavelength" of variation in U at 300 mb was about 20° latitude, the effective width of the "channel" (north-south extent of the major disturbances) was about 60° latitude, and the typical zonal dimension of the large-scale "eddies" was about 45° longitude at latitude 35° N. According to Riehl's Figure 5, the zonal average of the absolute value of the meridional wind at 300 mb was about 11 m/sec at latitude 35° N. Substituting these values for w, W, L and $\overline{|v|}$ in Eq. (32), we find that c is about 220 miles/day. The actual speed of migration may be estimated from Fig. 5 of CRESSMAN (1950), which shows that the main jet drifted southward about 20° latitude in a seven day period centered on 14 October 1945. This displacement corresponds to a speed of about 197 miles/day. Owing to the crudity of these estimates, one should probably not be impressed by the *closeness* of agreement between the predicted and actual speeds of migration. It is certainly safe, however, to say that the predicted speed of migration is of the correct order of magnitude.

8. Prediction of the Scale and Intensity of Turbulence

Once the sequence of mean zonal wind profiles has been tentatively predicted from Eq. (28), it is a simple matter to predict changes in some of the eddy statistics. Variations in the overall scale of the eddies, for example, can be computed from the predicted variations of U by means of Eq. (25). This, in fact, leads to the

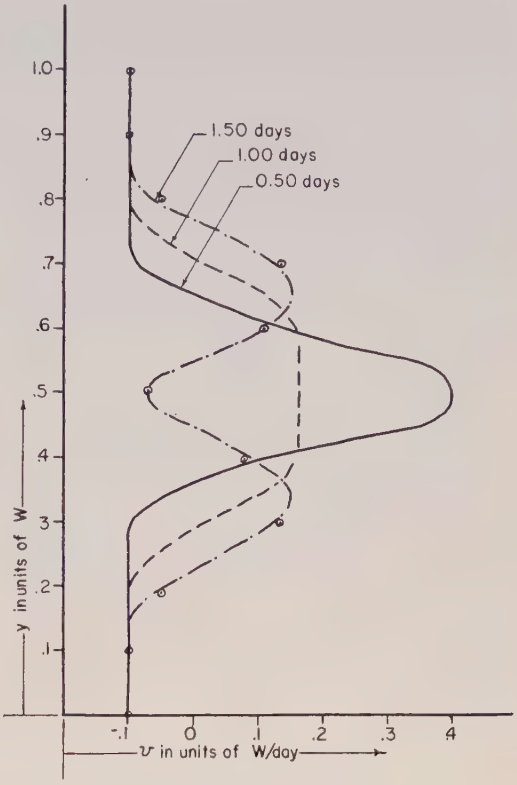

Fig. 7. (b) $\overline{v^2}$ constant.

general theory of mean motion, outlined in Section 3, in which Eqs. (21), (25) and (27) are regarded as a closed system of three equations involving the mean zonal wind, the eddy scale, and the intensity of turbulence.

Variations in the *overall* intensity of turbulence may be predicted from the equation for conservation of total kinetic energy, which relates the eddy kinetic energy to the predicted kinetic energy of the mean zonal flow. The changes in another and more informative index of the intensity of turbulence may also be expressed in terms of the variations of mean zonal wind. Multiplying Eq. (9) by ζ', and applying the bar operator,

$$\frac{\partial}{\partial t}\overline{\zeta'^2} + 2\left(\beta - \frac{\partial^2 \overline{u}}{\partial y^2}\right)\overline{v'\zeta'} + \frac{\partial}{\partial y}\overline{v'\zeta'^2} = 0$$

It was pointed out in section 3, during discussion of the auto-interaction of eddies, that correlations between one deviation field and the square of another tend to be uniformly

small. Thus, simultaneously eliminating $\overline{v'\zeta'}$ by means of Eq. (5), we may rewrite the equation above as

$$\frac{\partial}{\partial t}\overline{\zeta'^2} + 2\left(\beta - \frac{\partial^2 U}{\partial y^2}\right)\frac{\partial U}{\partial t} = 0 \qquad (33)$$

This equation relates changes in the variance of eddy vorticity *at any latitude* to the changes in the mean zonal wind at that latitude. Accordingly, Eq. (33) provides the basis for a method of predicting the *latitude of maximum eddy circulation*.

Interpreted by an experienced synoptic meteorologist, a time sequence of zonal wind profiles—together with accurate predictions of eddy scale, eddy kinetic energy, and latitude of maximum eddy circulation—would probably be of considerable use in forecasting changes of regime, periods of widespread cyclonic activity, and perhaps shifts in the major storm tracks. Thus, if the present theory can be extended to account for long-period velocity variations in the atmosphere, it may prove to be a practical aid in extended-range forecasting.

9. Summary and Conclusions

The mathematical development of the present theory of mean motions hinges on two fundamental equations—one of which relates changes in the mean zonal flow to the eddy velocity, and the second of which states how the changes of eddy velocity, in turn, are related to the mean flow. By combining these equations properly, it has been found possible to derive an equation that expresses the time variations of the mean zonal wind in terms of the mean zonal wind itself and certain statistics of the eddy velocity. If the characteristic dimension or scale of the eddies is comparable with the "width" of the flow, those eddy statistics take on the properties of autocorrelation functions and depend very little on the details of the flow pattern. One of these statistics is essentially a measure of the intensity of turbulence, another is a measure of the eddy scale, and the remainder depend primarily (but not critically) on eddy scale.

A brief theoretical investigation indicates that percentage variations of eddy scale are much less than the maximum percentage variations of mean zonal wind, a conclusion that is in general agreement with observation. Supported by this argument, we have assumed that those eddy statistics which depend only on eddy scale are invariant and retain their initial values over periods of several days to a week or so. With this hypothesis, the equations of mean motion comprise a complete system that is solvable by numerical methods.

The equation for the mean zonal wind—which has the form of a "wave-equation"—has been integrated numerically for two types of initial mean zonal wind profiles, beginning with no initial momentum transport. The results of those computations show that, as a result of the intrinsic dynamical properties of the system, extremes of the mean zonal wind maintain their identity over considerable periods of time, and migrate either northward or southward in a very regular way, the direction of motion depending on initial conditions. This feature is strongly reminiscent of the regular long period variations of mean zonal momentum reported by Riehl et al. (1950). The computations showed, further, that a narrow intense "jet" near the middle of the initial profile of the mean zonal wind tends to "split" into two jets of lesser intensity, which then rapidly move apart to form the "double-jet" structure typical of widespread "blocking". A similar phenomenon in the atmosphere has been described in highly evocative terms by Cressman (1950). Since the sole physical content of the present theory is expressed in the equations for barotropic flow, we tentatively conclude that *a mechanism for the initiation and development of blocking is contained in the theory of barotropic flow*.

A rather crude theoretical estimate of the "migration speed" of a pronounced mean zonal wind maximum was made from hemispheric data for 14 October 1945, previously published by Riehl (1950). The theoretical estimate of 220 miles per day is to be compared with an observed speed of 197 miles per day, taken from independent data published by Cressman (1950). One may conclude, at the least, that the theoretical speed of migration is of the correct order of magnitude.

In summary, the theory of mean motion outlined in the foregoing sections of this paper appears to describe—qualitatively and semi-

quantitatively—the most striking and regular features of long-period velocity variations in the atmosphere that have yet come to light.

The type of mean velocity variations discussed above has a characteristic time-scale of the order of a week or two, rather than a day or two. Thus, one is tempted to speculate that, if the theory of barotropic flow is adequate to describe *those* variations, then it is probably capable of predicting the general features of the large-scale circulation patterns over like periods of time, when taken *in the mean*. If this is indeed the case, the role of purely mechanical processes of the atmosphere (as distinguished from its thermodynamical processes) would be much more important from the standpoint of extended-range forecasting than previous studies of the *unaveraged* equations have indicated.

REFERENCES

Cressman, G. P., 1950: Variations in the structure of the upper westerlies. *J. Meteor.*, **7**, pp. 39—47.

Lorenz, E. N., 1952: Flow of angular momentum as a predictor for the zonal westerlies. *J. Meteor.*, **9**, pp. 152—157.

Phillips, N. A., 1955: The general circulation of the atmosphere: A numerical experiment. Submitted for publication in *Q. J. Roy. Met. Soc.*

Riehl, H., Yeh, T. C., and LaSeur, N. E., 1950: A study of variations of the general circulation. *J. Meteor.*, **7**, pp. 181—194.

Shuman, F. G., 1955: A method of designing finite-difference smoothing operators to meet specifications. *Tech. Memo. No. 7, Joint Numerical Weather Prediction Unit.*

Bergthorsson, P., Döös, B. R., Fryklund, S., Haug, O., and Lindquist, R., 1955: Routine forecasting with the barotropic model. *Tellus*, **7**, pp. 272—274.

Starr, V. P., 1953: Note concerning the nature of the large-scale eddies in the atmosphere. *Tellus*, **5**, pp. 494—498.

On the Theory of Comet Tails

By H. ALFVÉN. The Royal Institute of Technology, Stockholm

(Manuscript received June 22, 1956)

Abstract

According to Biermann's theory the repulsive force in comet tails is due to a corpuscular radiation from the sun. It is shown that some of the difficulties of this theory can be overcome if the assumed radiation consists of beams with a frozen-in magnetic field of the same type as required in the electric field theory of magnetic storms and aurorae.

The interaction between such a beam and the head of the comet produces an amplified magnetic field which determines the shape of the tail. The high accelerations, which have been observed in the tails may be due to electromagnetic forces.

§ 1

There are different types of comet tails. Some of them (type II and III) consist of dust and non-ionized gases. The motions in them show accelerations of the same order as the solar gravitational acceleration (0.56 cm sec^{-2} at a distance of one astronomical unit), or smaller. It seems possible to explain the motions as produced by the light pressure.

The main difficulty with the comet tails is associated with tails of type I. Such tails consist of ionized gases and exhibit usually a pattern of very narrow "streamers" and "envelopes". A representative pattern is shown in Fig. 1 (FOKKER 1953). Accelerations of the order of several thousand times the solar gravitation are often observed. The attempts to understand the formation of tails of this type have usually followed the "fountain model" according to which matter is ejected from the head of the comet and moves under the influence of a repulsive force deriving from the sun.

The fountain model meets three difficulties.

1. The ejection velocity from the head must be assumed to be high, often 25—40 km/sec. which e.g. for the CO^+ ions observed in the tails would correspond to a temperature of the order of a million degrees (cf. for example FOKKER 1953). It is difficult to understand how such high velocities could be produced in the head of the comet.

2. The repulsive force is up to thousand times the force which could result from the light pressure.

3. The fountain model should give a structure of "fountain" parabolas starting from the head. Instead the predominant shapes of the streamers are straight lines. The only parabola which is seen in Fig. 1 surrounds the head. In general, the luminous lines near the head are parabolas, but they surround the nucleus and do not start from it, as would have been most natural according to the fountain theory. It is important to note that according to Fokker there is a continuous transition between "envelopes" and "streamers".

§ 2. Biermann's theory

In order to avoid the second difficulty, BIERMANN (1953) has proposed that the repulsive force is due to the viscosity between

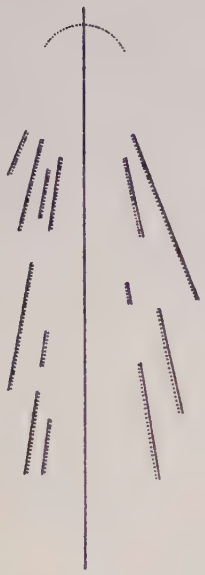

Fig. 1. Comet brooks 1911 nov. 3. Typical pattern ("envelope" and "streamers") in a comet tail according to FOKKER (1953).

gases ejected by the comet and an assumed corpuscular radiation emitted from the sun. The acceleration a, which he deduces, is numerically

$$a = 0.1\, n \text{ cm sec}^{-2}$$

where n is the density of the corpuscular radiation. Biermann assumes that the density is normally 10^2—10^3 cm^{-3} but that at intervals it may reach 10^5 cm^{-3}. The corpuscular radiation should be of the same type as assumed by Chapman and Ferraro in their theory of magnetic storms, and the assumed density are in agreement with this theory. Using these values Biermann finds accelerations of 10—100, and occasionally up to 10^4 cm sec^{-2}.

It seems difficult to accept the high densities of the corpuscular radiation, which Biermann's theory requires. The agreement with data derived from Chapman-Ferraro's theory is no real support because of the well-known difficulties of this theory. Further, a corpuscular radiation of this density cannot possibly pass the solar corona without being observed.

If a corpuscular radiation is ejected from the sun and moves out radially with a constant velocity, its density n is

$$n = \nu R^{-2} \tag{1}$$

where ν is a constant and R is the distance from the sun's centre, counted in solar radii. The maximum value which we could possibly attribute to ν is given by the minimum value nR^2 if for n we use the observational values of the density of the corona. Hence we obtain from van de Hulst's table (1953) of maximum corona.

R	1.1	2	3
n	$1.6 \cdot 10^8$	$2.8 \cdot 10^6$	$3.2 \cdot 10^5$
$\nu = n R_2$	$1.9 \cdot 10^8$	$1.1 \cdot 10^7$	$2.8 \cdot 10^6$
R	4	6	
n	$8.9 \cdot 10^4$	$2.9 \cdot 10^4$	
$\nu = n R^2$	$1.4 \cdot 10^6$	$1.0 \cdot 10^6$	

The minimum corona gives somewhat lower values.

Thus we find that even if the total light of the corona at 4—6 solar radii should derive from corpuscular radiation, the value of ν could not surpass 10^6. However, there are good reasons to suppose that the corona is essentially an atmosphere in thermal equilibrium (see van de Hulst). This means that a corpuscular radiation passing through the atmosphere must have a density which is considerably lower, and $\nu = 10^5$ would be a more reasonable upper limit.

With $\nu = 10^5$ the density at one astronomical unit is

$$n = 2.2 \text{ cm}^{-3} \tag{2}$$

Even the maximum value $\nu = 10^6$ does not bring us up to more than

$$n = 22 \text{ cm}^{-3} \tag{3}$$

With Biermann's formula this gives accelerations of only 0.22 or 2.2 cm sec^{-2} which is even less than the light pressure may give.

Higher densities can be obtained if the corpuscular radiation does not move radially but is focussed in some way. Certainly the intensity of the corpuscular radiation varies and is larger in some directions, as indicated by the occurrence of magnetic storms at the earth and associated increases in comet activity. But tail accelerations far above 0.25 or 2.5 cm sec^{-2} are observed during months and occur with

the comet at different heliographic latitudes. This puts a rather tight limit to the degree of focussing we should assume. In fact a density of $n = 10^5$, as required by Biermann's theory means a concentration by focussing by a factor of about 10^4. This implies that a beam which passes the corona under a solid angle of say $100° \times 100°$ should be concentrated to 1 square degree. It is difficult to invent a mechanism for this. Still more important is that a focussing implies that the chance that a comet at a random position is hit by a beam is only of the order 10^{-4}.

Finally it should be observed that Biermann's theory does not give any satisfactory solution to the first and third difficulty of the fountain theory.

§ 3. Magneto-hydrodynamic mechanism

As Biermann's basic idea that the repulsion is due to corpuscular radiation from the sun seems to be sound, we shall try to modify this theory by substituting Chapman-Ferraro's corpuscular radiation by the type of radiation which is required by the electric field theory of magnetic storms and aurorae (ALFVÉN 1955). This radiation is supposed to be emitted from the sun in form of beams in certain directions. The motion is essentially radial so that when the sun rotates the beam gets the form as shown in Fig. 4 similar to the beam of Chapman and Ferraro. The velocity is of the order 10^8 cm sec^{-1}. Contrary to Chapman-Ferraro's beam the density satisfies the condition (2). In fact, a density of $n = 10^{-1}$ or 10^{-2} is acceptable in the theory of magnetic storms and aurora. The beam carries a magnetic field of the order of 10^{-5} gauss which is frozen in. In the central parts of the beam the direction of the magnetic field is preferentially perpendicular to the sun's equatorial plane. There may be turbulence in the beam, but this vill be neglected here. At the borders of the beam the field may be essentially radial, but even this is not important in this connection. It should be observed that a beam of this type is compatible with cosmic ray data and is used in the theory of cosmic ray storm effects. In fact the value of the magnetic field derives essentially from cosmic ray data.

Suppose that a beam of this type hits the head of a comet, which consists of dust and of gas which is not ionized or only partially ionized. (The comet may also have a type II or III tail of neutral gas and dust, expelled by light pressure.) At the collision a shock wave is produced and an intense heating of the gas in the head occurs so that the degree of ionization increases. As the ionization, at least in part, takes place in the magnetic field of the beam, the lines of force are "frozen in" in the gas of the comet head. As the beam continues outwards from the sun the lines of force are dragged out.

Figs 2 and 3 show what is likely to happen when the beam moves outwards. After some time the lines of force are "hanged up" on the comet head and ending in the beam which now may be far out. On these lines magneto-hydrodynamic waves may travel, possibly giving rise to the wavy patterns which are sometimes observed. In absence of such waves the lines of force are *straight* lines except very close to the head, where they are curved because they take up the shock wave from the gases ejected from the head. It is natural to assume that ionized gas ejected from the comet forms "streamers" along the magnetic field lines. This gives us a pattern which shows a striking resemblance to the observed tail structure with its "streamers" and "envelopes". It is important to note that theories employing light pressure or viscous forces predict an essentially parabolic structure of the tails, whereas very often a rectilinear fan-like structure is observed (compare Fig. 1) which according to the present theory should be given by the magnetic field lines. These effects could of course also be described as produced by the electric field $E = v \times H$ associated with the beam. This field produces a current in the gas of the comet, and the magnetic field around the comet is produced by this current and the primary magnetic field of the beam. Hence the basic phenomenon is the same as in the electric field theory of magnetic storms and aurora. The difference between the phenomena around the earth and around the head of a comet are essentially due to the terrestrial magnetic field.

If the magnetic field of the beam is strictly homogeneous, the tail should be plane, so that when seen parallel to the field of the beam it should look like Fig. 3. Gas ejected from the head may be caught by the field lines and form a "condensation" which moves out close to the tail. If looked upon as in Fig. 2 the

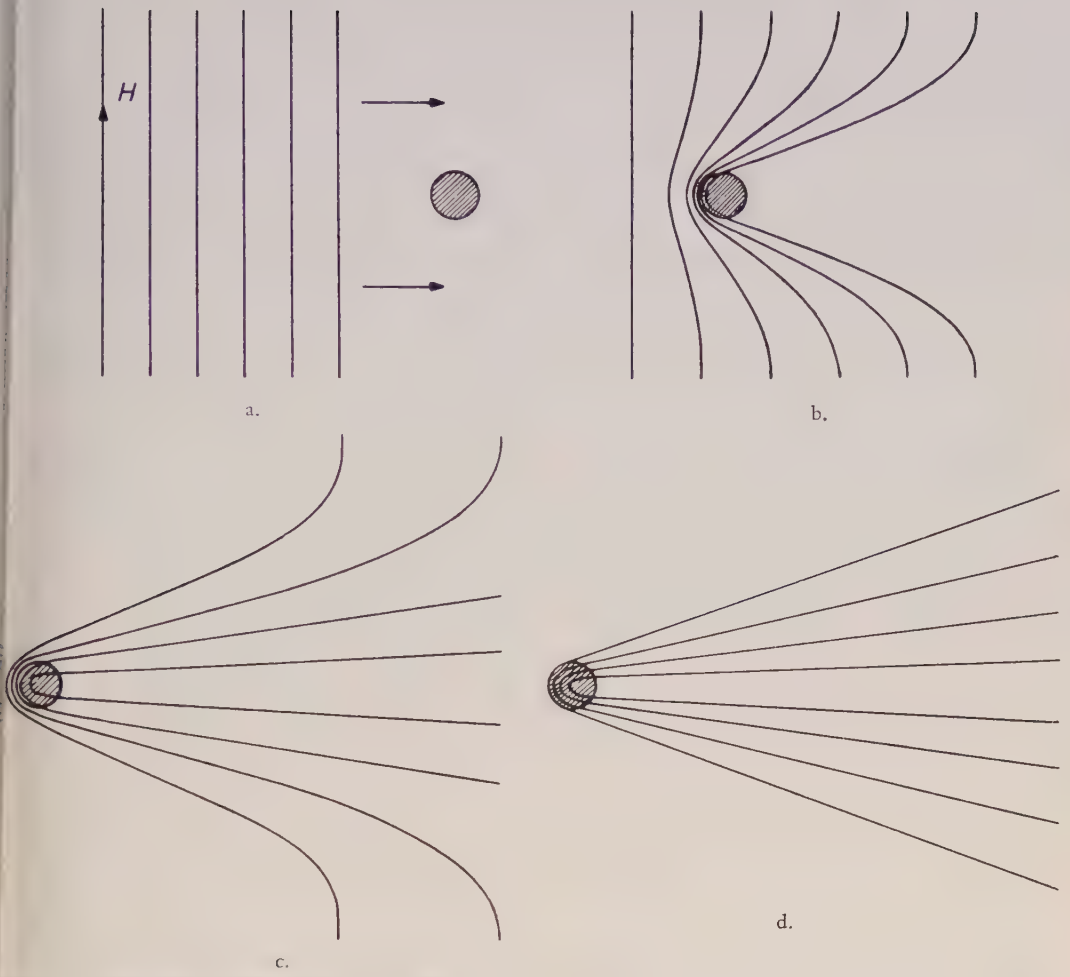

Fig. 2. A beam with a frozen-in magnetic field H approaches the head of a comet (2 a). The field is deformed (2 b and 2 c). Final state when the beam has passed (2 d). Viewed perpendicular to the field of the beam.

"condensation" would be identified as a part of the tail.

The possibility that comet tails are "flat" is interesting and may be checked observationally. Some comets with very thin tails may be comets of ordinary type looked upon parallel to the magnetic field. However, if there is a considerable turbulence in the beam, the conclusion may not be valid.

An important feature of the present theory is that a continuous tail activity need not necessarily mean that the sun continuously emits corpuscular radiation in all directions. If a beam has passed a comet, the lines of force are dragged out so that during some time the comet is "hanged up" on lines of force which are fastened in a part of the beam which may be very far out (see Fig. 4). As the beam elements move out radially, the magnetic drag acts essentially along the vector radius from the sun. In the moment when the beam passes the comet, the tail activity should increase, as it does according to Biermann, and thereafter the activity should in general decrease until a new beam hits it. In absence of beams during a sufficiently long time the comet should loose its type I tail.

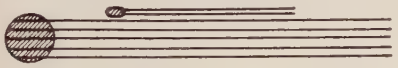

Fig. 3. The same as Fig. 2 but viewed parallel to the field of the beam.

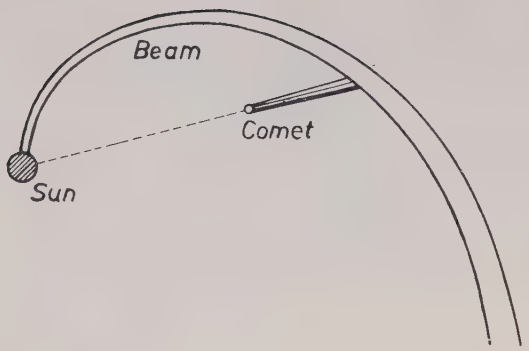

Fig. 4. Beam emitted from the sun, and comet.

§ 4. Properties of the tail

According to the present theory the problem which we should solve in order to understand the formation of comet tails is how a ball of gas and dust reacts when it is hit by a magnetized beam of rarified gas. We do not need to postulate any complicated mechanism ejecting gas in the head of the comet, a problem which leads to absurd assumption in the fountain model. In fact, the directions of the tail is given by the magnetic field, the direction of which is determined by the relative motion of the beam and the comet. The tail should no more be considered as gas moving freely in space. Instead the tail is a real part of the comet, fastened to the head by magnetic field lines.

Seen from the coordinate system of the comet the tail should point in the direction in which the matter of the beam moves. Hence if the velocity of the comet has a radial component v_r and a tangential component v_t and the beam moves out radially with the velocity v_b, the tail of the comet will make an angle α with the vector radius from the sun. The angle is given by

$$\operatorname{tg} \alpha = \frac{v_t}{v_b - v_r}$$

If for example $v_t = 3.10^6$ cm sec^{-1}, $v_r = 0$, and $v_b = 10^8$ cm sec^{-1}, we obtain $\alpha = 0.03 = 2°$. Larger angles are obtained if v_b is smaller. The value $v_b = 10^8$ cm sec^{-1} is derived from the delay of magnetic storms after a solar event and corresponds to a time of passage from the sun to the earth of $1.5 \cdot 10^5$ seconds.

As the direction and the structure of the tail is not immediately connected with the ejection of gas from the head of the comet, the ejection velocity may be quite small.

The structure of the "envelopes" and "streamers" is given by the magnetic field and the matter forming them need not necessarily move with a large velocity in relation to the comet. The high velocities which in some cases have been actually observed, may be due to magneto-hydrodynamic waves, travelling along the tail. In a beam with the density $\varrho = 10^{-25}$ g cm^{-3} corresponding to $n = 0.1$ cm^{-3}, and a magnetic field of 10^{-5} gauss the magneto-hydrodynamic velocity is $V = (4\pi\varrho)^{-1/2} = 10^7$ cm sec^{-1}. In a tail the field has been amplified considerably, so much higher velocities are possible. On the other hand the density is also larger. Wave velocities of 10^7 or 10^8 cm sec^{-1} seem reasonable. Another possibility is that the observed motion of "condensations" in the tail is due to small gas clouds torn away from the head as indicated in Fig. 3. The electromagnetic forces tend to make such a cloud move with the beam, and as the magnetic field may be amplified up to 0.01 gauss or more near the head, it is easily seen that they are strong enough to produce very large accelerations.

REFERENCES

FOKKER, A. D., 1953: Notes on the fountain model of cometary envelopes and streamers. *La Physique des Comètes*, Louvain.

BIERMANN, L., 1953: Physical processes in comet tails and their relation to solar activity. *La Physique des Comètes*, Louvain.

VAN DE HULST, H. C., 1953: The chromosphere and the solar corona, p. 262, *Kuiper's "The Sun"*, Chicago.

ALFVÉN, H., 1955: On the electric field theory of magnetic storms and aurora, *Tellus*, **7**, p. 50. Compare also: Alfvén, H., 1954. On the Origin of Cosmic radiation, *Tellus*, **6**, p. 232, and Alfvén, H., 1955: On the sun's general magnetic field, *Tellus*, **8**, p. 1.

Experiments on the Effect of Inhomogeneity and Obliquity of a Magnetic Field in Inhibiting Convection

By B. LEHNERT and N. C. LITTLE,[1] Royal Institute of Technology, Stockholm, Sweden

(Manuscript received May 11, 1956)

Abstract

Two experiments are described on the inhibition of convection in a magnetic field. In the first experiment a layer of mercury is placed in an inhomogeneous magnetic field and heated from below. Photographs show convection where the field is weak, but indicate no motion where the field is strong. The boundary between these two regions corresponds to a critical magnetic field in agreement with current theory. The boundary is well defined showing that the onset of convection is sensitive to variations in the magnetic field. In the second experiment with a homogeneous field, varied in direction from vertical to horizontal, it is the vertical component which controls the onset of motion. A strong horizontal field does not inhibit convection but causes motion in narrow cells elongated in the direction of the field.

Introduction

The theory of the onset of convection in a layer of an imcompressible fluid subject to thermal instability was originally treated by RAYLEIGH (1916) in the purely hydrodynamic situation and by THOMPSON (1951) and CHANDRASEKHAR (1952) when the fluid is electrically conducting and is placed in a homogeneous magnetic field. Papers which deal with experimental aspects of the magnetohydrodynamic problem are those of NAKAGAWA (1955), JIRLOW (1956) and LEVENGOOD (1956). Further references are given by CHANDRASEKHAR (1952) and by NAKAGAWA and FRENZEN (1955).

The theory shows that a layer of fluid heated from below first becomes unstable when the Rayleigh number, R, exceeds a certain critical value, R_0.

$$R = \frac{g\alpha\beta d^4}{\varkappa\nu}, \qquad (1)$$

where

d is the depth of the fluid layer
g, acceleration due to gravity
α, volume coefficient of thermal expansion
β, initial temperature gradient (directed downward to produce instability)
$\varkappa$, thermometric conductivity (the ratio of thermal conductivity to the product of the specific heat and the density)
ν, kinematic viscosity (ratio of coefficient of viscosity to density).

Motions with a cellular pattern depending on the boundary conditions ensue. If the fluid is electrically conducting and a magnetic field is introduced, electromagnetic forces will oppose these motions; R_0 will be increased to R_c. The ratio of R_c to R_0 has been given by CHANDRASEKHAR (1952) in terms of a parameter,

$$Q = \frac{B_z^2\sigma d^2}{\varrho\nu}, \qquad (2)$$

[1] Now at Bowdoin College, Brunswick, Maine, U.S.A.

where

B_z is the vertical component of the magnetic field
σ, the electrical conductivity
ϱ, the density.

To appreciate the physical significance of the rigorous theory consider roughly a horizontal layer of fluid at rest, which is heated from below so that a uniform vertical temperature gradient, β, exists between its hot lower surface and its cold upper surface. Let small disturbing cellular motions be introduced. Rising currents carry the fluid to regions of greater temperature and less density. The reverse is true for those parts of the fluid with downward components of velocity. The temperature at any point is deviated by an amount $\triangle T$ from its initial value. This results in a gravitational driving force per unit volume, tending to maintain the cellular motion which is given by

$$F_g = \varrho g \alpha \triangle T. \tag{3}$$

This driving force is opposed by a viscous force given roughly by

$$F = \text{const}\, \nu \varrho v / d^2, \tag{4}$$

where v is a velocity characteristic of the cellular motion. Finally, the temperature deviation, $\triangle T$, which controls the driving force is related to this velocity by the usual equation for heat conduction in a steady state, namely

$$(\mathbf{v} \cdot \nabla) T = \varkappa \nabla^2 T. \tag{5}$$

For small disturbances this equation reduces to

$$v\beta = \text{const}\, \varkappa \triangle T / d^2 \tag{6}$$

as far as orders of magnitude are concerned.

Convection starts when the driving force just balances the viscous force. From equations (3), (4), (6) and (1), this condition reduces to $R = \text{const} = R_0$. For small velocities the relation between v and $\triangle T$ [eq. (6)] is linear. However, since the temperature deviation cannot exceed the total temperature range across the fluid layer, this relation cannot hold indefinitely. Thus, if for small cellular velocities the driving force exceeds the viscous force, a limiting convective velocity eventually will be reached.

Now suppose that the fluid is without viscosity, but has a finite electrical conductivity, σ. In the presence of a magnetic field, $\mathbf{B}$, the motion generates an electromotive force proportional to $\mathbf{v} \times \mathbf{B}$, which in turn gives rise to electric currents and an electrodynamic force per volume of the order

$$F_\sigma = \sigma B^2 v. \tag{7}$$

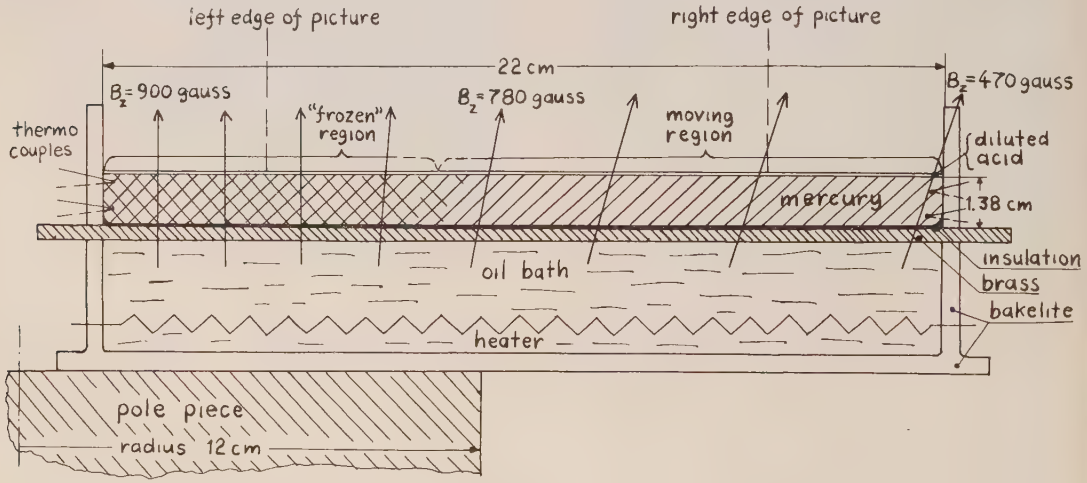

Fig. 1. Experimental arrangement used for investigation of thermal convection of mercury in an inhomogeneous magnetic field. Figure shows a cylindrical vessel composed of a lower part with a heat bath containing oil and an upper part containing a layer of mercury. Convective motion is observed at the upper surface of the mercury, which is kept clean by a thin layer of diluted acid. The directions of the magnetic field lines are indicated and the field strengths correspond to the situation of fig. 2 d. The temperature gradient is measured with thermo couples.

If magnetic and velocity fields are stationary, this force may be interpreted as a "viscous" force due to Joulean dissipation. Again equate the driving force to this "viscous" force as a condition for the onset of convection, and obtain from equations (3), (6), (7), (1), and (2)

$$\frac{\varrho g \alpha \beta d^2}{\varkappa \sigma B_z^2} = \text{const} = R/Q. \qquad (8)$$

It should be emphasized that the vertical component B_z and not the total field B has been introduced in formula (8). The horizontal component is not effective. With a purely horizontal field the convection takes place in narrow cells elongated in the direction of that field with no Joulean losses.

In general both viscous and Joulean dissipation will oppose the driving force and the onset of convection will be expressed in terms of R and Q as shown by the rigorous theory.

1. Experimental procedure

Two experiments were performed on thermal convection in a horizontal mercury layer, one with an inhomogeneous magnetic field and one with a homogeneous field forming oblique angles with the vertical direction.

Fig. 1 shows the experimental details in the first experiment. 80 watts were applied to the oil bath, which was separated from the mercury layer by a brass plate for eliminating horizontal temperature differences. Contact between mercury and all metals was prevented by a thin coating of insulating paint.

The mercury surface must be scrupulously clean in order to show convective motions. The mercury was passed through a bath of potassium hydroxide (15 %) and then through a bath of nitric acid (30 %) before each run. The mercury was always kept covered by a very thin layer of extremely dilute nitric acid which as far as could be observed had no effect on the motions of the mercury surface beneath it. Even with these precautions the surface became contaminated after an hour or so.

The temperature gradient in the mercury layer, which was 1.38 cm in depth, was measured by three pairs of copper-constantan thermocouples placed around the periphery of mercury layer. The vertical distance between the elements of a pair was 0.5 cm. The pairs were located where the applied magnetic field would have a maximum, a mean and a minimum value. Each couple had an independent circuit to avoid any possibility of short circuiting by the mercury. Temperatures were measured relative to an external constant temperature bath. The value of the temperature gradient was checked independently by the analysis of heating and cooling curves with the apparatus under similar conditions. Even so, the temperature gradient is by far the most uncertain of the experimental data.

When the mercury layer had reached a temperature of about 45° C and convective motion was clearly in evidence, magnetic fields of varying strength were applied. After the mass motion resulting from the change of the field had died down, a picture (exposure 5 sec) was taken. The method of investigating motion of the upper mercury surface was that devised by LEHNERT (1955). Clean grains of sand are sprinkled on the surface and illuminated from the side.

The pictures obtained by observing the surface on an inclined mirror show a region 13 × 9 cm in the experiment with an inhomogeneous field (Fig. 2). The cylindrical dish containing the mercury layer was placed between the pole pieces of a large electromagnet, but extended well out beyond edges of these poles into the region where the field became inhomogeneous. The central region of the pictures, as shown by Fig. 2h, comes where the field gradient was steepest.

The purpose of the second experiment was to study the effect of the direction of a homogeneous magnetic field. The dish of mercury was placed midway between the pole pieces and the magnet rotated about it. For varying values of this homogeneous field, the angle with the vertical at which the onset of convection starts was estimated. Fig. 3 was taken with a horizontal field of 4500 gauss with an exposure time of 5 seconds.

2. Experimental results

a. *Inhomogeneous magnetic field*

The pictures which map the velocity field as seen from above indicate from the length of the traces convective velocities from 0.5 to 2 mm/sec. Fig. 2a shows the convective pattern with no magnetic field and Fig. 2g

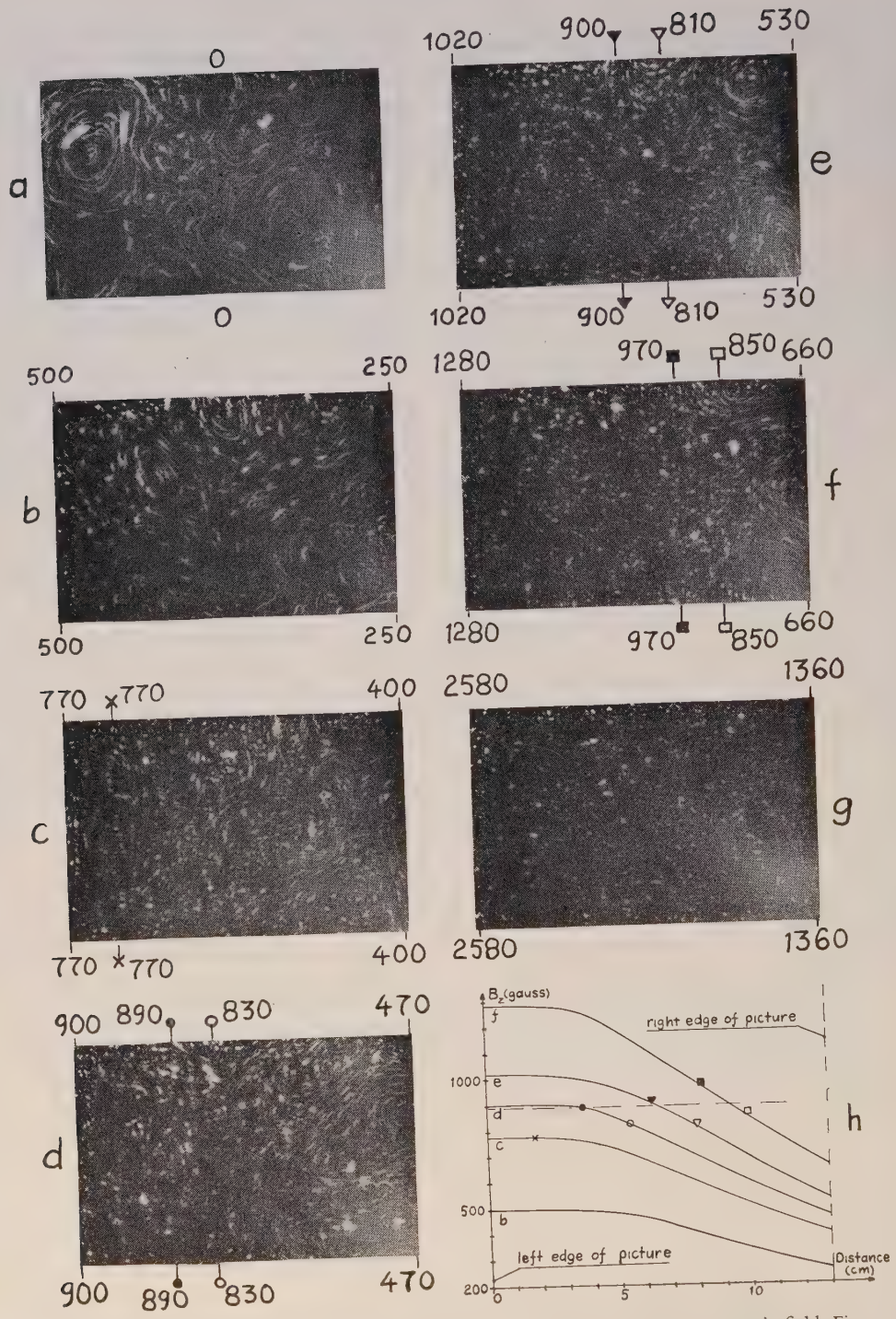

Fig. 2. Inhibition of thermal convection in mercury by an inhomogeneous magnetic field. Figs. a—g show mercury surface as seen from above. Lines of constant vertical magnetic field strength run from the top to the bottom of the pictures. Fig. h gives the distribution of the vertical field component B_z over pictures b—f from the left hand edge to the right hand edge. Fig. a is taken without magnetic field and data near the corners of figs. b—g indicate the range of field strengths in gauss. Solid marks in figs. c—h indicate lines to the left of which there is certainly no motion and open marks indicate lines to the right of which motion certainly exists. The broken horizontal line shows the estimated mean field strength 900 gauss for the onset of convection.

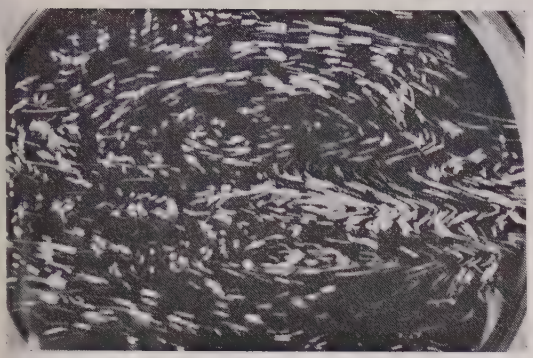

Fig. 3. Cellular convection in a layer of mercury in a magnetic field parallel to the free surface of the layer. The picture shows the surface as seen from above. The magnetic field (B = 4,500 gauss) runs from the right to the left and the cells are seen to be elongated in the field direction and to extend across the whole vessel. The flow pattern was observed to consist of alternating flow directions.

with a field strong enough to inhibit all convective motion or to "freeze" the surface. In Fig. 2b, although the maximum field is 500 gauss, there is no evidence of the inhibition of convection. The remaining pictures, Fig. 2c to f incl., clearly show the inhibiting effect of the field. Recall that the lines of constant field strength run from top to bottom of the pictures. This series of pictures was taken in quick succession keeping the attendant conditions as nearly constant as possible. As the magnetic field is increased the border line between stability and motion moves to the right. Estimates of the positions of a line to the left of which there is no motion (solid marks) and of a line to the right of which there is clearly motion (open marks) are recorded on the edge of the photographs together with the corresponding field strengths. These transition points are again indicated on the field strength curves of Fig. 2h. It may be seen that convection sets in within rather close limits for the magnetic field around a mean value of about 900 gauss.

In order to test quantitatively the theory, experimental values may be substituted in eq. (2) to find the parameter Q. Thus, in MKS rationalized units, with $d = 0.0138$ meters, $B_z = 0.090$ volt-sec./meter^2 (900 gauss), $\sigma = 1.04 \times 10^6$ mho/meter, $\varrho = 13550$ kilogram/meter^2, and $\nu = 1.08 \times 10^{-7}$ meters^2/sec., Q becomes 1100. From Chandrasekhar's values for a fluid layer with one surface free and the other fixed the corresponding critical value R_c is 6000. With this value of R_c, $g = 9.8$ meters/sec.^{2}, $\alpha = 1.81 \times 10^{-4}$ per degree and $\varkappa = 4 \times 10^{-6}$ meters^2/sec., eq. (1) yields a computed value of the temperature gradient of 40 degrees per meter. The range of experimental values was between 40 and 60 degrees per meter.

As seen from Figs. 1 and 2h, the difference between the total magnetic field and its vertical component is less than the range of values over which convection was estimated to have been inhibited. Therefore, from the results of this experiment one cannot say whether it is the total field or its vertical component (as used in eq. 2) which controls the onset of convection.

Appropriately, three regions of different states of motion might have been expected to have been found on the photographs. Following the magnetic field from high to low strengths, first might have come a "frozen" region with no motion, second a region of regular cellular convection and third a region of irregular non-stationary convection (turbulence). Only the first and third were observed. The absence of the second may be due to the fact that thermal conditions had not reached a steady state or that the cell size was too large to be uninfluenced by boundary conditions. Further, it should be remembered that the theory was developed for a homogeneous field. It might validly be applied to the inhomogeneous situation only if the size of the cells was small compared with the distance in which there was an appreciable change of field. There can be little doubt that the onset of convection alters the pattern of heat flow. With one region "frozen" and another adjacent to it in convective motion heat must flow across the boundary between them and indeed might alter the temperature of the bath below the mercury.

b. *Homogeneous, oblique magnetic field*

In the second experiment convection was studied in a homogeneous magnetic field forming oblique angles Θ with the vertical direction. The onset was estimated by visual observation of the free surface with an accuracy of about 10 % in the magnetic field strength. The estimated critical values of the total field B and the vertical component $B_z = B \cos \Theta$ are given in Table 1 for a range of different angles

Table 1. Critical values of the total magnetic field strength B and the vertical component $B_z = B \cos \Theta$ in a layer of mercury. The field forms the angle Θ with the normal direction to the free surface of the layer

Θ degrees	B gauss	B_z gauss	
0	936	936	mean: 799 ± 60
47	1080	734	
57	1440	785	
67	2160	844	
76	2880	696	
90	4500	no inhibition; see Fig. 3	

Θ. The computed value of B_z using experimental data, $d = 0.0130$ meters and a temperature gradient of 40° per meter, is 800 gauss. This agrees with the critical value given in Table 1. A picture was taken (exposure 5 sec.) with the field parallel to the free surface ($\Theta = 90°$) as shown by Fig. 3. Even with a field as strong as $B = 4500$ gauss, i.e., about five times the strength of a vertical field necessary to inhibit convection under the same attendant conditions, no inhibition could be observed. Convection took place in the form of elongated cells extended across the vessel and with stream lines running mainly parallel with the magnetic field. No measurement was made of the motion under the mercury surface. The presence of horizontal temperature gradients cannot be excluded.

The result is not fully understood at present. The dissipation for a convective pattern of cells which are "short" in the magnetic field direction is greater than that for a pattern of cells elongated in the field direction. But it is not obvious that this fact could be used as an argument for the observed effect, because one has to take into consideration the variation of the driving force with the cell shape. Further, one might as well have expected a motion in the form of long "rolls" rotating around an axis parallel with the magnetic field. As far as could be observed, no such motion was present in the experiment.

3. Conclusions

(1) The onset of convection in a horizontal layer of fluid heated from below with constant power input depends upon a critical field strength regardless of the distribution of the inhomogeneities of that field.

(2) The value of this critical field agrees with that calculated from current theory within the limits of experimental error.

(3) The boundary between moving and immovable regions is sharply defined and determined with an accuracy corresponding to a variation in field strength of about 10 percent.

(4) It is the vertical component of the magnetic field which is critical in limiting the onset of convection. A strong horizontal field does not inhibit convection.

(5) With a horizontal field the convection is limited to narrow horizontal cells elongated in the direction of the field. The motion observed was essentially along the axis and there was no evidence of motion around the axis of a cell.

At first sight the structure of sunspots might be connected with the influence of the magnetic field on convection as described in these experiments. The umbra, penumbra and the photosphere surrounding the spot would correspond to regions of thermal conduction, regular convection and turbulent motion, respectively. The needle-like structure of the granules in the penumbra would suggest a type of convective cells elongated in the directions of the diverging magnetic field of a sunspot. However, CHANDRASEKHAR (1952) has pointed out that the onset of convection is essentially different under terrestrial and astrophysical conditions. In the laboratory $1/\mu\sigma >> \varkappa$. Instability may give rise to convective motions sensitive to the magnetic field strength as shown in this experiment. In the photosphere where sunspots are seen, or in the interior of the sun under presently accepted models, $1/\mu\sigma << \varkappa$. Under this condition, instability can occur either as cellular convection or as an over-stability in the form of oscillations of increasing amplitude caused by magnetohydrodynamic waves. This latter form is insensitive to the magnetic field. Thus, the application of the results of these experiments to sunspots is of doubtful validity. However, a definite answer to the question of their applicability cannot yet be given.

Acknowledgements

The authors wish to express their thanks to Professor H. Alfvén for valuable discussions on the topics of this paper.

REFERENCES

Chandrasekhar, S., 1952: On the inhibition of convection by a magnetic field. *Phil. Mag.* [7], **43**, p. 501.

Jirlow, K., 1956: Experimental investigation of the inhibition of convection by a magnetic field. *Tellus*, **8**, p. 252.

Lehnert, B., 1955: An instability of laminar flow of mercury caused by an external magnetic field. *Proc. Roy. Soc. A*, **233**, p. 299.

Levengood, W. C., 1956: Influence of a magnetic field on thermal convection patterns. *Nature*, **177**, p. 631.

Nakagawa, Y. and Frenzen, P., 1955: A theoretical and experimental study of cellular convection in rotating fluids, *Tellus*, **7**, p. 1.

Nakagawa, Y., 1955: An experiment on the inhibition of thermal convection by a magnetic field. *Nature*, **175**, p. 417.

Rayleigh, Lord, 1916: Convection currents in a horizontal layer of fluid, when the higher temperature is on the under side. *Phil. Mag.* [6], **32**, p. 529.

Thompson, W. B., 1951: Thermal convection in a magnetic field. *Phil. Mag.* [7], **42**, p. 1417.

Herdmechanische Vorgänge bei einigen zirkumpazifischen Erdbeben[1]

Von SIEGFRIED MÜHLHÄUSER, z. Zt. Uppsala, Meteorologiska institutionen, Avdelning för seismologi

(Manuscript received July 31, 1956)

Abstract

Earthquake mechanisms can be determined by a method given by P. BYERLY and later developed by J. H. HODGSON and his collaborators. By a comparison with the tectonics of the earthquake region, it is possible in most cases to decide which of the two nodal planes represents the fault plane. As a certain arbitrariness cannot be avoided, also the stikes of the auxiliary planes have been given. If the arrows, indicating the direction of motion, have been drawn perpendicularly to the fault plane, this may mean that no auxiliary plane could be determined.

The mechanisms have been determined for 11 earthquakes in the years 1931—1950 in the Pacific area. It results that there is no general rule for the mechanisms, although the strikes of the fault planes in general coincide with the Circum-Pacific structural lines. The dip of the fault plane is as small as 31° in one case (earthquake no. 7), whereas the dip for the other cases is at least twice as large. Most of the earthquakes have a very large dip of the fault plane, in the range 70—88°. Dip values above 80° are especially frequent. The cases with smaller dip are localized to the north and northwest part of the Circum-Pacific belt.

The coastal earthquake belts of Central and South America exhibit a normal dip of the fault plane under the continent; this is also true for the northwest part of the Circum-Pacific belt. The conditions are similar at the southeast coast of Kamchatka, in Alaska, in western part of the Aleutians, and in the area between the Loyalty Islands and New Hebrides. In the other cases the fault plane dips toward the Pacific.

In northwestern Pacific belt the motions are often perpendicular to the strikes of the fault planes, whereas in the other areas the vertical motions are combined with horizontal displacements.

The number of observations for a single earthquake varies between 22 and 47. A few earthquakes in the Alpide belt have also been investigated, and comparisons with the results of other authors (A. R. RITSEMA, 1955; A. N. TANDON, 1955) showed good agreement in spite of the fact that these authors have used 4—5 times as many observations. In a particularly favourable case (HINDU KUSH, Jan. 9, 1933), 14 reliable observations of the initial motion of P waves gave the same result as 7 times as many observations, used by RITSEMA. Nevertheless, as many reliable observations as possible should be used for earthquake mechanism studies.

Allgemeines zur Rekonstruktion herdmechanischer Vorgänge bei Erdbeben

Mit plötzlichen Dislokationen verbundene geotektonische Vorgänge lassen sich rekonstruieren, wenn das Netz der Erdbebenstationen eine genügende Anzahl von Beobachtungen über die Richtung der ersten Bodenbewegung an der Erdoberfläche liefert. Die Grundlage für die Rekonstruktion eines derartigen Vorganges besteht im gesetzmässigen Zusammenhang zwischen der räumlichen Orientierung und der Tiefenlage eines Scherungsbruches einerseits, und den Impulsrich-

[1] Nach einer, an der Württembergischen Hauptstation für Erdbebenforschung ausgeführten Dissertation der T. H. Stuttgart.

tungen der von ihm ausgehenden longitudinalen Raumwellen andererseits. Bei einem Beben werden in bestimmten Zonen Dilatationsimpulse beobachtet, während die übrigen Gebiete von Compressionsimpulsen getroffen werden. Bei dem stetigen Übergang von Compression zu Dilatation im Erdkörper, bzw. bei jedem Vorzeichenwechsel der Impulsrichtung der direkten longitudinalen Raumwelle muss der Wert o durchlaufen werden. Dies ist in den Knotenflächen der Fall. Nach der allgemein herrschenden Vorstellung liegt *eine* Knotenfläche zwischen den beiden Bruchflächen eines Scherungsbruches.

Die Knotenflächen kann man in sehr grober Näherung mit Kugelschalen vergleichen, die ihre konkave Seite stets der Erdoberfläche zukehren. In Wirklichkeit weichen sie jedoch stark von dieser Form ab, da sie ja von Strahlen longitudinaler Wellen umschlossen, bzw. erfüllt sind. Die Kenntnis ihrer Lage im Erdkörper ist für ein Erdbeben zwangsläufig mit dem Wissen um die Orientierung der beiden Scherungskräftepaare im Hypozentrum, und damit ganz allgemein um den Herdvorgang identisch. Man nennt die beiden durch die Knotenflächen abgeschnittenen Kalotten zweckmässig »Nebenräume«. Ausserhalb dieser Nebenräume erstreckt sich der »Grossraum«, der die entgegengesetzte Impulsrichtung der ersten longitudinalen Raumwelle aufweist wie jene. Ist die Herdtiefe $h > 0$ so durchdringen sich die beiden Nebenräume, wobei ihre Knotenlinien auf der Erdoberfläche ein sphärisches Zweieck bilden. Der diesem Bereich anliegende Teil des Erdkörpers führt analog zum Grossraum die Bezeichnung »Kleinraum«. Für $h \to 0$ verschwindet er praktisch vollkommen. Die Existenz des durch Überschneidung beider Knotenlinien gebildeten sphärischen Zweiecks kann dann nur bei Vorhandensein sehr herdnaher Stationen nachgewiesen werden.

Die Analyse der Herdvorgänge der in dieser Veröffentlichung behandelten Erdbeben geschieht im Wesentlichen mit Hilfe der Byerlyschen Methode. Es muss jedoch schon eingangs erwähnt werden, dass der Idealzustand — zwei unmittelbar benachbarte Stationen weisen gegensätzliche erste Bodenbewegung auf — wie zu erwarten, selten zur genauen Festlegung einer, oder gar beider Knotenlinien dienen kann. Die Annahme der beiden Knotenlinien ist häufig in gewissen Grenzen variabel.

Das Beobachtungsmaterial und seine Darstellung — (Methodik der Untersuchung herdmechanischer Vorgänge)

Aus einer, im Jahre 1952 an der Württembergischen Hauptstation für Erdbebenforschung in Stuttgart erfolgten Zusammenstellung von etwa 1 500 Weltbeben der Jahre 1931—1951, die mit erkennbarem Richtungssinn der ersten Bodenbewegung aufgezeichnet worden waren, wurden 11 für herdmechanische Studien ausgewählt (MÜHLHÄUSER, 1953). Massgebend waren dabei vor allem Aufzeichnungen solcher Stationen, von denen auf Grund ihrer Instrumentierung mit Benioff-, Galitzin-, Grenet-, Hiller- oder Sprengnetherseismographen zuverlässige Angaben über die Richtung der ersten Bodenbewegung bei den betr. Erdbeben zu erwarten waren. Die Beobachtungsangaben solcher Stationen werden in den Figuren durch vollflächige Bewegungssymbole dargestellt, während die übrigen nur konturiert wiedergegeben sind.

In jeder Figur ist der Herdvorgang in einer kleinen Kartenskizze des Epizentralgebietes dargestellt.

1. Alaska — Pazifik, 17. 11. 1938 — 03h54m34s. 55,6° N—157,7° W

Beobachtungsstationen:

1	Manila	iP	C	12	Toledo	iP	D
2	Hongkong	P	C	13	Triest	iP	C
3	Vladivostok	iP	D	14	Kopenhagen	iP	C
4	Christchurch	iP	C	15	Hamburg	iP	C
5	Pasadena	iP	D	16	Stuttgart	iP	C
6	Tucson	iP	D	17	Zürich	eP	C
7	Weston	iP	C	18	Strassburg	iP	C
8	Helwan	iP	D	19	De Bilt	iP	C
9	Moskau	P	C	20	Uccle	iP	C
10	Pulkovo	P	C	21	Kew	iP	C
11	Rom	iP	C	22	Ksara	iP	C

a) Herdlage: Die hauptsächlich mesozoisch gefalteten Gebirgsketten der Kordilleren setzen sich im Norden im Hochland von Alaska in südwestlicher Richtung fort. Der Herd liegt am Ostrand des Aleuten-Grabens in normaler Tiefe. Die Entfernung des Epizentrums von der Küstenlinie beträgt etwa 65 km. Der Herd fügt sich nach Lage, Tiefe und Richtung der ersten Bodenbewegung in Pasadena (BÅTH, 1952) und Stuttgart (MÜHLHÄUSER, 1953) zwanglos in die für diese Region bekannte Regelmässigkeit ein.

b) Herdvorgang: Die Beobachtungsangaben

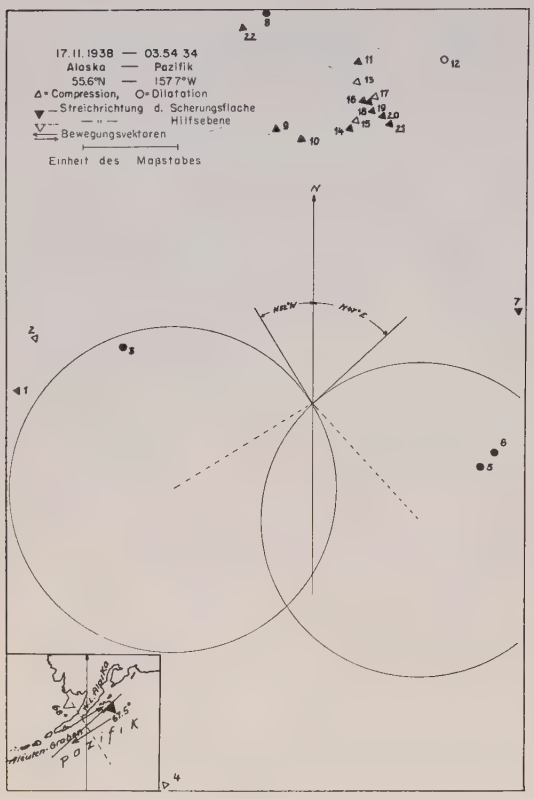

Fig. 1.

weisen besonders im Norden eine überdurchschnittliche Dichte auf. Hier liegen in einem Sektor von 33° ausser den europäischen Stationen noch Helwan und Ksara. Mit Ausnahme Toledos, Belgrads und Helwans liegt in diesem Sektor Compression vor.

Manila, Hongkong und Vladivostok legen einen westwärts gerichteten Sektor fest. Das herdnähere Vladivostok gibt Dilatation, die ferneren Stationen Manila und Hongkong Compression an.

In südwestlicher Richtung liegt Christchurch mit Compression.

Der nach Osten gerichtete amerikanische Sektor weist im Norden Compression auf (Weston), während die südlichen Stationen Tucson und Pasadena Dilatation angeben. Die zwischen beiden Bereichen liegenden Stationen Florissant und St. Louis sind nicht in der Lage, die Richtung der ersten Bodenbewegung anzugeben. Wahrscheinlich rührt dies von der Nähe der Knotenlinie her.

Die dem Epizentrum am nächsten liegenden Stationen sind im Westen Vladivostok, im Osten Pasadena und Tucson. Alle drei Stationen haben Dilatation beobachtet. Die Vermutung liegt daher nahe, dass die beiden Nebenräume Bereiche mit Dilatation sind. Im Widerspruch hierzu stehen die Angaben von Helwan (8) und Toledo (12). Diese beiden Stationen können ihrer Lage nach nicht auf der Oberfläche der beiden Nebenräume liegen, da sie vom Epizentrum eine Zone mit Compression trennt. Ein Vergleich der theoretischen Laufzeit mit der beobachteten zeigt für die Angabe von Helwan eine Verzögerung des P-Einsatzes von 7 Sekunden (H. Jeffreys und K. E. Bullen, 1940). Bei der Auswertung des Seismogrammes wurde wahrscheinlich erst die der Compression nachfolgende Dilatation als P-Einsatz angesprochen. Ähnliche Fehldeutungen liegen möglicherweise auch für Belgrad und Toledo vor.

Nach der Byerlyschen Formulierung steht die Hilfsebene (d. i. die dem sekundären Scherungskräftepaar zugehörige Knotenfläche) senkrecht auf dem, den Bruch bewirkenden primären Scherungskräftepaar. In Karte 1 streicht die nach Südosten einfallende Fläche unter einem Winkel von 47° E. Diese Richtung entspricht ungefähr dem integrierten Verlauf der Küstenlinie in diesem Bereich. Die Annahme, dass diese Fläche die Scherungsfläche ist, liegt daher nahe. Sie fällt unter einem Winkel von $\sigma_1 = 68°$ ein. Der Ergänzungswinkel zu 90° ist 22°. Die Hilfsebene ist also so zu konstruieren, dass eine im Epizentrum auf der Streichrichtung der Scherungsfläche senkrecht stehende Gerade in sie zu liegen kommt, wenn sie unter einem Winkel von 22° nach Nordwesten eintaucht. Die so bedingte Ebene streicht N 32° W und fällt unter einem Winkel von $\sigma_2 = 68°$ gegen Südwesten ein.

Der Herdvorhang vollzog sich unter der Annahme, die N 47° E streichende, und unter 68° nach Südosten einfallende Ebene sei die Bewegungsfläche, folgendermassen: Die pazifische Seite bewegte sich relativ zur kontinentalen unter einem Winkel von $(90 - \sigma_1) = 22°$ nach oben und gleichzeitig in südwestlicher Richtung. Die Projektion dieser Bewegungsrichtung in die Kartenebene ist S 58° W.

In Figur 1 ist das Ergebnis der Rekonstruktion der den Bruch bewirkenden Scherungs-

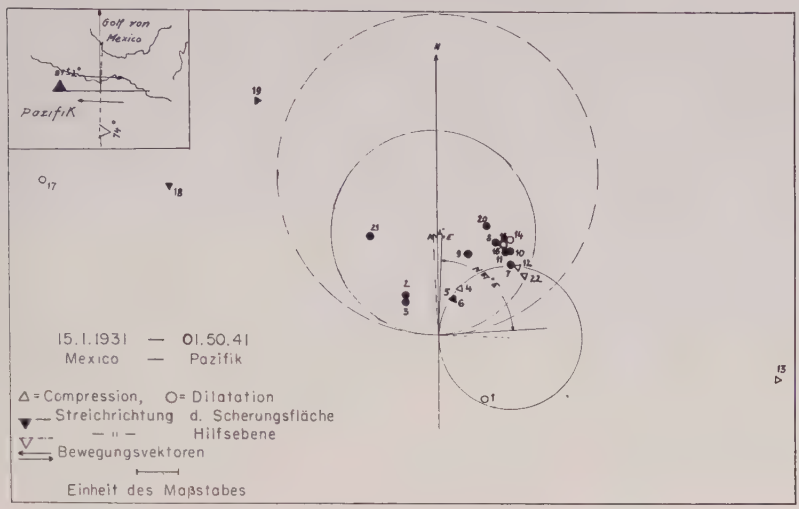

Fig. 2.

kräfte eingezeichnet. Die in der Randskizze mit einem vollflächigen Dreieck versehene Gerade stellt die Streichrichtung der wahrscheinlichen Verschiebungsfläche dar, entsprechend strich-punktiert die der Hilfsebene. Die bei den Dreiecken stehenden Gradzahlen geben die Neigung der betr. Ebene an. Die Dreiecke weisen in die Einfallsrichtung. Die beiden parallelen Pfeile symbolisieren das primäre Scherungskräftepaar. Zeigt ein Pfeil gegen die Streichrichtung auf der Einfallsseite, so ist damit der obere Vektor symbolisiert und umgekehrt.

2. Mexiko — Pazifik, 15. 1. 1931 — 01h50m41s. 16,4° N — 96,3° W

Beobachtungsstationen:

1	La Plata	iP	D	12	Toledo	iP	C
2	Berkeley	iP	D	13	Tananarivo	ePKP	C
3	Pasadena	iP	D	14	Wien	iP	D
4	Toronto	iP	C	15	Göttingen	iP	D
5	Florissant	iP	C	16	Hamburg	iP	D
6	St. Louis	iP	C	17	Batavia	iPKP	D
7	Kew	iP	D	18	Manila	iPKP	C
8	Kopenhagen	iP	D	19	Zi-Ka-Wei	ePKP	C
9	Scoresby-Sund	iP	D	20	Pulkovo	?	D
10	Strassburg	iP	D	21	Vladivostok	?	D
11	Uccle	iP	D	22	Cartuja	iP	C

a) Herdlage: Der Herd liegt in der Küstenzone Pazifik-Cordilleren, am Ostrand des Acapulco-Grabens. Im Gegensatz zu der im übrigen amerikanischen Küstenbereich vorherrschenden Nordwest-Südostrichtung der Faltengebirgsketten überwiegt im Herdbereich die Ost-Westrichtung, gleichsam als ob durch eine Bewegung der amerikanischen Kontinentalschollen nach Süden hier eine Stauzone vorliegen würde, deren Streichrichtung senkrecht auf der Bewegungsrichtung steht.

b) Herdvorgang: Sämtliche beobachtenden Stationen verteilen sich auf eine, vom Epizentrum aus gesehen, nordöstliche Hemisphäre. Wegen der grossen Epizentraldistanzen von Tananarivo ($\triangle = 145{,}5°$), 13, und Manila ($\triangle = 131.9°$), 18, können die Nebenräume keine Bereiche mit Compression sein.

Ein Kreis ist genau festgelegt. Er umschliesst sämtliche Stationen mit Compression innerhalb einer Herdentfernung von $\triangle = 82.3°$, ausserdem la Paz mit Dilatation und geht durch das Epizentrum. Weiterhin muss dieser Kreis zwischen Kew (Dilatation) und Toledo (Compression) verlaufen. Eine Fläche, die diesem Kreis entspricht, streicht im Epizentrum N 2° E und fällt unter einem Winkel von $\sigma_1 = 74° 20'$ gegen Osten ein. Diese Werte legen den zweiten Kreis innerhalb gewisser Grenzen fest, auf Grund der Rechtwinkligkeitsbeziehung zwischem primärem Scherungskräftepaar und Hilfsebene. Der zweite Kreis muss sämtliche Stationen mit Dilatation, und ausserdem die im ersten liegenden mit Compression einschliessen. Da er darüberhinaus die Rechtwinkligkeitsbedingung erfüllen muss ergeben

sich für ihn folgende Lagewerte: Die kleinste mögliche Fläche streicht im Epizentrum N 87° E und fällt unter einem Winkel von 79° gegen Norden ein. Die Maximalfläche ist durch zwei Bedingungen festgelegt, denen sie genügen muss: 1. Die Radien der beiden Kreise können keinen kleineren Winkel als 90° miteinander bilden, da die Senkrechte auf der Streichrichtung einer Fläche im Epizentrum in der zweiten Fläche liegen muss. 2. Die Knotenlinie muss zwischen Epizentrum und Zi-Ka-Wei (19) verlaufen. Diese Forderungen erfüllt eine Fläche, die genau in Ost-Westrichtung streicht und unter einem Winkel von 83° gegen Norden einfällt.

Das Übereinstimmen der Streichrichtung dieser Fläche mit dem Küstenverlauf gibt dieser bei der Wahl der Bewegungsfläche den Vorzug vor der nach Osten einfallenden. Demnach streicht die Scherungsfläche etwa Ost—West $\pm 2°$ und fällt unter einem Winkel von $\sigma_2 = 81 \pm 2°$ nach Norden ein. In diesem Fall ist der mechanische Vorgang im Herd durch ein relatives Untertauchen der pazifischen Masse unter den Kontinentalrand, bei gleichzeitiger Ost-Westbewegung, zu erklären. Der Bewegungsvektor weist eine Neigung von $(90° - \sigma_1) = 15° 40'$, bei einer Streichrichtung von N 88° W (in der Horizontalprojektion) auf.

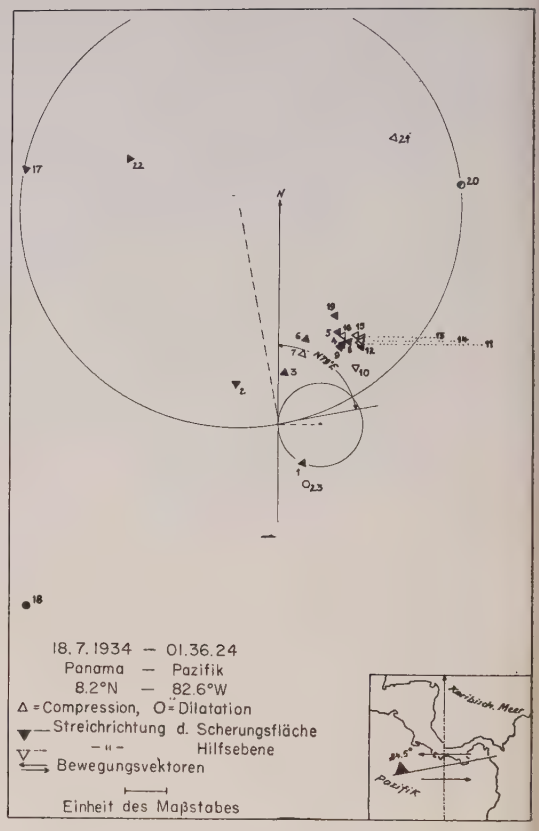

Fig. 3.

3. Panama — Pazifik, 18. 7. 1934 — 01h36m29s. 8,2° N — 82,6° W

Beobachtungsstationen:

1	La Paz	iP	C	13	Belgrad	iP	C
2	Pasadena	iP	C	14	Zagreb	eP	C
3	Washington	iP	C	15	Wien	iP	C
4	Kew	iP	C	16	Hamburg	iP	C
5	Kopenhagen	iP	C	17	Manila	iPKP	C
6	Scoresby-Sund	iP	C	18	Riverview	iP	D
7	Ivigtut	iP	C	19	Pulkovo	i	C
8	Strassburg	iP	C	20	Baku	eP	D
9	Uccle	iP	C	21	Tashkent	?	C
10	Cartuja	iP	C	22	Vladivostok	?	C
11	Triest	iP	C	23	La Plata	iP	D
12	Firenze	iP	C				

a) Herdlage: Der Herd liegt südöstlich Kap Burica in der pazifischen Grenzzone. Die von Osten kommenden tertiären Falten der mittelamerikanischen Cordilleren biegen im Hinterland des Herdgebietes nach Nordwesten um.

b) Herdvorgang: Der Lage der Beobachtungspunkte in Figur 3 zufolge müssen die Nebenräume Bereiche mit Compression sein, da es keine Knotenlinien gibt, welche die Stationspunkte mit Dilatation umschliessen und gleichzeitig sinngemäss gegen die Beobachtungsstationen mit Compression abgrenzen.

Für die beiden Kreise von Bewegungs- und Hilfsebene bestehen folgende Konstruktionsbedingungen: Der erste muss alle Stationen mit Compression, ausgenommen La Paz (1), umschliessen und zwischen Tashkent (21) mit Compression und Baku (20) mit Dilatation verlaufen. Durch die letztgenannte Bedingung ist seine Grösse in gewissen Grenzen festgelegt. Der zweite Kreis muss im Südosten zwischen La Paz (1) und La Plata (23) hindurchgehen. Die Möglichkeiten, die zur Konstruktion beider Kreise — jeden für sich betrachtet — bestehen, werden durch die Rechtwinkligkeitsbeziehung zwischen Bewegungsvektoren und Hilfsebene auf eine einzige zurückgeführt. Sie genügt jedoch der theoretischen Gesetzmässigkeit insofern nicht, als die Streichrichtung des kleinen Kreises genau nach Norden weist, anstelle von 48° W.

Interessant ist der e-Einsatz im Seismogramm von Baku (20), das ja nach Figur 3 in unmittelbarer Nähe der Knotenlinie liegt. Diese entspricht einer N 79° E streichenden Fläche, die unter einem Winkel von $\sigma_1 = 84{,}5°$ nach Nordwesten einfällt. Die zweite streicht Nord-Süd, bei einem Einfallswinkel von $\sigma_2 = 63°$. Der Kleinraum ist frei von Beobachtungsangaben, während der Grossraum Dilatationsbereich ist.

Die Richtung der nördlich einfallenden Fläche tritt bevorzugt unter den Bruchlinien der pazifisch-kontinentalen Grenzzone auf, sodass die Annahme gerechtfertigt erscheint, dass diese Fläche die Bewegungsebene enthält. Die vorliegende Verteilung von Compression und Dilatation wurde demnach durch einen Vorgang bewirkt, der in einer Abwärtsbewegung des kontinentwärts liegenden Teils bei gleichzeitiger Westdrift bestand.

4. Kermadek-Inseln, 10. 12. 1950 — 13h23m04s. 28,7° S — 179° W. h = 300 km

Beobachtungsstationen:

1	Apia	iP	D	14	Prag	?	D
2	Brisbane	iP	D	15	De Bilt	iPKP	D
3	Riverview	iP	D	16	Kew	iPKP	D
4	Fukuoka	iP	D	17	Stuttgart	iPKP	D
5	Osaka	iP	D	18	Strassburg	iPKP	D
6	Sapporo	?	D	19	Zürich	ePKP	D
7	Pasadena	iP	D	20	Chur	ePKP	D
8	Berkeley	iP	D	21	Rom	?	D
9	Seattle	iP	D	22	Lissabon	?	D
10	Victoria	iPKP	D	23	Cartuja	iPKP	C
11	Helwan	iPKP	C	24	Alger	iPKP	D
12	Uppsala	iPKP	D	25	Tamanrasset	iPKP	C
13	Belgrad	ePKP	D				

a) Herdlage: Der Herd liegt nordwestlich der Kermadek-Inselgruppe in einer Bruchlinie, die vom Kermadek-Graben durch einen schmalen Rücken getrennt wird. Diese aufragende Zone streicht wie der Kermadek-Graben in Richtung SSW—NNO.

b) Herdvorgang: Auffallend ist das völlige Übereinstimmen in den Angaben über die Richtung der ersten Bodenbewegung bei den japanischen Stationen, sodass die ganze Nordhemisphäre, mit Ausnahme von Cartuja und Helwan, Dilatationsbereich ist. Daher muss der grosse Kreis Cartuja (23) und Helwan (11) mit Compression ausschliessen, die auf Dilatation lautende Angabe von Alger jedoch in den Dilatationsbereich einbeziehen, Die Fläche, die diesem Kreis entspricht, streicht im Epi-

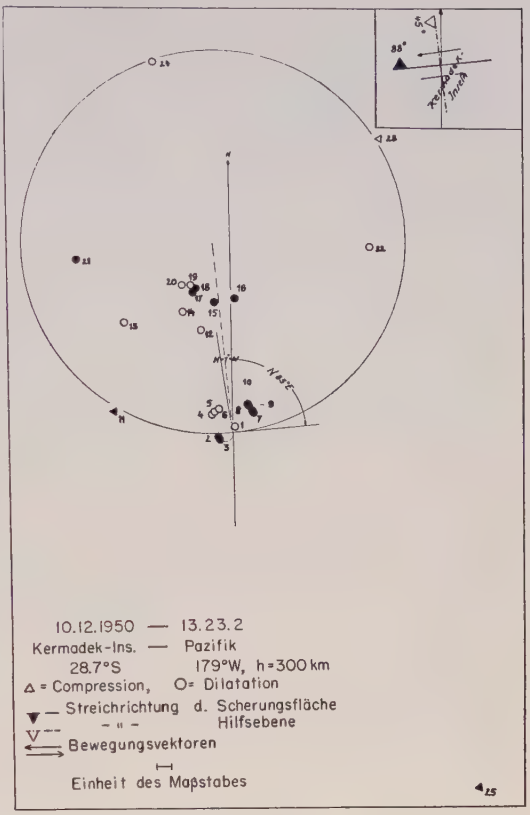

Fig. 4.

zentrum N 85° E und fällt unter einem Winkel von $\sigma_1 = 88°$ gegen Norden ein.

Der Verlauf des kleinen Kreises ist durch die Lage von Brisbane (2) und Riverview (3) festgelegt. Sein Radius entspricht einem Maximalwert, da er sowohl durch das Epizentrum gehen, als auch Apia (1) ausserhalb seiner Fläche belassen muss. Nach der Rechtwinkligkeitsbeziehung streicht diese, unter einem Winkel von $\sigma_2 = 45°$ gegen Westen einfallende Fläche in Epizentrum N 7° W.

Die Bewegungsfläche stellt wahrscheinlich die unter einem Winkel von 88° nach Nordwesten einfallende, N 85° E streichende Ebene dar. Die starre pazifische Tafel führt entlang der Bewegungsebene eine nahezu vertikale Bewegung (88° Neigung) aus, und zwar steigt der nördlich der Trennungsebene liegende Teil relativ zum südlichen auf, unter gleichzeitiger Bewegung in Richtung S 83° W. Die Bewegungsrichtung bildet mit der Horizontalen den Winkel $(90° - \delta_2) = 45°$.

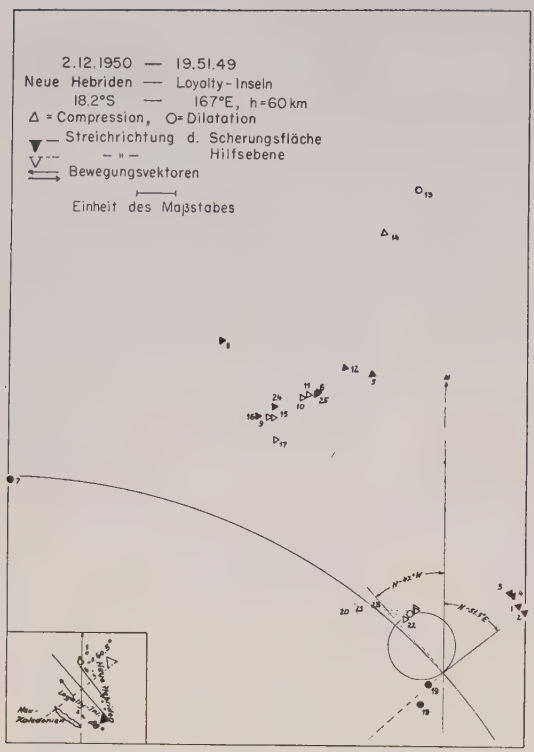

Fig. 5.

5. Neue Hebriden—Loyalty-Inseln, 2. 12. 1950 — 19h51m49s. — 18,2° S — 167° E. h = 60 km

Beobachtungsstationen:

1	Berkeley	iP	C	14	Lissabon	?PKP	C
2	Pasadena	iP	C	15	Triest	iPKP	C
3	Seattle	iP	C	16	Rom	iPKP	C
4	Victoria	iP	C	17	Belgrad	ePKP	C
5	Kew	iPKP	C	18	Riverview	iP	D
6	Strassburg	iPKP	C	19	Brisbane	iP	D
7	Tamanrasset	iPKP	D	20	Sumoto	?	D
8	Alger	iPKP	C	21	Sendai	?	C
9	Basel	ePKP	C	22	Nagasaki	?	C
10	Chur	ePKP	C	23	Morioka	?	C
11	Zürich	ePKP	C	24	Firenze	?	C
12	De Bilt	iPKP	C	25	Stuttgart	iPKP	C
13	Cartuja	iPKP	D				

a) Herdlage: Der Herd liegt in einem SO—NW gerichteten Senkungsfeld des pazifischen Untergrundes, zwischen den Neuen Hebriden und den Loyalty-Inseln. Dieses Senkungsfeld wird im Osten von dem in gleicher Richtung streichenden Hebriden-Rücken gegen die innerpazifische Tiefseeflur abgeschlossen.

b) Herdvorgang: Die Verteilung von Compression und Dilatation weist ähnliche Züge auf wie beim Kermadekbeben vom 10. 12. 1950, jedoch sind hier die beiden Einsatzsymbole vertauscht. Durch die Lage Sumotos (20), das mit Dilatation verzeichnet ist, scheidet die Möglichkeit aus, die dargestellten Beobachtungspunkte im Compressionsbereich mit einer Knotenlinie zu umschliessen. Es ergibt sich daher die Notwendigkeit, die Nebenräume als Dilatationsbereiche anzunehmen und beide Kreise so zu legen, dass sie die dargestellten Stationen mit Dilatationsangabe umfassen, und gegen die übrige Fläche des Gross-, sowie des Kleinraumes abgrenzen. Eine Knotenlinie ist durch die Lage Sumotos (20) zwischen Sendai (21) und Nagasaki (22) genau festgelegt. Die diesem Kreis zukommende Fläche streicht im Epizentrum N 51,5° E und fällt unter einem Winkel von $\sigma_1 = 60{,}5°$ gegen Nordwesten ein. Die zweite Knotenlinie umschliesst Tamanrasset (7), Riverview (18) und Brisbane (19) mit Dilatation. Für die Streichrichtung der zweiten Fläche ergibt sich der Wert N 42° W und ein Einfallswinkel von $\sigma_2 = 88°$ gegen SW.

Die auf Dilatation lautende Angabe über die Richtung der ersten Bodenbewegung in Cartuja (13) beruht offensichtlich auf einer Fehldeutung des ersten Einsatzes im Seismogramm. Bei einem Vergleich der theoretischen Laufzeit (H. Jeffreys and K. E. Bullen 1940) mit der beobachteten ergibt sich für die letztgenannte eine Verspätung der direkten longitudinalen Welle von 19,2 Sekunden. Die Beobachtungsangabe Cartujas beruht auf der Registrierung der E-Komponente, da eine Vertikalbewegung wohl nicht mit genügender Deutlichkeit aufgezeichnet wurde.

Die gute Übereinstimmung in der Streichrichtung der gegen SW einfallenden Ebene mit dem Verlauf der Inselkette der Neuen Hebriden bzw. Neu-Kaledoniens und der zwischen beiden sich erstreckenden Tiefzone weist dieser Fläche mit grosser Wahrscheinlichkeit die Funktion der Scherungsebene zu. Unter dieser Voraussetzung bewegt sich die innerpazifische Seite entlang einer unter 88° gegen SW einfallenden Ebene abwärts und gleichzeitig in Richtung S 38,5° E. Die Bewegungsrichtung schliesst im Epizentrum mit der Horizontalen einen Winkel von $(90° - \sigma_1) = 29{,}5°$ ein.

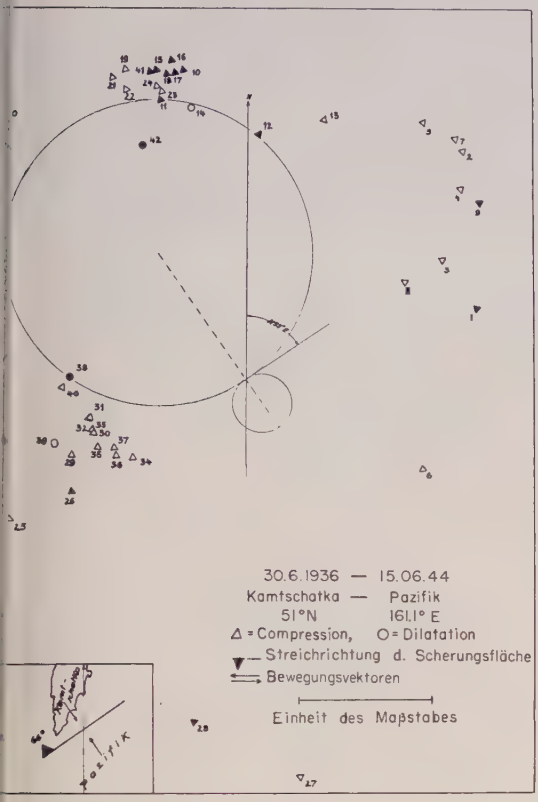

Fig. 6.

6. Kamtschatka — Pazifik, 30. 6. 1936 — 15h06m44s. 51° N — 161,1° E

Beobachtungsstationen:

1	Pasadena	iP	C	22	Wien	iP	C
2	Harvard	iP	C	23	Göttingen	iP	C
3	Bozeman	iP	C	24	Hamburg	iP	C
4	Chikago	iP	C	25	Batavia	iP	C
5	East Madias	?	C	26	Manila	iP	C
6	Honolulu	iP	C	27	Christchurch	iP	C
7	Philadelphia	iP	C	28	Riverview	iP	C
8	Sitka	iP	C	29	Taihoku	P	C
9	Florissant	iP	C	30	Husan	iP	C
10	Kew	iP	C	31	Keizyo	iP	C
11	Kopenhagen	iP	C	32	Zinsen	iP	C
12	Scoresby-Sund	iP	C	33	Taikyu	iP	C
13	Ivigtut	iP	C	34	Numadu	iP	C
14	Bergen	iP	D	35	Hukuoka	P	C
15	Strassburg	iP	C	36	Kobe	iP	C
16	Paris	iP	C	37	Toyooka	P	C
17	Uccle	iP	C	38	Chiufeng	iP	D
18	De Bilt	iP	C	39	Hongkong	P	D
19	Triest	iP	C	40	Nangking	iP	C
20	Ksara	iP	C	41	Stuttgart	iP	C
21	Zagreb	iP	C	42	Moskau	iP	D

a) Herdlage: Der Herd liegt im nördlichen Bereich der grossen nordwestpazifischen Störungszone, im Mittelteil des Kamtschatkagrabens. Das Hypozentrum ist das nödlichste der folgenden Reihe von Beben aus der nordwestpazifischen Zone.

b) Herdvorgang: Die auf Dilatation lautenden Angaben machen weniger als 10 % des reichhaltigen Beobachtungsmateriales aus. Dies ist der Grund, weshalb nur *eine* Knotenlinie durch Beobachtungsstationen belegt werden kann. Stationen, die als erste Beobachtung Compression angeben sind in fast sämtlichen Azimuten vorhanden. Der Grossraum stellt somit offensichtlich einen Bereich mit Compression dar.

Eine Knotenfläche ist, wie Figur 6 zeigt, mit grosser Genauigkeit festgelegt. Ihre kreisförmige Begrenzung muss die Stationen, Bergen (14), Moskau (42) und Chiufeng (38) mit Dilatation einschliessen. Kopenhagen (11) liegt mit Compression in unmittelbarer Nähe dieses Kreises, sodass dieser sowohl nach Durchmesser als auch nach Lage bestimmt ist. Der Einfallswinkel dieser Knotenfläche ist $\sigma_1 = 66° 20'$, ihre Streichrichtung beträgt N 55,5° E.

Für die Definition der zweiten Knotenebene besteht nur die Möglichkeit, die Neigung dieser Fläche der Forderung nach zu bestimmen, dass primäres Scherungskräftepaar und Hilfsebene aufeinander senkrecht stehen. Von den zahlreichen Möglichkeiten, die es für die Lage der zweiten Knotenfläche gibt, stellt die in Figur 6 gewählte die einfachste Lösung dar. Bei gleicher Streichrichtung wie Knotenebene 1 kommt ihr ein Einfallswinkel von $(90° - \sigma_1) = 23° 40'$ zu.

Die Streichrichtung der gegen Nordwesten einfallenden Knotenebene enspricht ungefähr dem integrierten Verlauf des Kamtschatkagrabens, sodass sie wohl als Scherungsfläche angesehen werden darf. Wird die Hilfsebene so gewählt wie es auf Figur 6 der Fall ist, vollzog sich der Herdvorgang folgendermassen: Entlang einer unter 66° 20′ nach NW einfallenden, N 55° E streichenden Bewegungsebene, schiebt sich die pazifische Masse relativ unter die eurasische Randzone hinab.

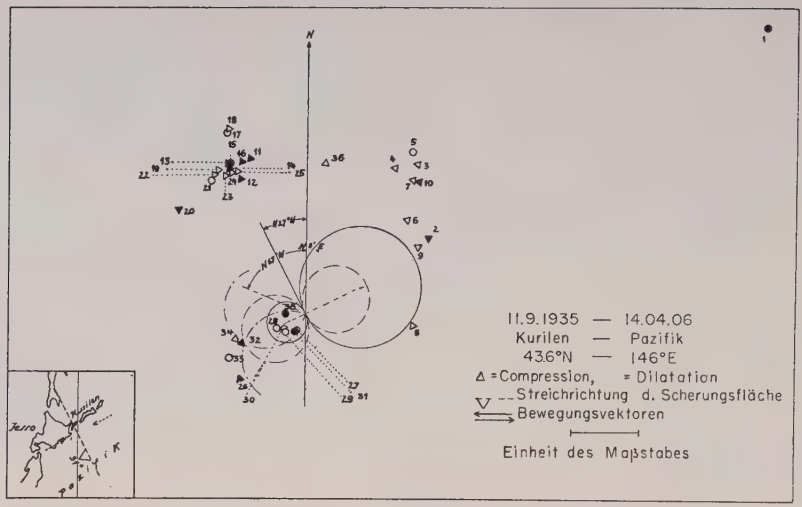

Fig. 7.

7. Kurilen — Pazifik, 11. 9. 1935 — 14h04m06s. 43,6° N — 146° E

Beobachtungsstationen:

1	La Paz	iPKP	D	19	Triest	iP	C
2	Pasadena	iP	C	20	Ksara	iP	C
3	Harvard	iP	C	21	Belgrad	iP	D
4	Toronto	iP	C	22	Zagreb	eP	C
5	Charlottesville	iP	D	23	Wien	iP	C
6	Bozeman	?	C	24	Leipzig	iP	C
7	Chikago	?	C	25	Göttingen	iP	C
8	Honolulu	?	C	26	Manila	iP	C
9	Ukiah	?	C	27	Tyosen	iP	D
10	Florissant	?	C	28	Husan	iP	D
11	Kew	iP	C	29	Kobe	iP	D
12	Kopenhagen	iP	C	30	Toyooka	eP	D
13	Zürich	eP	C	31	Tokyo	?	D
14	Strassburg	i	D	32	Zi-Ka-Wei	iP	C
15	Stuttgart	iP	C	33	Hongkong	P	D
16	Uccle	iP	C	34	Nangking	iP	C
17	Cartuja	iP	D	35	Vladivostok	iP	D
18	San Fernando	P	C				

a) Herdlage: Der Herd liegt 50 km östlich des Ostkaps der japanischen Nordinsel Jesso, in unmittelbarer Nähe des Bereiches in welchem die Inselkette der Kurilen gegen den japanischen Inselbogen stösst. Das Herdgebiet ist ausserdem durch die Nähe des Japangrabens ausgezeichnet, in den der Schelfbereich auf der Höhe des Epizentrums abbricht.

b) Herdvorgang: In den mit Beobachtungsstationen besetzten Kreisausschnitten lassen sich angesichts Figur 7 mehere widerspruchsvolle Angaben über die Richtung der ersten Bodenbewegung feststellen. Hierher gehören im europäischen Sektor diejenigen von Belgrad und Strassburg. Beide Stationen liegen in einem mehrfach belegten Bereich mit Compression, geben aber als Richtung der ersten Bodenbewegung Dilatation an. Ähnlich liegen die Verhältnisse bei Charlottesville und Hongkong.

Wenn man annimmt, dass die Nebenräume Bereiche mit Dilatation darstellen, muss eine Knotenlinie die südwestlichen Stationen mit Dilatation umschliessen und zwischen Husan (28) und Zi-Ka-Wei (32) verlaufen. Es gibt für die Lage dieses Kreises zahlreiche Möglichkeiten. Den einfachsten Fall stellt der kleine ausgezogene Kreis dar. Er, sowie der einem Grenzfall entsprechende gestrichelte kommen Ebenen zu, die im Epizentrum N 27° W streichen. Als zweite Fläche ergänzt die dem grossen, nordwestlich liegenden Kreis angehörende Ebene mit ihrem Einfallswinkel die Neigung des kleinen südwestlichen Kreises, die 31° beträgt, zu 90°. Entsprechendes gilt für die beiden gestrichelten Kreise.

Die nördliche, bzw. südliche Grenzlage der westlichen Knotenfläche ist durch zwei fragmentarische, strich-punktierte Kreise symbolisiert. Die Streichrichtung der dem nördlichen Kreis entsprechenden Fläche ist N 8,5° E, ihr Einfallswinkel 50° gegen Westen. Die Werte für die südliche Grenzlage sind analog N 67° W und 54° SW.

Die pazifische Seite tauchte demnach beim Herdvorgang unter den Kontinentalrand hinab,

und zwar entlang einer Fläche deren wahrscheinlichste Streichrichtung (s. oben) etwa N 27° W beträgt und die unter einem Winkel von etwa 31—45° gegen Südwesten einfällt. Da die Hilfsebene nicht bestimmbar ist, kann über die Neigung der Bewegungsvektoren innerhalb der Scherungsfläche nichts ausgesagt werden.

8. Japanisches Meer, 13. 11. 1932 — 04h46m45s. 43,4° N — 137° E. h = 330 km

Beobachtungsstationen:

1 La Paz	iP	C	17 Sapporo	?	D
2 Berkeley	iP	C	18 Akita	?	D
3 Pasadena	iP	C	19 Morioka	?	D
4 Kew	iP	D	20 Nemuro	?	D
5 Strassburg	iP	D	21 Sendai	?	D
6 Uccle	iP	D	22 Nagano	?	D
7 Cartuja	iP	D	23 Mito	?	D
8 Belgrad	iP	D	24 Toyooka	?	D
9 Göttingen	iP	D	25 Hatidyozima	?	D
10 Hamburg	iP	D	26 Nagasaki	?	D
11 Batavia	iP	C	27 Miyazaki	?	D
12 Riverview	iP	C	28 Zi-Ka-Wei	iP	C
13 Taihoku	P	D	29 Chiufeng	iP	D
14 Zinsen	iP	C	30 Sverdlovsk	?	D
15 Hukuoka	iP	D	31 Stuttgart	iP	D
16 Kobe	iP	D			

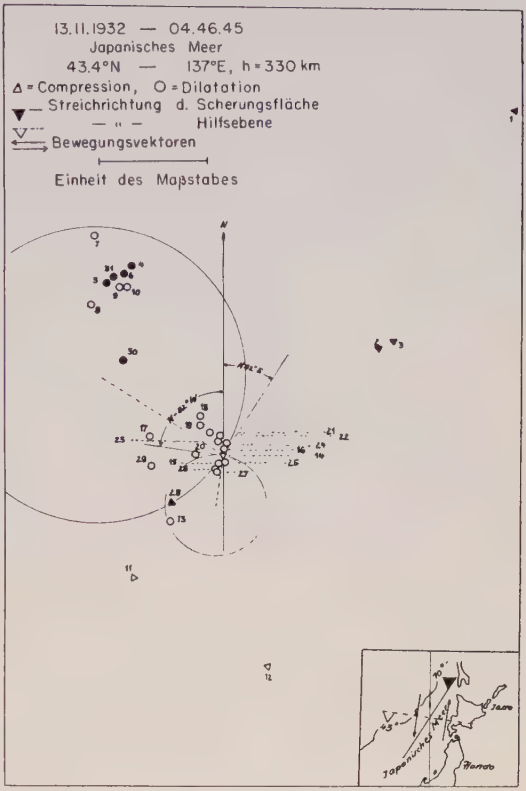

Fig. 8.

a) Herdlage: Das Mandschurisch-Ochotskische Staffelland und der Westteil der Muldenzone, im vorliegenden Fall des japanischen Beckens, zeichnen sich durch tiefliegende Erdbebenherde aus. Frühere Bearbeitungen haben gezeigt u. a. (MÜHLHÄUSER, 1955), dass hierbei die Herdtiefen von Südosten in nordwestlicher Richtung zunehmen.

b) Herdvorgang: Figur 8 zeigt sehr deutlich, dass die Nebenräume Bereiche mit Dilatation sind, und die beiden Knotenlinien, ohne Widerspruch in der Impulsverteilung konstruiert werden können. Der erste Kreis muss die Dilatationspunkte der japanischen Stationen 15, 25, 26, 27 und 13 umschliessen. Dies ist nur möglich, wenn auch Zi-Ka-Wei mit Compression in diese Fläche einbezogen wird. Durch diese Bedingungen, sowie durch die Lage von Nemuro (20) ist diese Knotenlinie eindeutig festgelegt. Sie gehört einer Ebene an, die unter einem Winkel von $\sigma_1 = 43° 10'$ gegen Süden einfällt und N 82° W streicht. Die zweite Knotenlinie bezieht die übrigen japanischen Stationen mit den europäischen in einen zweiten Bereich mit Dilatation ein, und schneidet aus der ersten Kreisfläche ein Zweieck aus, in dem Zi-Ka-Wei (28) mit Compression liegt.

Die Streichrichtung der Ebene, die diesem Kreis entspricht, stimmt sehr gut mit der allgemeinen, NE—SW verlaufenden Richtung des Ostabbruches des Mandschurisch-Ochotskischen Staffellandes überein. Diese Tatsache weist dieser Fläche mit grosser Wahrscheinlichkeit die Funktion der Scherungsfläche zu. Unter dieser Annahme ist der mechanische Vorgang im Herd auf ein Untertauchen der südöstlichen, dem Pazifik zugewandten Seite unter den eurasischen Kontinent zurückzuführen. Gleichzeitig mit dieser relativen Abwärtsbewegung findet eine Verschiebung der pazifischen Seite in Richtung N 8° E statt. Die Bewegungsrichtung ist gegen die Horizontale um $90° - \sigma_1 = 46° 50'$ geneigt und liegt in einer Ebene, die N 32° E streicht und unter einem Winkel von $\sigma_2 = 70°$ gegen NW einfällt.

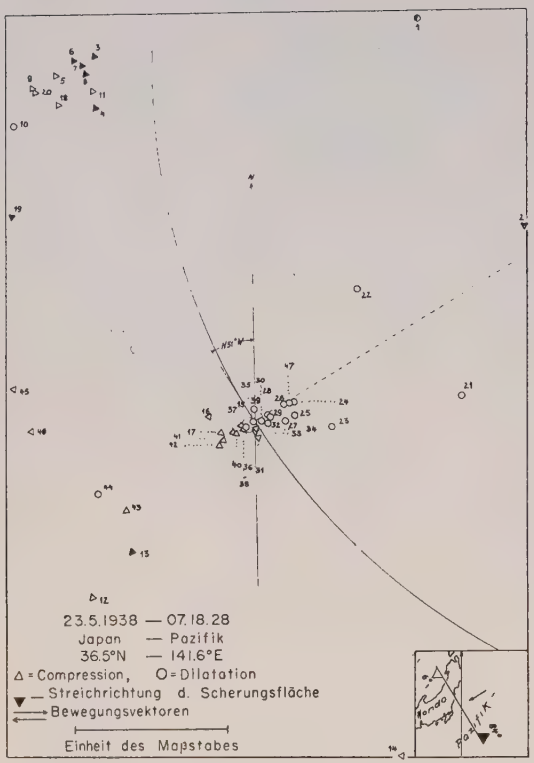

Fig. 9.

9. Japan — Pazifik, 23. 5. 1938 — 07h18m28s. 36,5° N — 141,6° E

Beobachtungsstationen:

1	Weston	eP	D	25	Kumagaya	?	D
2	Tucson	eP	C	26	Yokohama	?	D
3	Kew	iP	C	27	Maebasi	?	D
4	Kopenhagen	iP	C	28	Funatu	?	D
5	Zürich	eP	C	29	Misima	?	D
6	Paris	iP	C	30	Kofu	?	D
7	Uccle	iP	C	31	Mizusawa	?	C
8	De Bilt	iP	C	32	Nagano	?	D
9	Padua	iP	C	33	Miyako	?	C
10	Belgrad	iP	D	34	Morioka	?	D
11	Hamburg	iP	C	35	Wazima	?	D
12	Batavia	iP	C	36	Kyoto	?	C
13	Manila	iP	C	37	Toyooka	?	C
14	Christchurch	iP	C	38	Osaka	?	D
15	Koti	?P	C	39	Mori	?	C
16	Zinsen	?P	C	40	Muroto	?	C
17	Hukuoka	iP	C	41	Miyazaki	?	C
18	Prag	?	C	42	Yakusima	?	C
19	Ksara	?	C	43	Kosyun	?	C
20	Triest	?	C	44	Hongkong	?	D
21	Mito	?	D	45	Agra	?P	C
22	Tyosi	?	D	46	Calcutta	?	C
23	Utsunomyia	?	D	47	Komaba	?	D
24	Tokyo	?	D				

a) Herdlage: Der Herd liegt im Schelfbereich der pazifischen Randzone, zwischen der Ostküste Hondos und dem Westrand des Japangrabens.

b) Herdvorgang: Für dieses Beben liegen neben Beobachtungsangaben ferner Stationen vor allem sehr zahlreiche Aufzeichnungen der ersten Bodenbewegung an Nahstationen vor. Die auf Dilatation lautenden Beobachtungsangaben von Hongkong und Belgrad beruhen sehr wahrscheinlich auf Fehldeutung des ersten Einsatzes im Seismogramm, da beide Stationen in einem Bereich mit Compression liegen.

Die Nebenräume sind durch das Auftreten von Dilatation charakterisiert, da keine Bereiche mit Compression bestehen, deren Umgrenzung mit Knotenlinien den Bedingungen genügt, die an diese gestellt werden müssen. In Figur 9 muss der erste Kreis die nordöstlich vom Epizentrum liegenden Stationen umschliessen. Sein Verlauf ist durch die Lage von Wazima (35), Morioka (34) und Mori (39) festgelegt. Die diesem Kreis entsprechende Ebene streicht N 31° W und fällt unter einem Winkel von $\sigma_1 = 84°$ gegen NE ein. Dabei wird allerdings Tucson (Compression) in einen Bereich mit Dilatation gelegt. Da es sich jedoch sowohl bei Weston (1) als auch bei Tucson (2) um e-Einsätze handelt, sind die Angaben beider Stationen nur bedingt zu werten.

Der zweite Kreis umschliesst einen sehr kleinen Bereich mit Dilatation in unmittelbarer Herdnähe, in dem die Stationen Wazima (35) und Kyoto (36) liegen. Seine zugehörige Fläche hat annähernd dieselbe Streichrichtung wie die oben erwähnte, und ihr Einfallswinkel ergibt sich zu $(90 - \sigma_1) = 6°$. Dieser Wert entspricht dem graphisch bestimmbaren Einfallswinkel sehr genau.

Die Streichrichtung der beiden Ebenen stimmt gut mit dem Verlauf der Ostküste Hondos südlich der Epizentrumsbreite überein. Da nach den Erfahrungen, die bei anderen randpazifischen Beben gemacht wurden, die Bewegungsfläche meist eine Neigung $> 60°$ aufweist, ist wahrscheinlich die unter 84° gegen Nordosten einfallende Ebene als Scherungsfläche anzusehen. Dies bedeutet, dass sich beim Herdvorgang die pazifische Seite an einer unter 84° gegen Nordosten einfallenden Fläche, relativ zum Festland, gehoben hat.

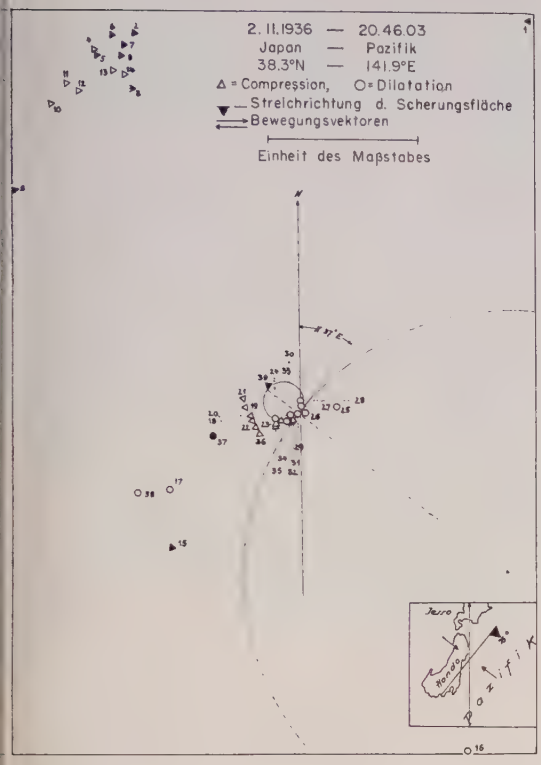

Fig. 10.

10. Japan — Pazifik, 2. 11. 1936 — 20h45m56s.
38,3° N — 141,9° E

Beobachtungsstationen:

1 Harvard	iP	C	21 Heizyo	iP	C
2 Kew	iP	C	22 Hukuoka	iP	C
3 Kopenhagen	iP	C	23 Kobe	?P	C
4 Zürich	eP	C	24 Toyooka	?P	D
5 Strassburg	iP	C	25 Sendai	?	D
6 Paris	iP	C	26 Mizusawa	?	D
7 Uccle	iP	C	27 Morioka	?	D
8 De Bilt	iP	C	28 Hatinohe	?	D
9 Ksara	iP	C	29 Tukubasan	?	D
10 Belgrad	iP	C	30 Yokohama	?	D
11 Zagreb	?P	C	31 Hunatu	?	C
12 Wien	iP	C	32 Misima	?	C
13 Göttingen	iP	C	33 Hamamatu	?	D
14 Hamburg	iP	C	34 Hikone	?	C
15 Manila	iP	C	35 Sumoto	?	C
16 Christchurch	eP	D	36 Miyazaki	?	C
17 Taihoku	?P	D	37 Zi-Ka-Wei	iP	D
18 Husan	iP	C	38 Hongkong	?P	D
19 Taikyu	iP	C	39 Vladivostok	iP	C
20 Keizyo	iP	C	40 Bergen	iP	D

a) Herdlage: Die Herdlage dieses Bebens stimmt hinsichtlich der Breite annähernd mit der vom 18. 6. 1933 überein. Die Entfernung des Epizentrums von der Nordostküste Hondos ist etwa 100 km kleiner als am 18. 6. 1933.

b) Herdvorgang: Gegen die Richtigkeit der auf Dilatation lautenden Beobachtungsangaben von Zi-Ka-Wei, Hongkong und Taihoku sprechen vor allem die zwischen Herd und diesen Stationen liegenden Punkte mit Compressionsbeobachtungen von Heizyo (21), Taikuy (19), Keizyo (20), Husan (18), Hukuoka (22) und Miyazaki (36).

Wie beim vorigen Beben sind die Nebenräume offensichtlich wieder Bereiche mit Dilatation. Für die Konstruktion der Kreise, die Bereiche mit Dilatation umschliessen, gibt es jeweils nur eine Möglichkeit. Der erste muss die Stationen Toyooka (24), Yokohama (30), Tukubasan (29), Morioka (27) und Hatinohe (28) gegen die Beobachtungspunkte Hunatu (31), Misima (32) und Hikone (34) abgrenzen. Hierdurch ist sein Verlauf genau festgelegt. Die Ebene die diesem Kreis zuzuordnen ist streicht im Epizentrum N 37° E und fällt unter einem Winkel von $\sigma_1 = 15°$ gegen Nordwesten ein. Der zweite Kreis ist einerseits durch die Lage von Hunatu (31) und Misima (32) mit Compression und andererseits durch die Lage von Morioka (27) und Tukubasan (29) mit Dilatation bestimmt. Die Streichrichtung der zugehörigen Ebene ist mit der der ersten Fläche identisch. Deshalb ergibt sich ihre Neigung zu $(90° - \sigma_1) = 75°$ gegen Südosten. Dieses verhältnismässig steile Einfallen gibt der nach Südosten geneigten Fläche bei der Wahl der Bewegungsebene den Vorzug vor der unter einem Winkel von 15° gegen Nordwesten einfallenden.

Bei diesem Beben hob sich die Randzone der pazifischen Masse relativ zur eurasischen, entlang einer unter 75° gegen Südosten einfallenden Bewegungsebene. Eine Verschiebung in horizontaler Richtung trat hierbei nicht auf.

11. Japan — Pazifik, 17. 4. 1948 — 16h11m28s.
33° N — 135,5° E

Beobachtungsstationen:

1 Berkeley	iP	C	10 Lissabon	iP	C
2 Pasadena	iP	C	11 Helwan	iP	D
3 Kew	iP	C	12 Triest	iP	C
4 Uppsala	iP	C	13 Rom	iP	C
5 Helsinki	iP	C	14 Ksara	iP	C
6 Zürich	eP	C	15 Belgrad	iP	C
7 Strassburg	iP	C	16 Prag	iP	C
8 De Bilt	iP	C	17 Riverview	iP	D
9 Cartuja	iP	D	18 Wellington	?	C

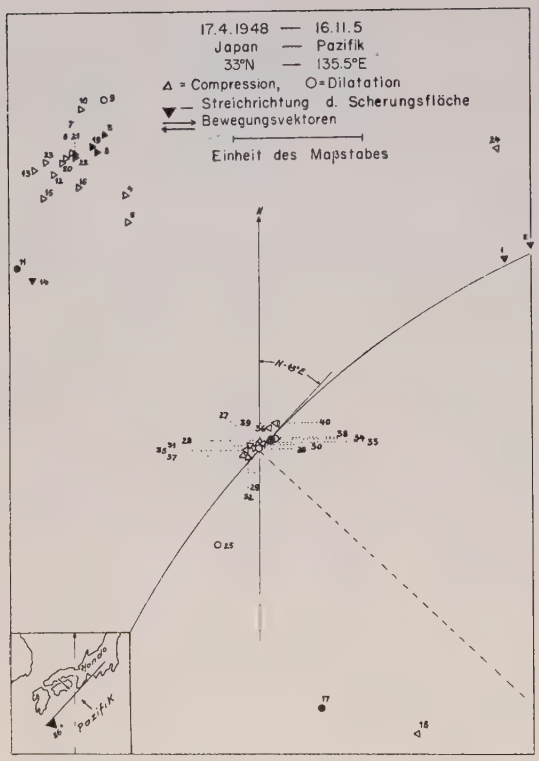

Fig. 11.

19	Uccle	?	C	30	Gifu	?	C
20	Chur	?	C	31	Hiroshima	?	C
21	Basel	?	C	32	Miyazaki	?	C
22	Stuttgart	iP	C	33	Yokohama	?	D
23	Firenze	?	C	34	Tokyo	?	D
24	Cleveland	?	C	35	Kumamoto	?	C
25	Shionomisaki	?	D	36	Kumagaya	?	C
26	Sumoto	?	D	37	Kagoshima	?	C
27	Kobe	?	C	38	Mito	?	D
28	Kyote	?	C	39	Morioka	?	C
29	Kochi	?	C	40	Miyako	?	C

a) Herdlage: Der Herd liegt vor dem Südkap Hondos in der Linschoten-Strasse, nordöstlich des Liu-Kiu-Grabens.

b) Herdvorgang: Die in Figur 11 in ihren Bewegungssymbolen dargestellten Beobachtungsstationen gestatten durch ihre dichte Lage in Herdnähe eine sehr genaue Festlegung von Scherungs- und Hilfsebene. Gleichzeitig treten die Fehlbeobachtungen von Helwan (11), Cartuja (9) und Wellington (18) deutlich als solche in Erscheinung. Für die Laufzeit der P-Welle ergibt sich für Helwan nach Jeffreys-Bullen (H. Jeffreys and K. E. Bullen, 1940) der Wert 743 Sekunden. Dieser weicht vom beobachteten von 757 Sekunden um 14 Sekunden ab. Diese Verspätung der P-Welle ist ein Hinweis dafür, dass die fragliche Bodenbewegung auf einen späteren Welleneinsatz zurückzuführen ist.

Die herdnahen Stationen scheiden die Möglichkeit der Existenz von Nebenräumen mit Compression aus. Die Knotenlinien müssen vielmehr Bereiche mit Dilatation umfassen. Der erste Kreis ist durch die Lage von Miyazaki (32), Sumoto (26), Gifu (30) und von Yokohama (33), ausserdem durch Tokyo (34) und Mito (38) festgelegt. Ein Kreisbogen der diesen Bedingungen genügt belässt die Stationen Berkeley (1) und Pasadena (2), wie erforderlich, im Compressionsbereich. Die diesem Kreis zukommende Ebene streicht N 43° E und fällt unter einem Winkel von $\sigma_1 = 86°$ gegen Südosten ein. Unter der Annahme, dass es sich bei dieser Fläche um die Scherungsebene handelt, fällt die Hilfsebene unter einem Winkel von $(90° - \sigma_1) = 4°$ gegen Nordwesten ein.

Der mechanische Vorgang im Herd bestand aus einer relativen Aufwärtsbewegung des südöstlichen Teils im Hypozentrum, entlang einer unter 86° nach Südosten einfallenden Fläche.

Nachwort

Herrn Professor Dr. Wilhelm Hiller, dem Leiter des Landeserdbebendienstes Baden-Württemberg, danke ich herzlich für die Ermöglichung der vorliegenden Arbeit, sowie für wertvolle Anregungen und Literaturhinweise. In gleicher Weise möchte ich Herrn Dozenten Dr. Markus Båth, dem Leiter des Schwedischen Erdbebendienstes, für anregende Diskussionen und freundliche Unterstützung bei der Umarbeitung für die Drucklegung herzlich danken. Die letztgenannte Arbeit wurde am Seismologischen Laboratorium des Meteorologischen Instituts der Universität Uppsala ausgeführt.

LITERATURVERZEICHNIS

Båth, M., 1952: Initial motion of the first longitudinal earthquake wave, recorded at Pasadena and Huancayo. *Bull. of the Seis. Soc. of America*, **42**, pp. 174—195.

Byerly, P., 1942: *Seismology*. Prentice Hall Inc. New York, pp. 233—239.

Gutenberg, B. and Richter, C. F., 1954: *Seismicity of*

the earth and associated phenomena. Princeton University Press, Princeton, New Jersey.

Hodgson, I. H. and Allen, I. F. I., 1954: *Tables of extended distances for PKP and PcP.* Edmond Cloutier, C.M.G.O.A., D.S.P. Queen's Printer and Controller of Stationery Ottawa.

Hodgson, I. H. and Bremner, P. C., 1952: Direction of faulting in the Ancash, Peru, earthquake of November 10, 1946, from teleseismic evidence. *Bull. of the Seis. Soc. of America,* **43**, pp. 121—125.

Hodgson, I. H. and Milne, W. G., 1951: Direction of faulting in certain earthquakes of the North Pacific. *Bull. of the Seis. Soc. of America,* **41**, pp. 221—242.

Hodgson, I. H. and Milne, W. G., 1953: Tables extending Byerly's fault-plane techniques to earthquakes of any focal depth. *Bull. of the Seis. Soc. of America,* **43**, pp. 49—61.

Hodgson, I. H. and Storey, R. S., 1954: Direction of faulting in some larger earthquakes of the 1949. *Bull. of the Seis. Soc. of America,* **44**, pp. 57—83.

Jeffreys, H. and Bullen, K. E., 1940: *Seismological tables'* London office of the British Association, Burlington House, W. 1.

Mühlhäuser, S., 1953: Die Richtung der ersten Bodenbewegung in Stuttgart für die Hauptbebengebiete der Erde, als Grundlage für grosstektonische Betrachtungen. *Zeitschrift für Geophysik.* Verlag Friedrich Vieweg & Sohn, Braunschweig, Sonderband 1953, Seite 78—91.

Mühlhäuser, S., 1953: *Betrachtungen über den mechanischen Vorgang im Herd bei einigen Grossbeben.* Dissertation der T. H. Stuttgart 1955.

Ritsema, A. R., 1955: The fault-plane technique and the mechanism in the focus of the Hindu Kush earthquakes. *Indian Journal of Meteorology and Geophysics,* **6**, pp. 41—50.

Tandon, A. N., 1955: Direction of faulting in the Great Assam Earthquake of 15 August 1950. *Indian Journal of Meteorology and Geophysics,* **6**, pp. 61—64.

A Consideration on Earth Tidal Change of Gravity

By EIICHI NISHIMURA, TOKIO ICHINOHE, and ICHIRÔ NAKAGAWA, Geophysical Institute, Kyoto University, Kyoto

(Manuscript received July 26, 1956)

Abstract

Gravimetric observations with the portable Worden gravimeter were made at three stations in our country to obtain accurate values for the earth tidal factor of gravity (G) and to detect, if possible, the local characters of these values. The observation period was respectively one month for each station, and the three stations were specially selected from the stand-point of diversity in conditions with regard to the supposed effect by ocean tides and subterranean structure. Judging from the observation results the G-values observed at three stations are generally well in accord with each other, but, if the numerals in the third figure of the G-value obtained can be assumed to have any significance, it should be said that the problem of the local character of the G-value remained unsolved and awaits the future investigation. The effect by ocean tides upon the G-value is discussed somewhat in detail, and the highly sensitive gravity variometer of double bifilar suspension type is also introduced.

1. Introduction

Since the first theoretical treatment by LORD KELVIN (1863), the phenomena of earth tides have ever been an attractive and important subject of research in the field of physical geodesy. E. v. REBEUR-PASCHWITZ (1892) was the first to succeed in detecting and instrumentally observing earth tides by the tiltmeter of the horizontal pendulum type, and after him many observations on earth tides have been made, especially with tiltmeters, by many researchers at various places in the world. Thus the study on earth tides has a comparatively long history extending about a century and becomes one of the old research items, but the recent development of techniques in measurement and observation has rejuvenised it and again made it an important research item for investigating the nature of the earth and its interior. In reality, to tap the earth with great earthquakes and to twist the earth with earth tides are certainly two powerful methods for diagnosing the earth's interior, and in this sense the study on earth tides will everlastingly afford us new clues for exploring the earth and advancing our knowledge on the nature of the earth's interior.

The observation of earth tides with tiltmeters have been made by many researchers since the first observation by E. v. REBEUR-PASCHWITZ in 1892, and the problem on the value of the so-called "diminishing factor", D ($\equiv 1+k-h$), and the secondary effect by ocean tides were fully studied. The dimensionless numbers, k and h, above mentioned are those introduced by A. E. H. LOVE (1909) in his theoretical treatment on earth tides, and they play an important role in the investigation of the earth and the interior by the aid of observational results. On the contrary, there are few examples of the observations of earth tides with gravimeters since the first gravimetric observation by W. SCHWEYDAR (1914), owing mainly to its instrumental difficulty. Consequently the value of $G\left(\equiv 1-\frac{3}{2}k+h\right)$—which is the

ratio of gravimetrically observed tidal change of gravity on the real earth to that observed on the hypothetically perfect rigid earth, and is called "earth tidal factor of gravity" or, in short, "gravimetric factor"—has not yet been accurately determined in comparison with the value of D. Really, the values of G, obtained by some recent provisional observations of short period of from several days to half a month with the portable gravimeter for prospection use, show a considerably large diversity among them, varying from 0.9 to 1.5. The causes of this diversity are considered to be attributed mainly to the following three effects: first, the observational errors and computational errors in analysing the data of short period observation; secondly, the secondary effects caused by ocean tides; and thirdly, the effects introduced by the difference of subterranean structure. Concerning these three points a consideration will be presented in the following.

2. Observational results

(1) Observation stations

In order to examine the above described effects, observation stations were effectively selected to fit the purpose of detecting the maximum effect caused by ocean tides and subterranean structure. Namely, the three stations of Kyoto, Chikubushima, and Shionomisaki were selected whose position, sea shore distance, Bouguer anomaly, and observational period are as listed in the following table and shown in Figure 1.

(2) Instrument

The instrument used in the present series of observations is the Worden gravimeter, No. 127. Its sensitivity given by the factory is 0.18473 mgal/div, and for practical purposes it can be read to one tenth of the scale division by the vernier. According to the experiments on the reliability of the scale constant, made by the comparison with the North American gravimeter, *AG*-1,108, the accuracies of the scale constants of both gravimeters accord well with each other within the limits of experimental error. Although the problem concerning the absolute value of the gravimeter scale constant is generally very troublesome owing to the difficulties on the method of checking,

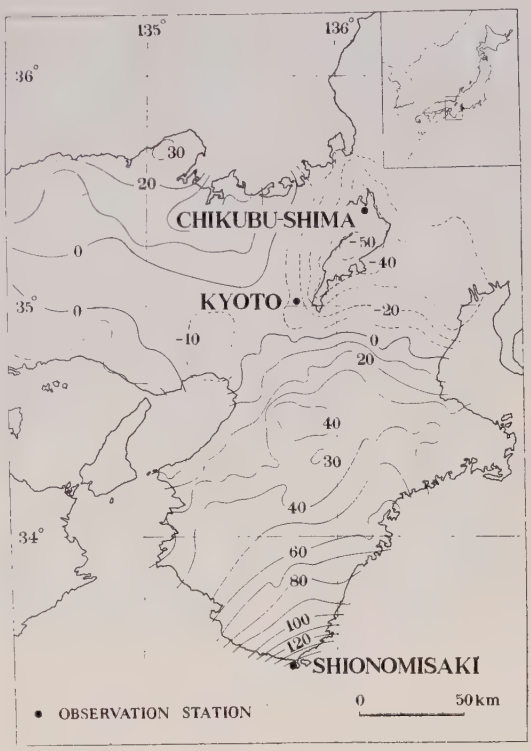

Fig. 1. The position of observation stations and the distribution of Bouguer anomaly in mgal-unit.

it may safely be said from various considerations that the scale constant given by the factory is trustworthy at least to the third significant figure. Consequently, when discussing the earth tidal factor of gravity to its third significant figure, the value of the scale constant given by the factory will be regarded as correct in the present observations. Moreover, judging from our own experiments as well as from those made independently by the members of the Geological Institute of Kyoto University, the above described scale constant has remained constant within the limits of experimental error since the time of its importation (1953) to the present; in other words, there is no noticeable time variation in the scale constant of that gravimeter. The plastic flow of the main spring, or simply expressed "drift", of the gravimeter has been farily large, and moreover, the drift speed was never uniform. The average values of drift speed were estimated, in the present case, to be 0.60 mgal/day, 0.94 mgal/day, and 0.86 mgal/day for the

Table

Station	Latitude (N)	Longitude (E)	Height (m)	Bouguer anomaly (mgal)	Distance from the nearest sea shore of Pacific Ocean (km)	Observation period
Kyoto	35° 02′	135° 47′	58	— 12	110	June 11—July 13, 1954
Chikubushima	35° 25′	136° 09′	98	— 45	140	Sept. 28—Oct. 30, 1955
Shionomisaki	33° 27′	135° 46′	74	+ 139	0.4	Nov. 16—Dec. 17, 1955

$H\cos(nt-\zeta)$, observed

Station	M_2		S_2		O_1		K_1	
	H_{obs}	ζ_{obs}	H_{obs}	ζ_{obs}	H_{obs}	ζ_{obs}	H_{obs}	ζ_{obs}
Kyoto	59.4 μgal	181°.96	27.2 μgal	176°.67	33.7 μgal	178°.07	53.3 μgal	202°.73
Chikubushima	60.2	181 .20	28.5	182 .22	32.8	174 .30	54.1	180 .95
Shionomisaki	64.0	182 .42	30.0	185 .37	28.2	179 .61	54.1	199 .62

$H\cos(nt-\zeta)$, theoretical

Station	M_2		S_2		O_1		K_1	
	H_{theor}	ζ_{theor}	H_{theor}	ζ_{theor}	H_{theor}	ζ_{theor}	H_{theor}	ζ_{theor}
Kyoto	50.3 μgal	180°.00	23.4 μgal	180°.00	29.3 μgal	180°.00	41.2 μgal	180°.00
Chikubushima	49.8	180 .00	23.2	180 .00	29.4	180 .00	41.4	180 .00
Shionomisaki	52.2	180 .00	24.3	180 .00	28.6	180 .00	40.3	180 .00

Station	M_2		S_2		O_1		K_1	
	G	$\varkappa$	G	$\varkappa$	G	$\varkappa$	G	$\varkappa$
Kyoto	1.18±0.02	+ 1°.96	1.16±0.03	— 3°.33	1.15±0.04	— 1°.93	1.29±0.07	+ 22°.73
Chikubushima	1.21±0.02	+ 1 .20	1.23±0.02	+ 2 .22	1.12±0.05	— 5 .70	1.31±0.13	+ 0 .95
Shionomisaki	1.23±0.02	+ 2 .42	1.23±0.02	+ 5 .37	0.99±0.05	— 0 .39	1.34±0.10	+ 19 .62

periods of the observations at Kyoto, Chikubushima, and Shionomisaki respectively.

(3) Results of the observations

The gravity changes at three stations were read at intervals of half an hour during the respective one month, and the obtained values were corrected by applying drift reduction. After the reduction on drift, the hourly values during one month were harmonically analysed by Darwin's method, giving the following component tides. The values shown in the following table are corrected for the augmenting factor in analysis and reduced to the mean inclination of the moon's orbit to the equator, the phase being referred to the respective meridian of the observation stations.

Corresponding to the above values obtained from the observational data, the theoretical values calculated for a perfectly rigid earth are as follows:

Taking the ratios between the observed values and the theoretical, the following values

of G and $\varkappa(\zeta_{obs.} - \zeta_{theor.})$ for the respective component tide at each station are obtained.

As shown in the above table, the values of G and $\varkappa$ at the three stations and for each component tide, especially the M_2-component, are quite consistent with each other within the limits of observational and instrumental error. From these results it may safely be said that the earth tidal factor of gravity and phase difference in a certain small area can correctly be determined within the above mentioned accuracy by one month's observation with a gravimeter of ordinary sensitivity. But whether the same value for the tidal factor ofgravity can be expected or not at places of greatly different latitudes from those of the present three stations, or at the middle of the continent, or at an isolated island in the middle of the ocean is quite another problem to consider, and this sort of observation is highly recommended to be put into effect through the cooperation of many countries at the opportunity of the coming Geophysical Year (1957—1958).

3. Effects of ocean tides

As above stated, the values of the earth tidal factor of gravity obtained at the three stations during the present observations are well in accord with each other, but if, in this case, it is provisionally assumed that the third figure of the numerical G-value in the above listed table is trustworthy and the differences between the three stations have any significance, they should be attributed to the differences in effects of ocean tides and of the subterranean structure upon the G-values obtained at each station. In this section a brief discussion will be made on these secondary effects upon the G-values.

Concerning the effect caused by the difference of subterranean structure which is represented by the distribution of Bouguer anomaly in the present treatment, the theoretical calculation is considerably difficult. But as H. TAKEUCHI has recently taken up the problem and has been working out the computation, the amount of this effect upon the G-value will be estimated before long. In the present case only the effect caused by ocean tides will be discussed in some detail. Before entering into the treatment on ocean tidal effect, the effect caused by the height differences of observation stations should briefly be mentioned. In the present case, the maximum height difference between the three stations is only 40 meters, and the difference of vertical component of gravity due to this height difference calculated from the tide-generating potential is estimated to be 1/160,000 of the original force. With regard to Love numbers, they are also influenced by height, but the effect of height difference upon them is negligibly small in the similar order of the above described vertical component. Hence the effect of the height difference between the three stations upon the G-value which is the algebraic summation of the vertical component of tidal force and forces relating to Love numbers may safely be disregarded in the present case.

The supposed effects upon the G-value caused by ocean tides are generally divided into three principal parts. One is the effect of the vertical component of attraction by the tidal height change of sea water, the second, the effect of the vertical displacement of the ground at the observation station caused by the tidal load of sea water, and the third, the effect caused by the distortion of gravitational potential field as a result of deformation of the ground and sea bottom. Beside these, the effect originating from the horizontal displacement of the ground at the observation station caused by the tidal load of sea water may also to be taken into account, but this effect was ascertained to be negligibly small.

On the effect of attraction by tidal change of sea water height, the station to be discussed is certainly considered to be only Shionomisaki whose observation point is 74 meters high above the sea level and 400 meters distant from the sea shore of Pacific Ocean. Concerning the other two stations, Kyoto and Chikubushima, the effects concerned with the ocean tides were ascertained to be negligibly small, because the distances from the nearest sea shore of the Pacific Ocean are 110 kilometers and 140 kilometers respectively. The vertical component of attraction of the M_2-period caused by the neighbouring sea water within 1,000 kilometers distance from the observation station for Shionomisaki is calculated as nearly

$$0.9\ \mu\text{gal} \cos(2t - 165^\circ).$$

Secondly, the effect originating from the vertical displacement of ground at the observa-

tion point caused by the tidal load of sea water will be calculated. The quantity of vertical displacement is calculated from the formula derived by NAGAOKA (1906) in his study on the elastic deformation of the ground by surface load. Assuming tentatively the values of Lamé's elastic constant as $\lambda = \mu = 5 \times 10^{11}$ c.g.s. units, the vertical ground displacement of M_2-period at the station of Shionomisaki caused by the tidal load of the neighbouring sea water within 1,000 kilometers distance from the station is estimated as nearly

$$7.3 \text{ cm} \cos (2t - 165°).$$

Converting the above value of vertical ground displacement into change of gravity concerned with the M_2-period is

$$22.5\ \mu \text{ gal} \cos (2t - 165°).$$

The calculated effect concerning the vertical ground displacement is by itself of an exceedingly large amount, and it contains many problems to examine.

And thirdly, the effect originating from the distortion of gravitational potential field as the result of deformation of the ground and sea bottom should be discussed. But it is a hard task to calculate accurately the amount of this effect under practical circumstances, and its amount is supposed to be so considerably large as to nearly cancel the effect caused by the vertical ground displacement by the tidal load of sea water. Because, if only the correction of effect caused by the vertical displacement is applied to the observed result in the present case of Shionomisaki, the earth tidal change of gravity and the G-value derived therefrom show the following absurdly small values: namely the change of gravity of M_2-period is nearly 42.2 μgal cos $(2t - 192°.02)$ and the G-value is reduced to nearly 0.81. From this fact and many other considerations on the normal value of G derived from many other gravimetric observations, it is safely concluded that the large effect upon the earth tidal change of gravity caused by the vertical displacement of the ground at the station near the sea coast should generally be cancelled in balance by the effect originated from the distortion of gravitational potential field caused by the tidal deformation of the surrounding ground of the station. The calculation of the latter effect under each set of practical circumstances is certainly desirable for a complete discussion of secondary effects by ocean tides upon the tidal change of gravity.

In the present case, the theoretical treatment by H. TAKEUCHI (1951) on the deformation of the earth by surface loads will tentatively be applied for correcting the observed value at Shionomisaki. After his theory, the total effect upon the tidal change of gravity by ocean tides which is the algebraic summation of the above described three effects caused by the attraction of sea water, vertical displacement of the station ground, and distortion of gravitational potential field due to deformation of the ground is calculated as nearly 1.1 times the effect caused by the attraction of sea water, when the tidal deformation of the earth by ocean tides is simply expressed by a spherical harmonic of 20th degree, in case of the earth of Bullen's model. Under these assumptions the secondary effect of ocean tides is roughly estimated for the station of Shionomisaki as 1.0 μgal cos $(2t - 165°)$, and consequently the G-value corrected for the ocean tidal effects at Shionomisaki becomes $G = 1.21$. Actually, the total effect of ocean tides at Shionomisaki is reasonably supposed to be a little larger than 1 μgal. Thus the secondary effects of ocean tides upon the earth tidal change of gravity, is in any case, supposed to be small in quantity compared with the original primary value of the tidal change of gravity, and really it plays any role in discussing the significance of numerals in the third figure of the G-value.

When the observed value of G at Kyoto—which is supposed to be little influenced by ocean tidal effects and to have a normal crustal structure of 30 kilometers, as estimated from seismic observations—is representatively adopted as the standard in our region, the numerical values of the Love numbers, h and k, are simply calculated by combining the G-value with the D-value. When adopting the numeral obtained by E. NISHIMURA (1950) as the D-value, the values of the Love numbers become as follows:

$$G \equiv 1 - \frac{3}{2} k + h = 1.18$$

$$D \equiv 1 + k - h = 0.66$$

$$h = 0.66, \qquad k = 0.32.$$

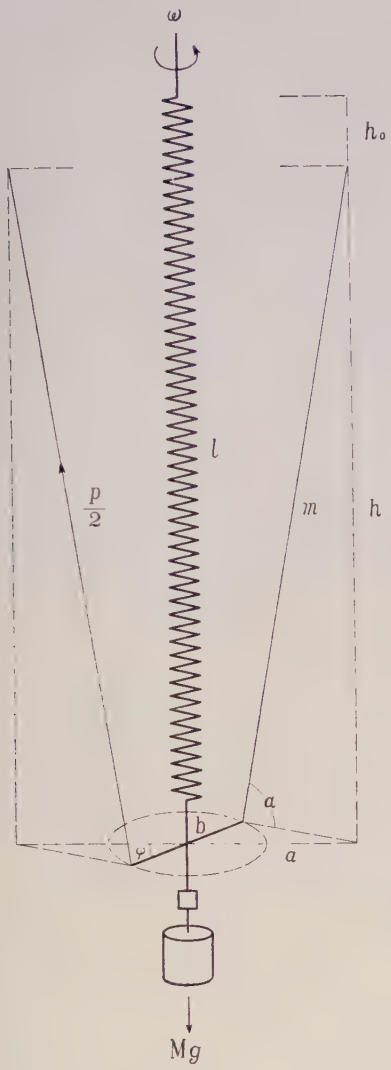

Fig. 2 a. Schema on construction of an ordinary bifilar gravity variometer.

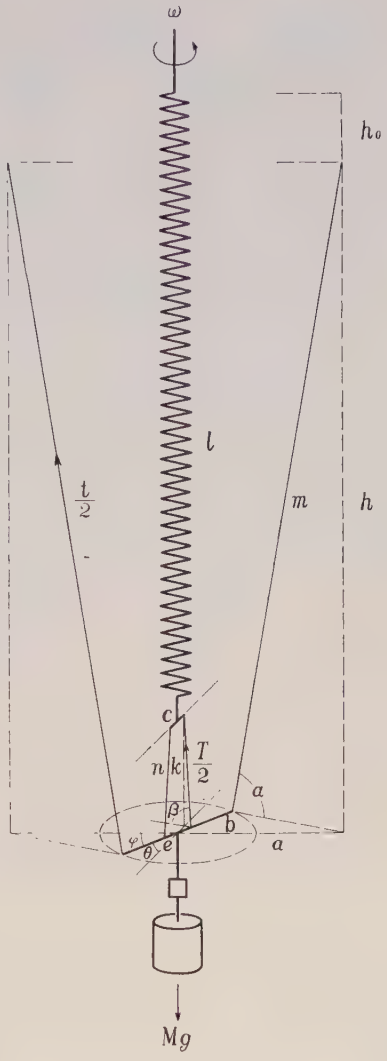

Fig. 2 b. Schema on construction of a double bifilar gravity variometer.

Applying the value of h calculated above to the expression of the radial displacement, $U = h\,W_2/g$ (W_2: tide-generating potential), at Kyoto, the tidal upheaval of the ground is estimated as follows:

Tidal upheaval of the ground at Kyoto for M_2-component: 21.3 cm.

Total tidal upheaval of the ground at Kyoto: 50.5 cm. And the greatest tidal upheaval of the ground that could occur on the earth is calculated as 51.5 cm.

4. Gravity variometer of double bifilar suspension type

In the preceding section, it is repeatedly mentioned that the precise observation of earth tidal change of gravity during a period of more than one year with a more sensitive gravity variometer than 1×10^{-9} g/mm of automatic recording is highly recommended for the development of the study of the earth tidal phenomena and the advancement of our knowledge on the nature of the earth's interior. For

this purpose the double bifilar gravity variometer, for example, devised by ICHINOHE (1951, 1955) will certainly be serviceable, and its construction and function are briefly described in this section.

The double bifilar gravity variometer is the same in principle as the ordinary bifilar gravity variometer, but its sensitivity is largely and easily raised, and moreover stabilised compared with that of the ordinary bifilar gravity variometer, by applying the second inner bifilar suspension to the part between the main helical spring and the hanging bob as shown in Figure 2b. These two thin strings composing the second inner bifilar suspension play an important role in greatly raising the sensitivity of the instrument, and in addition, are effectively serviceable for minimizing the undesirable deflection caused by temperature changes and the drift, or plastic flow, of the instrument. This depends on the fact that the torsional force, which has a share in the causes of undesirable deflection and instrumental drift, is the couple produced by the horizontal components of tensional forces of strings in the case of the double bifilar gravity variometer in contrast to the elastic force produced by the torsion of a helical spring in the case of the ordinary bifilar gravity variometer.

The sensitivities for the two types of gravity variometer are approximately expressed as follows:

$$\frac{d\varphi}{dg} \cong -\frac{abM \sin\varphi}{mf + abp\cos\varphi}$$

for the ordinary bifilar suspension type,

$$\left.\begin{aligned} \frac{d\varphi}{dg} &\cong -\frac{\left(abM \pm \frac{mf}{gF}\right)\sin\varphi}{mf\left(1 \pm \frac{q\cos\varphi}{F}\right) + abqMg\cos\varphi} \\ \text{with } F &\equiv \sqrt{\frac{(cem)^2}{(abn)^2} - (q\sin\varphi)^2} \end{aligned}\right\}$$

for the double bifilar suspension type,

where φ denotes the turning angle of the bob; g the acceleration of gravity; M the mass of the bob; m and n the length of the outer and inner bifilar strings; f the torsional elastic constant of the helical spring; p the tension of the outer strings in the ordinary bifilar suspension type; q the ratio of the tension of outer bifilar strings to that of inner bifilar strings in the double bifilar suspension type; and a, b, c, e are the constructional constants having

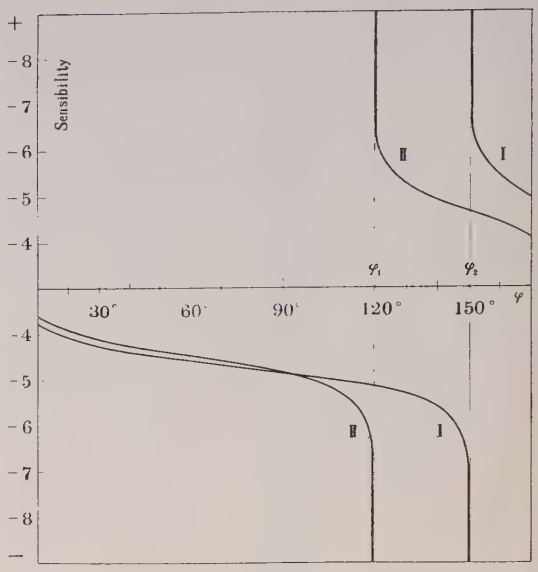

Fig. 3 a. Sensitivity curve of an ordinary bifilar gravity variometer.

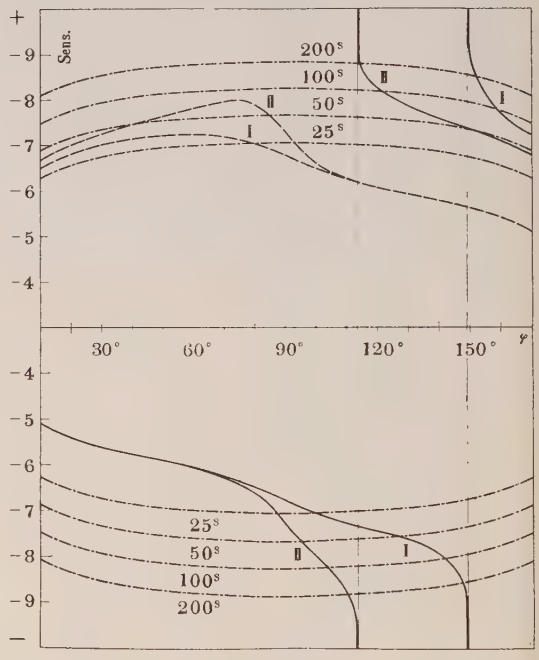

Fig. 3 b. Sensitivity curve of a double bifilar gravity variometer.

the dimension of length as shown in Figure 2b. And the relation between q, φ, and $\frac{d\varphi}{dg}$ in the double bifilar suspension type is represented in Figure 3b, with the sensitivity curve of ordinary bifilar type for comparison in Figure 3a, the numerical values of constructional constants adopted in the calculation being as follows: $g = 980$ cm/sec^2; $M = 50$ gr; $m = 130$ cm, $n = 10$ cm; $f = 1{,}000$ dyne cm; $a = 6$ cm, $b = 3$ cm, $c = e = 0.1$ cm; and $q = 7.0/1{,}000$ for curve I, and $= 7.2/1{,}000$ for curve II. In the Figure, the full-line curves correspond to the plus sign of the above sensitivity formula and the broken-line curves to the minus sign. The numerals in the ordinate indicate dg/g in the common logarithms, corresponding to 1 mm displacement of the optical image on the recording paper with 5 meters optical distance. The chain-line curves show the relation between the free oscillation period of the bob and $\frac{d\varphi}{dg}$ in case of $r^2 = 2$ cm^2, r being the radius of gyration of the bob. From the comparison of Figure 3b with Figure 3a, it is clearly understood that the sensitivity of the double bifilar gravity variometer is easily raised up with a great stability compared with that of ordinary bifilar type. A double bifilar gravity variometer was early in 1949 constructed for testing at the ordinary underground room of the building of the Abuyama Seismological Observatory attached to Kyoto University; its constructional constants were nearly the same as mentioned above in Figure 3b, and the sensitivity could be raised up to 3×10^{-9} g/mm/5 m with the free oscillation period of the bob of 200 seconds, but in practical observation the instrument was inevitably used in considerably reduced sensitivity by reason of the great disturbances due to microseisms, local ground tremors, and minute but restless oscillations and pressure changes of the surrounding air. And, moreover, the drift of the instrument caused by the plastic flow of the main spring was also greatly enlarged according to the raise of instrumental sensitivity, but the problem of drift was temporisingly solved by applying the artificial control at the part of outer bifilar suspension for recovering the permanent flow of the main spring. An example of record thus obtained is inserted in Figure 4, in which the effect of microbarometric change upon the instrument is largely observed.

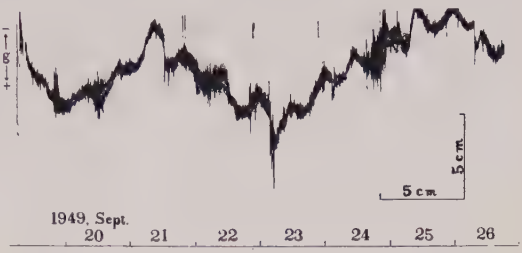

Fig. 4. An example of records obtained with a highly sensitive gravity variometer of double bifilar suspension type (sensitivity: 1×10^{-8} g/mm/2 m).

Under such circumstances as above stated, observations with highly sensitive gravity variometer has again recently been planned, and, in the present schedule, the instrument should be evacuated at least to 0.1 mm Hg for avoiding buoyancy changes and convection of the surrounding air, and should be set up in a deep seated thermostatic room of more than 500 meters depth for avoiding the microseisms and ground tremors. The drift of the instrument is to be controlled by any suitable method of artificial regulation. In this way the sensitivity of the double bifilar gravity variometer will be raised to the degree of 3×10^{-10} g/mm/5 m by the multiple reflection method of recording, and the gravimetric observation with it is expected to be greatly useful for studying the earth tidal change and, if existing, non-periodic micro-variation of gravity. Gravimetric observations with super high sensitive gravity variometers at two stations are planned for the international cooperative observation period during the coming Geophysical Year (1957—1958), and they are also scheduled to be operated in conjunction with concurrent gravimetric observations with the station gravity variometers of the double bifilar suspension type having an ordinary sensitivity of 1×10^{-8} g/mm/2 m at ten suitable stations in our country, and with two portable pen recording gravimeters of the Askania Gs-11 type at more than thirty points in our country for detecting the local character of the G-values. On the results of these observations, a detailed report will be made in due time.

REFERENCES

ICHINOHE, T., 1951: Highly sensitive double bifilar gravimeter. *Journ. Seism. Soc. Japan*, 2nd Series, **3**, pp. 49—56.

ICHINOHE, T., 1955: Study on change of gravity with time. Part I. On the tidal change of gravity. *Mem. Col. of Science, Univ. of Kyoto*, Series A, **27**, pp. 289—316.

KELVIN, LORD, 1863: Dynamical problems regarding elastic spheroidal shell. On the rigidity of the earth. *Phil. Trans. Roy. Soc. London*, **153**, pp. 583—616, pp. 573—582.

LOVE, A. E. H., 1909: The yielding of the earth to disturbing forces. *Proc. Roy. Soc. London*, A 82, pp. 73—88.

NISHIMURA, E., 1950: On earth tides. *Trans. Amer. Geophys. Union*, **31**, pp. 357—376.

REBEUR-PASCHWITZ, E. v., 1897: Horizontal Pendel-Beobachtungen auf der Kaiserlichen Universität-Sternwarte zu Strassburg 1892—1894. *Gerl. Beitr. z. Geophys.* **2**, s. 211—535.

SCHWEYDAR, W., 1914: Beobachtung der Änderung der Intensität der Schwerkraft durch den Mond. *Sitz. d. König. Preuss. Akad. Wiss.*, **14**, s. 454—465.

TAKEUCHI, H., 1951: On the earth tide. *Journ. Faculty of Science, Tokyo Univ.*, II 7 Part 2, pp. 119—153.

NOTES

Report on the Third Annual Conference on Atmospheric Chemistry, May 28—30, 1956

By W. A. MORDY, International Meteorological Institute in Stockholm

The third in a series of conferences on Atmospheric Chemistry was held at the Meteorological Institute, May 28—30, 1956. The two previous conferences have been reported in Tellus (1954, No. 3 and 1955, No. 3).

The purpose of the third conference, in addition to the necessary discussions related to the maintenance, extension and improvement of the European atmospheric chemical observational network, was to formulate ideas and recommendations for the types, numbers, and locations of atmospheric and geochemical observations needed during the International Geophysical Year.

In attendance at the conference were 27 scientists representing 18 scientific organizations as listed below:

J. Bouquiaux, Ministère de la Santé Publique, Brussels, Belgium.
G. Brodin, R. Agr. College, Uppsala, Sweden.
K. Buch, Helsingfors, Finland.
H. R. Byers, University of Chicago, U.S.A.
L. K. Coachman, Institute of Zoophysiology, Oslo, Norway.
L. J. L. Deij, Kon. Ned. Meteor. Instituut, Holland.
H. Egnér, R. Agr. College, Uppsala, Sweden.
E. Eriksson, Institute of Meteorology, Stockholm, Sweden.
S. Fonselius, Institute of Meteorology, Stockholm, Sweden.
R. M. Goody, Department of Meteorology, Imperial College, London, England.
E. Gorham, Freshwater Biological Association, Ambleside, England.
Edv. Hemmingsen, Institute of Zoophysiology, Norway.
S. L. Jansson, R. Agr. College, Uppsala, Sweden.
O. Johansson, R. Agr. College, Uppsala, Sweden.
F. Koczy, Oceanographic Institute, Gothenburg, Sweden.
F. Koroleff, Institute of Marine Research, Helsinki, Finland.
J. Låg, Agr. Coll. of Norway, Vollebekk, Norway.
J. Van Mieghem, Inst. Royal Météorologique de Belgique, Belgium.
W. A. Mordy, Institute of Meteorology, Stockholm, Sweden.
G. Neumann, Institute of Meteorology, Stockholm, Sweden.
H. Riehm, Landw. Versuchsanstalt, Augustenberg, Karlsruhe, Germany.
C.-G. Rossby, Institute of Meteorology, Stockholm, Sweden.
E. Schmacke, SMHI, Stockholm, Sweden.
P. F. Scholander, Institute of Zoophysiology, Oslo, Norway.
C. O. Tamm, Forest Research Institute of Sweden, Stockholm, Sweden.
S. L. Tierney, Meteorological Service, Dublin, Ireland.
H. Wexler, US Weather Bureau, Washington D.C., USA.

The conference was supported largely by funds granted by the International Union of Geodesi and Geophysics.

The first day of the conference was devoted to reports and discussions on the present state of and future plans for the networks in the different countries. This was followed by a general discussion aimed at formulating recommendations from the group concerning the desirable observational density, techniques and frequency, analysis control, network extension and data publication, and also means of financing and obtaining the necessary cooperation in the analysis of the gas and precipitation samples.

United States

Dr. Wexler, US Weather Bureau, reported on four aspects of the atmospheric chemistry and geochemical programs under way or planned by scientists in the U.S.: atmospheric investigations; oceanic investigations; the chemical composition of river waters, and investigations of the chemical composition of glaciers.

Atmospheric chemistry:

Dr. Junge has been analysing precipitation samples for Mg and Cl from 63 stations scattered over the United States. As these stations are much more widely separated than the Swedish stations a different scale of geographic variation in these constituents has been noted and therefore different patterns. As Dr. Junge's primary interest in this work has been in its relation to condensation nuclei, he now feels that he has no further need for the continuation of the network. Dr. Wexler indicated that the Weather Bureau is prepared to take over the network for the IGY as soon as necessary when provision can be made for the analysis of the precipitation samples. Three possible cooperating agencies for this work, he mentioned, are the U.S. Department of Agriculture, the U.S. Public Health Service, and the U.S. Geological Survey.

In addition to the program in the United States, 6 stations have been planned for the IGY in Antarctica. Samples of precipitation from these stations will be collected and analysed on return of the Antarctic parties to the United States.

In reference to CO_2 in the atmosphere, observations are currently being made on the West Coast of the United States and they are planned for selected stations in Antarctica during IGY. Dr. Charles Keeling, working with Dr. Harrison Brown at the California Institute of Technology, has been using a new technique for the measurement of CO_2. An instrument, developed by the Research Corporation of Pasadena, California, operating on the principle of infra-red absorption and subsequent heating of CO_2, records continuously the content of this gas with an accuracy of 0.3 ppm by volume. It is hoped that this instrument will work satisfactorily in Antarctic conditions although there are some complications related to corrections necessary for water vapor in the atmosphere. One instrument will be installed at Little America. Bottled samples for CO_2-analyses will be collected at inland stations in the Antarctic and Arctic as well as samples collected by reconnaissance aircraft of the Air Weather Service during IGY. In this regard Dr. Wexler mentioned the very cooperative attitude of Brig. Gen. Thomas Moorman of the USAF Air Weather Service toward assistance during the IGY.

Some interesting results of Dr. Keeling's work in California and Washington have been his determination that the variability of CO_2 decreases with altitude (even though the total amount seems to be generally the same as at sea level) and that different ratios between C^{13} and C^{12} exist at high and low altitudes. C^{13} is present in relatively large amounts at high levels. A diurnal effect is also seen in this ratio which reflects the diurnal effect in CO_2 near the earth's surface. CO_2 is rather more abundant at night as is C^{12} hence the ratio goes down, even at higher levels.

Oxygen (O_2) *measurements* are planned also for a number of stations. Dr. Wexler said that the objective of these measurements was to investigate further the annual variation in oxygen and to try to resolve certain differences in these measurements which appear in the literature. Glückauf has reported values of approximately 20.5 % by volume in summer and 20.8 % in winter. Kanwisher & Wolf have reported 20.83 % in summer and 20.95 % in winter. Observations will be made in Antarctica by bottled samples which will be sent to the US for analysis.

Ozone measurements by means of the Dobson ozone spectrophotometer will be made at Fairbanks, Alaska and Ice Island T-3 in the North. In the Continental United States,

observations are planned at Washington, D.C., Caribou, Maine, Green Bay, Wisc., Bismarck, N.D , Flaggstaff, Ariz., and Forth Worth, Tex. A Dobson instrument is also planned for Mauna Loa, Hawaii. An instrument has been shipped to Little America, Antarctica.

The Canadians are planning ozone measurements with the Dobson instrument at Alert, Resolute, Moosonee and Edmonton.

In reference to ozone it was reported that there has been some success in the United Kingdom in using the moon as a light source. It is hoped that this method will be established for use during the IGY. Total O_3 at the surface will also be measured at Little America using the chemical method developed by V. Regener.

Particulate matter is being investigated in air pollution research by Dr. James P. Lodge of the U.S. Public Health Service on the Farallon Islands, 40 miles west of San Francisco and at San Nicolas Island and Point Piedras Blancas in Southern California. The US Weather Bureau recently began investigations of the relationship of these particles to meteorological conditions. Of interest to date has been the fact that amounts of this particulate matter have been greater for air approaching from the open sea than from the land.

Oxidants are being measured in California at Mt. Hamilton, San Clemente Island, Crescent City, and numerous points in Los Angeles using the phenothalein-colorimetric technique. In addition approximately 30 locations in California are making oxidant measurements using the Haagen-Smit "rubber-band" method.

Measurement of water vapour by infra-red absorption is planned for the Antarctic and Arctic.

Tritium is being measured in precipitation samples for a number of locations by Dr. Libby, Atomic Energy Commission.

Dr. Irving Friedman of the U.S. Geological Survey is making measurements of *Deuterium* in sea water, precipitation and rivers.

Radioactivity measurements made over the world by U.S. scientists will be reported shortly in *Science* (Sept. 14, 1956). These show the world-wide extension of radioactive clouds from the Pacific experimental explosions.

Oceanic investigations:

The exchange of CO_2 between the sea and the atmosphere is an important question in meteorology and oceanography. During the IGY oceanographers will be making many routine analyses of the *chemical constituents of sea water*. Cores of *ocean sediments* will be analysed.

Chemical composition of river waters:

Dr. Friedman hopes to furnish kits to willing cooperators in an effort to get a world-wide sampling of river waters. Mr. William Rubey (US Geological Survey) is interested in salts contained in river waters as indicated by their chemical constituents.

Glaciers:

A 1,000 ft bore into the Greenland icecap is planned for the summer of 1956. Other deep drillings are planned in Antarctica during the IGY. A series of pits 5 to 10 meters deep may yield information on the annual accumulations of snow and the average annual temperature for Polar regions. O^{16}—O^{18} determination will be made of about 200 samples of snow and ice.

Professor Rossby said that he was concerned that nothing had been planned for synoptic measurements of CO_2 in the continental US and the Pacific.

Dr. Wexler answered that 10 or 15 stations were included in the original plans. These plans will be revised later.

Mexico

Following Dr. Wexler's paper Professor Rossby read from a letter from Dr. Fournier D'Albe, now a UNESCO adviser to Mexico, which reported that *precipitation samples* were being analysed from two stations (Mexico City, and a 4,160 m station not far from the city). They hope to extend the network soon.

Belgium

Dr. Van Mieghem reported that four routine stations are now in operation at Uccle, Bruges S:t André, Dorubes and Botrange. Air and precipitation samples are being taken. He mentioned some practical problems related to power transmission which appear to be correlated with atmospheric-chemical variations. Corona discharges occur from the power lines when the weather is foggy, the winds light and the relative humidity high.

Trial measurements of *radioactivity* by air filter samples are being made at Dourbes, Uccle and Moll. It is hoped to establish two additional

stations shortly. Measurements of radioactivity of the residue of large filtered rain samples are being made in Moll.

Dr. Bouquiaux reported on the analysis of the samples from the four Belgian stations made by the Public Health Service.

The Netherlands

Dr. Deij reported that radioactivity measurements in air and precipitation have been made for more than a year at the Medical Biological Laboratory of the National Defence Organization of the Netherlands. In the near future it is planned to augment these measurements with the filtered rainfall method in use elsewhere. Two new atmospheric chemistry stations are planned which will make routine measurements.

Germany

The German network was reported on by Dr Riehm. He hoped that twelwe stations in Austria, Switzerland and Germany will be in operation by August of this year, with the Germans doing the analyses.

Ireland

An Irish network is planned, according to Dr. Tierney, for the near future. It is expected that the network of these stations will be essentially the same as the synoptic network for Ireland. Observations will first consist of precipitation constituents and later, it is hoped, aerosols. Radioactivity measurements using filtered rainwater have been made for several months at Valencia. Background counts of air radioactivity are also being made.

England

The proposed English network was discussed by Dr. Goody, who mentioned problems in arranging for the analysis of samples. The density of the English network will necessarily depend upon analysis facilities but Dr. Goody requested recommendations about what would be desirable.

Norway

Norwegian stations were described by Professor Låg. Three precipitation stations are currently in operation and 10 new stations, including a 3,000 meter altitude station, are planned.

Finland

The Finnish network, as described by Professor Buch, includes 4 precipitation stations at present and will add 2 more, one at Sodankylä in the north, and one in the southeast. Beginning in July the analysis of Finnish samples will be done in Helsinki by Dr. Koroleff.

After the network reports were presented practical problems connected with the maintenance of the chemical program were discussed.

1. *Elements to be sampled*

At the present time the Scandinavian network is analysing precipitation samples for Na, K, Ca, Mg, H_3N, NO_3, S, and carbonates. The pH and the conductivity of the samples is also determined.

Gas samples are examined for the same factors, except, NO_3, and, of course carbonates, pH, and conductivity.

Because of their importance in agriculture it was suggested that boron and phosphorus determinations should be added to current measurements. Iodine was also mentioned but is to difficult to sample and measure reliably.

Eriksson mentioned the desirability of measuring organic matter and separated, particulate matter. A quantity of approximately 5 mg/l of organic matter, probably from the sea, and 5 mg/l of inorganic matter including atmospheric dust and insolubles, has been found in Finnish snow. The possible importance of these organic and particulate materials is demonstrated by the fact that 1 to 5 μ silica particles have been found in snow in Sweden and that there is no known adjacent source for these particles. They must come from great distance, possibly the Sahara, and doubtless could provide important information about the origin and history of air in which they are contained.

Dr. Scholander asked if *living matter* in sufficient quantities for identification exists in the rainwater. Eriksson mentioned the appearance of spores and pollen in some samples. Quite a number of pollen counts have been made, Dr. Gorham mentioned, and would be interesting to look at from the standpoint of air trajectories.

The concensus was that boron should be sampled at a few stations, but other suggestions

were left pending further preliminary investigations.

2. *Sampling techniques*

A small committee was set up to bring forth sampling recommendations six months before the beginning of the IGY. The Group, which was later appointed, was Dr. Egnér (chairman), Dr. Låg, Dr. Koroleff, Dr. Bouquiaux, Dr. Goody and Dr. Riehm.

3. *Frequency of measurements*

Although there is no established criterion for optimum observation frequency, a number of practical matters dominate this decision. Weekly observations would quadruple the work of analysis, and this task is the major bottleneck in the present program.

Eriksson suggested that a rather dense network of *annual stations* could be established with relatively little additional work, which could provide results of climatic and agricultural interest. Occasional daily sampling will be made at six stations in southern Sweden this fall.

It was felt that very little could or should be done to change the frequency of observations at the present time.

4. *Density of Stations*

Dr. Van Mieghem requested a group recommendation concerning station spacing so that recommendations for atmospheric chemical stations could be prepared for CSAGI. The subject has been discussed also in connection with WMO recommendations for a hygroscopic nuclei survey.

After discussion it was agreed that a spacing of stations roughly corresponding to the spacing of stations on the synoptic meteorological charts would be desirable. Highest station density should be in coastal areas because of the role of sea salt particles.

5. *Control of analysis*

A method of comparing analytical techniques was suggested through the exchange of samples between analysis centers. Essentially the same techniques are now in use in all of these places so that only this exchange is required.

6. *Extension of the network.*

When Ireland and Great Britain have been added to the net it was felt that the network would be satisfactory for current objectives.

The second day of the Conference began with a paper by S. Fonselius concerning recent work on the variation of CO_2 in the Atmosphere in Scandinavia. (Fonselius & Koroleff 1956: *Tellus*, **8**, 3, pp. 176—183).

Following Mr. Fonselius' paper Dr. Buch indicated his belief that the CO_2 measurements which have been reliably made, tend to show an increase in CO_2 with the growth of industry.

Professor Rossby asked if a selection of reliable observations could be made objectively.

Dr. Tamm asked if meteorological data for the times of the CO_2 samples were available. Mr. Fonselius indicated that they were.

Dr. Scholander asked how high above the ground the samples were taken. They were taken at chest height by a man standing on level, bare ground, Mr. Fonselius said. The time of day (1300) was chosen to avoid, as much as possible, a local vertical CO_2 gradient.

Professor Rossby mentioned that emphasis in this work has been to get cheap and reasonably accurate results. When looking for large scale variations, more accurate methods may not be necessary. Because they are also more expensive and difficult they limit the possibility of developing an extensive network of stations.

In the next paper Dr. Goody presented an argument for the measurement of gases by spectrographic methods. He pointed out that the advantages of this method are that it is accurate, it is absolutely specific, and the measurements do not disturb the sample. He mentioned the importance of the work done on ozone as an example of the use of this method.

In illustration he gave an account of the work which he and his colleagues had done measuring nitrous oxide concentrations in the atmosphere. He showed that it was possible to do a very complete job of reasoning about the source, distribution, and destruction of this gas using spectroscopic measurements.

Mr. Eriksson remarked that it is apparent from spectroscopic measurements that nearly all the NH_3 must be in particulate form, and that this is quite important in considering the transport of NH_3 in the air as it must mean that the sea is an important source.

Dr. Goody emphasized that it is important to distinguish between gaseous and particulate NH_3.

Mr. Eriksson said that although Dr. Junge had filtered air through millipore filters he nevertheless found appreciable amounts of NH_3 in the filtered gas. Dr. Egnér added that ammonia cannot exist as a gas very long in the atmosphere as it is combined with acids to form ammonium salts.

Professor Rossby asked Dr. Goody what the "Umlaufzeit" was for nitrogen forms in soil to become N_2O. Dr. Goody estimated it about 100 days although it is very dependent on moisture.

In a paper by Dr. Egnér the balance of cations and anions found in precipitation was discussed. In most cases this balance is excellent, in some cases there is a slight imbalance of cations over anions. To calculate the balance it was necessary to determine the bicarbonate in the samples. This was done by titration to a pH low enough to ensure that all bicarbonate ions were converted to carbonic acid.

It was pointed out that such a titration would also affect weak organic acids, like fatty acids, when present in precipitation. Therefore one would expect good agreement between cations and anions using this method, even if there were organic acids present. When comparing the carbonate determined by titration with that calculated from pH and a normal concentration of CO_2 in the air, the titration values were always much greater than those calculated, indicating the presence of some organic compounds.

Dr. Tamm said that the agreement which Dr. Egnér had shown was very impressive. He wondered whether the measurements had been made at their given pH or adjusted to a particular pH.

Dr. Egnér indicated that they were not adjusted and went on to say that caution should be exercized in translating determinations from one laboratory to another. Using the same spectrophotometer is not enough. A slight difference in the atomizer, use of a different gas as fuel etc. can influence results.

Dr. Koczy asked if it was not possible from a titration curve of precipitation to determine whether organic acids were present or not. Dr. Egnér thought this was possible.

In his paper Dr. Gorham described the work he had been doing in England with precipitation samples. Collecting daily samples of rainwater at two hill locations, at top and bottom of a 65 foot tower, Dr. Gorham studied chloride/sulphate variations in relation to wind, season and rainfall conditions. Ratios of the elements in precipitation were in general agreement with those found in sea water except in the cases where there was reason to believe that industrial smoke was present. "Sulphate rains" dominate there in summer when winds are more commonly from industrial areas. In winter the rains were primarily "chloride". Sulphate rains were more common when the rainfall was moderate. Chloride rains occurred both for very heavy and very light rains. Salt content of the precipitation water was higher at the higher elevation station.

Dr. Egnér asked whether the sampling funnels were covered (they were not) between rains and if there were hills between the sea and the sampling stations. The stations were located in hilly country approximately twenty miles from the sea.

Prof. Rossby said that he felt three points in Dr. Gorham's lecture should be considered together.

1) The fact that the Cl to Na ratio was in nearly perfect agreement with sea water.
2) The Mg to Cl ratio agreed with the Mg to Cl ratio in sea water.
3) The chloride deposits and wind speed are related.

Each of these factors seems to point to a local source for the sea salts. Dr. Goody commented that the sampling stations were well inland but that for similar distances in Sweden the changes in the Cl/Na ratio were much greater.

Professor Byers said that chloride decreases inland in Puerto Rico and the sea spray could be seen to be the main source there even at some distance inland.

Mr. Rooth suggested that differences in the samples taken at high and low elevation might be due to the evaporation of small drops between the higher and lower stations.

Mr. Mordy asked about the difference in wind between the low and high station. Since the funnels were not covered any coating of salt by impingement might be expected to be greater with increased wind speed. This could perhaps be seen by comparing first and second day's rains after a dry period.

Professor Rossby asked if the Cl/Na ratio as well as the proportion of sulphur in lake waters in the vicinity was in agreement with the sea water ratio. Dr. Gorham said they were but there were significant variations in the ratio of Mg/Cl and K/Cl which could be accounted for by rock weathering and the washing down of minerals by rain.

Mr. Eriksson asked about the possibility of industrial sources for the chloride. The Cl content of coal is fairly small, and as the ratio of S/Cl is around 30—50 the contribution by combustion should not be very great.

In a lecture describing the chemical work done in connection with the University of Chicago Cloud Physics Research Professor Byers first decribed measurements of condensation nuclei. These measurements were made by Dr. Lodge with the use of membrane ("millipore") filters treated after the collections with appropriate reagents which provided enlarged spot tests where particles impigned. Particles larger than 0.1 μ are caught in this way. Samples are taken by drawing air through the filters. Professor Byers showed optical and electron photomicrographs of spots produced by the different chemical components of nuclei.

As the interest of the Chicago group was largely in the precipitation process, measure-

ments in Puerto Rico were made only of Mg and Cl particles. The measurements were generally in agreement with those made by Woodcock earlier in similar climates.

Measurements of SO_4/Cl and some other particles were also made from aircraft over the middle western part of the United States. The Chicago group expected to find a gradient in the salt particle concentration inland from the Gulf of Mexico Coast but this was not found. Professor Byers indicated that at high levels almost as much salt was present in the middle west as in Puerto Rico.

Professor Byers described work done by T. Larson and I. Hettick at the Illinois State Water Survey in measuring chemical content of rainwater. Cations are found in slightly less quantity than anions. CO_2 content varied greatly with the length of storage of the samples. (No pH determinations were made although acidity causes deviation in the ion balance.)

During the discussion Mr. Eriksson pointed out that the strong decrease in numbers of chloride particles, near the ground must indicate the ground itself could not be the source. Professor Byers answered that this was true for the giant nuclei. Mr. Eriksson also pointed out that the size distribution itself was not a good guide for the mass of chloride in the air without some related mathematical considerations. It therefore should not be concluded that there was no decrease in mass from the Gulf of Mexico to Illinois even if the number of particles were about the same. Professor Byers agreed that the number could not be used to infer the amount of chloride in the air but he attributed the depletion of particles near the ground to the sweeping up of nuclei by vegetation.

The next lecture was given by Mr. Eriksson who discussed the geochemical balance of chloride and sulphur between sea and land. From data available on volcanic production, weathering, and human activities it is not possible to account for the rather large amounts of cloride and sulphur in river water without assuming a substantial transport of these two from the sea to land via the atmosphere. In the case of chloride this has been realized for some time. As to sulphur, the lack of balance was first pointed out by an Irish scientist, Conway, who suggested that H_2S produced in the blue mud of the continental shelfs diffused into the air, was oxidized to SO_2 and SO_3 and precipitated. The sulphur could be accounted for in this way. From the rainwater analyses on sulphur made at various places in the last fifty years, the amount precipitated would be sufficient, but it is necessary to accept the hypothesis of Conway to account for it. A great deal of specific study on this mechanism has yet to be made but it seems acceptable by quantitative reasoning.

In the discussion Dr. Egnér mentioned that the sulphur in precipitation was not the only quantity of sulphur brought to the ground. Much direct absorption takes place. This furnishes more evidence of the importance of the sea as a source for sulphur.

Dr. Gorham asked about the possibility of sulphur being released over land from soils. Mr. Eriksson said that he thought that sulphur is probably released everywhere anaerobic conditions exist, i.e. in bogs, swamps and marshes, but that it is difficult to estimate the quantities involved. They are presumably great but also do not effect the balance between the sea and land which has to be maintained anyway.

On the third day, conferees were guests of Dr. Egnér at the Agricultural College, Uppsala, In addition to the discussions and the presentation of papers, the day's activities included a pleasant boat trip into Lake Mälaren, and a visit to the laboratories where the techniques Dr. Egnér uses for the analysis of air and precipitation could be seen at first hand.

The first paper of the day, presented by Prof. Rossby, was a resumé of some large scale synoptic variations observed in the precipitation analysis. He showed the geographic variation in the ratio between chloride and sodium (Cl/Na), and maps of sulfur in precipitation. Prof. Rossby pointed out the difference in the gradients on the Cl/Na maps and the sulphur maps and how these gradients can give indications of the source region.

The geographic variation of the Mg/Na ratio was quite similar to the Cl/Na ratio. This distribution is strikingly different from the patterns of sulphur distribution.

Finally Mr. Eriksson commented on a chart of the geographic variation of sulphur as found in river waters in Sweden. This chart was quite similar in configurations to the chart showing sulphur found in rain water.

In the discussion following, Dr. Koczy mentioned that in considering the sea as a source for sulphur, one should keep in mind seasonal variations in the sea which could influence the quantity liberated to the atmosphere, principally variations in the thermocline and resulting changes in convection and eddy diffusivity. The most favorable convection periods in the sea are March-April and October-November. He asked whether these periods showed an increase in sulphur.

The highest sulphur content in rainwater was found in March, Prof. Rossby replied, but in his recollection

the winds were in the wrong direction for it to have come from the sea.

A paper by Dr. Koczy described some oceanic characteristics favorable to surface film formation and some observations of them. Surface films reducing surface tension by as much as 6 to 12 dynes/cm were common in coastal regions while in harbors he had measured a reduction as high as 22 $^1/_2$ dynes/cm. The normal surface tension of sea water is slightly higher than that of distilled water (max. 72 dynes/cm), whereas a characteristic value in an open sea area is only 66 dynes/cm. These surface films can often be observed as a streak on the sea and are largely formed by fatty acids. They gradually become oriented in streaks parallel to the wind. This orientation is largely due, Dr. Koczy felt, to long horizontal wind vortices or convective wind cells which separate them, i.e. Bernard cells.

Motion pictures were shown of the formation of similar streaks on the sea under various conditions.

In discussing this paper Dr. Welander questioned the explanation given the formation of the film streaks. He did not feel that they were reflection of the presence of Bernard cells, but possibly of wind shear.

Dr. Koczy said he had not made a theoretical investigation of this phenomenon. The streaks, he said, are very stable and last many hours.

Prof. Rossby asked whether it wasn't equally probable that they are convection cells in the water, which might be produced by evaporation.

Mr. Eriksson then gave a brief description of the molecular nature of the fatty acid molecules and made a particular point of their polarity in reference to their affinity to water, and different orientation resulting when in monomolecular as opposed to multimolecullar films.

He then mentioned that 20 % of the materials produced by phytoplankton were of this chemical nature. Such films would preferably absorb calcium from sea water and, as they are carried into the air by spray the calcium would also be carried away.

Dr. Egnér described some investigations which Prof. Köhler, and later he, had tried in bubbling air through sea water to determine whether any separation of sea salt components would take place. The experiments were unsuccessful as there was no detectable difference between the sea water samples and the tiny droplets collected. In this case, however, there was probably not enough surface material present to get separation.

Dr. Tamm asked if methods were worked out for collecting organic material in sea water.

Mr. Fonselius mentioned that he had been successful in extracting fatty material from fresh water lake samples.

In his lecture to the conference Dr Riehm paid tribute to M. Nessler whose method of ammonia detection had made the present microanalysis of rain water possible.

Dr Riehm then went on to emphasize the importance of boron in agriculture and to show the surprisingly large amount which can be received in rainwater. In the rainwater for December 1955 he found 8.9 γ/l of boron and in April 1956, 1.2 γ/l.

The rapid method used by Dr. Riehm in his boron determinations was described in detail.

In the discussion which followed this paper Dr. Egnér added additional emphasis to Dr. Riehm's contention that boron measurements should be started. He also mentioned that boron fertilization is needed in sugar beet production in southern Sweden.

Prof. Rossby asked what the possible sources of boron are. Because boron distribution by the atmosphere is probably quite irregular and because deficiencies exist over wide areas, it should be quite interesting to look at data which could show seasonal or annual variation in the boron deficiencies.

Dr. Philipsson said that in the samples analysed in Ultuna he had found 5 to 8 γ/l in rainwater (7 week collection period) and that these values had been nearly constant with only a 10 % variation.

The final lecture was given by Dr. Egnér who discussed the results of air sampling by Dr. G. Arrhenius from Scripps Oceanographic Institution in the South Pacific during the "Capricorn" cruise. The samples were taken by scrubbing air with dilute nitric acid solution. The sea salt components in these regions were several orders of magnitude higher than in other regions. An exception to this was ammonia. In the doldrums, only one sample was taken, but concentrations were similar to continental regions. The composition of the sample was similar to sea water when concentrations were high but differed significantly for lower concentration samples.

In the discussion Eriksson gave figures on total atmospheric salt concentration in oceanic regions. He mentioned that Hawaiian rainfall contained different proportions of salts than sea water. These proportions were similar to the one example Arrhenius gave for the doldrums.

Dr. Koczy mentioned that divergence in the sea occurs in this area south of the equator. This would favor surface film formation due to the amount of organic material brought to the surface in the divergence area.

The conference reflected a considerable increase in interest and activity since the work in atmospheric chemistry began a few years ago.

Letters to the editor

On Sub-Tropical Jet Stream and its Role in the Development of Large Scale Convention

Dear Sir,

In a recent paper, RAMASWAMY (1956) has discussed the method of forecasting more than 12 hours ahead the broad regions in which thunder in general and thundersqualls or Nor'westers and convective dust-storms in particular would develop on the basis of his studies of vorticity patterns at 500 and 300 mb levels.

The writer of this letter would like to present the following points in connection with the claims made by Ramaswamy in the above-mentioned paper:

(i) It is known that Nor'westers and dust-storms in northern India and Pakistan *are most frequent generally late in the afternoons or evenings* in the plains and that only *a small number occurs at other times of the day or night;* this has also been stated by RAMASWAMY (loc. cit.). According to the instances quoted by Ramaswamy in his paper, the mass divergence associated with upper tropospheric vorticity patterns at 500 and 300 mb levels on the evening of any particular day is responsible for the Nor'westers and dust-storms in northern India and Pakistan during the 24 hours after the next morning. On referring to the synoptic charts, it is seen that a large number of the dust-storms and Nor'westers shown in Figs. 10 to 14 of his paper had occurred during the 6 hours or so in the afternoon or evening of the next day, i.e., after about 20 hours of the upper vorticity patterns in question. One should have expected the dust-storms or Nor'westers to occur over any particular area throughout the period of existence of such upper tropospheric vorticity patterns at all times of the day in stead of only after about 20 hours of their appearance and that too being most frequent in the afternoon or evening. Further, as seen from the synoptic charts, the upper vorticity patterns in question have on the illustrative occasions chosen by Ramaswamy, actually moved eastwards as seen from changes in wind directions by the time the phenomena developed over the areas in question. It would thus appear that some agencies in the lower troposphere particularly operative in the afternoon and evening over those areas play a vital role in the majority of dust-storms and Nor'westers although the existence of divergence in the upper troposphere would undoubtedly, under certain circumstances, help in the extension or intensification of the phenomena.

It is considered that it would be more appropriate to associate the upper tropospheric vorticity patterns on any evening with the weather produced during the 24 hours of that morning to the next morning, evening being about the mean time of the period, than with that produced during the 24 hours period after the next morning as done by Ramaswamy; but, by doing so, the utility of the evening patterns in forecasting 12 hours or more ahead as contemplated by him may not be directly recognised except through the persistence or slow movement of the patterns.

(ii) If the usual inversion at a height of about 5,000 ft. is destroyed by the large scale divergence in the upper troposphere which favours mass convergence in the lower troposphere as shown in Fig. 29 b of Ramaswamy's paper and not by insolation etc. (Fig. 29 a), one would also expect the Nor'westers to occur equally at all hours of the day and not particularly in the afternoons and evenings. Sounding balloon and radio-sonde ascents have shown that on many days of intensive activity of Nor'westers the inversion in question is noticed to persist practically till about the time of occurrence of the Nor'westers. The inversion would appear to be broken up mostly due to the effect of insolation (DESAI and MAL 1938; DESAI 1950) rather than due to large scale divergence in the upper levels giving rise to mass convergence in the lower levels.

It has also been stated that with large scale convergence in the upper troposphere and divergence in lower troposphere, there will be strong downward

motion of the dry air above the inversion and spreading of the moist air below it, which will probably intensify the already existing inversion. This has yet to be supported by actual observations when there is fair weather over northeast India. Further, it is considered that downward motion will be gentle and extensive rather than strong and localised as contemplated by Ramaswamy.

From what has been stated above, it will be seen that the claim made by Ramaswamy that one can forecast, more than 12 hours ahead, the broad regions of thundersqualls or Nor'westers and convective dust-storms on the basis of vorticity patterns in the upper troposphere at and above 500 mb level is not justified although the same will undoubtedly cause extension or intensification of these phenomena under certain circumstances.

Poona, June 5, 1956.

B. N. Desai
Meteorological Office

REFERENCES.

Desai, B. N., 1950: Mechanism of Nor'westers of Bengal, *Indian J. Met. & Geophys.*, **1**, pp. 74—76.

Desai, B. N., and Mal, S., 1938, Thundersqualls of Bengal, *Gerl. Beitr. z. Geophysik*, **53**, p. 285.

Ramaswamy, C., 1956: On the sub-tropical jet stream and its role in the development of large scale convection, *Tellus*, **8**, pp. 26 – 60.

Reply

Dear Sir,

Most of the points raised by B. N. Desai in the above note have already been discussed by the present writer in his paper ((Ramaswamy, 1956). However, the following very brief remarks are offered for the purpose of clarification: —

(a) Desai's note would give the impression that the author does not attach any importance to the local factors such as insolation, nocturnal valley convergence, orographic influences etc. in the development of large-scale convection. This is not so: these factors do play a part in the development. The main thesis of the author, however, is that these local factors are either a constant feature (e.g. orographic effects) or are often present during fair weather as well as severe convective weather (e.g. insolation and nocturnal valley convergence) while, in contrast, upper level *divergence* is invariably present during occasions of large-scale convection and upper level *convergence* prevails during unusual spells of fair weather. In other words, upper level divergence seems to be an 'invariable factor' in the development of large-scale convection while insolation, valley convergence etc. appear to be "local perturbing factors" of the lower troposphere which determine, when coexistent with upper divergence, the times of occurrence of violent convection. These are the reasons which have led the author to conclude that large-scale convection is 'overwhelmingly determined' by the upper divergence field (see pages 26 and 54 of the original paper).

(b) Desai's note may give the impression that the upper air systems illustrated in figures 10—14 in the paper moved away eastwards during the subsequent 24 hour-period and that the convective developments shown in these figures actually took place when the vorticity systems referred to by the author were not present. Considerations of space do not permit the author to publish in this reply the charts for the 3 subsequent days referred to. All that the author would state here is that the eastward movement of the systems on these occasions was small and was, in any case, much slower than the movements of high-level systems usually observed in middle latitudes. It may be incidentally added that it is the slow movement of upper level patterns which seems to provide adequate time for the transmission of the associated upward motion to the lower parts of the troposphere.

(c) One of the important objectives in this investigation was to find out a significant scientific criterion for forecasting large-scale convection over Indo-Pakistan. As stated by Desai himself, there would have been no scope for achieving this objective if the synoptic hour for the high level flow patterns had been chosen as suggested by him. Regarding the other reasons which led the author to choose 09/15 GMT hours of the previous day for the high level patterns, the reader is referred to the original paper (pp. 30 & 31). It will also be quite relevant to mention in this connection that an extensive chart showing the sea level pressure changes in *24 hours* ending at 03 GMT is used on a routine basis by the Indian forecasters along with the 03 GMT sea level chart for prognosticating weather and pressure systems during a period of

36 hours commencing from 03 GMT. The *mean synoptic hour* of this pressure change chart is *15 GMT of the previous day.* In view of this, the choice of the upper air charts of 12 GMT (mean hour) of the previous day, by the author, for prognosticating broad zones of the thunderstorms and duststorms during a *24 hour*-period commencing from 03 GMT appears to be justified. The author would also take this opportunity to suggest that, as a further step in this investigation, it would be interesting to attempt a prognostic high-level contour chart for the next 24 hours on the basis of the 09/15 GMT (mean hour 12 GMT) chart and determine the zones of convective activity on the basis of this chart.

(d) In explaining the schematic diagrams in figures 29(a), (b) and (c), the author has discussed the role of the dynamical processes and the local factors separately, only for the sake of simplicity in discussion. These local factors and their contribution to the actual development of large-scale convection have been more fully discussed in the later para in the same section of the paper (p. 53) and again in Section 12 (p. 56) where the effects of these local factors in helping the upper divergence field to overcome the resistance to lifting of the moist air have been specifically mentioned.

(e) The author has not stated that the downward motion induced by the dynamical processes is localised. The downward motion must obviously be extensive as it has been attributed to the effect of large-scale patterns. The word 'strong' was used by the author to qualify the downward motion only in a relative sense. The speed of the downward motion will obviously depend upon the amount of upper convergence, which, in its turn, will depend (to a first approximation) upon the amount of negative vorticity advection i.e. upon the negative value of the term

$$-V^2\left(\frac{\partial k_s}{\partial x}+k_s k_n\right)$$

(p. 51 of the original paper). No quantitative assessment of the downward or upward motion has been made by the author.

In view of the above, the author is still of opinion that the high level vorticity patterns provide a useful tool for the prognostication of the *broad areas* of development of thunderstorms and dust-storms in northern India and Pakistan in the pre-monsoon period, more than 12 hours ahead, whenever adequate Radio-wind and Radio-sonde data are available.

Madras 31, November 9, 1956.

C. Ramaswamy.

Regional Meteorological Centre.

REFERENCES

Ramasway, C., 1956: On the sub-tropical Jet Stream and its role in the development of large scale convention, *Tellus*, **8**, pp. 26—60.

Oxygen in Antarctic Air

Dear Sir,

In reviewing the many determinations of atmospheric composition Carpenter (1937) and Paneth (1937) concluded that the amount of oxygen in air is always the same at open places all over the world. The values generally range from 20.93 to 20.96 volume per cent. Hock et al. (1952) have since published a series of 320 determinations made during an 18 months stay at Pt. Barrow, Alaska, at 71 N. All of these fell between 20.91 and 20.96 per cent and the variation was not considered significant. In sharp contrast to this essentially constant composition of arctic air are the determinations of Lockhart and Court (1942) on the oxygen in ground level air in the Antarctic. Their values ranged from 20.76 to 20.48 volume per cent, a surprising amount lower than those from any other place on the earth. In addition they noted a seasonal variation, the summer values being generally lower than the winter ones. Gluckauf and Paneth (1946) objected to these measurements because no check analyses on normal air were carried out.

The icebreaker Atka collected a series of air samples off the Antarctic continent in 1955. When these became available[1] it seemed worthwhile to determine the oxygen in them. Empty helium cylinders were filled to 2,000 pounds pressure by a compressor on board ship. Smaller cylinders were later filled from these.

[1] Mr. Paul Humphrey of the U.S. Weather Bureau was responsible for the collection of the gas samples. They were made available to the author through the kindness of Dr. F. T. Haremann of the Argonne National Laboratory.

Triplicate oxygen determinations were made with the $^1/_2$ cc analyser of SCHOLANDER (1947). The instrument is considered accurate to .02 per cent. Measurements were only made after values for local air showed that the instrument was working well. Woods Hole air has never been found to vary significantly from 20.94 per cent over a period of several years. The data are presented in Table 1.

Table 1. Per Cent Volume of Oxygen in Antarctic Air

Sample	Latitude	Longitude	Date	Analysis			Average
				1	2	3	
SP-1	10 S	100W	12/16/54	20.90	20.91	20.88	20.90
9	73 S	163W	1/27/55	20.82	20.84	20.83	20.83
10	72 S	131W	1/30/55	20.82	20.82	20.85	20.83
11	69 S	100W	2/3/55	20.88	20.87	20.85	20.87
12	65 S	65W	2/6/55	20.86	20.89	20.85	20.87
15	72 S	15W	2/15/55	20.88	20.87	20.85	20.87
21	12 N	38W	4/2/55	20.86	20.86	20.86	20.86
Woods Hole...	42 N	70W	5/7/56	20.93	20.94	20.96	20.94

All of the samples are significantly below local air by amounts varying from .04 to .11 per cent. Two of the samples are from the tropics where normal values have always been reported. In view of this it is believed that the slightly lower oxygen percentage arose during the sampling and storage of the gas. Because of the greater solubility and reactivity of oxygen nearly all of the conceivable errors would tend to lower it in relation to nitrogen. DOLE ET AL. (1954) found that they had to allow for chemisorption of oxygen in the steel cylinders used to take atmospheric samples from rockets. One is not able to calculate how large such an effect might be. The measurements given here probably do not represent a significant departure from normal atmospheric composition. Since they are as much as .4 per cent above the summer values of Lockhart and Court, their earlier work is not substantiated. It is hoped that the large amount of Antarctic work during the International Geophysical year will include more atmospheric composition measurements.

Woods Hole, Massachusetts, December 25, 1956.

JOHN KANWISHER
Woods Hole Oceanographic Institution.

REFERENCES

CARPENTER, T. M., 1937: *J. Am. Chem. Soc.*, **59**, p. 358.
DOLE, M., LANE, G. A., RUDD, D. P., and ZAUKELIES, D. A., 1954: *Geochim. et Cosmochim. Acta*, **6**, p. 65.
GLUCKAUF, E., and PANETH, F. A., 1946: *Proc. Royal Soc.*, A-185, p. 89.
HOCK, R. J., ERIKSON, H., FLAGG, W., SCHOLANDER, P. F., and IRVING, L., 1952: *J. Meteorol.*, **9**, p. 441.
LOCKHART, E. E., and COURT, A., 1942: *Monthly Weather Rev.*, **70**, p. 93.
PANETH, F. A., 1937: *Quart. J. Roy. Met. Soc.*, **63**, p. 433.
SCHOLANDER, P. F., 1947: *J. Biol. Chem.*, **167**, p. 235.

On Short-Period Magneto-Hydrodynamic Waves in the Ionosphere

Gentlemen,

An interesting paper by Dr. B. Lehnert was published in *Tellus*, 1956, **8**, No. 2, p. 241. This paper explains the giant pulsation in terms of magneto-hydrodynamic waves travelling between the different ionospheric layers in the auroral zone. It is assumed that the velocity of Alfvén's waves is $H(4\pi\varrho)^{-1/2}$, where ϱ is the density of the atmosphere including neutral atoms. I see some difficulties in this suggestion. The periods of waves T lay in the range between 60 and 300 sec. For the ionosphere the time t_n of mean collisions is according to Dr. B. Lehnert (private communication)

Layer	D	E	F_1	F_2
t_n (sec)	$5 \cdot 10^{-6}$	$5 \cdot 10^{-4}$	1	300

for neutral atoms.

In the D, E and F_1 layers the value of $t_n < T$. However this condition is insufficient to make the neutral part of the atmosphere to oscillate with the ions.

Let the velocity of ions in the wave be v_i. Let the ions reach this velocity due to the action of the magnetic force during the time $t < t_n$. As a result of collisions the ions can transmit their momentum to the neutral atoms. But the abundance of neutral atoms is much greater than that of ions. The total momentum of the atmosphere will be about $\frac{\varrho_i}{\varrho}\varrho v_i$ after one collision. N collisions are needed in order that the whole atmosphere should acquire the wave matter velocity. If the wave energy is expressed in terms of the strength of the disturbing magnetic field h, the velocity of ions in the magneto-ionic waves will be about $v = h\,(4\pi\varrho)^{-1/2}$. If the whole atmosphere takes part in magneto-hydrodynamic oscillations, the velocity of matter will

be about $v = h\,(4\pi\varrho)^{-1/2}$. We have an approximate condition

$$N \cdot \frac{\varrho_i}{\varrho}\,\varrho v_i \approx \varrho v \text{ and } N \approx \frac{v\varrho}{v_i \varrho_i} \approx \left(\frac{\varrho}{\varrho_i}\right)^{1/2}$$

The wave period must exceed $4Nt_n \approx 4\left(\frac{\varrho}{\varrho_i}\right)^{1/2} t_n$ in order that the atmosphere would be able to take part in the magneto-hydrodynamic oscillations. If this condition is not fulfilled only the magneto-ionic waves will exist. The velocity of their propagation is about $v = H(4\pi\varrho_i)^{1/2}$ and the damping of these waves is very large according to Dr. J. Piddington's investigations. Calculations show that this condition is not fulfilled in the normal E, F_1 and F_2 layers.

Crimea, USSR, December 28, 1956.

I am, Gentlemen,
Yours faithfully

S. B. Pickelner
Crimean Astrophysical Observatory.

Dear Sir,

In a recent paper (*Tellus*, 1956, **8**, No. 2, p. 241) an attempt has been made to explain the giant pulsations in the auroral zones in terms of hydromagnetic waves. Prof. S. B. Pickelner has pointed out in the preceding note that the coupling between the ions and the neutral gas is too poor for the total mass of gas to oscillate as a whole. I fully agree that, with the present knowledge of ionospheric data, such a type of oscillations is impossible outside the auroral zones. What speaks in favour of such oscillations inside the auroral zones is that the periods of oscillation of ordinary hydromagnetic waves can be made consistant with the observed periods of giant pulsations (between 60 and 300 seconds). In order not to conflict with the difficulties pointed out by Pickelner the ionization degree has to be high inside the region of a giant pulsation. Consequently, reliable data have to be obtained for the ionization degree inside such a region before it can be decided whether a hydromagnetic approach is relevant or not.

Stockholm, Sweden, January 7, 1957.

Bo Lehnert
The Royal Institute of Technology.

Errata

Volume 8, number 4. Page 434, 2nd column, line 7 from below: For "alone on giant hygroscopic nuclei" read "in the life of one cumulus bubble".

Current Data on the Chemical Composition of Air and Precipitation VIII

(For further information see Egnér, H., Eriksson, E., *Tellus* **7**, pp. 134—139, **8**, p. 285 and 517)

Code	mm	mg/m²								pH	HCO_3^- $\frac{\mu val}{l}$	$\frac{\varkappa \cdot 10^6}{\Omega \cdot cm}$	$\mu g/m^3$ (= kg/km³)						
		S	Cl	NO_3–N	NH_3–N	Na	K	Mg	Ca				S	Cl	NH_3–N	Na	K	Mg	Ca
	Precipitation August 1956 (D 608)												Air August 1956 (L 608)						
Ri	67	13	104	0	0	46	11	8	21	6.0	6	9	1.2	9.6	2.0	1.7	1.2	3.3	10.0
Ki	36	10	16	0	0	8	5	2	23	6.2	14	7	*	*	*	*	*	*	*
Ar	87	37	16	2	2	14	4	4	22	5.7	4	6	0.6	0.0	1.6	1.8	0.8	1.0	5.9
Öj	61	48	26	1	3	14	17	6	57	6.3	28	10	2.4	5.1	4.1	2.6	4.3	2.0	6.8
Rö	102	76	27	2	7	25	9	13	32	5.4	0	7	*	*	*	*	*	*	*
Of	115	68	41	0	0	57	49	11	45	6.0	18	9	3.1	0.0	3.4	2.3	1.5	7.5	11.0
Br	80	29	7	1	1	8	4	3	14	5.2	0	7	1.1	2.1	0.7	0.6	0.2	2.3	2.9
ÅF	64	34	18	0	1	14	6	4	23	5.8	4	6	1.1	3.2	1.7	0.9	2.5	7.3	12.
ÅH	82	26	21	0	1	16	7	6	21	5.6	1	6	—	—	—	—	—	—	—
Sv	106	56	13	0	0	14	7	10	47	5.5	0	6	—	—	—	—	—	—	—
Rä	110	40	19	0	0	19	10	7	226	6.5	61	15	1.5	4.2	1.4	1.1	1.5	2.1	3.8
Åm	176	54	38	2	0	25	13	8	35	5.3	0	7	1.5	4.7	1.6	1.1	1.3	0.4	9.0
Sa	92	69	28	3	3	17	11	8	47	5.0	0	12	0.6	2.4	1.2	0.5	0.5	1.5	3.7
Ul	69	43	19	4	10	12	8	6	28	5.0	0	13	1.1	2.4	1.4	0.6	0.5	0.4	2.0
Er	112	92	52	4	52	24	45	7	25	5.9	13	10	1.2	3.0	1.7	2.1	1.4	2.7	5.7
St	83	58	25	3	5	24	11	7	50	4.8	0	15	2.5	0.0	1.8	2.1	1.9	0.6	7.9
Fo	102	58	38	0	0	31	34	8	57	5.4	0	10	2.9	0.9	4.1	0.9	0.4	1.2	8.7
Kv1	105	464	80	8	47	37	32	23	510	4.4	0	63	37.	0.0	1.8	0.8	1.4	2.7	14.
Kv7	100	82	51	6	22	23	19	9	54	4.8	0	18	—	—	—	—	—	—	—
VK	—	—	—	—	—	—	—	—	—	—	—	—	—	—	—	—	—	—	—
La	85	61	150	5	11	75	51	16	69	5.7	9	17	*	*	*	*	*	*	*
Bo	104	94	354	8	9	201	15	32	95	5.7	5	20	1.7	7.1	1.5	4.4	0.6	1.1	7.5
Vi	52	125	1 590	11	25	795	55	107	97	5.9	9	123	27.	520.	7.3	254.	15.	36.	34.
Fa	118	16	51	7	5	37	22	13	126	6.3	21	13	1.7	1.7	5.5	1.2	1.3	0.9	4.1
Fl	124	77	67	6	8	47	38	14	53	5.4	0	11	5.9	6.3	1.3	0.9	1.1	0.5	9.1
Am	145	91	166	7	12	103	21	17	57	5.6	4	11	—	—	—	—	—	—	—
Si	190	103	556	14	19	305	42	37	77	5.0	0	21	—	—	—	—	—	—	—
Pl	98	87	606	15	21	365	31	42	91	5.7	9	33	1.6	2.7	2.7	1.9	0.8	0.7	4.6
Sö	108	86	77	9	11	41	11	11	57	5.1	0	13	—	—	—	—	—	—	—
Sm	124	79	71	9	3	33	19	10	84	6.1	10	9	1.3	19.	1.7	1.0	0.6	0.7	15.
Sy	64	50	40	6	14	23	26	6	78	6.3	25	14	—	—	—	—	—	—	—
BH	70	47	81	9	9	47	15	15	69	5.2	0	19	4.2	3.3	2.1	0.9	0.5	1.1	6.3
Sk	85	85	146	20	34	79	21	14	180	5.3	0	22	—	—	—	—	—	—	—
Al	94	84	140	13	18	72	18	13	138	5.6	4	20	6.0	3.7	3.4	1.8	1.0	4.8	8.4
Hi	40	37	44	5	13	30	5	4	32	5.7	5	17	—	—	—	—	—	—	—
Ås	106	55	33	4	0	27	18	8	30	4.8	0	14	0.4	11.	3.0	1.8	1.2	2.4	18.
Vå	81	50	18	0	0	19	17	8	46	5.9	15	7	*	*	*	*	*	*	*
Li	154	96	2 130	20	28	1085	71	142	115	4.6	0	70	6.5	58.	1.0	26.	2.0	4.6	6.8
Ka	54	49	20	2	2	15	13	5	59	6.1	15	9	2.2	11.	2.4	2.0	1.5	0.6	11.
Ku	93	75	15	2	1	12	6	5	23	5.2	0	7	*	*	*	*	*	*	*
Jy	79	78	46	0	0	17	12	7	50	5.3	0	10	1.0	2.5	1.1	0.5	0.3	2.2	12.
Tv	105	87	106	0	0	59	21	12	48	5.4	0	11	0.0	6.9	0.4	1.2	0.2	1.0	5.6
Öd	84	107	180	14	24	92	13	15	60	4.9	0	24	3.1	7.8	4.7	3.0	0.9	0.7	8.1
As	104	115	510	20	39	320	23	43	77	5.0	0	33	6.2	12.	5.3	5.7	0.6	1.4	1.7
Ty	69	88	544	24	57	460	47	60	200	6.9	157	65	0.5	17.	4.5	9.7	1.0	2.4	22.
Ab	93	144	284	11	7	175	19	324	61	5.2	0	24	9.0	7.0	3.0	2.8	1.1	2.7	14.
Ed	196	175	178	22	15	97	22	575	156	4.8	0	20	8.9	7.2	2.0	1.3	0.3	1.3	14.
Le	156	177	213	24	36	75	36	36	126	4.6	0	28	17.	22.	4.7	7.4	1.3	4.1	35.
Ro	128	172	128	22	27	63	22	15	138	5.1	0	19	19.	13.	3.8	3.3	1.1	5.6	53.
NA	96	101	288	9	7	184	31	29	207	6.0	33	27	4.5	6.5	4.7	1.9	0.8	2.6	11.
Au	67	124	41	12	31	26	12	29	251	6.1	23	25	0.5	42.	5.4	0.9	1.2	11.	16.
Ba	131	63	33	10	20	25	13	15	80	6.0	14	9	0.0	3.3	2.9	1.5	1.6	3.8	30.
Fe	145	127	52	14	19	33	11	14	127	6.2	18	10	0.0	3.1	1.2	1.4	0.5	0.8	11.
Sc	132	212	527	26	15	300	51	44	276	5.8	13	32	0.8	17.	5.2	9.6	2.1	1.7	13.

Code	mm	mg/m²								pH	$HCO_3 - \frac{\mu val}{l}$	$\varkappa \cdot 10^6 / \Omega \cdot cm$	$\mu g/m^3$ (= kg/km³)						
		S	Cl	NO_3-N	NH_3-N	Na	K	Mg	Ca				S	Cl	NH_3-N	Na	K	Mg	Ca
	Precipitation August 1956 (D 608)												Air August 1956 (L 608)						
BV	69	185	89	19	18	42	21	22	239	5.2	0	36	5.5	1.7	2.9	1.4	1.5	0.8	3.4
Ho	92	261	46	9	112	23	93	33	210	6.6	109	30	11.	11.	2.8	5.5	2.1	2.5	14.
Bn	106	282	102	28	39	41	22	34	434	6.4	48	33	10.	9.7	6.7	4.6	1.7	2.3	18.
U	99	122	43	42	40	60	18	14	151	5.0	0	26	17.	5.6	4.2	1.6	1.0	0.3	2.2
SA	106	80	199	27	30	118	28	17	72	5.3	0	17	6.6	8.5	4.5	2.2	0.6	0.3	0.8
B	112	98	80	27	28	43	12	11	63	4.9	0	16	5.1	2.6	1.9	0.8	0.3	0.0	0.7
D	59	74	103	21	21	58	9	11	80	5.2	0	23	2.1	7.1	3.1	1.3	0.1	0.1	1.6
DB	106	127	190	28	29	150	20	20	56	4.6	0	28	4.9	12.	4.6	3.7	0.5	0.5	2.0
	Precipitation September 1956 (D 609)												Air September 1956 (L 609)						
Ri	88	38	83	4	4	49	7	7	25	5.7	0	9	0.0	5.2	0.6	1.4	0.8	1.0	8.3
Ki	21	16	3	1	0	2	4	2	7	5.9	8	7	0.0	0.0	1.0	1.3	0.9	1.6	11.
Ar	12	17	9	2	4	13	2	3	25	6.5	45	26	0.0	2.1	1.9	1.5	1.2	0.9	5.0
Öj	24	21	21	2	3	11	8	4	41	6.3	31	21	2.7	0.0	2.4	1.0	1.4	1.2	8.9
Rö	56	46	31	4	5	41	11	7	42	5.9	2	12	0.4	3.2	1.1	0.8	0.8	0.4	5.5
Of	21	22	12	0	1	13	77	5	20	6.7	69	25	1.6	3.3	2.3	0.8	0.3	3.8	8.1
Br	12	9	6	1	4	4	2	3	5	5.9	0	12	1.3	0.0	1.3	1.1	0.1	2.5	5.4
ÅF	86	43	69	1	2	41	13	7	23	5.6	0	8	3.9	0.0	2.0	1.1	3.7	1.9	14.
ÅH	69	41	33	4	6	26	6	5	23	5.7	0	9	*	*	*	*	*	*	*
Sv	37	25	8	2	3	8	5	3	21	5.9	5	9	—	—	—	—	—	—	—
Rä	55	24	13	6	7	8	6	5	178	6.9	108	27	1.4	3.6	1.7	0.8	0.6	2.7	11.
Åm	77	56	25	4	9	14	7	5	18	4.8	0	14	0.6	1.9	1.6	1.3	0.9	0.8	16.
Sa	35	40	16	4	6	9	7	5	39	5.5	0	15	3.2	2.0	1.1	0.9	0.9	1.0	4.2
Ul	27	25	14	3	7	8	5	2	22	5.2	0	16	2.8	0.2	1.2	0.6	0.6	1.5	3.3
Er	36	31	26	1	2	27	25	18	27	6.0	22	14	2.1	0.6	1.1	0.5	1.0	1.6	7.4
St	27	37	14	4	2	18	8	8	65	6.6	45	24	0.0	0.9	2.3	0.9	0.6	0.6	5.4
Fo	52	62	44	9	8	34	20	11	53	5.7	4	18	0.0	0.8	1.1	1.0	0.3	1.0	4.7
Kv1	52	574	51	7	33	22	31	24	495	4.2	0	117	46.	4.6	5.2	0.7	0.8	1.7	7.6
Kv7	10	29	50	1	3	27	5	6	25	4.6	0	54	*	*	*	*	*	*	*
VK	—	—	—	—	—	—	—	—	—	—	—	—	—	—	—	—	—	—	—
La	42	52	192	7	9	98	57	16	53	5.7	10	32	*	*	*	*	*	*	*
Bo	42	91	920	6	7	507	32	69	103	6.4	35	102	4.7	4.7	1.5	3.0	0.7	1.0	17.
Vi	51	325	4 300	15	13	2380	133	287	153	5.3	0	314	16.	395.	3.4	224.	11.	28.	43.
Fa	68	86	21	14	20	17	8	11	42	4.9	0	19	1.6	6.3	2.5	1.8	0.6	1.8	6.2
Fl	49	57	99	6	7	56	43	8	34	5.3	0	20	1.6	4.1	1.7	1.1	1.6	1.1	8.7
Am	70	78	231	9	12	138	15	18	42	5.1	0	26	—	—	—	—	—	—	—
Si	71	96	329	11	15	178	19	25	53	5.2	0	32	—	—	—	—	—	—	—
Pl	44	86	206	14	19	112	17	20	66	5.8	7	37	*	*	*	*	*	*	*
Sö	45	50	44	6	8	24	6	7	44	5.8	2	16	—	—	—	—	—	—	—
Sm	31	35	14	4	7	9	11	4	32	5.8	7	16	0.9	0.0	2.1	1.1	2.9	0.8	8.1
Sy	75	50	66	12	14	21	14	6	74	5.9	8	16	0.8	16.	3.0	1.1	0.8	0.7	12.
BH	*	*	*	*	*	*	*	*	*	*	*	*	*	*	*	*	*	*	*
Sk	42	67	140	12	31	79	11	17	57	5.5	0	35	—	—	—	—	—	—	—
Al	34	63	115	9	16	64	16	21	67	5.6	0	36	5.7	4.2	3.3	2.4	0.8	0.9	6.1
Hi	27	36	65	6	11	39	5	5	38	6.2	10	25	—	—	—	—	—	—	—
Ås	107	93	50	11	16	35	23	9	31	4.8	0	18	10.	8.4	3.2	1.0	0.6	2.2	8.5
Vå	23	22	9	2	2	9	13	4	30	6.3	24	15	1.5	9.8	4.7	0.9	2.2	14.	18.
Li	112	287	3 030	19	20	1640	109	222	146	4.8	0	113	3.4	13.	1.8	9.1	0.8	1.4	4.6
Ka	37	29	14	2	3	11	8	4	39	6.2	17	12	2.4	2.6	1.9	1.4	0.6	1.7	17.
Ku	41	24	11	1	1	8	5	2	16	5.6	0	7	6.6	0.0	4.4	0.9	1.4	13.	33.
Jy	34	20	17	1	1	11	4	2	25	5.7	0	10	1.4	1.6	0.7	0.5	0.3	0.8	3.8
Tv	23	25	63	0	1	35	11	6	27	6.0	14	25	*	*	*	*	*	*	*
Öd	32	67	101	10	16	56	11	8	36	4.8	0	37	4.6	8.4	4.3	3.4	0.8	1.7	8.6
As	43	103	212	17	34	121	15	24	65	5.1	0	45	3.7	4.1	3.5	1.6	0.4	0.7	6.4
Ty	51	107	164	20	37	173	22	22	83	6.4	80	45	3.0	9.0	7.2	3.6	1.2	2.8	26.
Ab	114	234	254	25	43	178	29	29	124	5.3	0	27	12.	16.	5.5	6.2	2.5	8.3	72.

Code	mm	mg/m² S	Cl	NO_3–N	NH_3–N	Na	K	Mg	Ca	pH	HCO_3^- – µval/l	$\varkappa \cdot 10^6$ / $\Omega \cdot$ cm	µg/m³ (= kg/km³) S	Cl	NH_3–N	Na	K	Mg	Ca
	Precipitation September 1956 (D 609)												Air September 1956 (L 609)						
Ed	100	124	162	23	93	100	41	17	77	5.5	0	25	8.8	0.2	2.9	1.8	0.4	1.4	7.2
Le	65	123	149	25	52	71	16	33	136	5.2	0	35	29.	12.	7.2	4.4	1.7	4.0	42.
Ro	64	112	110	17	14	61	15	14	142	5.2	0	27	16.	9.6	5.3	5.2	1.2	5.4	40.
NA	224	236	347	35	45	242	20	55	257	6.2	17	19	3.1	6.4	5.3	2.8	1.1	4.2	27.
Au	53	108	17	13	22	9	6	25	96	5.8	1	21	4.4	6.7	0.5	8.7	1.4	2.6	10.
Ba	48	38	32	6	9	10	8	7	53	6.1	16	13	8.6	3.7	1.4	1.6	1.6	16.	15.
Fe	53	33	13	8	9	8	4	4	40	5.9	7	13	1.6	3.2	1.5	1.6	1.4	4.5	11.
Sc	39	107	164	16	17	85	12	22	96	5.0	0	42	7.8	22.	1.8	6.9	2.6	0.8	6.3
BV	42	232	113	17	20	71	20	36	286	5.6	0	61	25.	2.6	7.0	1.9	1.7	2.0	19.
Ho	52	146	34	14	132	12	62	29	105	6.4	16	43	18.	17.	1.2	1.4	0.8	0.9	8.6
Bn	84	378	81	25	34	19	23	51	677	6.6	90	68	4.8	1.1	11.	68.	3.8	2.7	80.
U	57	130	69	17	30	35	13	11	115	5.8	4	26	9.2	10.	6.2	1.4	1.3	0.9	3.5
SA	44	78	48	17	21	29	15	8	56	4.7	0	28	7.8	2.5	3.1	0.8	0.5	0.2	0.5
B	81	123	55	31	30	30	13	10	68	4.5	0	25	3.3	13.	2.8	0.9	0.4	0.5	3.1
D	65	78	47	27	30	20	8	8	70	4.9	0	20	2.4	4.6	2.9	0.8	0.5	0.3	1.2
DB	34	93	88	18	36	45	12	11	47	4.6	0	43	9.2	7.9	7.0	1.8	1.0	0.9	1.9
	Precipitation October 1956 (D 610)												Air October 1956 (L 610)						
Ri	68	21	152	0	0	71	7	9	19	5.8	5	12	5.6	9.1	1.3	3.6	1.0	2.6	15.
Ki	8	5	4	0	0	6	3	2	7	6.4	31	10	0.0	0.0	0.9	0.5	0.3	0.2	5.1
Ar	19	11	3	0	3	5	2	3	5	6.2	18	11	2.2	0.0	1.4	0.9	0.4	0.3	4.8
Öj	37	26	28	4	4	14	8	6	38	6.0	15	12	1.9	0.0	2.4	0.5	0.9	0.3	3.0
Rö	8	3	0	0	0	1	2	1	7	5.4	0	6	1.8	4.9	1.1	0.7	0.9	0.1	3.8
Of	47	26	18	2	2	20	28	6	30	6.1	19	10	0.3	2.1	1.6	0.5	0.5	0.2	2.6
Br	51	18	9	1	2	7	3	3	24	5.7	0	5	—	—	—	—	—	—	—
ÅF	103	73	86	0	0	66	13	8	29	5.9	10	8	4.3	6.5	1.0	0.5	0.8	0.8	5.8
ÅH	—	—	—	—	—	—	—	—	—	—	—	—	—	—	—	—	—	—	—
Sv	22	13	4	2	1	7	4	2	20	6.2	14	10	—	—	—	—	—	—	—
Rä	19	27	24	2	1	26	6	5	93	7.0	184	42	4.8	0.0	2.2	0.5	0.6	0.4	5.2
Åm	31	20	21	2	1	18	8	5	22	6.0	8	11	1.9	0.0	1.0	0.6	6.7	0.2	2.5
Sa	37	46	32	0	0	21	57	15	50	6.6	66	24	3.1	0.9	1.7	1.5	0.9	1.2	6.1
Ul	31	34	48	5	8	29	8	6	35	5.3	0	20	4.0	3.1	1.1	1.1	0.2	0.4	1.0
Er	27	25	39	0	0	21	47	7	5	5.9	19	18	6.9	0.0	1.0	0.5	0.7	3.4	4.4
St	25	33	38	3	2	30	11	7	47	6.4	49	27	5.3	2.2	1.6	1.0	0.3	0.9	4.5
Fo	50	44	47	3	1	30	8	7	29	5.0	0	17	3.3	2.5	0.9	0.7	0.4	0.3	2.2
Kv1	33	450	27	5	21	40	24	15	392	3.6	0	203	59.	3.9	4.4	0.6	0.6	1.3	8.6
Kv7	31	45	50	0	0	27	47	5	24	5.2	0	27	—	—	—	—	—	—	—
VK	—	—	—	—	—	—	—	—	—	—	—	—	—	—	—	—	—	—	—
La	40	47	139	6	23	77	18	14	76	6.7	75	36	—	—	—	—	—	—	—
Bo	54	79	581	10	9	370	20	46	58	6.4	33	58	2.6	29.	0.5	15.	0.7	1.7	1.8
Vi	27	130	1590	9	7	848	45	96	73	5.8	8	237	8.3	190.	4.2	108.	6.7	19.	28.
Fa	12	23	70	1	0	19	41	5	15	5.7	5	44	3.0	0.0	1.2	0.6	0.7	1.5	11.
Fl	41	37	97	7	5	56	28	14	31	5.9	12	22	1.8	0.1	1.1	1.1	0.6	0.2	3.6
Am	74	77	167	16	20	102	12	13	20	4.8	0	26	—	—	—	—	—	—	—
Si	85	99	346	21	22	186	20	26	28	4.6	0	38	—	—	—	—	—	—	—
Pl	55	71	364	13	28	210	15	71	47	5.9	10	42	2.6	3.4	2.7	1.8	0.4	0.5	3.7
Sö	29	35	79	11	6	47	16	9	41	6.1	15	29	—	—	—	—	—	—	—
Sm	37	28	45	5	0	24	26	12	40	6.0	20	17	2.5	0.0	1.2	0.6	0.6	0.0	2.0
Sy	23	24	69	5	5	21	16	6	38	6.1	15	26	3.2	9.3	2.7	1.2	0.8	1.1	6.4
BH	56	51	80	4	0	45	46	14	44	5.8	5	18	—	—	—	—	—	—	—
Sk	60	82	113	19	38	99	12	14	43	4.9	0	33	—	—	—	—	—	—	—
Al	61	92	98	16	29	81	14	16	75	4.8	0	33	18.	3.2	2.9	0.8	0.4	1.7	16.
Hi	18	15	41	2	3	26	4	3	20	6.2	21	22	—	—	—	—	—	—	—
Ås	28	36	66	8	11	45	30	8	33	6.1	18	28	3.7	1.6	3.9	1.3	2.8	17.	15.
Vå	23	19	18	1	0	14	14	4	25	6.6	70	15	0.0	0.3	5.9	0.0	0.2	5.4	5.4
Li	85	294	4650	13	12	2520	120	360	137	5.0	0	213	2.8	40.	0.9	20.	0.7	2.3	2.7

Codes	mm	mg/m² S	Cl	NO_3—N	NH_3—N	Na	K	Mg	Ca	pH	HCO_3 μval/l	$\varkappa \cdot 10^6$ $\Omega^{-1} \cdot cm^{-1}$	μg/³ (= kg/km³) S	Cl	NH_3—N	Na	K	Mg	Ca
	Precipitation October 1956 (D 610)												Air October 1956 (L 610)						
Ka	37	21	21	2	2	14	7	15	18	5.9	7	10	4.1	4.2	3.1	1.3	1.9	1.2	8.6
Ku	77	38	12	3	0	10	8	5	15	5.5	0	6	3.0	1.0	0.9	0.1	0.2	1.0	7.7
Jy	82	46	24	5	0	20	9	5	24	5.3	0	8	2.1	6.5	0.7	0.1	0.3	0.1	2.5
Tv	53	53	77	1	0	47	21	9	30	5.6	0	15	5.0	18.	1.6	4.0	0.5	2.9	28.
Öd	36	58	202	7	25	114	17	15	44	5.4	0	44	7.3	14.	4.2	6.5	0.3	0.9	4.7
As	62	93	689	12	35	326	98	42	66	5.7	7	58	9.2	2.2	5.1	2.4	0.1	0.6	8.1
Ty	37	82	218	16	29	267	21	38	78	6.6	175	65	*	*	*	*	*	*	*
Ab	56	102	320	6	2	218	15	31	73	6.3	50	40	12.	0.0	3.0	0.3	0.0	2.4	20.
Ed	40	74	162	6	18	81	12	13	40	5.4	0	32	16.	13.	3.3	2.4	0.0	0.9	5.1
Le	27	91	238	12	45	104	34	25	74	5.7	20	71	36.	25.	6.6	7.3	0.3	2.4	14.
Ro	30	65	98	10	8	46	15	9	75	4.9	0	42	28.	14.	4.5	1.4	0.6	1.0	9.6
NA	43	64	235	7	25	107	13	23	97	6.6	57	45	19.	4.6	5.6	1.7	0.3	0.4	7.4
Au	105	235	81	34	78	39	28	43	114	5.4	0	23	10.	3.8	2.5	1.8	2.9	5.2	10.
Ba	120	126	38	17	103	31	2	29	48	5.3	0	10	12.	9,9	1.7	11.	0.7	1.4	7.8
Fe	92	82	31	19	8	33	2	8	39	5.3	0	12	5.7	8,2	1,0	19.	1.0	1.2	7.0
Sc	94	139	517	25	27	29	12	41	73	4.8	0	37	14.	26,	1,8	12.	4.6	1.0	9.2
BV	75	183	89	14	65	39	14	25	165	5.2	0	26	14.	5,0	0	1.4	0.7	0.8	3.5
Ho	51	63	0	6	57	16	86	16	48	6.1	43	15	16.	15.	1.6	1.9	0.5	2.1	15.
Bn	71	68	106	18	85	19	12	45	122	6.4	70	57	8.0	20.	3.7	31.	8.1	4.8	21.
U	103	133	299	29	33	185	18	29	141	5.6	1	30	5.4	6.5	5.4	0.7	0.9	0.8	1.9
SA	122	175	1128	31	22	645	53	81	143	5.0	0	45	10.	9.7	4.4	1.2	0.9	0.6	6.8
B	172	170	344	46	43	116	22	24	100	4.8	0	20	2.7	3.5	2.6	0.5	0.3	0.4	0.5
D	95	93	160	26	29	97	13	16	84	5.1	0	18	4.5	8.2	3.6	0.4	0.4	0.5	0.7
DB	70	118	328	22	32	189	17	26	53	4.7	0	39	6.1	8.4	5.5	0.6	0.4	0.5	1.0

— No sampling. * Sample discarded. Stations Ri—NA analyzed at R. Agric. College, Uppsala. Stations Au—Bn analyzed at Staatl. Landw. Versuchs- u. Forschungsanstalt, Grötzingen. Stations U—DB analyzed at Institut d'Hygiene et d'Epidémilogie, Bruxelles.

G. Brodin, Uppsala H. Riehm, E. Quellmalz, Grötzingen J. Bouquiaux, A. Mertens, Bruxelles

CO_2-values Aug.—Oct. 1956 in Scandinavia

(Cf. Fonselius, Koroleff: Tellus 7, pp. 258—265)

Station	Aug. Date	°C	Wind	Weather	CO_2 ml/10 l.	Sept. Date	°C	Wind	Weather	CO_2 ml/10 l.	Oct. Date	°C	Wind	Weather	CO_2 ml/10 l.
Ab	1	15.5	ENE 4	3	3.04	1	4.5	WNW 4	0	2.94	1	1.0	W 5	7	3.24
	10	6.6	WNW 5	5	2.91	10	7.0	NNW 4	● 10	2.97	10	— 1.4	N 1	✳° 5	2.92
	20					20	2.0	WNW 9	▽ 10	3.37	20	0.8	W 5	▽ 10	3.25
Öj	1	17.1	SE 6	=° 3	3.00	1	13.6	W 3	8	3.35	1			✳°	
	10	16.4	N 6	5	3.19	10	18.0	SW 4	5	2.84	10	1.2	Calm	● 10	3.14
	20	16.7	E 1	4	2.98	20	14.6	W 2	10	3.44	20	9.1	W 6	9	3.33
Br	1	15.0	NE 1	5	2.94	1	8.0	W 5	5	2.98	1	0.0	SE 1	≡ 10	3.20
	10	10.0	N 4	2	3.10	10	17.0	SW 1	2	3.01	10				
	20	11.0	NE 1	●° 10	3.17	20	7.0	W 5	5	3.39	20	5.0	W 5	1	3.03
Er	1	15.7	E 2	● ▽ 10	3.08	1	16.8	WNW 2	2	3.15	1	12.1	W 4	8	3.26
	10	14.6	NNW 5	5	3.23	10	14.4	S 2	3	2.84	10	6.1	W 3	4	3.33
	20	18.4	SW 2	9	3.06	20	13.9	W 2	1	3.49	20	6.1	W 4	2	3.19
Fl	1	12.2	SW 1	, 10	2.99	1	15.8	SW 1	6	3.02	1	15.0	SW 2	8	3.18
	10	18.2	NE 1	● 0	3.12	10	12.7	E 1	5	2.81	10	11.8	W 1	0	3.11
	20	15.8	SW 2	▽ 7	3.07	20	12.5	SW 1	7	3.33	20	9.6	W 1	5	3.26
Pl	1	14.0	S 4	9	2.98	1	15.0	Calm	1	2.98	1	14.0	SW 2	6	3.46
	10	17.0	SW 4	1	3.09	10	16.0	SW 1	10	2.87	10				
	20	15.0	W 1	3	3.07	20	14.0	SW 1	1	3.38	20	0.0	SW 6	10	3.48
Ka	1	16.5	E 2	5	3.34	1	14.8	WSW 3	0	3.10	1	6.0	Calm	8	3.22
	10	13.0	N 5	5	3.21	10	14.6	W 2	5	3.25	10	4.6	SSW 3	9	3.04
	20	15.0	ENE 3	10	3.17	20	13.7	WSW 1	10	3.06	20	8.3	NNW 5	5	3.07
Ri	1	17.2	SE 2	5	3.01	1	13.0	WSW 3	0	3.26	1	5.8	SW 1	5	3.10
	10	10.8	NW 3	8	3.15	10	7.9	S 3	0	3.03	10	0.9	WNW 3	0	3.08
	20	18.8	E	10	3.23	20	11.8	WSW 3	7	3.08	20	6.6	WSW 3	5	3.20
Lu	1	15.3	ESE 1	5	3.16	1	11.7	WNW 3	5	3.11	1	2.5	SSE 2	10	3.25
	10	10.7	NW 3	10	3.17	10	12.5	SSW 3	0	3.27	10	2.5	S 2	10	3.12
	20	10.9	NE 3	● 10	3.26	20	10.2	SW 3	8	3.07	20	6.3	W 2	0	3.04
Tv	1	17.0	S 4	5	3.17	1	14.0	SW 2	0	3.22	1	13.0	SW 4	10	3.08
	10	16.0	N 3	5	3.12	10	13.0	S 1	10	3.07	10	17.0	SW 1	10	3.10
	20	17.0	S 1	10	3.27	20	11.0	W 4	10	3.13	20	8.0	W 3	0	3.22
Bo	1	20.6	NE 4	=° 0	3.03	1					1	6.0	ENE 3	=° 4	2.98
	10	10.3	ESE 4	=° 0	3.17	10	10.1	SW 1	=,° 10	3.16	10	6.3	W 3	●° ▽° 10	3.33
	20	11.5	NNE 3	=° 10	3.27	20	6.0	W 5	=° 0	3.45	20	4.4	W 4	=° 7	3.34
Vå	1	16.3	SW 3	7	2.99	1					1	8.3	SE 1	● ▽ 10	3.13
	10	14.2	ENE 2	0	2.96	10	13.4	NE 1	5	3.06	10	7,9	NE 1	●°	3.27
	20	9.2	SW 3	●° 10	3.02	20	13.6	E 1	5	3.30	20	1.4	SW 1	0	3.53
Be	1	12.1	NNW 2	●° ▽ 10	3.18	1					1	12.2	SE 5	● ▽ 10	3.09
	10	14.4	NW 1	5	3.25	10	15.0	SE 1	●° ▽ 10	3.23	10	11.2	WSW 2	10	3.37
	20	14.9	NW 2	10	3.08	20	13.4	SSE 1	=° 4	3.07	20	8.7	Calm	5	3.23
Öd	1	13.7	SW 6	●° ▽ 9	3.08	1	16.7	SE 2	7	3.03	1	16.2	SSW 5	7	2.89
	10	21.0	NW 1	4	3.07	10	15.2	SE 3	9	3.00	10	13.2	SW 4	4	3.62
	20	16.5	SW 4	7	3.04	20	17.3	SW 1	1	3.18	20	10.2	SE 2	●° 10	3.35
As	1	15.4	W 4	5	3.11	1	15.8	SE 3	4	3.18	1	15.2	W 5	6	3.16
	10	17.9	NW 2	4	2.96	10	17.8	SE 3	6	3.02	10	12.4	WSW 3	6	2.89
	20	16.5	WNW 4	4	2.98	20	17.9	W 1	8	3.25	20	12.0	SW 2	● 10	3.24

Symbols used for description of weather conditions, are those, internationally used. The numbers in the weather-column give the cloudiness and the wind force i Beauforts.

S. Fonselius
Intern. Inst. of Meteor, Stockholm

F. Koroleff
Inst. of Marine Research, Helsinki